Skin Structure and Drug Permeation

Cláudia Liliana de Bastos Sousa Silva

Faculdade de Farmácia, Universidade de Coimbra, 2008

Dissertação apresentada à Faculdade de Farmácia da Universidade de Coimbra para obtenção do grau de Doutor em Farmácia, na especialidade de Tecnologia Farmacêutica.

Trabalho desenvolvido sob orientação científica do Professor Doutor João José Martins Simões de Sousa do Laboratório de Tecnologia Farmacêutica da Faculdade de Farmácia da Universidade de Coimbra e do Professor Doutor Alberto António Caria Canelas Pais do Departamento de Química da Faculdade de Ciências e Tecnologia da Universidade de Coimbra.

Ao Filipe

Agradecimentos

Ao Professor Doutor João José Martins Simões de Sousa e ao Professor Doutor Alberto António Caria Canelas Pais quero expressar o meu sentido agradecimento pela oportunidade de desenvolver este trabalho bem como pela valiosa orientação científica e revisão crítica da presente dissertação. Ao Professor Doutor João José Martins Simões de Sousa expresso o meu mais sincero agradecimento pela confiança desde sempre demonstrada e por todas as palavras de apreço e permanente encorajamento. Ao Professor Doutor Alberto António Caria Canelas Pais um especial agradecimento por me ter feito sentir em casa, desde o primeiro momento, no Departamento de Química da Universidade de Coimbra e pela inestimável ajuda no alargamento dos horizontes científicos.

Ao Professor Doutor Adriano de Sousa manifesto o meu reconhecimento pelo acolhimento no Laboratório de Galénica e Tecnologia Farmacêutica da Faculdade de Farmácia da Universidade de Coimbra.

Ao Professor Doutor Sebastião Formosinho, Presidente do Departamento de Química da Faculdade de Ciências e Tecnologia agradeço o amável acolhimento e facilidades concedidas na utilização dos laboratórios onde foi desenvolvida uma parte substancial do trabalho apresentado nesta tese.

Aos médicos da Unidade de Queimados da Universidade de Coimbra, Dr. Celso Cruzeiro, Dr. Luís Cabral e Dr. Luís Teles e à Dra. Beatriz Simões da Silva do Instituto de Medicina Legal de Coimbra os meus sinceros agradecimentos pelas produtivas discussões científicas e pela recolha das amostras de pele.

Ao Professor Doutor José Redinha e à Professora Doutora Maria Ermelinda Eusébio agradeço as facilidades concedidas na utilização dos equipamentos

utilizados na caracterização térmica da camada córnea e seus componentes, bem como pelo apoio científico. À Sandra Nunes agradeço a imprescindível ajuda na utilização dos mesmos equipamentos, a partilha dos conhecimentos científicos, as longas, mas sempre agradáveis horas, passadas no laboratório e a boa amizade que aí começou.

Ao Professor Doutor Björn Lindman e ao Professor Doutor Håkan Wennerström agradeço o acolhimento no *Center for Chemical & Chemical Engineering, Physical Chemistry 1, Lund University*. À Professora Doutora Emma Sparr reconheço o apoio científico facultado durante a minha permanência em Lund. Ao Dr. Daniel Topgaard agradeço o valioso apoio técnico e científico no âmbito dos estudos de espestroscopia de ressonância magnética nuclear e ao Dr. Vitaly Kocherbitov agradeço também o apoio técnico e científico na realização dos estudos de microcalorimetria isotérmica.

Ao Professor Doutor Amílcar Ramalho, professor do Departamento de Engenharia Mecânica da Faculdade de Ciências e Tecnologia da Universidade de Coimbra o meu agradecimento pelas facilidades, apoio técnico e científico gentilmente concedidos para a utilização do Microscópio electrónico de varrimento.

À INCARPO S.A. agradeço o fornecimento das amostras de pele de porco.

Ao Professor Doutor Jorge Costa Pereira, professor do Departamento de Química da Faculdade de Ciências e Tecnologia da Universidade de Coimbra a minha gratidão pelo precioso apoio técnico e científico facultado no âmbito das titulações potenciométricas e validação dos métodos analíticos.

Ao Professor Doutor Hugh Burrows, professor do Departamento de Química da Faculdade de Ciências e Tecnologia da Universidade de Coimbra, agradeço todos os sábios ensinamentos sempre tão gentilmente partilhados.

Ao Professor Doutor Francisco Veiga e à Professora Doutora Maria Eugénia Pina expresso o meu agradecimento pelos conselhos sempre oportunos e pela sempre

agradável convivência no Laboratório de Tecnologia Farmacêutica da Faculdade de Farmácia da Universidade de Coimbra.

À Professora Doutora Maria Helena Gil, professora do Departamento de Engenharia Química da Faculdade de Ciências e Tecnologia da Universidade de Coimbra, o meu sincero agradecimento pela disponibilidade concedida na utilização do espectrofotómetro de infravermelho.

Aos meus colegas e amigos de Laboratório (Rita, Camille, Andreia, Carla, Jucymary) agradeço de forma especial as discussões de ideias, a amizade, apoio e contribuições para o desenvolvimento deste trabalho. Muito obrigado também por todos os bons momentos que ficam para sempre.

À minha família e aos meus amigos que tornam a minha vida tão rica não é possível exprimir fielmente a minha gratidão e alegria por os ter. São a minha força e a minha determinação, obrigado pelo carinho e colo nos momentos de maiores dificuldades. Em particular tenho que agradecer imensamente ao Samuel porque ter sido o amigo que mais directamente influenciou as minhas decisões académicas. Obrigado por ires sempre à frente e nos beneficiares a todos com a tua experiência, a tua bondade e carácter humilde fazem de ti o ser humano e profissional extraordinário que todos conhecemos e admiramos.
Aos meus pais e à minha irmã agradeço especialmente por aceitarem as minhas escolhas.
Ao Filipe agradeço por me ouvir, por apoiar as minhas decisões e sobretudo pela nossa maravilhosa vida em comum.

À Fundação para a Ciência e Tecnologia agradeço o apoio financeiro sob a forma da Bolsa de Doutoramento com a referência SFRH/BD/14213/2003, sem o qual a realização deste trabalho não teria sido possível.

Table of contents

Resumo

A administração transdérmica de fármacos constitui uma via de administração de moléculas activas através da pele, inovadora, não invasiva, permite contornar o efeito de primeira passagem hepática, promove a adesão à terapêutica e reduz os efeitos adversos quando comparada com as vias mais tradicionais. Apesar das inúmeras vantagens, a sua aplicação encontra-se limitada pela grande resistência da pele à penetração de fármacos. De facto, a pele não é apenas mais uma membrana biológica simples. Pelo contrário, trata-se the uma estrutura extraordinariamente selectiva, cerca de 100 vezes menos permeável que as outras membranas biológicas e, para além disso, possui um sistema imunitário potente, capaz de reagir imediatamente contra qualquer agressão exterior. Em face destas características, os objectivos deste trabalho são a investigação da organização estrutural da camada exterior da pele (camada córnea) e o desenvolvimento de uma nova forma farmacêutica para a administração transdérmica de fármacos.

No Capítulo I encontra-se uma introdução geral a todos os conceitos principais necessários para seguir o trabalho desenvolvido e que serão discutidos ao longo da tese. O trabalho iniciou-se pela investigação das transições de fase induzidas pela temperatura na camada córnea (CC) e seus componentes, ilustrando a importância da análise térmica na compreensão do respectivo arranjo molecular e do papel deste na permeabilidade selectiva da pele (Capítulo II). Os resultados demonstraram que pelo menos oito transições de fase podem ser detectadas na CC desde a temperatura ambiente até cerca de 120ºC, em vez das quatro transições de fase geralmente descritas na literatura científica. Também foi possível confirmar

a existência de transições térmicas a baixas temperaturas que, muito provavelmente, afectam a permeabilidade da pele a temperaturas fisiológicas. Os resultados indicam que os lípidos da CC dos seres humanos se encontram organizados de forma heterogénea e que existe coexistência de fases a temperaturas fisiológicas e não fisiológicas.

A CC encontra-se sujeita a diferentes gradientes, tais como o conteúdo em água, temperatura e pH, que influenciam as suas funções e a sua permeabilidade. Após ter sido estudado o efeito da temperatura e sabendo-se que a permeabilidade da CC responde de forma não linear a variações no grau de hidratação, foi considerado relevante investigar o comportamento de fase da CC e seus componentes em condições isotérmicas e com diferente conteúdo em água (Capítulo III). Observou-se um intumescimento substancial da CC intacta assim como dos seus componentes isolados. Foi ainda detectada a presença de lipídos numa fase fluida, tanto na amostra de lípidos extraídos como na CC intacta, mesmo quando o contéudo em água é muito baixo. Foi possível detectar três novas transições de fase exotérmicas nos lípidos isolados, a humidades relativas entre 91-94%, que poderão estar relacionadas com a resposta não linear da permeabilidade da CC à hidratação.

Após a maior compreensão da estrutura e natureza físico-química da pele, uma nova forma farmacêutica constituída por complexos de polielectrólitos à base de quitosano foi desenvolvida e optimizada de forma a obter filmes com propriedades funcionais óptimas para serem aplicados na pele: flexibilidade, resistência, taxa de transmissão de vapor de água, bioadesão (Capítulo IV). A interação entre o quitosano e dois polímeros diferentes de ácido poliacrílico foi maximizada através do controlo do pH. O glicerol foi o plastificante utlizado que demonstrou ter a melhor influência nas propriedades funcionais dos filmes, com um nível óptimo a 30%. A aplicação de um adesivo sensível à pressão aumentou significativamente a capacidade bioadesiva dos filmes, apenas com um efeito mínimo na resistência e flexibilidade dos filmes. O filme obtido exibiu propriedades muito adequadas para a aplicação na pele e representa uma formulação muito promissora para a

incorporação de fármacos e subsequente administração por via tópica ou transdérmica.

De forma a avaliar o potencial do filme optimizado como veículo para a administração eficaz de fármacos através da pele, quatro princípios activos (paracetamol, ibuprofeno, galantamina HBr e galantamina base) com diferentes propriedades físico-químicas foram incorporados nos filmes (Capítulo V). A sua eficácia foi avaliada através da determinação do perfil de libertação e permeação de cada um dos fármacos. As propriedades bioadesivas e o potencial de induzir irritação do filme sem fármaco foram objecto de investigação em voluntários. Os filmes demonstraram ser permeáveis à água, não irritantes e capazes de aderir firmemente à pele. Para além disso, asseguram a libertação tanto de fármacos hidrofílicos como lipofílicos de forma fidedigna, reprodutível e sustentada, seguindo uma cinética de libertação aproximadamente de ordem zero. A forma dos perfis de permeação apresenta no início uma permeação invulgarmente rápida que é seguida por uma zona de fluxo de fármaco constante. Este perfil é extremamente benéfico na medida em que permite um início rápido da acção terapêutica do fármaco no organismo. De acordo com os resultados de permeação, bioadesão e irritação, os filmes desenvolvidos são uma opção viável para a administração eficaz de fármacos através da pele.

O objectivo final do trabalho aqui apresentado centrou-se na optimização de um filme para a administração transdérmica de galantamina, um fármaco terapeuticamente relevante, inibidor da colinesterase e usado no tratamento da doença de Alzheimer (Capítulo VI). Esta doença constitui a forma mais comum de demência nos idosos e, embora actualmente não existam fármacos capazes de a curar ou reverter a sua progressão, o tratamento dos seus sintomas pode atrasar a evolução da doença bem como melhorar significativamente a qualidade de vida dos doentes e suas famílias. O filme final representou uma melhoria da permeação percutânea da galantamina de cerca de 7 vezes comparativamente com a solução saturada do fármaco. Considerando estes resultados, o filme transdérmico final de galantamina constitui uma opção muito promissora para o tratamento eficaz da doença de Alzheimer.

Abstract

The transdermal drug delivery is an innovative and non-invasive route of drug administration through the skin, which circumvents the first-pass metabolism in the liver, offers higher patient compliance and reduces adverse effects when compared with the more traditional routes of drug delivery. Nevertheless, its applications are limited by the skin high resistance to the transport of drugs. The skin is not just another simple biological membrane. Instead, it is about 100 times less permeable than the other biological membranes, remarkably selective and has a powerful imune system that readly reacts to any agression. Therefore, the aim of this work is to investigate the structural organization of the outer layer of the skin, the *stratum corneum* (SC), as well as the development of a novel transdermal drug delivery system.

In Chapter I it is given a general introduction to all the main concepts that are needed for the development of the work and are explored throughout the thesis.
Considering the importance of the thermal analysis for the understanding of the SC and SC lipids molecular structure and their role in the selective permeability of the skin, the present work has been initiated by the investigation of the phase transitions induced by temperature in the both SC and SC lipids (Chapter II). The results have shown that at least eight transitions are detected in the SC from room temperature to ca. 120ºC, instead of the usual four described in literature. Also, it has been confirmed the existence of low temperature transitions that are likely to affect the SC permeability at physiological temperatures. These results indicate that human SC

lipids are organized heterogeneously, with coexisting phases at physiological and non-physiological temperatures.

The SC is subjected to several different gradients such as water level, temperature and pH that influence its functions and permeability. After studying the influence of temperature and with the knowledge that the SC permeability has a non-linear response to variations in the degree of hydration, it was considered relevant to investigate the phase behavior of the SC and SC components at different water contents under isothermal conditions (Chapter III). A substancial swelling of the SC and SC components and the presence of lipids in a fluid phase in both extracted lipids and intact SC was observed, even at remarkably low water contents. Three new exothermic phase transitions were detected in the SC lipids at RH=91-94% that may be related to the non-linear response of SC permeability to hydration.

After increasing the understanding of the structure and physicochemical nature of the skin, novel chitosan based polyelectrolyte complexes (PEC) were developed and optimized in order to obtain films possessing the optimal functional properties (flexibility, resistance, water vapour transmission rate and bioadhesion) to be applied on skin (Chapter IV). The interaction between chitosan and two polyacrylic acid polymers was maximized by pH control. Glycerol was the plasticizer with the best influence in the film functional properties at 30%. The application of a pressure sensitive adhesive significantly improved the films bioadhesion properties, with only a negligible effect in their resistance and flexibility. The optimized film exhibited very good properties for application in the skin and represented a very promising formulation for further incorporation of drugs for topical and transdermal drug administration.

In order to evaluate the drug delivering potential through the skin of the optimized chitosan based films, four drugs (paracetamol, ibuprofen, galantamine HBr, galantamine free base) with different physicochemical properties were incorporated in the films and the drug release as well as the skin permeation were evaluated. A second purpose of the work presented in Chapter V was the *in vivo* evaluation of the bioadhesive properties and irritation potential of the placebo film. The films

demonstrated to be water permeable, non-irritating and capable of firmly adhere to the skin. They also assure the release of both hydrophilic and lipophilic drugs in a reliable, reproducible and sustained manner following a quasi-zero order release kinetics. The shape of the permeation profiles reveals in the early stages an unusually fast permeation, followed by a region of constant flux. This behavior is most beneficial because it enables to rapidly attain the pharmacological action. According to the in vitro permeation results, bioadhesive properties and non-irritating potential, the developed films are a viable option for the effective delivery of drugs through the skin

The final purpose of the present work was the optimization of a film for the transdermal administration of galantamine, a therapeutically relevant cholinesterase inhibitor used in the treatment of the Alzheimer's disease, the most common form of dementia among older people (Chapter VI). Although at present there is no drug that cures or reverses the progression of the disease, the treatment of its symptoms can delay the evolution of the illness and, therefore, significantly improve the quality of life of the patients and their families. The optimized film exhibits an improvement of the percutaneous permeation of galantamine of ca. 7 times relative to the performance of the saturated solution of the drug. On the basis of these results, the final film is a very promising option for the effective treatment of Alzheimer's disease.

List of Papers

Silva, C.L., A.A.C.C. Pais and J.J.S. Sousa. 2007. Optimization of an anti-Alzheimer's transdermal film, submitted.

Silva, C.L., C. Vitorino, A.A.C.C. Pais and J.J.S. Sousa. 2007. Polyelectrolyte complexes as potential skin drug delivery systems of drugs with different lipophilicities, submitted.

Silva, C.L., J.C. Pereira, A. Ramalho, A.A.C.C. Pais and J.J.S. Sousa. 2007. Films based on chitosan polyelectrolyte complexes for skin drug delivery: development and characterization, submitted.

Silva, C.L., D. Topgaard, V. Kocherbitov, A.A.C.C. Pais, J.J.S. Sousa and E. Sparr. 2007. Stratum corneum hydration: phase transformations and mobility in stratum corneum, extracted lipids and isolated corneocytes. *BBA – Biomembranes* 1768: 2647-2659.

Silva, C.L., S.C.C. Nunes, M.E.S. Eusébio, A.A.C.C. Pais and J.J.S. Sousa. 2006. Study of human stratum corneum and extracted lipids by thermomicroscopy and DSC. *Chem. Phys. Lipids* 140:36–47.

Silva, C.L., S.C.C. Nunes, M.E.S. Eusébio, A.A.C.C. Pais and J.J.S. Sousa. 2006. Thermal behavior of human stratum corneum. A differential scanning calorimetry study at high scanning rates. *Skin Pharmacol. Physiol.* 19:132–139.

Reports not included in the thesis:

Burrows, H.D., M. J. Tapia, S.M. Fonseca, S. Pradhan, U. Scherf, C.L. Silva, A.A.C.C. Pais, A.J.M. Valente and K. Schillen. 2008. What spectroscopy, light scattering, electrical conductivity and molecular dynamics tell about the ability of non-ionic surfactants and polymers to solubilize poly{1,4-phenylene-[9,9-bis(4-phenoxy-butylsulfonate)]fluorene-2,7-diyl} in water, submitted.

Burrows, H.D., S.M. Fonseca, C.L. Silva, A.A.C.C. Pais, M.J. Tapia, S. Pradhan and U. Scherf. 2008. Aggregation of the hairy rod conjugated polyelectrolyte poly{1,4-phenylene-[9,9-bis(4-phenoxy-butylsulfonate)]fluorene-2,7-diyl} in aqueous solution: an experimental and molecular modelling study, submitted.

Burrows, H.D., M.J. Tapia, C.L. Silva, A.A.C.C. Pais, S.M. Fonseca, J. Pina, J.S. Melo, Y. Wang, E.F. Marques, M. Knaapila, A.P. Monkman, V.M. Garamus, S. Pradhan and U. Scherf. 2007. Interplay of electrostatic effects with binding of cationic gemini surfactants and a conjugated polyanion: Experimental and molecular modeling studies. J. Phys. Chem. B **111** (17): 4401-4410.

Ramalho, A., C.L. Silva, A.A.C.C. Pais and J.J.S. Sousa. 2007. *In vivo* friction study of human skin: influence of moisturizers on different anatomical sites. Wear 263: 1044-1049.

Ramalho, A., C.L. Silva, A.A.C.C. Pais and J.J.S. Sousa. 2006. *In vivo* friction study of human palmoplantar skin against glass. Tribologia – Finnish J. Tribol. 25:14-23.

List of Abbreviations

a	y-intercept
AD	Alzheimer's disease
AFM	atomic force microscopy
ATR	attenuated total reflectance
a_w	water activity
b	slope of the calibration curve
C_v	drug concentration in the vehicle
$C_{s,v}$	drug solubility in the vehicle
$C_{s,m}$	drug solubility in the membrane
D	drug diffusion coefficient of the drug in the SC
DL	detection limit
DSC	differential scanning calorimetry
DTA	differential thermal analysis
EB	elongation to break
ED	electron diffraction
EPR	electron paramagnetic resonance
ER_f	enhancement ratio of the formulation
ESR	electron spin resonance
FID	free induction decay
FTIR	Fourier transform Infrared spectroscopy
FT-Raman	Fourier transform Raman spectroscopy
GB	galantamine free base
GS	galantamine HBr
g(r)	radial distribution function
H_w^m	partial molar enthalpy of mixing of water

Hyper-DSC™	high-speed differential scanning calorimetry
IBU	ibuprofen
J	steady-state flux
K	drug partition coefficient between the formulation and the SC
K_0	zero-order release constant
K_H	Higuchi release constant
K_{KP}	Korsmeyer-Peppas release constant
L	drug diffusion pathlength
log P	logarithm of the octanol-water partition coefficient
LPP	long periodicity phase
MD	molecular dynamics
NMF	natural moisturizing factor
NMP	N-methyl pyrrolidone
NMR	nuclear magnetic resonance
PAA	poly(acrylic acid)
PAF	peak adhesion force
PAR	paracetamol
PBS	phosphate buffered saline
PEC	polyelectrolyte complexes
PLTM	polarized light thermal microscopy
PSA	pressure-sensitive adhesive
PVP	polyvinylpyrrolidone
PW	test value
Q	cumulative amount of drug permeated per unit of skin area
Q_{24h}	cumulative drug permeated at 24 h
Q_{48h}	cumulative drug permeated at 48h
QL	quantification limit
Q_t	amount of drug released in time t
Q_0	initial amount of drug in solution
R^2	coefficient of determination
RH	relative humidity
RSD	relative standard deviation
SAXD	small angle X-ray diffraction

SB	*Stratum basale*
SC	*Stratum corneum*
SG	*Stratum granulosum*
SL	*Stratum lucidum*
SPP	short periodicity phase
SS	*Stratum spinosum*
SSB	skin surface biopsy
S_{xo}	standard deviation of the method
S_y	residual standard deviation
T_2	transverse relaxation time
t_E	echo time
TEM	transmission electron microscopy
TEWL	transepidermal water loss
TS	tensile strength
V_{xo}	coefficient of variation of the method
WA	work of adhesion
WAXD	wide-angle X-ray diffraction
WVTR	water vapor transmission rate
Π_{osm}	osmotic pressure

List of Figures

List of Tables

I

General introduction

1. Introduction and objectives of the work

Over the past 30 years there has been a significant amount of research in the dermal and transdermal delivery of drugs and the transdermal devices have become a recognized technology for the variety of relevant clinical benefits that offers [1, 2]. Transdermal delivery systems are currently available to treat illnesses such as motion sickness, cardiovascular diseases, male hypogonadism, menopause and nicotine dependence [2-4].

The transdermal devices market is growing at an annual revenue rate of ca 12% for a worldwide market in 2005 of about US$12.7B and is expected to increase to $21.5B and $31.5B by the years 2010 and 2015, respectively [5]. About 50 new products candidate for dermal or transdermal delivery are being evaluated [3, 6]. These include formulations for the transdermal administration of drugs for the treatment of Parkinson's disease, Alzheimer's disease, skin cancer or depression [3].

In order to optimize the formulation of transdermal devices and broaden the number of drug candidates for administration through the skin, it is necessary to increase the understanding of the skin structure along with the mechanisms of percutaneous permeation. In fact, the exact nature of the skin lipid organization at the molecular level still possesses many unanswered questions. It constitutes a field of intensive research and development due to the advent of sophisticated instrumentation with increasing precision and sensitivity. Understanding the physicochemical and biological nature of the skin is necessary for a better understanding of the drug transport through the skin and for the continuous growth of the transdermal technology.

The purpose of the present work is to investigate the organization of the outer layer of the skin, the *Stratum corneum* (SC), and to develop a novel delivery system for the skin. Emphasis is laid on the investigation of the phase transitions induced by temperature and water in the SC components (e.g. lipids and proteins) and their role in the selective permeability of skin. A variety of techniques is used in this study.
The novel dosage form consists in a hydrogel film composed by chitosan and polyacrylic acid. In a first step, the desirable functional properties for film application on the skin will be optimized. Secondly, the potential of the films as universal transdermal drug delivery systems is evaluated by the incorporation of drugs with different lipophilicities. Finally, the film is optimized for the transdermal delivery of galantamine, an anti-Alzheimer's drug.

2. Skin functions

The human skin (**Figure 1.1)** is the most extensive organ of the human body with an area of 1.5-2 m^2, an average thickness of 0.5 mm, accounting for approximatelly 16% of the total body weight [7-9]. It constitutes the interface between the body internal enviroment and the external atmosphere, and is also responsible for protective, sensory and metabolic functions [10-12]. The skin barrier function is related with its multilayered structure (**Figure 1.1**) [13].

The skin protects the body against physical, chemical, microbial, electrical and thermal injuries, as well as UV radiation. The skin restricts the amount of water that is loss from the body preventing dehydration [12, 14]; limits the absorption of xenobiotics from the enviroment and prevents microbial infections [15]. Moreover, besides constituting a physical barrier for the penetration of microorganisms, several other processes make the skin surface very unfavourable for the microbial proliferation. The sebaceous and sweat glands (**Figure 1.1**) produce the acidic mantle (pH~5) that is a complex mixture of lipids with bacteriostatic and fungistatic activities [10, 14, 16]. The dry skin surface also accounts for this antimicrobial protection.

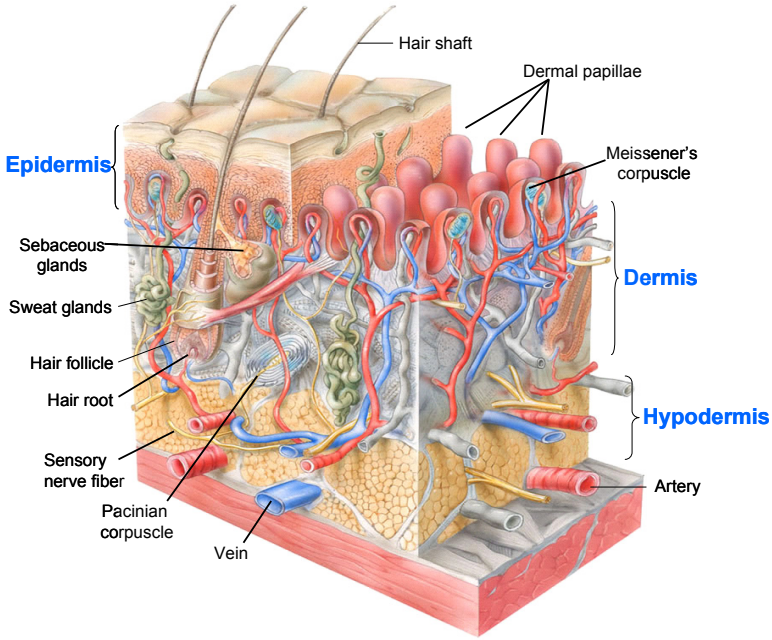

Figure 1.1 Schematic representation of the skin structure, modified from reference [17].

The skin also plays a protective role against ultraviolet (UV) rays due to the prodution of the pigment melanin in the melanocyte cells. Melanin has the ability to absorb and diffract the UV rays minimizing the sun induced trauma [7, 10, 12, 15,

16]. However, the UV rays are necessary for the chemical reactions that result in the synthesis of vitamin D, which is important for the absorption of calcium in the gastrointestinal tract and to the normal growth of bones and teeth [9, 14, 16].

The skin mechanisms of thermoregulation involve the sweat glands, the circulatory system and the hypodermis [10, 14]. The evaporation of sweat and water in the skin surface as well as the vasodilatation of blood vessels leads to a more rapid cooling. On the contrary, the vasoconstriction of blood vessels prevents the heat loss from the body [12, 14].

The skin is also a sensory organ: through the nerve endings and receptors the human being is able to perceive touch, pain and thermal stimuli [12, 14, 16].

3. Anatomy and physiology of the skin

The skin is divided in three functional layers, the epidermis, the dermis, and the hypodermis and each layer has different levels of cellular and epidermal differentiation [13].

3.1 Epidermis

The epidermis consists of stratified squamous keratinizing epithelial tissue, with an approximate thickness of 100-150 μm and is also avascular. The epidermis forms the outermost layer of the skin [14, 18, 19].
The epidermis is divided in four main layers, from the interior to the exterior, the S*tratum basale* (SB), the S*tratum spinosum* (SS), the S*tratum granulosum* (SG) and the *Stratum corneum* (SC) (**Figure 1.2**) [7, 14, 19, 20]. The S*tratum lucidum* (SL) is only present in the palms and soles, the areas of the body where the skin is very thick [7, 12, 18, 19].

Keratinocytes correspond to ca. 95% of the epidermal cells, although specialized cells such as Langerhans, melanocytes and Merkel cells are also present [7, 9, 12, 19]. The Langerhans cells are dendritic immune cells located in the SG that play a major role in the immunological defense [7, 14, 18]. They begin to process antigens, which is followed by the setting up of the inflammatory response [7, 12, 14, 16] (**Figure 1.2**). These cells also participate in the mechanism of contact allergy [7, 14].

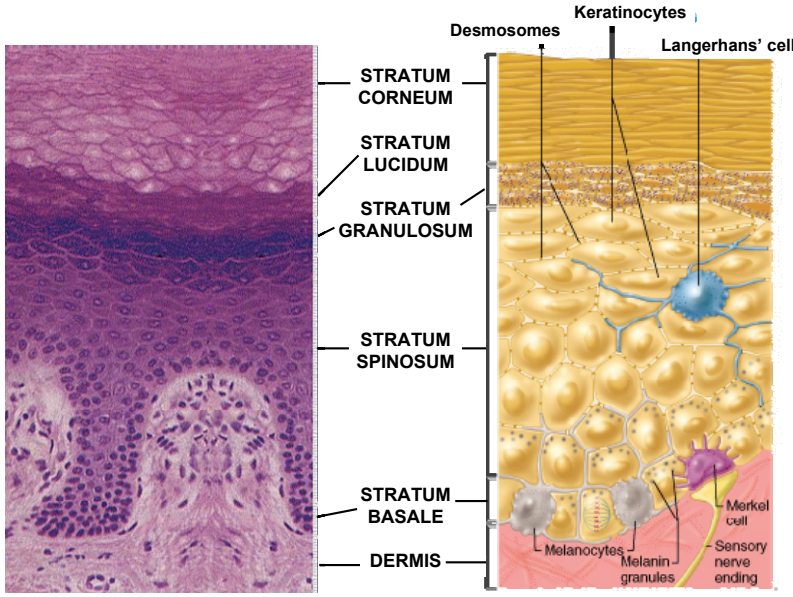

Figure 1.2 Structure of the human epidermis. On the left is shown a histological cut and on the right there is a schematic representation of the different epidermal layers and specialized cells.

Melanocytes are dendritic cells located in the SB and are also present in hair and eyes [12, 14, 18]. Their main function is to produce the pigment melanin that has the ability to absorb and diffract the UV rays minimizing the sun induced trauma and are also responsible for the skin color [7, 10, 12, 15, 16, 18]. Melanin is produced in the melanossomes of the melanocytes in response to a UV exposure and is then

transferred to the keratinocytes by a process that envolves phagocytosis [7, 14]. In this way, the pigment is uniformly distributed and conferes to the skin a protective role against UV rays [7, 10, 12].
Merkel cells are located in the SB, being tactile epithelioid cells associated with nerve endings (**Figure 1.2**) [12, 14].
Several skin appendages are specializations of the epidermis: the hair, sweat and sebaceous glands and nails (**Figure 1.1**) [14].

Keratinocytes undergo a process of proliferation, differentiation and keratinization during their migration from the SB to the skin surface, and give rise to the four major layers of the epidermis (**Figure 1.3**) [14]. During their migration, the cells flatten and the protein and lipids that constitute the SC are synthesized [10, 15]. The complete renewal of normal human skin takes approximately 1 month [12, 14, 21].

The SB is composed by a single layer of keratinocytes that are columnar, cuboidal and mitotically active with 6 to 8 μm in diameter [19]. The basal cells are connected to each other by desmossomes, and are attached to the basement membrane by hemidesmossomes [12, 14, 19, 22]. The basement membrane or epidermal dermal junction is an extracellular matrix that separates the dermis from the epidemis [14, 23].
The majority of the basal cells are stem cells that continuously undergo mitosis generating a daughter cell that is displaced from the older cells towards the epidermis surface (**Figure 1.3**) [12, 14, 18]. The basal cells exhibit a large nucleous, cell organelles and keratin filaments (tonofilaments) [19]. The major function of the remaining keratinocytes of the basal layer is to anchor the epidermis to the basement membrane [12].

The next layer is the SS as referred before and is the thickest layer of the epidermis (**Figure 1.2**) [19]. It consists of several layers of irregular polyhedral keratinocytes attached to each other and to the basal cells by desmossomes. They arise from the migration of the daughter cells generated in the basal layer [14]. These cells have a larger cytoplasm, a higher amount of keratin filaments, numerous organelles, a more flattened shape and lamellar bodies rich in lipids (Odland bodies) in its outer layers

(**Figure 1.4**) [12, 14, 19, 24]. The Odland bodies collect the lipids synthesized during the process of migration and differentiation of keratinocytes [10].

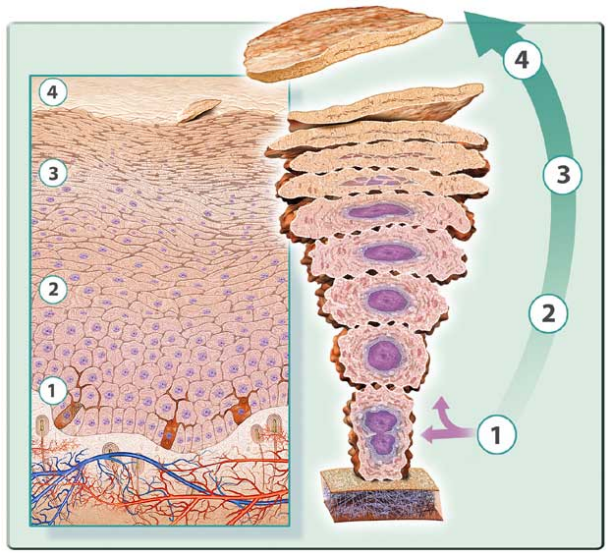

Figure 1.3 Schematic representation of the process of epidermis regeneration showing the keratinocytes proliferation, differentiation and keratinization (1-4). Reprinted from reference [25].

The SG consists of 3-5 layers of flattened keratinocytes that exhibit distinct keratohyalin granules, which usually appear darkly stained in the histological preparations (**Figure 1.2**) [14, 19]. The keratohyalin granules contain profilaggrin a precursor of the protein fillagrin that has the ability to aggregate and align the keratin filaments [14, 19, 21]. The keratinocytes of this layer are the last cells with nuclei. The Odland bodies are present in a higher number and size, and are filled with lipidic lamellar subunits, as well as some hydrolytic enzymes (proteases, lipases, glycosidases) (**Figure 1.4**) [11, 12, 14, 19, 26]. The stacked lipid lamellae are composed of precursors of the SC intercellular lipids: phospholipids, cholesterol and

glucosylceramides [11, 12, 21]. The Odland bodies migrate towards the cell membrane and in the interface between the SG and the SC they fuse with the cytoplasmatic membrane and extrude their content into the intercellular space [11, 12, 14, 15, 19, 21, 24, 27]. More recently, it has been proposed that this process may take place via a “continuous process of intersection-free membrane unfolding” without membrane fusion [28].

When the lipidic content is secreted, the co-secreted enzymes break down the phospholipids and convert the glucosylceramides to ceramides, the lipids that form the final epidermal barrier [11, 15, 19, 21]. The short lamellar stacked disks are also reorganized to form the typical lamellar sheets that are observed in the SC intercellular space [11, 29]. These processes are fundamental for the formation of the SC extracellular lamellae [19].

In the palms and soles where the skin is particularly thick and without hair, the next layer is the SL. It consists of several layers of flattened and compacted keratinocytes devoided of nuclei and cytoplasmatic organelles (**Figure 1.2**).

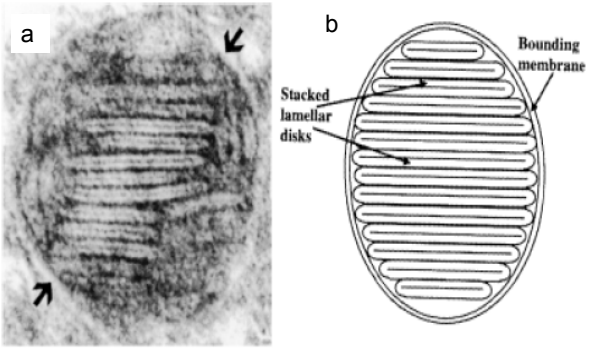

Figure 1.4 (a) Electron micrograph of a Odland body or lamellar granule of mouse skin. (b) Schematic representation of a Odland body according to the model of Landmann [30]. This figure is adapted from reference [11].

3.1.1 The skin barrier: *stratum corneum*

The outermost layer of the epidermis is the SC. It represents the end product of the differentiation process and the keratinocytes are now dead, fully keratinized, devoided of nuclei and cytoplasmatic organelles and are denoted as corneocytes. The corneocytes continuously undergo desquamation due to the action of the secreted proteases, which regulate the corneodesmosome cleavage (**Figure 1.3**) [11, 12, 14, 15, 19].

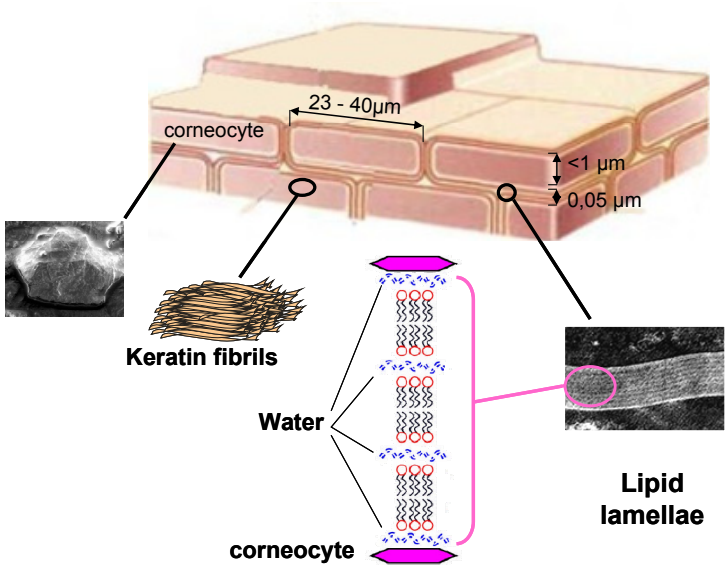

Figure 1.5 Schematic representation of the SC structure.

The SC consists of 10-15 layers of corneocytes with about 0.5 µm of thickness, 40 µm of diameter and 900 μm^2 in area, see **Figure 1.5** [15, 19, 31]. The corneocytes dimensions, their keratin filaments packing and the number of corneodesmosomes depends not only on the anatomical site, but also on their specific location in the SC and the age of the subject [19, 31].

The corneocytes are embedded in a matrix of stacked lipid lamellae in an array similar to "bricks and mortar" [32]. The intercellular lipid matrix represents approximately 20% of the total SC weight and constitutes the sole continuous region of the SC [31]. Due to this fact, the molecules that pass through the skin barrier must be mainly transported through this tortuous pathway [33-35].
The corneocytes have a protective function against physical and chemical injuries from the external environment, while the intercellular lipid lamellae provides the barrier for water diffusion, thus preventing dehydration [31, 36].

Corneocytes are filled with an insoluble protein complex mainly composed by highly organized keratin fibrills, aligned parallel to the corneocytes width and cross-linked by intermolecular disulfide bridges [12, 31, 36-38]. Keratin contributes to the mechanical properties of the SC, and is encapsulated by highly specialized structure, the cornified cell envelope (CE), with an approximate thickness of 15-20 nm (**Figure 1.6**) [31, 39-41]. The CE consists of a 15 nm thick interior layer of cross-linked proteins, an external 5 nm thick layer mainly composed by covalently bound long chain ceramides and represents 7-10% of the SC dry weight [12, 37, 39-44]. The lipid envelope represents ca 1.4% of the SC dry weight and has important functions such as acting as a permeability barrier as well as a template to orient intercellular lipid lamellae [31, 37, 39, 43-46].

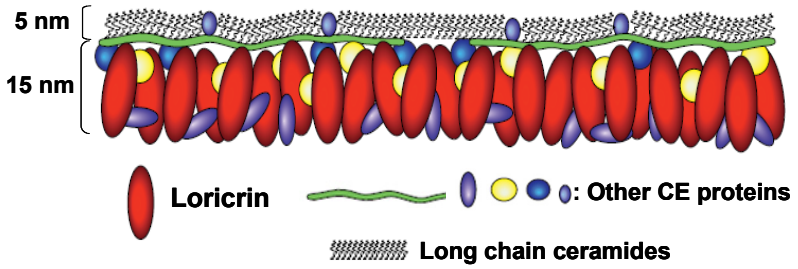

Figure 1.6 Schematic representation of the cornified cell envelope, adapted from reference [47].

The major components of the lipid matrix are long-chain ceramides (ca. 50-60% by mass), free fatty acids (ca. 10-20% by mass), cholesterol (ca 20% by mass) and cholesterol sulphate (ca. 5% by mass). They are responsible for the skin barrier function and its regulation [11, 31, 48-50]. The lipid composition differs considerably from most other biological membranes, having longer and more saturated lipids and basically no phospholipids [48, 51].

Nine subclasses of CER have been identified in the human SC and their structure can be found in **Figure 1.7**.

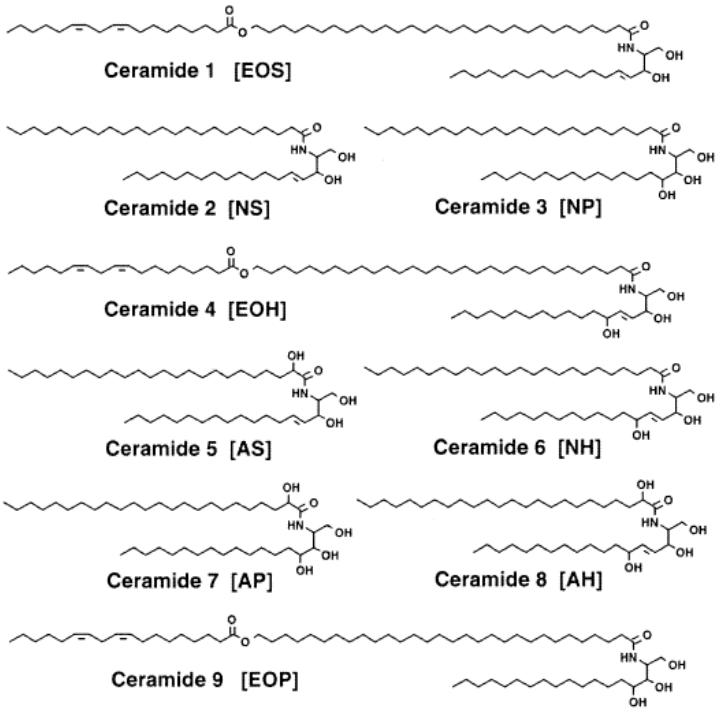

Figure 1.7 Subclasses of ceramides identified in human SC with the two conventions currently used. For details about the nomenclatures see text. From reference [11].

Two different conventions are currently used for naming ceramides, a numbering system from 1-9 and other related to structure. The latter was initially developped by Motta el al [52] and is based in the general form CER FB. B stands for the type of base: sphingosine (S), phytosphyngosine (P) or 6-hydroxysphingosine (H). On the contrary, F is related with the type of fatty acid: normal fatty acids (N), alpha-hydroxy fatty acids (A) or omega-hydroxy fatty acids (O). The letter E is used when there is an ester-linked fatty acid [11]. The two conventions are used in **Figure 1.7**

Free fatty acids are mainly saturated varying in chain lenght between C_{16} and C_{24} [49]. The long carbon chain lengths of the free fatty acids and ceramides contribute to a tight lateral packing that result in less fluid and less permeable lipid domains than the liquid crystalline organization of phospholipds in the biological membranes [11]. On the contrary, cholesterol seems to increase the fluidity of the extracellular lipid lamellae [11].
The extracellular lipid lamellae are clearly observed by electron microscopy using ruthenium tetroxide fixation [19, 31] or cryo-fixation [24, 53].

At physiological temperatures, the SC lipids in human, pig and mouse SC are arranged in a lamellar structure with two typical repeating units, a long lamellar structure or long periodicity phase (LPP) with a repeat length of ca. 134 Å and a short lamellar structure or short periodicity phase (SPP) with a repeat lenght of ca. 60 Å [54-57]. The LPP is not observed in phospholipid systems and is present in the SC of all species examined, being considered crucial for the permeability of the SC [54, 55, 58]. The LPP formation depends on the presence of long chain ceramides: CER1, CER4, CER9. On the contrary, free fatty acids promote the formation of the SPP, induce the transition from an hexagonal lateral sublattice to the predominant orthorhombic lateral sublattice and increase the fraction of SC lipids forming a liquid phase [59-64]. The existence of SC lipids in a fluid phase probably accounts for the non-negligible transepidermal water loss (TEWL) of about 100-150 ml per day and square meter of skin surface through the intact healthy skin [15], which appears difficult to explain on the basis of the solid SC lipids alone. It could also allow for the

high elasticity of the skin, and for the enzymatic activity in the SC intercellular space that is unlikely to take place in a crystalline phase [65].
A normal TEWL is necessary for the hydration of the outer layers of the skin [66, 67].

The organization of the intercellular SC lipids has been depicted in different models and is still under debate. The domain mosaic model of the SC organization proposed by Forslind [68] suggests that the lipids are organized in predominant crystalline/gel domains surrounded by grain boundaries where the lipids are in a fluid crystalline state and form a continuous pathway (**Figure 1.8**) [69].

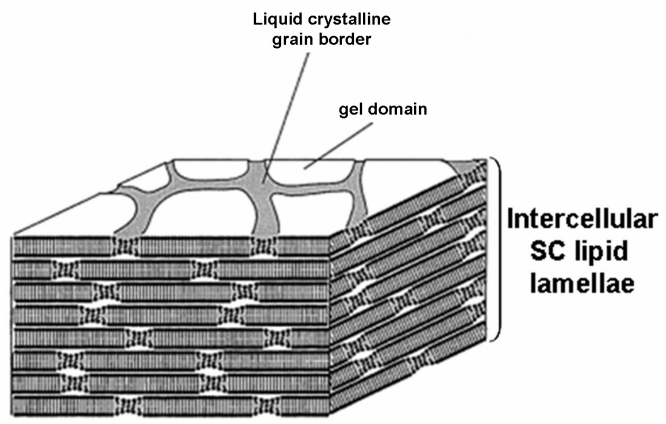

Figure 1.8 The domain mosaic model for the SC extracellular lipid organization, modified from [70].

Other models of the lipid matrix of SC emphasize the molecular arrangements of the lipids [70, 71]. One of thee, the sandwich model [71], also postulates the coexistence of crystalline and liquid crystalline lipid domains, while it describes a complex structure of connected bilayers for the LPP where lipids are organised in 3 layers: two broad crystalline layers on the sides and a narrow discontinuous fluid phase located in the center.
The discontinuous fluid phase is mainly composed by the fatty acid tail of the long chain ceramides (CER1, CER4, CER9) and cholesterol (**Figure 1.9**).

More recently, the single gel phase model [70] assumes an arrangement of lipids in the lower half of the SC in a single and coherent lamellar gel phase, excluding non-lamellar structures in continuous or bicontinuous arrangements - cubic, reversed hexagonal, reverse micelles or phase separation (**Figure 1.10**).

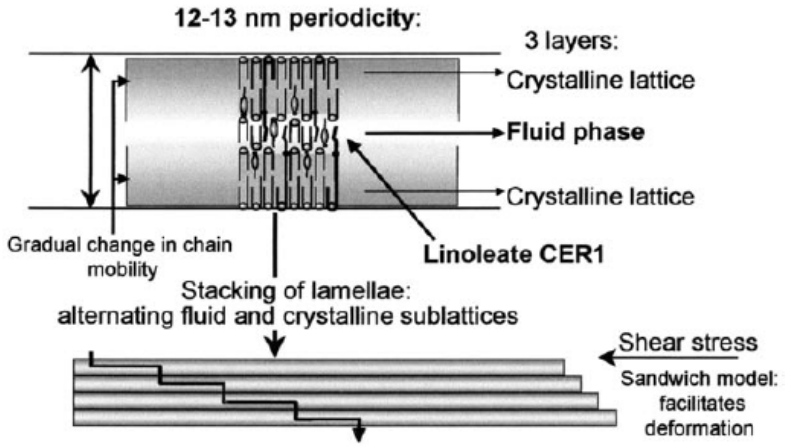

Figure 1.9. Schematic representation of the sandwich model for the extracellular lipid organization of human SC. From reference [72].

The SC integrity and cohesion is mainly attributed to the existence of corneodesmossomes that join corneocytes together in the plane of the SC and to adjacent layers [7, 31]. The desquamation process is one of the most important defensive process of the SC where the corneodesmossomes must be digested by proteolytic enzymes (corneodesmolysis) that are present within the extracellular lipid lamellae [16]. The activity of these enzymes is controlled by pH and water [31].

The water content in SC is important in regulating the SC permeability [73, 74], and it is also a determinant factor to other vital function of healthy skin in, e.g., its relation to the mechanical properties, the appearance and the enzymatic activity [66, 75] of the SC. The normal water content in SC is about 30 ± 5% [76] and depends on three

main mechanisms. First of all, the very unusual lamellar organization and composition of the intercellular lipids provide a very tight barrier to water diffusion. On the other hand, the corneocytes themselves increase the tortuosity and the diffusion pathlenght for the water across the SC. Finally, the water-holding capacity of the SC is intimately related to the presence of the so-called Natural Moisturizing Factor (NMF), a complex mixture of low molecular weight water-soluble compounds located in the intercellular as well as in the intracellular space [20].

The NMF is produced inside the corneocytes as a result of the hydrolysis of fillagrin [31, 65, 66]. After inducing the aggregation and alignment of the keratin filaments [14, 19, 21], fillagrin is converted by proteases in its amino acids: histidine, glutamic acid and glutamine [20, 65, 77]. Histidine is further converted to urocanic acid, while glutamic acid and glutamamine are converted to pyrrolidone carboxylic acid [20, 65, 77]. Additionally, NMF is also composed by lactic acid, urea, citrate and sugars [66]. The high concentration of these very hygroscopic components results in a high osmotic strength that has the ability to retain water [20, 66].

More recently, the involvement of aquaporin-3 in the skin physiology as well as the major role of glycerol in the SC water holding capacity has been also discovered [78, 79].

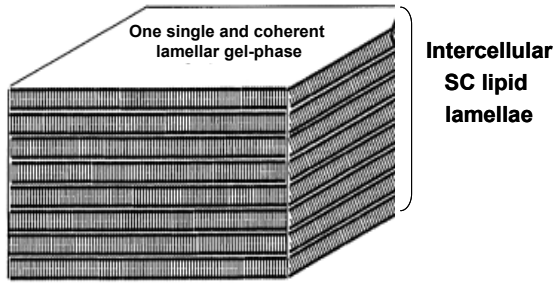

Figure 1.10 Schematic representation of the single gel phase model for the SC intercellular lipid organization. Modified from [70].

3.2 The dermis

The dermis is the main structural support and mechanical barrier of the skin [10, 12, 14]. It consists in a matrix of dense irregular connective tissue, ca. 0.1-0.5 cm thick and composed of collagen, elastin and reticular fibers embedded in a amorphous ground substance of mucopolysacharides (**Figure 1.1**) [10, 12, 14, 18]. The predominant cells present are the fibroblasts that produce the components of the connective tissue while the mast cells and macrophages are related with the immune and inflammatory responses [10, 12, 14, 18]. It contains an extensive circulatory system and lymphatic network, sensory nerve endings, hair follicles, sweat and sebaceous glands [10, 12, 14, 18].
The dermis vascular system provides the nutrients and oxygen to the skin while playing an important role in the body temperature regulation and in the removal of waste. The vasodilatation of the blood vessels leads to a rapid cooling while the vasoconstriction of the blood vessels prevents the heat loss from the body [12, 14].

3.3. The hypodermis

The hypodermis is the deepest layer of the skin, composed of loose connective tissue that connects the dermis to the underlying muscles or bones (**Figure 1.1)** [14, 18]. The main cells, adipocytes, are specialized in storing energy in the form of fat but it also contains fibroblasts and macrophages [12, 18].
The hypodermis is a heat insulator, protects against shock, enables the slide of the skin over the joints and carries the neural and vascular systems for the skin [12, 14].

3.4. Skin appendages

There are four types of skin appendages: the hair follicles, the nails, the sebaceous and the sweat glands (**Figure 1.1**). The hair follicles are located in all the body with

the exception of the palms, soles, lips and external genitalia. They always possess a sebaceous gland that produces the sebum which protects and lubricates the skin and helps to maintain the pH of the skin surface at around 5 [10, 12, 14].
The sweat glands are located in most of the body with the exception of the lips and genitalia. They secrete a hypotonic solution, with an approximate pH of 5 in response to the body overheat or emotional stress [10, 12, 14].
The nails have protective and manipulative functions [12, 18].

4. Drug delivery across the skin

The percutaneous absorption of drugs corresponds to the drug delivery across the skin into the systemic circulation. The percutaneous absorption involves three sequential processes. The penetration is the first process and corresponds to the entry of the drug in the skin. After the penetration, it follows the permeation of the drug that is defined as the passage of the active ingredient from one skin layer to another. The final process is the absorption that consists in the uptake of the drug into the systemic circulation.

Pharmaceutical active ingredients can be applied on the skin in a formulation to have a local or regional action (topical delivery) or to pass through the skin into the bloodstream or lymph system and develop a systemic action at the target site (transdermal delivery).

4.1. Advantages

The transdermal delivery of drugs offers a variety of well documented advantages over conventional routes of drug administration. These benefits include the maintenance of constant drug levels in the blood that reduces or eliminates the systemic side effects particularly for the drugs with short half-lives and/or a narrow

therapeutic window. Additionally, it increases the patient compliance due to simpler dosage regimens.
In addition, with the transdermal delivery, it is avoided the drug first pass metabolism in the gastrointestinal tract and liver, as well as other variables that influence gastro-intestinal absorption (e.g. changes in pH, food-intake, gastric emptying time and intestinal motility). These effects reduce the dose to be administered and, consequently, side effects [4, 12, 80, 81]. The drug administration is also easy to discontinue by removing the formulation from the skin, which is very advantageous in the case of adverse drug reactions.
The drug delivery across the skin constitutes a convenient, non-invasive and painless administration. Furthermore, it can be the route of drug delivery in circumstances where oral administration is compromised (e.g. unconscious or nauseated patients) [4, 12, 80, 81].

4.2 Limitations

Drug delivery across the skin has also some limitations [12, 13]. The main one is the very good barrier provided by the skin for the permeation of wanted, as well as unwanted molecules, as previously discussed. There is also intra and inter-variability in the skin permeability between different subjects that may produce different biological responses [12, 13].
The active pharmaceutical compounds may activate allergic reactions and be inactivated before entering the bloodstream, due to the activity of the bacterial flora in the skin surface or the enzymes present in the skin [12, 13, 82].

The function of the skin as a very effective barrier to the permeation of chemicals has been discussed in the previous sections. In spite of this action, the percutaneous absorption of drugs for local or systemic delivery can be a desirable process. For this reason, it is important to understand the mechanisms by which the drugs and other chemicals penetrate the skin and how the skin permeation can be modulated.

4.3 Routes of permeation

When a formulation is applied on the skin, the drug partition into the SC and go accross it by a mechanism of passive diffusion [12]. After transversing the highly lipophilic SC, the molecule has to partition to the water rich viable epidermis and after that to the dermis before it can enter the systemic circulation.

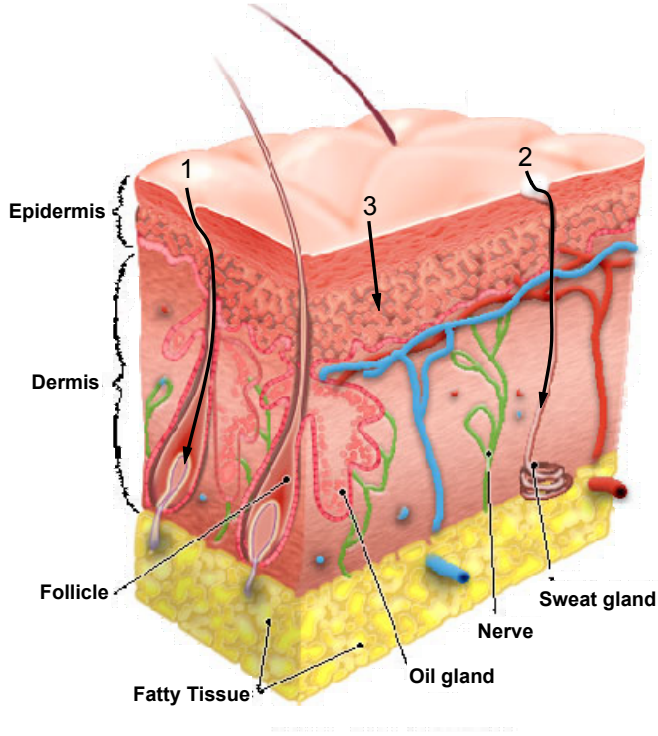

Figure 1.11 Possible routes for the drug delivery across the skin. (1) through the hair follicles with the associated sebaceaous glands, (2) via the sweat glands or (3) across the intact SC.

There are two possible pathways for a penetrant to cross the skin barrier: through the transappendageal route or the transepidermal route [10, 12, 83].

The transappendageal route includes the transport via the sweat glands as well as the transport through the hair follicles and associated sebaceous glands (**Figure**

1.11) [6, 10]. On the contrary, the transepidermal route comprises the diffusion of drugs across the intact SC and can be subdivided in transcellular and intercellular routes (**Figures 1.11** and **1.12**) [10].

Any chemical that penetrates the skin will diffuse through the path of least resistance, which is also dependent on both the physicochemical properties of the drug and the skin condition at the time [10].

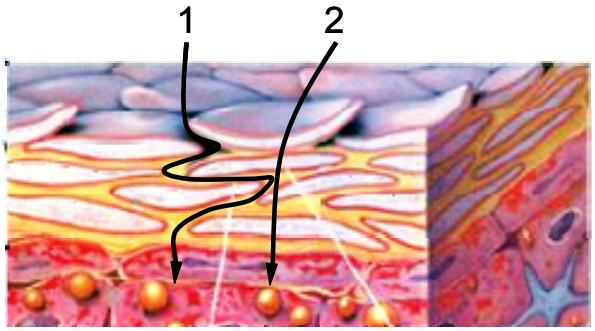

Figure 1.12 Transpidermal routes for drug permeation. (1) Intercellular route and (2) transcellular route.

The area available in the skin surface for the transappendageal transport is only ca. 0.1% in areas with less pilosebaceous units per area of skin and ca. 10% in the face and scalp where the density of pilosebaceous units is higher [12, 84-86]. This route of permeation circumvents the penetration of the SC because the openings of the pilosebaceous units conduct to an epithelial membrane more permeable than the SC [6, 12, 85, 87]. It seems to be important for large polar molecules and ions that are difficult to diffuse across the SC, and also some kind of delivery systems such as liposomes, nanoparticles and colloidal particles [6, 12, 85, 88, 89].

The drug diffusion through the transcellular route involves the sequential partition of the molecule between the lipophilic intercellular matrix and the hydrophilic corneocytes. The intercellular route concerns the diffusion of molecules through the continuous and tortuous pathway composed by the intercellular lipid lamellae. It is

generally accepted that the intercellular route provides the main pathway for most of the chemicals [6, 12, 33].

4.4 Factors affecting the percutaneous permeation

The transport of a molecule across the SC occurs by a process of passive diffusion. The steady-state diffusion through the SC can be described by Fick's first law [12]:

$$Q = D.K.Cv.\frac{t}{L} \qquad (\mathbf{1.1})$$

where *Q* is the cumulative amount of drug permeated per unit of skin area, *D* is the drug diffusion coefficient in the SC, *K* is the partition coefficient of the drug between the formulation and the SC, C_v is the drug concentration in the vehicle, *L* is the drug diffusion pathlength and *D.K.C/L* is the steady state flux (*J*).

It is thus clear that the percutaneous permeation of a drug depends on the:

- physicochemical properties of the drug;
- physicochemical properties of the vehicle;
- skin condition and physiological factors;
- application conditions.

4.4.1 Physicochemical properties of the drug

The ideal properties for the percutaneous absorption of a molecule are not the same as for the improved gastrointestinal absorption or other routes of drug

administration. The molecules that more easily permeate through the skin are small and have a moderate lipophilicity [90, 91].

The chemical structure of the drug influences its ability to diffuse through the skin. In fact, low molecular weight molecules (< 500 Da) have a higher diffusion coefficient (*D*) in the SC [3, 6, 92-95]. On the contrary, molecules with hydrogen bonding groups tend to diffuse slowly due to an increased ability to interact with the polar head groups of the intercellular SC lipids [81, 92, 94, 96].

The logarithm of the octanol-water partition coefficient (log P) is a good predictor of the partition behavior of the drugs within the skin [91, 95]. Generally, molecules with log P ranging from 1-3 have a good partition behavior due to their good solubility in both the lipophilic SC as well as in the hydrophilic and water-rich viable epidermis [3, 81, 90, 92, 95]. If the drug is too hydrophilic, the partition to the SC will be small and in the case of a very lipophilic drug, there will be a good partition to the SC but the drug tends to be retained there [97].

The concentration gradient influences the drug flux within the skin and is mainly determined by the *K* of the drug [**Equation** (**1.1**)] [81]. The solubility characteristics of the molecule have also a high influence in its ability to penetrate a membrane. A low melting point of the drug is related with a good solubility and is beneficial for the permeation [6, 90].

The ionization potential is another important property that influences permeation. The degree of ionization influences the drug solubility in the membrane as well as the partition (*K*) into the skin [6, 90]. Although unionized molecules partition better to the SC, the ionized species may permeate the skin through the transappendageal route (**Figure 1.11**) or may form ion pairs with ions present in the skin forming neutral compounds [6, 90].

Along with the physicochemical properties of the drugs, the pharmacokinetic parameters are also very important when analyzing the suitability of an active compound as candidate for transdermal drug administration. The drug must be

pharmacologically potent so that the therapeutic dose is small enough to compensate the limited amount that can enter the skin through a reasonable area [97]. Furthermore, the drug should not be directly irritant to the skin or prone to stimulate immune reactions [4].

4.4.2 Physicochemical properties of the vehicle

The first step in the transdermal drug delivery is the drug partition between the vehicle and the skin [1]. The vehicle can influence drug release from the formulation, change the barrier function of the skin and increase the dug solubility in the SC [1, 12, 98-100]. The alteration of the barrier function includes the interaction with the intercellular lipid lamellae, as well as with the protein components, and the increase of the SC hydration by an occlusive effect [10, 12].
The rate of vehicle evaporation, the dissolution kinetics, the solvent flux through the SC and the alteration of the vehicle composition with time are other important effects that affect the molecules permeation through the skin [1, 12, 81].
In general, it is favourable to select vehicles that have a low affinity to the permeants and in which the drug is less soluble [1, 12].

4.4.3 Skin condition and physiological factors

Several physiological factors are known to influence the percutaneous permeation of drugs: age, hydration, surface microflora, pH, surface lipids, metabolism, the body site, race, gender, temperature, blood flow [1, 10, 12, 101, 102].

The aging of the skin induces structural and biophysical alterations such as the decrease in the SC hydration, global deficiency in SC lipids, increased size of individual corneocytes, decreased blood flow, TEWL and epidermal turnover [12, 103-107]. All these alterations can modify the skin permeability and it has been

demonstrated the reduction of the permeability of hydrophilic compounds in aged skin [12, 103]. Moreover, premature neonates have an imperfect barrier that is very permeable and the absorption of exogenous chemicals is a matter of concern [1, 12, 101, 107, 108].

The percutaneous absorption varies according to the anatomical site due to differences in the skin thickness, lipid content, blood flow or density of the hair follicles [12, 48, 102, 104, 109]. It is generally accepted that the skin permeation tends to increase in the following order: genitals > head and neck > trunk > arm > leg [101, 103].

There are no significant differences between the skin permeability in the same body site of males and females, although there are marked differences in the appearance [10, 12, 101, 104].

The skin permeability changes between human races due to differences in the physicochemical properties of the skin [101-103], but this relation is not unequivocal. The SC of the blacks have more cell layers and higher density which justifies the smaller permeability [10, 103].

The skin hydration has a pronounced effect on drug permeation. An increase in the water content of the SC always produces a concomitant increase in the permeation [73]. In fact, occlusion is one of the most widely used techniques to improve the permeation of drugs due to its effect in the increase of the amount of water in the skin by preventing TEWL [12, 101, 110-112].

The skin has a significant metabolic activity due to its enzymes and the natural surface microflora that can transform many molecules that enter the skin [12]. This metabolism can inactivate the drugs or can be used to overcome the problem of drugs with disadvantageous physicochemical properties for the transdermal delivery. A prodrug with suitable physicochemical properties can be synthesized and within the skin this molecule is metabolized into the active form [12].

The temperature also modifies the skin permeability, and an increase in the skin temperature is accompanied by a non-linear increase of the skin permeability [12, 35, 113-118]. The temperature increases the fluidity of the intercellular lipids [119-121], it also changes the blood perfusion due to the mechanisms of thermoregulation, increases the drug solubility and contributes to the activation energies for the diffusion of molecules across the SC [1, 10, 12, 117].

In the case of the skin disorders or damaged SC, the barrier properties are compromised and the skin permeation is normally increased [122, 123]. Some examples of skin disorders with impaired barrier include psoriasis [124], eczema, dermatitis, infections, ichthyoses and tumours [10, 125-127].

4.4.4 Conditions of application

The most determinant application conditions for the percutaneous permeation of drugs are: the application method, dose level, exposure time, area of application and method for removing the dosage form when necessary [12, 14, 102].

There are two main application methods: the infinite and the finite dose technique [12, 128]. The infinite dose technique consists in the application of an amount of permeant high enough so that the variations in the donor concentration during the time of the experiment can be considered negligible [12, 14]. The infinite dose technique enables the determination of the steady-state flux according to Fick's first law of diffusion.
The finite dose technique consists in the application of a small dose in order to mimic the in-use conditions. There is a marked depletion of the dose during the time of the experiment that is reflected in a permeation profile with a characteristic plateau [12, 14].

5. Skin penetration enhancement

The equation of Fick's first law of diffusion can also be written as follows, in order to describe the flux (*J*) of a molecule through the SC [129]:

$$J = \frac{Cv}{Cs,v} \times \frac{D \times Cs,m}{L} \quad (\mathbf{1.2})$$

where C_v is the drug concentration dissolved in the vehicle, $C_{s,v}$ and $C_{s,m}$ are the drug solubility in the vehicle and in the membrane, respectively, $C_v / C_{s,v}$ corresponds to the degree of saturation of the drug in the formulation, *D* is the diffusion coefficient of the drug in the SC, and *L* is the drug diffusion pathlength through the membrane.

Most of the times, in order to achieve the required therapeutic level it is necessary to improve the amount and the rate of the transdermal drug delivery. Based on **Equation (1.2)**, three evident enhancement strategies can be used to improve the drug flux through the skin:

- increasing *D;*
- increasing $C_{s,m}$;
- increasing $C_v / C_{s,v}$.

Several penetration enhancing techniques have been developed based on these enhancement strategies and can be divided in passive and active (physical) methods [13]. In **Figure 1.13** there is a schematic diagram of the principal strategies used for the optimisation of the transdermal drug delivery.

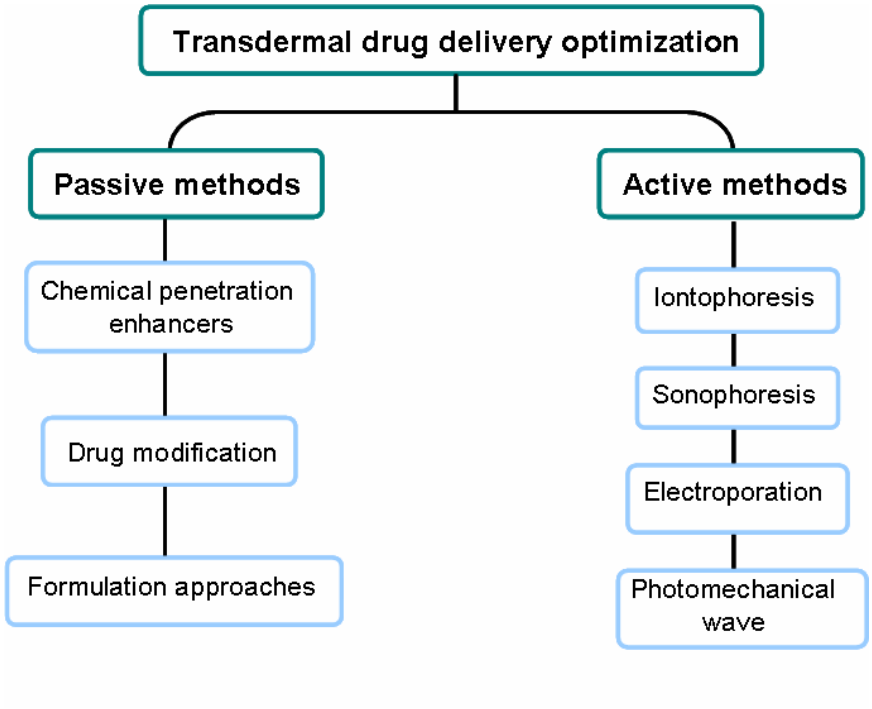

Figure 1.13 Principal strategies for the enhancement of the drug delivery across the skin.

5.1 Passive methods

The passive methods are the most widely used approach to overcome the SC barrier. They include chemical penetration enhancers, drug modification and the manipulation of the formulation (e.g. supersaturated systems, liposomes, microemulsions).

5.1.1 Chemical penetration enhancers

The chemical penetration enhancers are molecules that have the ability to reversibly reduce the barrier function of the SC and in that way improve the penetration of the molecules in the skin and into the bloodstream [14, 81, 97]. They are also known as sorption promoters or accelerants and include an extensive list of diverse classes of

chemicals such as water, sulphoxides, terpenes, pyrrolidones, fatty acids, alcohols, azone, surfactants. The desirable properties for an ideal skin penetration enhancer are shown in **Table 1.1** [4, 14, 130].

Table 1.1 Desirable properties for the chemical penetration enhancers.

Absence of pharmacological action within the body.
Non-toxic, non-irritant and non-allergenic.
Action: rapid onset, predictable, reproducible, reversible and suitable duration according with the drug.
The mechanism of action should allow the penetration of the drugs while preventing the efflux of endogenous substances from the body.
After being removed from the skin the barrier properties of the skin should recover rapidly and entirely.
Chemically and physically compatible with the drug and excipients of the formulation.
Odorless, colorless, inexpensive as well as pharmaceutically and cosmetically acceptable.

There are several potential mechanisms of action of the skin penetration enhancers [3, 6, 12, 97, 130-133]. They can interfere with the normal SC structure by disrupting the intercellular lipid lamellae, through the interaction with the SC proteins inside the corneocytes and/or by the disruption of the cornified envelope. Some penetration enhancers have the ability to promote the partition of the drug to the SC while, in others cases, the enhancing effect is related with modifications in the dosage form such as the increase of the effective concentration of the drug in the vehicle.
Most of the chemical penetration enhancers combine more than one of these mechanisms of action.

The penetration enhancers can interfere with the intercellular lipid domains in several ways as depicted in **Figure 1.14** and, in that way, they are able to increase the drug diffusion coefficient (*D)*.

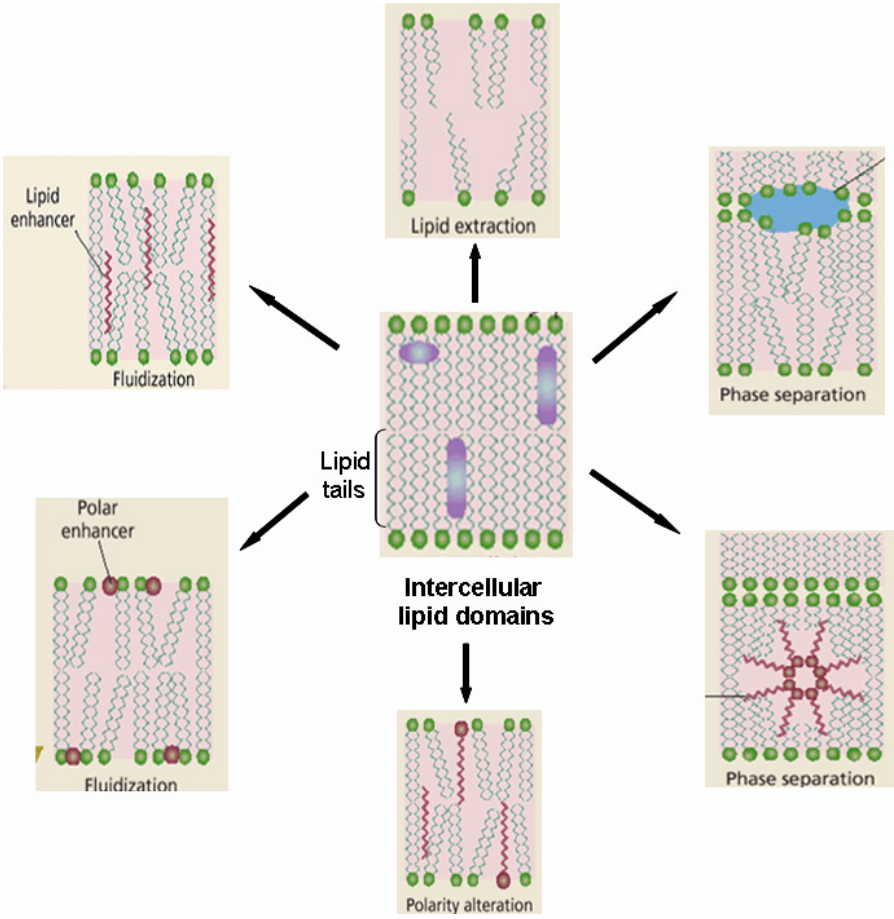

Figure 1.14 Chemical penetration enhancers mechanisms to disrupt the intercellular lipid domains. Modified from [134].

The sorption promoters can induce a fluidizing effect by insertion in two different zones of the intercellular lipid lamellae of the SC, the lipid tail regions (e.g. phospholipids, azone, sefsols) or the polar headgroups region (e. g. polar solvents)

[12, 130, 135]. Other accelerants, rather than being homogeneously distributed in the intercellular lipid lamellae, phase separate in the membrane [12, 130]. This is the case of fatty acids such as oleic acid [136].

In the case of some solvents (e.g. DMSO, alcohols, acetone) they are able to solubilise and extract part of the lipids, inducing a disorganization of the intercellular lipid domains [12, 130, 137].

The last mechanism known to disrupt the intercellular lipid domains of the SC is the formation of water pools in the region of the polar head groups, contributing for the creation of a facilitated polar pathway. That is the case of DMSO [12, 134].

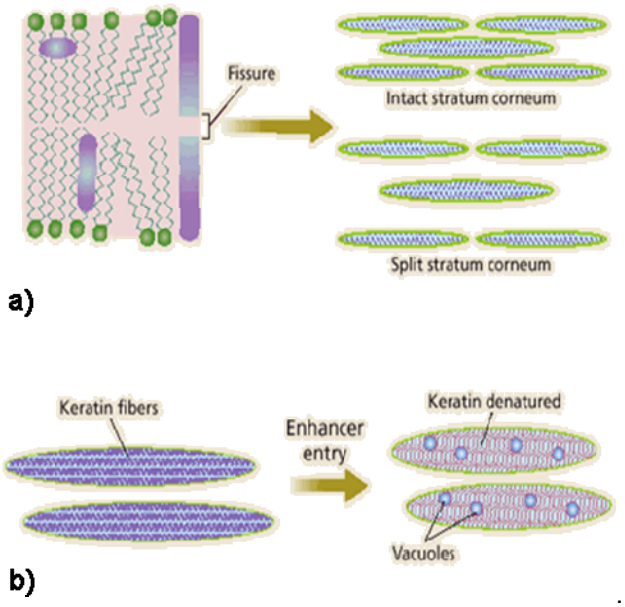

Figure 1.15 Interaction of the chemical penetration enhancers with the SC proteins. (a) Disruption of the corneodesmosomes with the consequent separation of corneocytes into the individual cells. (b) Within the corneocytes, the sorption promoters induce swelling, keratin denaturation and vacuolation. Modified from [134].

In **Figure 1.15** it is shown the mechanisms by which the chemical penetration enhancers interact with the SC proteins. Some molecules such as ionic surfactants or sulphoxides have the ability to interact with the SC intracellular keratin. This interaction produces a decrease of the corneocytes density, which makes them more permeable [3, 12, 131, 134]. On the other hand, caustic solvents, phenols and acids can break the corneodesmosomes, which promotes the separation of the individual corneocytes [12, 134]. These two mechanisms produce an increase of the diffusion coefficient of the drug within the SC and hence the permeability.

The majority of the penetration enhancers that are able to increase both the drug partitioning between the vehicle and the SC [K in **Equation** (**1.1**)] and the solubility of the drugs in the SC [$C_{s,m}$ in **Equation** (**1.2**)] are solvents. Some examples of such solvents are ethanol, propyleneglycol, transcutol, N-methyl pyrrolidone [3, 131, 132].

In terms of safety and effectiveness, water is the best penetration enhancer. One of the most common approaches to improve the transdermal drug delivery is by increasing the water content of the SC [130, 138]. The normal water content is ca. 20% (of the dry weight of the skin) but this value can be increased by soaking the skin with water, in high relative humidity or by occlusion [3, 6, 130, 138].
Occlusion with plastic films, paraffins, oils, ointments or others can increase the SC water content up to 400% of its dry weight [130, 138]. It prevents the normal TEWL and can cause a 10-100 fold increase in drug percutaneous permeation [4]. The main disadvantage is the possibility to cause local skin irritation [4, 111, 112, 139].
An increase in the SC hydration results in a higher elasticity and permeability of the SC for hydrophilic as well as for some lipophilic molecules [3, 6, 112, 130, 140-142]. The water produces the swelling of the compact structure of the SC and the texture becomes softer [3, 6, 112, 130, 138, 140, 141].
Despite the extensive number of studies, the exact mechanism by which the water increases the percutaneous permeation of drugs is still unclear. It is also unclear if water has the ability to disrupt the intercellular lipid lamellae [130, 143, 144].

5.1.2 Drug modification

The synthesis of drugs or prodrugs with physicochemical properties more desirable for the transdermal drug delivery is another possible strategy for the skin penetration enhancement [145]. More lipophilic molecules can be obtained by esterification of carboxylic groups or acetylation of amines [3, 97, 146]. When considering the prodrug approach, it should be taken into consideration that the metabolic capacity of the skin is very limited when compared with the liver [146, 147]. This strategy have been well succeeded in drugs such as buprenorphine [148], propranolol [149], 5-aminolevulinic acid [150] or morphine [151].

As discussed in **Section 4.4.2**, ionized drugs have generally a small partition coefficient between the vehicle and the SC [3]. Two different strategies can be used to increase the skin permeation of charged species, the ion-pair approach or the conversion of the drug to its free base [3, 152, 153].
The ion-pair approach consists of the addition of an oppositely charged specie to the ionized drug, forming a neutral ion-pair that has a more favourable *K* for the skin permeation. After passing through the SC, the ion-pair dissociates in the epidermis releasing the ionized drug [3]. An increase in the flux of ca. 7.3 and 11 times has been described for diclofenac and salycilates, respectively, due to the ion-pair formation [154, 155].

Most of the drugs were designed for oral drug delivery and for this reason only the salt forms are commercially available for the majority of the actives. The conversion of the salt form of a drug to the corresponding base (free base form) can render molecules with more desirable properties for the drug delivery across the skin such has higher log P, lower MW and lower MP. The benztropine free base exhibited a 2-60 times higher flux, in comparison with its mesylate salt, when delivered from the neat solvents [152], while the steady-state flux of primaquine free base was 75-230 times higher than the value obtained with the salt form [156].

5.1.3 Formulation approaches

5.1.3.1 Supersaturation

The supersaturation of the drug in the vehicle increases the driving force for the release and penetration of the drug in the skin without alteration of the SC structure [3, 157]. Looking again to **Equation (1.2)**, it is clear that the mechanism of enhancement via drug saturation is due to the increase of the fraction $C_v / C_{s,v}$.

In a saturated solution, the fraction $C_v / C_{s,v}$ (thermodynamic activity or degree of saturation) is equal to unity; thus, in a supersaturated system the degree of saturation is higher than the unity [12, 138]. Several strategies are used to prepare supersaturated systems [12, 138], as discriminated below.

Alteration of the vehicle composition

A widely used technique is to dissolve the drug in a solvent system composed by one volatile solvent combined with less volatile or non-volatile solvents. When the formulation is applied on the skin, the volatile solvent evaporates leading to the supersaturation of the drug in the skin surface.

Preparation of supersaturated systems of amorphous forms of the drug

Amorphous states of the drugs can be prepared by grinding with carrier or deposition on carrier. Skin permeation is higher from the amorphous states than from the crystalline forms.

Use of a binary cosolvent system

In these formulations the drug is dissolved in two solvents. Immediately before the administration, one of the solvents is added to the formulation in order to decrease the drug solubility in the vehicle and produce a supersaturated system.

The major problem of the supersaturated formulations is that they are thermodynamically unstable and recrystallization tends to occur over time [12, 138]. Supersaturated systems can be stabilized by the addition of antinucleant polymers (e. g. PVP, HPMC, CMC) that have the ability to delay recrystallization [158-160].

5.1.3.2 Eutectic Systems

An eutectic system consists in a mixture of two components that do not react to form a new molecular entity but, at certain ratios, inhibit the crystalization of each other. The eutectic system has a single melting point that is lower than the melting point of each component isolated [3, 161].

As previously described in **Section 4.4.2**, the lower the melting point of the drug, the greater is the solubility of that molecule in the solvents, including the SC lipids [3].

Most of the eutectic systems prepared for the skin permeation enhancement are formed by a drug and a known penetration enhancer (e.g. menthol, fatty acids, thymol) as the second component [161-163]. In these cases not only the melting point depression is contributing for the increase in skin permeation but is also likely that the interaction between the sorption promoter and the SC lipids accounts for the improvement of the drug flux.

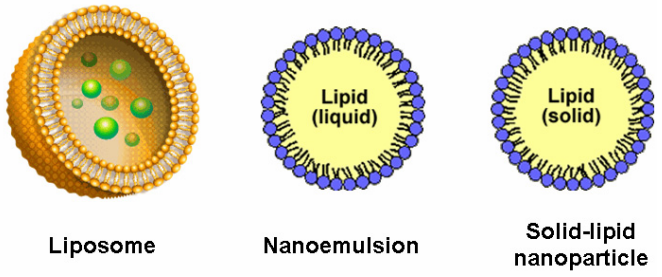

Figure 1.16 Structure of some colloidal carriers used as vehicles for skin penetration enhancement.

5.1.3.3 Colloidal carriers

Liposomes [89, 164, 165], niosomes [165, 166], transfersomes [165], ethosomes [167, 168], proniosomes [169, 170], nanoemulsions [171-173], solid-lipid nanoparticles [171, 174] are some examples of colloidal carriers with entrapped

active pharmaceutical ingredients used with the aim of increasing the actives percutaneous permeation (**Figure 1.16**) [3, 6, 131].

These carriers accumulate in the SC, without penetrating further into the viable epidermis, where they seem to interact with the SC lipids and release the encapsulated drugs [3, 6, 131]. The effectiveness of these carriers is debatable and further research is needed.

5.2 Active methods

In the active methods, an input of external energy is necessary as driving force for improving the drug permeation or to reduce the barrier properties of the skin [4]. These type of methods are generally employed in large (> 500 daltons), hydrophilic and polar molecules, with low potency, such as proteins [4, 13].
A variety of active methods have been evaluated, including those discriminated below.

Iontophoresis

In the iontophoresis technique, a small electric current is applied on the skin and works as the driving force to increase the delivery of charged drugs through the skin [6, 138, 175]. The charged molecules are forced to enter the skin by electrical repulsion although other mechanisms also contribute to the drug penetration enhancement, such as the flow of electric current that may increase the skin permeability and the electroosmosis which induces a solvent flow across the membrane [6, 138, 176, 177].

Phonophoresis or sonophoresis

An ultrasonic energy of low frequency is applied over the skin where the drugs are going to be delivered. The energy induces a perturbation in the SC due to cavitation, heating, radiation pressure and acoustic microstreaming effects which produce the increase of the drug percutaneous permeation [6, 138, 178-180].

Electroporation

The electroporation acts by the application of short pulses of high voltage current on the skin that transiently opens hydrophilic pores in the SC intercellular lipid lamellae [3, 6, 181, 182]. These hydrophilic pores constitute new pathways for drug permeation.

Photomechanical wave

A drug formulation applied on the skin is irradiated with a laser pulse that generates photomechanical waves. This technique produces alterations on the SC that increase the percutaneous permeation of drugs [6, 183].

6. *In vitro* permeation experiments

The *in vitro* permeation studies using diffusion cells are routinely conducted in order to evaluate the percutaneous permeation of drugs [184]. The data obtained from these experiments are predictive of the *in vivo* percutaneous absorption, since the barrier properties of the SC are essentially maintained in excised skin [184].

Franz diffusion cells are one of the most widely used diffusion cells and consist of a donor and a receptor compartment (**Figure 1.17**) [185, 186]. The excised skin is placed between the two compartments and the system is closed with a clamp. The formulation is applied in the donor chamber, and the drug permeation rate through the skin is determined by measuring the amount of drug in the receptor compartment over time with an appropriate analytical method (e.g. HPLC, spectropothometric detection, scintillation).
The design of the diffusion cells should ensure a good seal around the skin membrane, an easy sampling technique, a proper mixing of the receptor solution and a rigorous temperature control of the system [184, 187, 188].

I*n vitro* methods offer several advantages over the *in vivo* methods. In the former, the experimental conditions are controlled with precision in order to closely mimic the normal *in vivo* exposure, and the only variables are the skin membrane and the

formulation under study [14]. The permeation of the compound is directly evaluated by collecting the samples immediately beneath the skin, instead of quantifying the amount of drug in the systemic circulation or urine [12]. These methods also avoid the expensive and time consuming *in vivo* experiments with animals or humans.

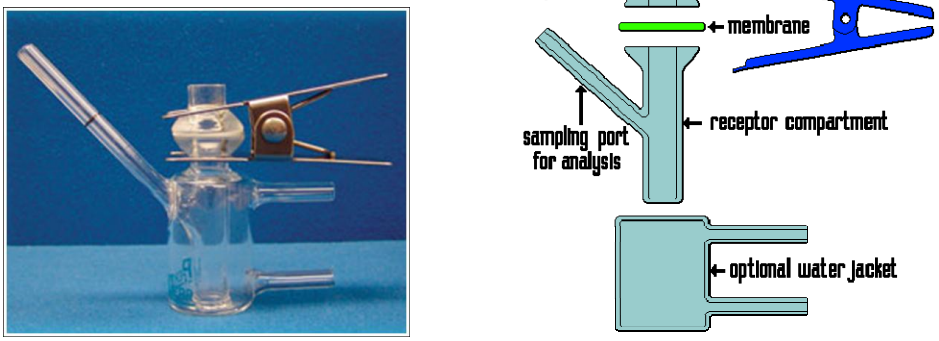

Figure 1.17 Franz diffusion cells.

6.1 Excised skin

Several studies have examined the differences in the percutaneous absorption of chemicals between different animal species and human skin, mainly due to the difficulties in obtaining human skin [189-193]. Animal skin is easier to obtain and is more uniform [12, 80]. The major differences between animal and human skin are the number of hair follicles, sebum and SC thickness [12, 80].

From all the species evaluated (e.g. pig, mouse, rat, guinea pig, rabbit, dog, monkey), the pig ear skin seems to have the closest resemblance to human skin in terms of permeability characteristics [12, 189, 191, 194], SC thickness, lipid composition, biochemical properties and histological appearance [12, 192-194]. Rat, mouse, rabbit and guinea skin are not predictive of the drug permeation through

human skin [12, 191, 194]. Pig skin is also the recommended *in vitro* model for human skin according to the reference guidelines [187, 188, 195, 196].

The number of skin layers used can also significantly affect the results of the permeation experiments. Different methods can be used to prepare the skin membranes. The full-thickness skin is composed by the epidermis and dermis while the dermatomed skin consists in a slice of skin cut with a dermatome in order to remove the lower dermis. The epidermal membranes are composed by the viable epidermis and a membrane composed exclusively by the SC can also be used in *in vitro* permeation experiments [12, 187, 188].
Dermatomed skin and epidermal membranes are the most widely used and the more appropriate. Full-thickness skin is not indicated in lipophilic drugs because the drug permeation is artificially prevented, *in vitro,* by the dermis [12, 187, 188].

It is recommended to check the integrity of all skin samples used in the permeation studies in order to avoid abnormally high values of permeability. Skin integrity may be qualitatively assessed by visual inspection or through quantification of the TEWL, the flux of low MW markers or by measuring the electrical conductivity [12, 184, 187, 188].

6.2 Receptor solution

The receptor solution must provide the sink conditions for the test chemical during the entire time of the experiment so that it does not act as a barrier to absorption. Furthermore, it must not damage the skin membrane, alter the physicochemical properties of the drug to be tested or interfere with the analytical method [184, 188, 194].
The receptor fluid must be maintained at a constant temperature because variations in the temperature may affect the drug absorption process. When the receptor solution is kept at 37ºC the temperature at the skin surface is approximately 32ºC which is considered to be the normal temperature of human skin [12, 184, 188, 194].

Generally, a buffer solution such as phosphate buffered saline (PBS) or a similar physiological buffer (pH 7.4) is suitable for conducting the *in vitro* permeation studies [14, 194].

7. Hydrogels

Hydrogels are three dimensional networks of linear hydrophilic polymers that absorb large amounts of water or biological fluids, while remaining insoluble and maintaining their 3D structure [197-200]. The network insolubility is due to the presence of chemical or physical crosslinks between the polymer chains. Due to their high water content, the soft consistency and resemblance with natural living tissues, hydrogels possess excellent biocompatibility [199]. The main advantage of hydrogels in the controlled drug delivery lies in the near constant release rates obtained [200].

Hydrogels can be classified in chemical and physical gels based on the crosslinking nature.
Chemical hydrogels are obtained by radical polymerization in the presence of crosslinking agents which results in the formation of irreversible covalent crosslinks between the polymeric chains [197, 199, 201, 202]. They are characterized by a permanent network, good mechanical properties and are very resistant to dissolution even in extreme conditions [202]. However, the use of crosslinking agents originates several disadvantages. Most of them are toxic compounds that must be removed from the hydrogels by an additional purification step before they can be safely administered [203]. In fact, there is a small amount of data concerning their biocompatibility and their fate in the human body. Moreover, free unreacted crosslinkers can affect the integrity of the drugs to be incorporated in these hydrogels [197, 202, 204].

On the contrary, physical hydrogels have reversible crosslinks between the polymeric chains. Physically crosslinked hydrogels can be formed by ionic

interactions, secondary interactions or be grafted or entangled hydrogels [197, 199, 201, 202].

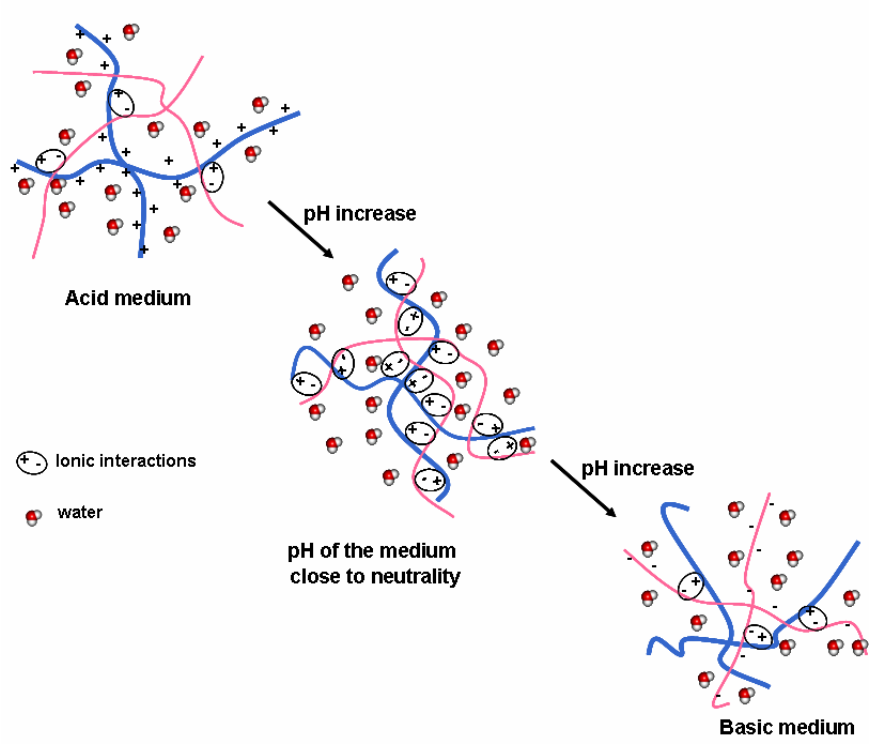

Figure 1.18 Schematic representation of a polyelectrolyte complex interaction between two oppositely charged polymers, according to the pH of the medium.

Polyelectrolyte complexes (PEC) are physical hydrogels in which ionic interactions are established between two polymers with opposite charges and a broad MW distribution (**Figure 1.18**) [197, 199, 201, 202]. These type of hydrogels offer several advantages over the chemically crosslinked ones. The reaction occurs in aqueous solution and mild conditions [201] which enables the direct incorporation of the drug in the formulation during the preparation of the PEC. The electrostatic interactions are strong enough to prevent dissolution in water, and PEC films are capable of

maintaining their mechanical strength [201, 202]. They are biocompatible, offering a wider range of potential medical and pharmaceutical application than covalently linked hydrogels [202]. The swelling of PEC hydrogels is sensitive to both pH and, in minor extent, to ionic strength; therefore they are very versatile drug delivery systems that can be used in pH controlled drug delivery [201].

The properties that were discussed justify the increased interest in the development and optimization of physical hydrogels. The main limitations are the moderate mechanical stability, the risk of dissolution in extreme pH conditions and their complex preparation method [201, 202].

The high water content of hydrogels is important in the skin moisturization and elasticity providing a better feeling when applied on the skin. For these reasons, hydrogels are a good alternative to more conventional dosage forms used in the transdermal delivery of drugs such as creams, ointments and patches [199].

II

Thermal behavior of human *stratum corneum*

1. Introduction

The characterization of the thermal behavior of the SC and SC lipids has been done over the past 3 decades [64, 116, 205-211]. It still constitutes a field of intensive research due to the development of more sensitive and precise instrumentation.

The information obtained from thermal analysis is crucial for understanding the SC and SC lipids molecular structure and their role in the selective permeability of the skin, which is still a matter of large debate [28, 70, 212, 213]. The structural arrangement of SC lipids at different temperatures can be directly correlated to water permeability [35] and, in a more practical sense, thermal analysis allows to assess the enhancing or retarding effect of specific molecules [214-221], that are used to reversibly alter the barrier properties of the skin. The presence of these molecules affects the temperatures at which phase transitions occur, and the temperature shift may be easily correlated to the effect upon the skin barrier, e.g. the lipids degree of fluidization. This gives the possibility of optimizing transdermal drug

delivery.

These studies have resorted to several techniques, such as differential scanning calorimetry (DSC) [205, 216, 217, 221-223] and differential thermal analysis (DTA) [214, 224, 225]. The information obtained concerns the thermal alterations in the SC that may be correlated with phase-transitions in the lipid lamellar-structures and also to modifications in other skin components, such as proteins or the interaction between lipids and these components.

Four endothermic transitions between 40 ºC and 115 ºC have been identified in a significant number of previous studies on the SC matrix and have been assigned essentially to lipid, lipid-protein and protein alterations [225]. Most results from other authors reflect this trend. The thermal transition at approx. 40°C has been ascribed to a change in the lateral lipid packing of the intercellular SC lipids from orthorhombic to hexagonal [121]. Between 65 and 75ºC the SC intercellular lipid structure evolves from lamellar to disordered and the lateral packing from hexagonal to liquid [55, 225, 226]. When the temperature is further increased until approx. 80°C, the lipids associated to proteins evolve from gel to liquid, and at temperatures above 90°C the skin upper layers suffer irreversible protein denaturation [206, 207, 225, 227]. More recently, a new transition has been detected in the SC thermogram at about 55ºC and is probably related with the covalently bound lipids of the corneocyte envelope [64, 216]. At the same time, it has been shown that proteins do not play a major role in the SC lipid phase behavior. This behavior is, to a large extent, observed in extracted lipids [71].

Other techniques, usually based in spectroscopy, may also be used in conjunction with temperature variations. A correlation between structural or conformational changes and temperature could, in principle, be readily obtained, but it is difficult to establish an uncontroversial interpretation of the data. This interpretation is usually made from indicators (such as specific vibrational frequencies) of transitions that result from alterations in some degrees of freedom of the constituting molecules. Different techniques originate complementary information. Examples are Fourier transform infrared spectroscopy (FTIR) [221, 228] and Fourier transform Raman spectroscopy (FT-Raman) [222, 223, 229], where effects of fluidization are assessed through shifts in the frequencies of certain vibrational modes. Similarly, electron paramagnetic resonance (EPR) [210, 230] inspects rotational degrees of freedom,

while electron diffraction (ED) [211] or wide-angle X-ray diffraction (WAXD) [121] techniques look more directly into structural aspects.

A variety of techniques has also been employed in selected lipid components of SC and simplified models for SC lipids. These include atomic force microscopy (AFM) [231, 232], small angle X-ray diffraction (SAXD) [59], transmission electron microscopy (TEM) [233], electron spin resonance (ESR) [127] and many others. These studies intend to mimic the behavior observed on the skin in order to give valuable information related to SC structural organization [59, 233-235] and the role of specific molecules in the barrier function [60, 61, 236, 237].

In spite of the above mentioned studies and many others, the SC system and the respective structure and behavior are still controversial. This can be seen from the number of different models suggested for the SC organization and discussed in more detail in the general introduction of this thesis [68, 70, 212]. Recent work have shed light directly on the organization of the repeat units in the intercellular lamellar structure [237], without detailing the thermotropic phase behavior. It is therefore extremely important to carry out new studies to obtain additional information.

The existence of a significant amount of irrelevant amorphous material in SC makes most transitions almost negligible from the energetic standpoint. The lipids are only a part of the whole matrix and large quantities of the SC layer are necessary to obtain quantitatively significant results. Even the identification of actual transitions is sometimes difficult both due to peak overlap and to less well-defined transitions. When resorting to human skin, obtaining large samples is not an easy task, and it is thus extremely important to employ less material-consuming techniques.

High-speed differential scanning calorimetry (Hyper-DSC^{TM}) has been reported to have high sensitivity when operation takes place at very high scanning rates, clearly above 100 °C/min [238]. Using high scanning rates significantly increases sensitivity and resolution because it leads to a higher heat-flow and also facilitates throughput. Transitions that are difficult to discern using conventional DSC can be more easily identified [239]. It is also to be stressed that these higher rates provide a better picture of the original sample as reorganization during the heating process is greatly reduced. It allows not only the detection of very weak transitions, but may

additionally avoid changes often induced by classical heating rates, such as recrystallization and decomposition [238]. This technique is used with sample masses well below those of conventional DSC, emphasizing the heterogeneity in the analysed material.

Although DSC is a technique widely used in studies of the skin, the coupling with polarized light thermal microscopy (PLTM) is not yet properly explored in this area. DSC is a method that allows the detection of the sign, temperature, rate of change and magnitude of phase transitions. However, in the study of multiphase systems we can often obtain very complex DSC curves with different superimposed signals that have a very difficult interpretation. The association with optical methods such as PLTM enables the observation of texture [240], partial melting, segregation, eutectic formation, decomposition [241], the distinction between solid-solid, solid-liquid or liquid-liquid transitions. In conclusion, the association of these two methods facilitates the elucidation of the type of transition in very complex systems such as those under study [242-244].

In what follows, we present results concerning phase transitions starting at room temperature, and including physiological and higher temperatures. The latter provide information on the organization of lipids and other components that may indirectly be associated to the behavior of the skin barrier at physiological temperatures.

2. Materials and Methods

2.1 Isolation of the *stratum corneum*

Human skin from the thigh was obtained after reconstructive surgery, and from post-mortem collection. The dermatomed skin is placed dermal side down on filter paper soaked with a 0.1% trypsin (type IX-S, Sigma Chemical Company, St. Louis, MO), in phosphate buffer saline (PBS) solution, pH 7.4. Digestion occurs during the night at 37ºC [214], see **Figure 2.1**. The SC is separated from the underlying tissue and

rinsed with ultrapure water, dried and stored in a desiccator with P_2O_5 for 24 hours. It is then hydrated in the presence of a 27% NaBr solution for a period of 2 days, before analysis [225].

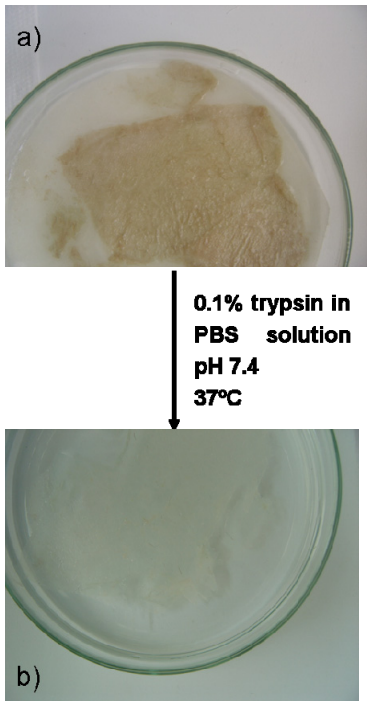

Figure 2.1 Schematic representation of the *stratum corneum* isolation. It can be seen the (a) dermatomed skin and the (b) *stratum corneum*.

2.2 Extraction and preparation of SC lipids

The SC is briefly rinsed with hexane to remove contaminating substances [206]. For the actual extraction we have followed the procedure described in [43]. The samples are sequentially immersed for 2h in three different HPLC-grade chloroform/methanol mixtures (2:1, 1:1, 1:2) each at room temperature. The extractions are then repeated for 1h each, and the sample is extracted overnight with methanol. All the extracts

are combined and re-covered by filtration through a Whatman grade 44 fillter. The final extract is dried under vacuum in a rotary evaporator.

Samples were prepared with two degrees of hydration. For obtaining the dehydrated lipids they are kept in a desiccator in the presence of P_2O_5. The more hydrated lipids are, in turn, stored in the presence of a NaBr solution (27g /100 ml) solution; it should be noted that the latter procedure is considered appropriate for obtaining the water content in the SC that is found in normal healthy skin [225]. The minimum residence time in the desiccator is 48h in both cases.

2.3 DSC measurements

A DSC Pyris 1 calorimeter from Perkin-Elmer, equipped with a Cryofill cooling system, was used. Samples of SC weighing 2-9 mg and samples of extracted lipids weighing 1-4mg were encapsulated in 10L aluminium pans adequate for volatile samples. The calorimeter was calibrated for temperature [245] with 99.9% pure cyclohexane, T_{fus}=6.66±0.04ºC, 99.9% naphtalene, T_{fus}=80.20±0.05ºC, and 99.99% indium, T_{fus}=156.60ºC. A 20 ml/min helium purging flow was used. Typically, samples initially cooled to -170ºC, are subjected to heating and cooling cycles between -170ºC and 160ºC at 400, 200 and 100ºC/min (heating) and 50ºC/min (cooling) rates.

Results for no less than three replicates were obtained from each sample.

2.4 Polarized light thermal microscopy

A slightly modified version of the original skin surface biopsy (SSB) technique [246] was employed for obtaining thin layers of the SC, approximately two to three cells thick, so as to be used in PLTM observations. A layer of cyanoacrylate is placed directly on the skin. After drying, the slide is rolled off the skin removing the SC layer. The technique is used in skin obtained from living donors, which has not

suffered any treatment or even washing in the previous 2h. The SC structure is maintained and the collected sample is immediately subjected to observation.

The hot stage/DSC video microscopy analysis was performed using a Linkam system DSC600. The optical observations were conducted resorting to a Leica DMRB microscope and registered using a Sony CCD-IRIS/RGB video camera. The image analysis used a Linkam system software with the Real Time Video Measurement System (**Figure 2.2**). The images were obtained combining the use of polarized light with wave compensators, at a 200x magnification.

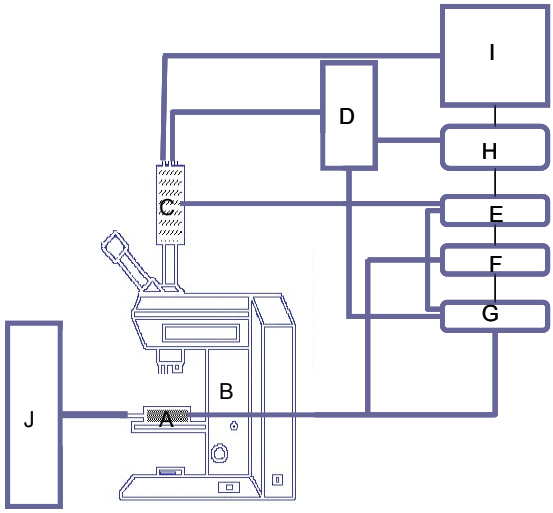

Figure 2.2 Schematic representation of the Linkam system DSC600. **A**: DTA cell, **B**: microscope, **C**: video camera, **D**: PC, **E,F,G**: central unit, **H**: video recorder, **I**: monitor and **J**: liquid nitrogen.

Samples consisted of SC layers, placed face down, and SC extracted lipids. The latter were prepared by dispersing a small amount of the material at the bottom of a covered 7 mm quartz crucible. In some experiments, the cover is placed directly over the sample in a thin flat preparation.

The behavior of the lipids was studied in heating/cooling cycles between 20 ºC and 120 ºC, at scanning rates of 10 ºC/min. The scans were made under a nitrogen atmosphere through the use of nitrogen flow.

3. Results

In this section we present the results obtained from thermoanalytical measurements using DSC, and observations from thermomicroscopy under polarized light.

3.1 High scanning rate DSC

The thermal transitions that are difficult to discern using conventional DSC are more easily identified using high scanning rate DSC or Hyper-DSC™. The higher rates provide also a better picture of the original sample, once reorganization during the heating process is greatly reduced. Hyper-DSC™ is used with sample masses well below those of conventional DSC, emphasizing the sample heterogeneity in the analyzed material.

3.1.1 *Stratum corneum*

Thermograms for hydrated SC were obtained at three scanning rates, i.e. 400, 200 and 100°C/min. For the higher, intermediate and lower rates, 18, 16 and 6 traces were registered, respectively. Samples were obtained from 6 donors, as seen in **Table 2.1**. The **Figure 2.3** exhibits the results obtained in the samples at these three heating rates. These particular thermograms were selected on the basis that they display a significant number of concomitant transitions.

Table 2.1 Characterization of the donors and number of determinations, for each scanning rate. Samples from donors 1-6 were hydrated, while those from donors 7 and 8 correspond to the dehydrated SC and delipidized matrix determinations, respectively.

		number of determinations per scanning rate (ºC/min)		
Donor	**gender, age**	**100**	**200**	**400**
1	female, 42			4
2	female, 65		9	7
3	female, 19		2	2
4	male, 20		2	1
5	male, 47	3	1	1
6	male, 51	3	2	3
7	male, 45		4	
8	male, 50		5	

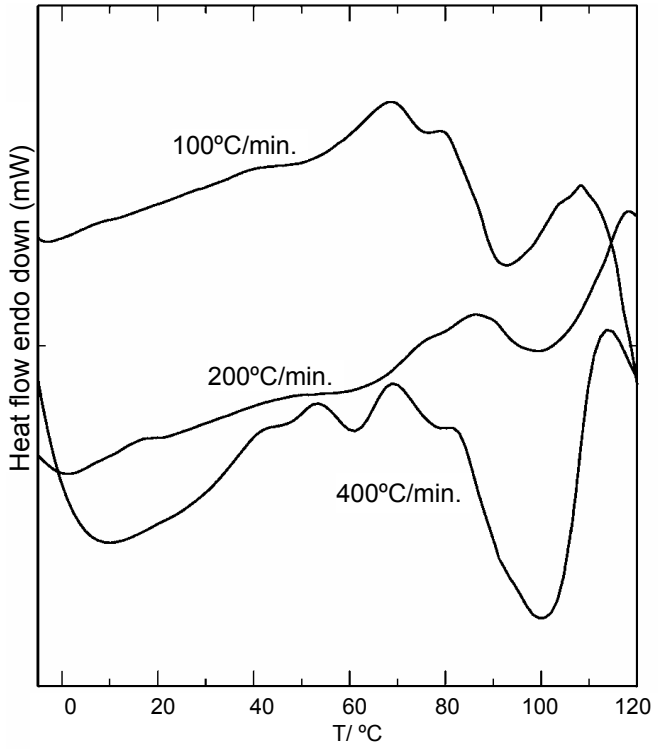

Figure 2.3 Examples of DSC traces, for the first heating run, obtained for hydrated human SC at different scanning rates (400, 200 and 100° C/min).

At least eight transitions were found in the 20-120ºC range, instead of the usual four. **Table 2.2** summarizes the transition temperatures detected in the present work, labelled from A to H and taken as the peaks maxima in the curves. It also includes a number of those found in previous studies by other authors and the literature data are organized in columns according to the similitude to processes identified in this work. Relevant sample and operational conditions are indicated in the order: scanning rate, temperature range, mass (or area) of SC, pre-treatment. All data were obtained from DSC, except where indicated. The temperature ranges correspond to the spread in peaks maxima (T_m).

The observation of the thermograms indicates, as usual, a broad endothermic peak starting slightly above 0°C, with the internal structure corresponding to transitions A-F, reaching its maximum near transitions E and F, then decreasing and raising again near H. The initial four peaks are placed in the ascending part of the overall peak and are thus clearly less visible. The first and second derivatives of the original traces (**Figure 2.4**) facilitate the location of less marked features. Zeros in the first derivative, from positive values, were assigned to definite T_m. In the cases where peak overlap is significant the zeros of the first derivative were used to identify the temperature in the T_m of the thermal transitions. Inflection points and inverted peaks given by the second derivative were used for confirmation.

The labelling of transitions was based on the fact that all these transitions were individually detected, i.e., they were present in some thermograms in conjunction with contiguous ones. They were also frequently detected, as shown in **Table 2.3**. The labels were based on an elementary cluster analysis that grouped values of peaks maxima obtained in different determinations. These groups are shown as a temperature range in **Table 2.2**, limited by the extreme values for each group. To avoid further subdivision, low temperature peaks were grouped under A, but correspond to a set of different transitions as clearly seen in some thermograms. Structure corresponding to higher temperature processes (temperature >120°C) can also be discerned.

Table 2.2 Transitions found in hydrated human SC, in ºC. Literature data are organized in columns according to the similarity to processes identified in this work.

A	B	C	D	E	F	G	H	Reference	Conditions
9, 21-24	30-35	43-49	50-58	68-79	81-89	91-103	108-115	This work	400ºC/min;-170ºC to 160ºC; 2.4 to 6.7 mg
6, 15-19, 24	30-37	40-49	50-60	68-79	81-88	91-108	111-118	This work	200ºC/min; -170ºC to 160ºC; 2.3 to 9.2 mg
8-9,13-19		40-43	51-57	68-74	79-87	92-109	111-116	This work	100ºC/min; -170ºC to 160ºC; 6.5 to 10.2 mg
10-23	28		51-60	75				[127]	0.25ºC/min; 0ºC to100ºC; normal human scales
	35			65	80	95		[207]	0.5 to 0.75ºC/min; 25 to 105ºC; 30 mg; washed w/ hexane
	35.9		55	70				[64]	0.6ºC/min; 10 to 110ºC; 15 to 25 mg; washed w/ hexane
		40		70	85	100		[224, 225]	2ºC/min; -130 to 120ºC; 10 to 30 mg; DTA
		40		65-75	85		115	[228]	2ºC/min; 25 to 145ºC; 20 to 30 mg; 60ºC [(a)]
				65	78	97		[221]	2ºC/min; 10 to 140ºC; 20 mg; 60ºC[a]
	36		51	72	83	100		[216]	10ºC/min; -10 to 140ºC; 10 mg dry; 60ºC; washed w/ acetone
	35			70	80	90		[217]	10ºC/min; 20 to 100ºC; 2 cm^2 (4 mg dry); 60ºC; washed w/ hexane
	37			72	83	100		[247]	10ºC/min; 10 to 140ºC; 8 to 12 mg; 60ºC; washed w/ acetone
		40		75	85	107		[206]	20ºC/min; -50ºC to 170ºC; 6 cm^2; 60ºC; washed w/ hexane
		42		72	87		112	[214]	2ºC/min; ≈7 to 127ºC; washed with acetone; DTA
		40		70			110	[248]	≤ 20ºC/min; ≈ 30 to 140ºC; blistering, strips of callus; washed with acetone

[(a)] Epidermis separation using immersion in water at 60ºC for approximately 1 minute.

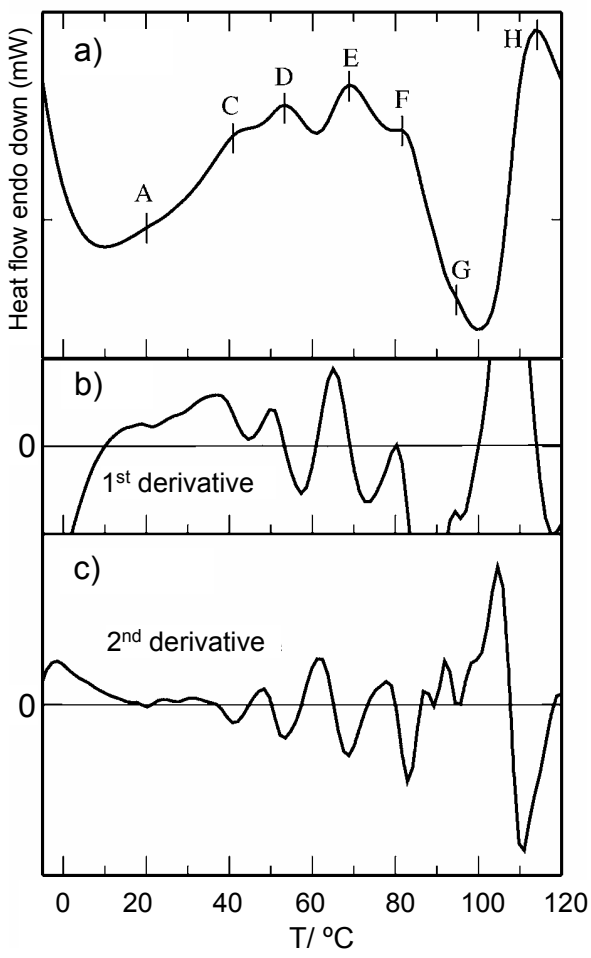

Figure 2.4 DSC trace shown in Figure 2.3 for 400ºC/min (a), and the respective first (b) and second derivatives (c). Approximate peaks maxima are shown in the top panel, for the labelled transitions. See corresponding zeros in the first derivative (b) and inverted peaks (c) for the second derivative used in identification.

The two highest scanning rates have produced similar results for the amounts of sample material employed, with a slightly enhanced resolution for 200° C/min. Effect of mass or donor is not detectable in the experiments. In fact, a variable number of groups (3-6) were organized with samples, each sample defined by a binary variable in which the presence of each of the eight transitions considered is marked with 1

and absence with 0. Using a centroid method [249] and Euclidean distance, it could be seen that each group of most similar samples had a tendency to include different scanning rates, masses and donors. This result was obtained irrespective of the number of groups tested.

Table 2.3 Data for hydrated SC concerning reproducibility for each transition temperature identified in this work. All three scanning rates tested are considered.

Transition	Frequency	
	Thermograms	Different donors
A	16	5
B	11	6
C	20	5
D	22	6
E	37	6
F	36	6
G	28	6
H	30	6

In the lowest scanning rate, transition B has not been detected, and a significant subdivision in transitions for temperatures higher than 100°C was observed, with sharp peaks that apparently result from the deconvolution of broader ones.

Reheating the samples (**Figure 2.5**), after cooling at a rate of 50°C/min, produces results that complement previous work from other authors such as Duzee [206] and Cornwell et al. [216]. The lowest transition, A, is essentially absent in the 2nd heating run. The transition B cannot be found in most samples either, although in some samples there are still signs of its presence. For higher temperatures, transitions C and D are scarce and transitions E-G, although not as well-defined or frequent, are still detectable in a significant number of samples. In summary, peaks obtained upon reheating are broader, transitions are less frequent, but partial reversibility may be associated to most transitions, except for very low temperatures (<30°C).

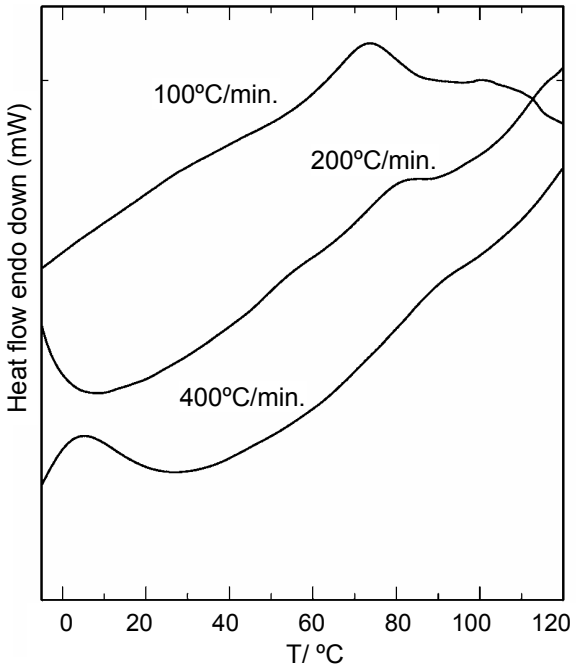

Figure 2.5 Thermograms of the 2nd heating run, corresponding to those samples previously depicted in Figure 2.4. The corresponding heating rates are indicated in the figure.

Additional tests were conducted in dehydrated and delipidized SC of two donors, at the heating rate that gave the best results (200°C/min)and the results are presented in the last entries of **Table 2.1**. Values for transition temperatures found in these samples are gathered in **Table 2.4**, with other values obtained from the literature. The dehydrated SC presents peaks slightly more defined than the hydrated counterpart. Transitions A-H are all detected; transition D was found in all samples, while transition C was only determined in 1/5 of the samples. For the other cases, the frequency was similar to that corresponding to the hydrated SC.

In the delipidized SC matrix, two major endothermic signals are found, corresponding to transitions D, G and H, close to 55ºC and 100ºC. Traces of transition E were also detected in two of the samples and F in one sample. Transition A was also found in only one of the samples.

Table 2.4 Transitions found in dehydrated human SC and in the respective delipidized matrix, in ºC, for a scanning rate of 200ºC/min. All data are organized according to Table 2.2.

	A	B	C	D	E	F	G	H	Reference
Dehydrated	16, 22	30	49 41	52-60 57	76-78 73	83-89 86	91-102	105-115	This work [205]
Delipidized				52-60			96-99 95 90 100	103-116	This work [207] [206] [216]

3.1.2 Extracted SC lipids

Two sets of lipids, hydrated and dehydrated as described above, have been subjected to the DSC study. Both originated from the same living donor and were extracted from SC that was part of a larger sample.

The DSC heating curves of both sets (see the examples displayed in **Figures 2.6.** and **2.7.**) display as a major feature a pronounced peak with a maximum close to 60ºC, starting at ≈40ºC and extending up to 80ºC.

The degree of hydration does not seem to affect the position of the transitions, but there is a significant alteration in the relative peak heights. For instance, high temperature transitions (T >90ºC) are much more emphasized in the less hydrated lipids. As a consequence, the general appearance of the corresponding thermograms is quite different. However, resorting to the second derivative (see bottom panels in **Figures 2.6** and **2.7**) it is shown that the thermograms display much more similar characteristics than visible at first glance, and confirms that the positioning of peaks maxima (T_m) does not differ significantly at these two hydration levels. However, transitions are broader and slightly less defined in the hydrated lipids.

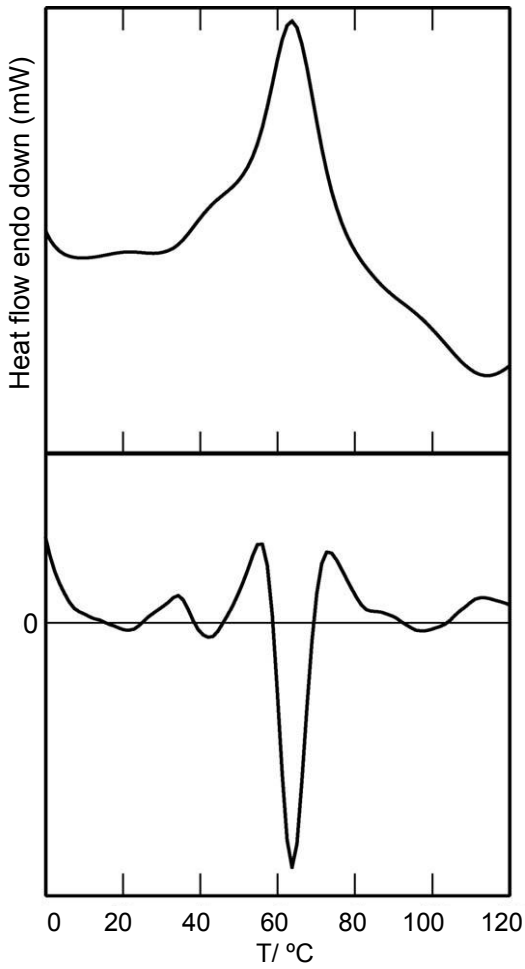

Figure 2.6 Thermogram obtained in one of the hydrated samples of lipids extracted from human SC, top, and respective second derivative, bottom. Both were used for the identification of the position of the T_m.

These results are compiled in **Table 2.5**, that also gathers the results from hydrated human SC described in the previous section for easier comparison. The data indicates that essentially the same transitions are found in hydrated SC and in the extracted lipids, even if the degree of hydration is varied in the latter. Additionally, both sets of lipids lack the transition close to 55 ºC.

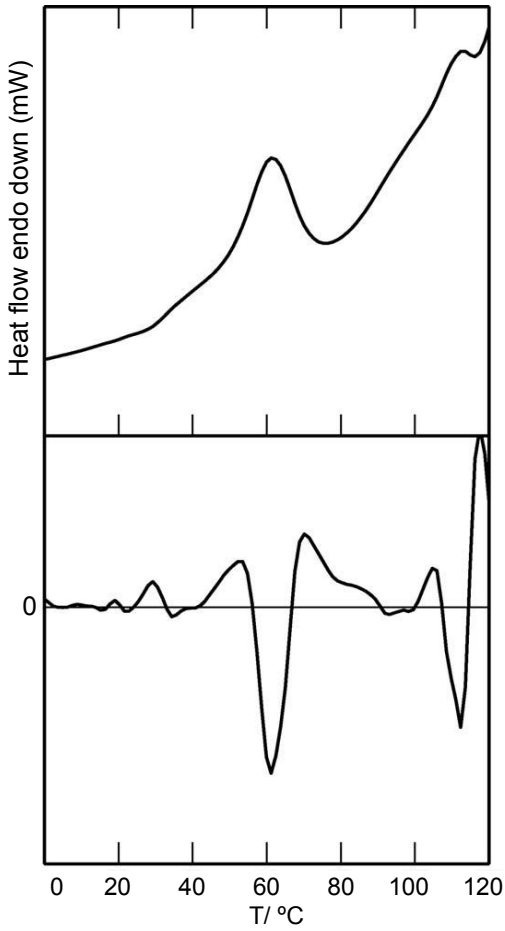

Figure 2.7 Thermogram obtained in one dehydrated sample of lipids extracted from human SC, top, and respective second derivative, bottom. Both were used for the identification of the position of the T_m.

High temperature transitions (T > 90 ºC) are found in these samples consisting of lipids only. Interestingly, and in spite of the presence of broader peaks, the interval corresponding to the various values of T_m, the maximum value in the peak, is narrower in the more hydrated set of lipids. The values found in SC and extracted lipids do not have systematic deviations, except for transition E, that occurs for higher temperatures in the SC matrix.

Table 2.5 Thermal transitions in ºC, for a scanning rate of 200ºC/min, labelled from A to H, detected by DSC in the systems studied. All data are organized according to Table 2.2.

System	A	B	C	D	E	F	G	H
SC (NaBr, 27g/100ml)	19,24	30-37	40-49	50-60	68-79	81-88	91-108	111-118
Extracted lipids (P_2O_5)	20-22	32-34	41-48		61-65	87	93-103	107-117
Extracted lipids (NaBr, 27g/100ml)	21-22	38	41-43		63-64	80-86	96-106	117-120

3.2 Thermomicroscopy

The thermal behavior of SC layers and extracted SC lipids was followed by PLTM. This technique is a valuable tool to study phase transformations since the visual follow-up gives important information to help their understanding. The association of PLTM results with information obtained by DSC allows a deeper insight into the organization of lipids in the SC layer and on the thermal transitions that takes place when the system is subjected to thermal cycles.

3.2.1 *Stratum corneum* layer

The direct observation of the SC layer, previously separated from the dermatomed skin using a trypsin solution, as previously described, allows the visualization of the most relevant structural features. Samples obtained from SSB correspond to layers of 1/5 to 1/4 of the whole SC thickness (**Figure 2.8**). In this Figure, the corneocytes borders are clearly seen, and marked with arrows. This layer displays different regions, also illustrated in **Figure 2.9** for which a higher contrast was imposed. These regions, or domains, result from differential lipid organization, since corneocytes are essentially amorphous. In **Figure 2.9**, the brighter areas correspond to more crystalline structures.

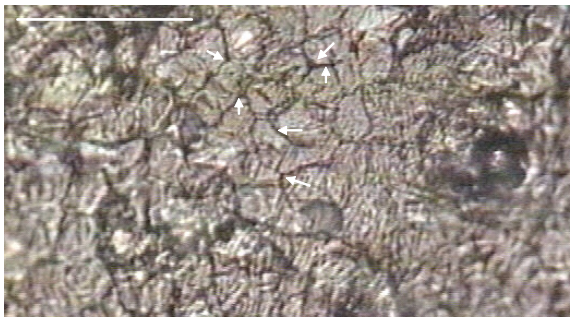

Figure 2.8 Intermediate layers of the SC (two to three cells thick), obtained from surface skin biopsy, observed under PLTM at room temperature. The corneocytes are easily discerned, and some of the respective borders are marked with arrows. The amount of amorphous material prevents the identification of clear domains. Bar= 100 μm.

As the temperature increases, the domains that are visible in the upper panel of **Figure 2.9**, tend to fade. At higher temperatures an almost uniform texture is observed (centre panel), which is compatible with the disruption of the lamellar structure. The sample does not retain the original appearance on lowering the temperature, lower panel, but the contours are similar. The amount of amorphous material in these samples prevents, however, a clear-cut identification of domains existent in the intercellular lipid matrix, and suggests the direct observation of SC lipids alone, especially if phase changes are to be associated to definite ranges of temperature.

3.2.2 Extracted lipids

Samples comprising extracted SC lipids possess at room temperature an overall appearance in which different regions are distinctly present. When heated from 20ºC to 120ºC, a sluggish fusion process of part of the material is the first observed alteration, slightly above 20ºC. This is particularly evident as there is a visible movement of the solid mass in the material that melts. Observations correspond to

the fusion of small subsets of the lipids (note that the lower temperature transition consistently detected by DSC is also slightly above 20ºC).

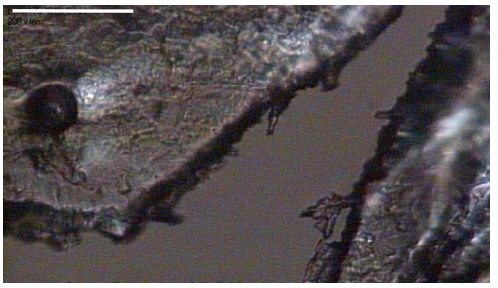

T= 29ºC

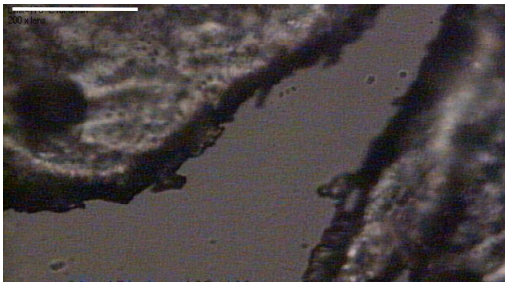

T=125ºC

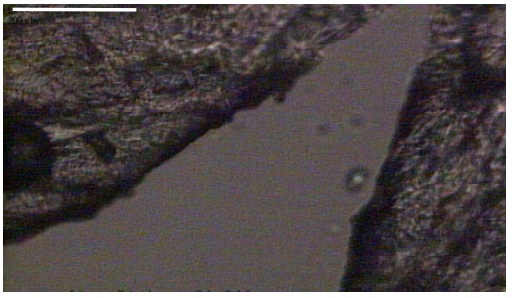

T=27ºC

Figure 2.9 SC obtained from SSB observed under PLTM, with cross polarization at the indicated temperatures. Note the areas of different contrast, more homogeneous at higher temperatures. Brighter areas correspond to more crystalline structures. The appearance upon cooling also differs from that of the original sample. Bar = 100 µm.

The lipid sample suffers no visible alterations up to temperatures close to 35ºC, in which similar changes can be discerned. This low temperature behavior is not clearly illustrated resorting to static pictures, for which they are omitted.

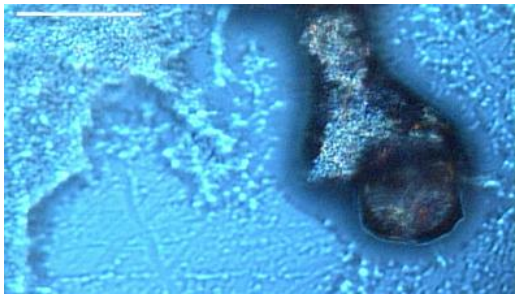

T=43ºC

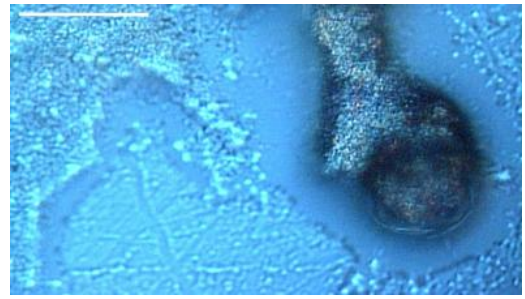

T=56ºC

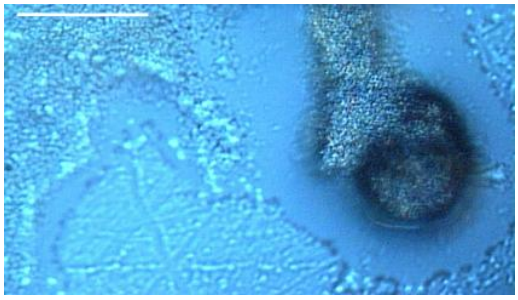

T=60ºC

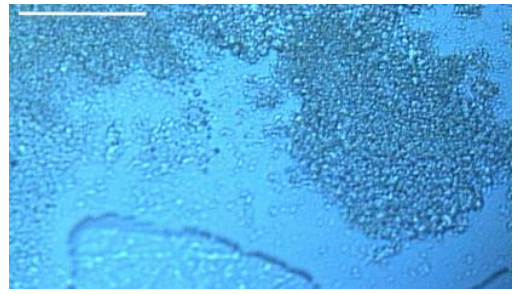

T=70ºC

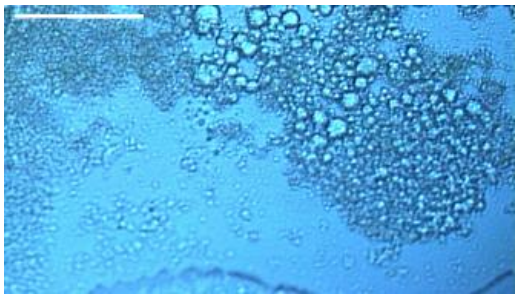

T=73ºC

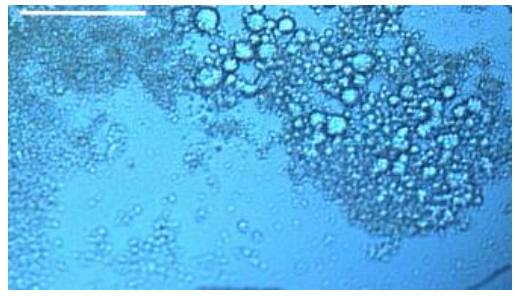

T=77ºC

Figure 2.10 PLTM images for a heating process in extracted lipids, without cover slip. An almost continuous evolution is seen up to ca. 60ºC. At the latter temperature, the system undergoes a process of overall fluidization into an isotropic liquid lipid mixture. Above 70ºC there is a very reduced mobility within the system, and two immiscible liquids are visible. Bar = 100 µm.

From above 40ºC to close to 55ºC a continuous disappearance of portions of lipids contrasting to the background and fluidization of the domain borders is visible, see **Figures 2.10** and **2.11**. **Figure 2.11** also exhibits the initial appearance of a sample.

T=24ºC

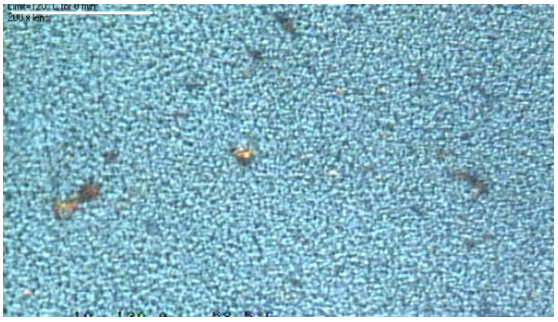

T=58ºC

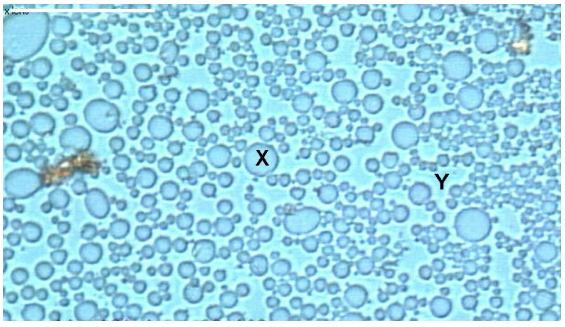

T=100ºC

Figure 2.11 Extracted lipids observed under PLTM at the indicated temperatures, in a heating process. Characteristic phases (X and Y) are marked. Bar = 100 µm.

It should be noted that these pictures correspond to the observation of the sample under polarized light with the combination of whole and quarter-wave compensators. In this way, instead of a dark visual field as it would be the case if using crossed polarizers, the background image is colored. Therefore, the anisotropic region corresponds to the same color as the background, while anisotropy results in several different colors.

At temperatures close to 60ºC almost all the material is involved in a rapid transition to a liquid state, but different isotropic immiscible phases coexist. The fusion process apparently promotes the segregation of different lipid domains but, simultaneously, more similar ones tend to coalesce. This phenomenon is particularly evident as the temperature reaches 75ºC. At this point the floating material aggregates and some isotropic crystals present in the complex mixture become evident. These are preferentially distributed in the phase denoted as X (see **Figure 2.11**, bottom panel).

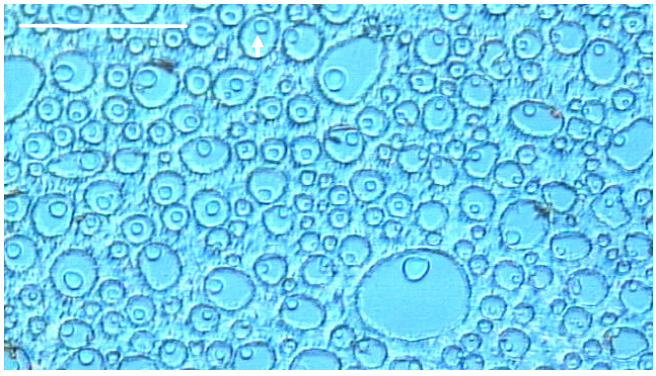

Figure 2.12 Appearance of the hydrated lipids sample of Figure 2.11 after cooling, at room temperature. Bar = 100 µm.

Phase X is viscous, as indicated by the respective contours, in comparison to Y. When the temperatures reaches 90ºC, the immiscibility between these two “liquid phases“ of apparently different viscosity, becomes even more noticeable. In the

cooling process the number of isotropic crystals tends to increase, and the existing ones grow in size. At the temperature of 55ºC a transition from isotropic to anisotropic material is observed in the more fluid regions (phase Y). At the same time, domains X alter to what seems an amorphous solid phase. The crystallization takes place through the slow formation of small crystalline aggregates, giving rise to a heterogeneous globular solid texture. The crystallization determines a striated texture in the frontiers of the floating material (see **Figure 2.12**, obtained immediately after cooling the sample).

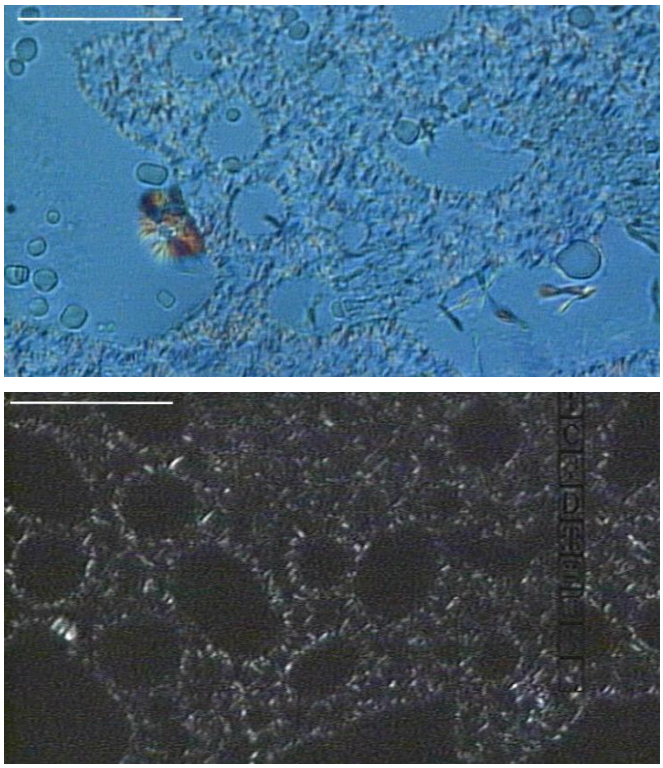

Figure 2.13 Evolution for ca. 1 week of a dehydrated lipids sample, after being subject to heating and cooling cycles. Top and bottom panels correspond to different field views, and are obtained without and with the use of cross polarizers, respectively. Bar = 100 μm.

The cooling process additionally evidences different domains of the SC lipids; a complex mixture of colored crystalline material with a globular texture, at least one isotropic non crystallizable phase X, isotropic crystals, and some amorphous/isotropic material. This appearance is particularly evident after some days, **Figure 2.13**.

The observation of the sample through the use of crossed polarizers gives support to the idea that phase Y is formed by small anisotropic crystals together with some isotropic material. In the second heating run (not shown) phase Y shows some structural transformation, and crystal growth is apparent. As the temperature reaches approximately 60ºC, the small crystalline aggregates tend to melt, but the process is much more subtle than that occurring in the first heating run. At this time the fusion appears almost as a fading of the globular texture. In the remaining phases no transformation could be detected. The heating run was followed up to T=120ºC, and up to that temperature no fusion of the isotropic crystals was observed.

4. Discussion

Most studies consider four main transitions in human SC, above room temperature. This set of four temperatures was first determined almost 30 years ago [206]. That study added an additional transition to those found earlier through differential thermal analysis (DTA) [248], due to the deconvolution of the lower temperature peak. Peaks at 40 and 75°C are seen to be reversible, with a clear decrease in the intensity of the former, but those transitions detected at around 85 and 107°C were not detected upon reheating and were considered irreversible. In contrast, high temperature transitions in dry SC were partly reversible. These results are similar to those found 10 years later [207], which however presented transitions that were lower by 5-12°C. After that, a new transition was presented at 23ºC from results in normal human scale, with no posterior confirmation [127]. Transition D was

determined at least three times [64, 205, 216] and received a new label, T_x, as it was found in conjunction with the usual four.

Considering only four peaks (T_1-T_4) and the data present in **Table 2.2** from other authors, the first one would thus be located in the interval 35-42°C and the 3 others at 65-75, 78-86 and 90-115°C. These are clearly large intervals, almost overlapping in some cases. Assuming 8 transition temperatures labelled from A to G, and making the correspondence to previous assignments, we have A as a new group, B and C as subdivisions of T_1, D as T_x, G and H as subdivisions of T_4. Transition T_1 spans an interval of 7 °C in the literature, which is reduced to 2°C both in B (except for one value [127]) and C. From the data present in the literature (**Table 2.2**), transition T_4 varied 25°C. That span was reduced to 10°C with the new label G (again, except for the value in Duzee [206]) and to 5°C in the transition denoted as H. This reinforces the idea that one is dealing with different transitions, difficult to deconvolve.

The higher number of peaks determined in the present work results essentially from the higher scanning rates; discrepancies may also result from sample treatments and different levels of hydration. In fact, it is very usual to perform a variety of pre-treatments in the skin layer from which the SC is isolated as can be seen in the experimental conditions described on **Table 2.2**. Rinsing with organic solvents, acetone and hexane, and heat separation of dermis and epidermis are the most common. As the presence of sebum has previously been discarded as responsible for inducing additional transitions [64], washing with organic solvents was not deemed necessary. In fact, these solvents have frequently been used in delipidization tests (see, e.g., Grubauer et al. [67]), resulting in disruption of the skin barrier. The use of a trypsin solution directly on the whole dermis, after removing the subcutaneous fat, was also sufficient to obtain the SC layer. The samples undergoing analysis in this work were therefore not subject to pre-treatment, which may also partially account for the differences encountered.

We would also like to point out the fact that most of the processes detected by DSC in this work are, at least partially, reversible. This seems to come as a result of the use of higher scanning rates, both in the heating and cooling processes, which makes reorganization of microdomains more difficult in the correspondingly shorter

time scale. Consequently, processes associated to reversible lipid behavior are emphasized and may be visible in spite of concurrent phenomena ascribed to SC proteins.

Results concerning the dehydrated SC have confirmed previous observations that the thermotropic behavior is not dramatically affected by the degree of hydration [64]. A higher level of hydration has been associated to an increase in the sharpness of the transition peaks [206, 207]. We have found, however, a slight enhancement in the resolution of a number of transition peaks. The relative intensity of the peak at 55°C clearly increases for dry SC, in agreement with other observations in dry SC [64] and with the fact that the intensity of D tends to decrease with hydration [216].

Our DSC and PLTM results are, overall, consistent with the heterogeneous nature of the lipid organization in human SC. The number of temperature induced transitions in the 0-120ºC range detected by DSC, and the clear distinction between coexisting domains, both in the SC matrix and extracted lipids, observed in thermomicroscopy are in accordance with the perspective that tightly packed lipids [237], gel phases, crystalline cholesterol and possibly also liquid-crystalline structures coexist at normal skin temperatures [62, 216, 250]. Different transition temperatures are, obviously, associated with different processes involving or not all visible phases.
Both hydrated SC and extracted SC lipids present low temperature transitions at ca. 20ºC (transition A). They correspond to textural changes affecting only a small portion of the observed material, that occur in a definite interval spanning about 2-3ºC. Values of T_m are consistent for dry or hydrated SC and SC lipids. Transition A probably corresponds to the melting of low-molecular-weight lipids, a process that have been previously attributed to a transition detected at ca. -9°C [224]. Although rare, previous works reported changes in a similar temperature range in dehydrated human SC lipids [206] and human SC [127].

The present results also indicate that the thermal transitions labelled as B and C result from the deconvolution in two different transitions of the phase transformation that has been denoted in the literature as T_1 [216]. The fact that these two transitions are simultaneously detected in the same sample by DSC determinations in both SC and SC lipids may thus shed some light on the conflicting results concerning

transition T_1, obtained from FTIR at ca 35ºC [64] and WAXD at approximately 40ºC [121]. In fact, determinations by FTIR closer to the temperature of B [64] indicate that the phase transformation has no direct relationship to an orthorhombic to hexagonal transition, which is the usual explanation for transition T_1. These experiments detected at ca 35ºC an inflexion for higher values in the CH_2 symmetric stretching, which is associated to a solid to fluid transition [64, 251]. Moreover, in the vicinity of the temperature associated with transition C, WAXD results [121] have shown a clear change in the packing lattice of the lipid alkyl chains from orthorhombic to hexagonal, while the lamellar repeat distance is not affected [55]. The fact that both transitions seem to be very sensitive to the degree of hydration [216], makes them very difficult to deconvolve and explains why they have been, until now, related with only one thermal transition (T_1).

PLTM observations show an almost continuous evolution of the system starting at about 40ºC. This is consistent with the progressive transformation in the lateral packing. Evidence from FTIR [64] and ED [211] have shown that this transformation may start, in some cases, at temperatures as low as 30ºC. However, above 40-45ºC there is a significant increase in the rate of transformation and at temperatures close to 60ºC most of the system is already in the hexagonal lateral packing.

The study of the SC delipidized matrix served to pinpoint the thermal behavior that is more directly associated to lipids covalently linked to proteins and proteins, since the type of extraction employed in this work does not remove the former. Transition D has been found in SC thermograms, delipidized SC but is not detected in our determinations with extracted lipids (see **Table 2.5**). To the best of our knowledge, it is the first time that this transition is detected in delipidized SC samples. In a previous work, it was only been detected in 1/5 of the SC samples and the phase transformation was attributed to another “solid-to-fluid” phase change in a subset of lipids [64]. More recently, transition D has been associated to lipids covalently bound in the corneocyte envelope [230], resorting to EPR, which is corroborated by the present observations by the fact that it is seen in the SC delipidized matrix and its absence in the extracted SC lipids.

When the temperature reaches 60ºC, an almost overall fluidization is visible in PLTM, see **Figure 2.10**. The lipid mixture becomes isotropic and liquid. Again, this is consistent with observations in model systems [252] and SC [216, 221, 228] that

suggest the transformation of the lamellar structure in a disordered phase and, concerning the lateral packing, a hexagonal to liquid transition as explanation for transition E [225]. Also, 60ºC marks an abrupt increase in the water vapor permeation through porcine SC [35]. At this point it should be also noted that SAXS scattergrams obtained by the authors in dehydrated extracted lipids have shown structures very similar to those found in human SC, consisting of short and long periodicity stacked lipid lamellae (SPP and LPP) [34].
Observations of SC lipid model systems above 60ºC, and up to approximately 80ºC have indicated that the lamellar phase may be followed by a hexagonal one, H_{II} [253-255]. The PLTM observations in this work show a much reduced mobility within the system, after transition E is completed, where two liquids are visible. The relation of these observation to those in model mixtures is not, however, straightforward.

DSC results indicate that the same transitions, F to H, are present in extracted lipids and SC for temperatures above 70ºC. The transition in SC slightly above 80ºC, transition F, was explained on the basis of a further gel to liquid phase change [216], in lipids bound to the corneocytes [225]. Our results in the delipidized SC samples indicate that transitions E [116] and/or F [221] are most likely not related to the above covalently linked lipids. They are detected in these samples, but they are infrequent and characterized by low intensity, which suggests incomplete extraction in a minute number of instances. Other authors [221] have suggested that transition F can also be explained in terms of disruption in the arrangement of the polar head groups of the lipids. A mixture of cholesterol and polar lipids is probably involved in this process [256].
It is clear from our results that this high temperature thermal behavior of SC is not associated exclusively to proteins or to covalently bound lipids, **Table 2.5**.

The transitions observed at higher temperatures have been grouped under T_4. The data from the present work show that at least two different processes may be identified in the 90-118°C range (transitions G and H). These transitions are generally related to irreversible protein denaturation, and have been frequently detected in the delipidized SC matrix [206, 207, 216], like in the present work. Early work in SC has also shown that denaturation of epidermal keratin may occur above 180ºC [257]. Also, no major structural changes seem to occur at 157ºC, and heating

up to 190ºC has shown a reversible pattern [248], although color changes may occur if samples are heated for long periods. We have subjected a SC sample, obtained from SSB, to a heating cycle from room temperature to 170ºC and cooling to room temperature again. Three indicative temperatures in this cycle are depicted in **Figure 2.9**. It is seen that the sample looses its texture, slightly shrinks (from 120ºC), in part due to dehydration, but maintains its overall appearance. PLTM observations on lipids above 90ºC indicate essentially the fluid behavior of the mixture, and do not provide further information (**Figure 2.11**).

The existence of lipid transitions, not involving proteins, for higher temperatures is not surprising. Mixtures consisting of polar lipids and cholesterol display transitions above 70ºC [216], which may be as high as 108ºC [253]. Also, some segregated ceramides may have points of fusion clearly above 90ºC [209, 258, 259].

Note that higher temperature transitions have also been associated to the loss of bound water [257]. Some major differences are detected if we compare thermograms obtained from hydrated SC, dehydrated and hydrated lipids. The main feature in the lipid traces corresponds to the peak centered at 60ºC. This contrasts with results for SC, in which peaks at 60ºC and 80ºC are very similar. In fact, although the transition at 80ºC is still visible in extracted lipids, it is much less pronounced. It is apparent, thus, that proteins do play a definite role close to that temperature.

5. Conclusions

The importance of the identification of the SC thermal transitions, and of a careful check on their reversible nature, is twofold. First, they provide information on the structural organization of the skin barrier. Second, they are used to correlate with other properties (e.g. permeation of substances) and as a previous assessment of the degree of fluidization induced by permeation enhancers. The present results show that the number of transitions is higher than usually determined and that the thermal transitions significantly overlap, i.e., instead of being sequential, some of the processes result directly from the existence of segregated phases and are thus almost concomitant. PLTM observations clearly showed the existence of domains

resulting from phase segregation. All these data strongly indicates that human SC lipids are organized heterogeneously, with coexisting phases at physiological and higher temperatures and allows rationalizing discrepancies resulting from the use of different techniques (usually at slightly different temperatures).

This work has confirmed the existence of a low temperature transition previously found in SC only, and now determined in the corresponding extracted lipids. Except for one transition (≈55ºC), we have corresponding results in SC and extracted lipids.
The transition T_1 of the literature has been shown to correspond to one phase transformation at about 35ºC and to another one above 42ºC, corresponding to different physical changes, according to previous results from different techniques.
The transition at 55ºC is absent in both sets of extracted lipids (dehydrated and hydrated in the presence of NaBr) and is present in the SC delipidized samples, which substantiates an EPR study that relates this transition with the corneocyte lipid envelope.
High temperature transitions are, at least partially, associated with lipids. They can be found in samples consisting of extracted lipids only.
The transition right above 60ºC is displaced to lower temperatures in the lipids, relative to SC. Also it is, in relative terms, much more intense with hydrated lipids than dehydrated, which is compatible with its interpretation as the disruption of the lamellar structure. This structure is partially supported by the corneocyte envelope in the SC matrix, and is also more structured in the presence of water.
PLTM observations of extracted lipids illustrate most of the behavior depicted above. Gradual variations are visible at temperatures corresponding to most transitions, but the disruption of the lamellar structure at ≈60ºC is illustrated by a drastic change in the texture of the sample. Alterations are visible at high temperatures, thus reinforcing that the thermotropic behavior of lipids extends to this high temperatures without the direct participation of proteins.
There is an appreciable correspondence between what is found through DSC both in the SC matrix and in extracted lipids, and what is observed by PLTM in the latter.

III

Stratum corneum hydration: phase transformations and mobility

1. Introduction

The most important function of the skin is probably its ability to serve as an efficient barrier to molecular diffusion, which is assured by the very outer epidermis layer, the SC as explained in detail on the general introduction of this thesis [122]. It is however important to bear in mind that, even though SC has a very low permeability, it is not totally tight. As an example, there is the TEWL of about 100-150 ml per day and square meter of skin surface through intact healthy skin [15].

The SC is exposed to large variations in the chemical surroundings, which are able to affect its structure and functions. Furthermore, the SC is subjected to several different gradients in, e.g. water level, temperature and pH, which can also influence its function. Important examples are the observations of a non-linear response in SC permeability to variations in the degree of hydration, and that the barrier properties can be regulated by, e.g., the relative humidity (RH) of the environment [35, 73, 74, 260, 261]. In a theoretical model for transport in responding lipid membranes in the

presence of a water gradient, this non-linearity was explained by structural transformations induced by this water gradient, which largely affects the overall permeability [262].

The normal water content in SC is about 30% ± 5% [76], it establishes the SC permeability [73, 74], and is also a determinant factor to other vital function of healthy skin in, e.g., its relation to the mechanical properties, the appearance and the enzymatic activity in SC [66, 75]. This intimate coupling between structure, function and hydration of SC motivates the investigations of the SC ultrastructural organization and how it responds to variations in the environment. Several studies on the hydration of human SC indicate a swelling limit in the interval 22-33 wt% [263-267].

It is important to remember at this point that the extracellular SC lipids constitute the sole continuous regions of the SC, the molecules that pass through the skin barrier must be mainly transported through them [33-35]. Here, the multilamellar arrangement of the lipids represents an almost ideal barrier towards strongly polar as well as non-polar substances. Due to its direct impact on the barrier properties, the organization and composition of these lipids have been extensively studied [50, 119, 120, 268]. Most of these studies concern the phase behavior at various temperatures. However, when considering the skin system, it is equally relevant to consider the phase behavior at different RH/water contents under isothermal conditions, which is the aim of the present work.

The majority of the SC intercellular lipids are in a solid state at normal RH and ambient temperature [61, 63, 68, 269-271]. However, there are several indications that a small fraction of the lipids is in a fluid state [59, 63]. The existence of fluid lipids could account for the non-negligible TEWL, which appears difficult to explain on basis only of the solid SC lipids. It could also allow for the high elasticity of the skin and for the enzymatic activity in the SC intercellular space that is unlikely to take place in a crystalline phase [65]. Several models that combine the structural information with the chemical and physical properties of the SC have been developed: the domain mosaic model [68], the sandwich model [71] and the single gel phase model [70]. A detailed description of these three models was provided on the general introduction of this thesis.

Taken together, it is well recognized that the mobility (fluidity) of the different SC components, as well as the SC hydration, is very important to several aspects of the vital functions of SC. However, the actual mechanisms of the SC-water interaction, how it is related with the hydration of the individual building-blocks (lipids and corneocytes) and whether these components have independent or cooperative roles in the hydration of SC are still unresolved issues whose solution forms the goal of the present study.

Extracted SC lipids, isolated corneocytes and whole SC were investigated at different RH/water contents by means of isothermal sorption microcalorimetry, and relaxation and wideline ^{1}H NMR. The sorption calorimetric technique allows for simultaneous measurement of the sorption isotherms and sorption enthalpies. The combination of the thermodynamic characterization of the hydration process and the structural information from the ^{1}H NMR measurements provides deeper molecular insight in the SC response to hydration. The characterization of this process is crucial to the understanding of skin structure and physiology, as well as for the development of new therapies for the prevention and correction of dermatological disorders related with low water content (e.g. eczema, psoriasis), and to the development of new pharmaceutical formulations for transdermal drug delivery and new cosmeceutics.

2. Materials and methods

2.1 Isolation of the *stratum corneum*

The pig skin from two different animals was a kind gift from “Slakteriprodukter i Helsingborg AB”. The hair was removed with an electric shaver and the dermatomed skin was placed dermal side down on filter paper soaked with a 0.2% trypsin (Sigma Chemical Company, St. Louis, MO) in PBS solution, pH 7.4. Digestion occurred during the night [214]. In order to remove any traces of viable epidermal cells, the

SC is rubbed and extensively rinsed with ultrapure water [Durapore (0.22 μm), Millipore, Bedford, MA], dried under vacuum and stored at -20ºC until used.

2.2 Extraction of SC lipids

The SC was rinsed with hexane to remove any lipids which might have contaminated the SC surface, such as sebaceous or subcutaneous fat [206]. For the actual extraction we have followed the procedure described in reference [43]. Briefly, the samples are sequentially immersed in three different HPLC-grade chloroform/methanol mixtures (2:1, 1:1, 1:2) for 2 hours each at room temperature. The extractions are then repeated for 1 hour each, and the sample is extracted overnight with methanol. Methanol is used to extract any polar lipids that are still remaining in the SC after the previous extraction steps [43]. All the extracts are combined and recovered by filtration through a filter paper. The final extract composed by the SC free lipids is dried under vacuum in a rotary evaporator and stored at -20ºC.

2.3 Isolation of corneocytes

The SC membranes recovered after extraction of SC lipids, are suspended in 1 M NaOH in 90% methanol and heated at 60ºC for 1 hour in order to extract the covalently linked lipids of the cornified cell envelope. The mixture is acidified to pH 4 by addition of 2M HCl and agitated with chloroform [43]. After filtration, the remaining SC material is washed with chloroform to eliminate residual lipids. In order to eliminate NaCl resulting from the extraction procedure, isolated corneocytes are extensively rinsed with ultrapure water, dried under vacuum and stored at -20ºC until used. Earlier studies demonstrated that the bulk keratin conformation is not modified by the delipidation procedure [272] nor by the treatment with solutions with a pH < 12 [273].

2.4 Sample preparation

After isolation and freeze-drying, all samples (intact SC, extracted SC lipids and isolated corneocytes) are dried in vacuum at room temperature in contact with 3Å molecular sieves during 24 hours. This procedure is necessary to remove all traces of water and organic solvents as confirmed by self-diffusion NMR experiments.
The transfer of the samples to the calorimetric cell and to the NMR tubes takes place in a dry nitrogen atmosphere. H_2O is added to each sample used in the NMR experiments after the samples being transferred into 4-mm diameter NMR tubes in N_2 atmosphere, in order to achieve the desired hydration. To avoid evaporation the sample tubes are flame-sealed.
The samples were allowed to equilibrate for at least 1 week at constant agitation before the measurements. Condensation of water was never observed in the tubes in any of the samples.

2.5 Sorption microcalorimetry

A double twin isothermal microcalorimeter was used to study the water vapor sorption of the SC and its components. A detailed description of the instrument is presented elsewhere [274]. The method of sorption calorimetry was used to monitor the water activity a_w and the partial molar enthalpy of mixing of water, H_w^m. A two-chamber calorimetric cell (diameter 20 mm) with the sample chamber on the top and water chamber on the bottom was used. The calorimetric cell was inserted into the double-twin microcalorimeter [274]. Water evaporated in the bottom chamber diffused through the tube connecting the two chambers and was absorbed by the studied sample in the top chamber, see **Figure 3.1**. The thermal powers corresponding to the evaporation of water in the vaporization chamber and to the sorption of water vapor in the sorption chamber were used to calculate the H_w^m with the sample. For the calculations of the H_w^m, the sorption calorimeter was calibrated using magnesium nitrate hexahydrate as a standard substance [275]. Water activity was calculated from the thermal power measured in the vaporization chamber as

described in ref [276]. The experimental set-up could be looked upon as a continuous titration of an initially dry lipid with water vapor. The rate of water diffusion in the vapor is controlled by the geometry of the vessel and the boundary conditions. We have confirmed that sorption process takes place under quasi-equilibrium conditions by conducting separate experiments with samples of different size. The complete sorption calorimetry experiment in the present study took approximately 13 days for the SC lipid samples, 3 days for the corneocyte samples and 7 days for the intact SC.

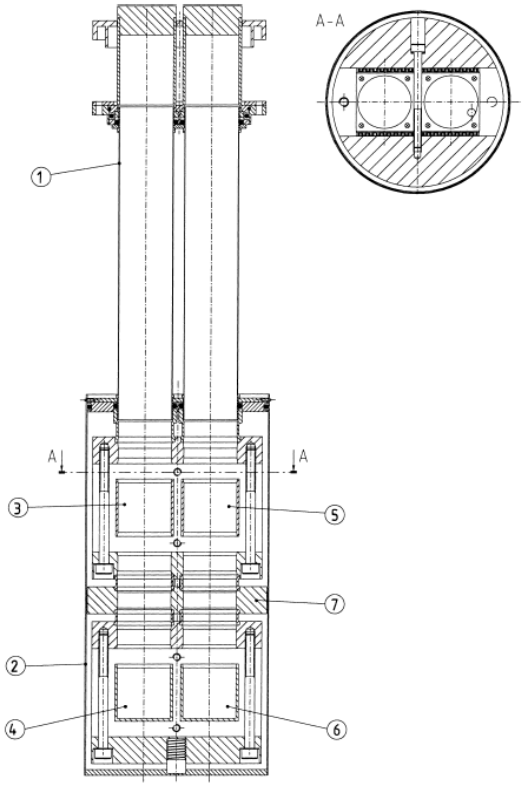

Figure 3.1 Schematic representation of the double twin microcalorimeter reprinted from [277]. (1) Tubes to charge the calorimeter; (2) steel can; (3) and (4) top and bottom reference ampoule position, respectively; (5) and (6) top and bottom measuring ampoule position, respectively; (7) heat flow breaker.

2.6 NMR

^{1}H NMR spectra were obtained on samples of extracted SC lipids, isolated corneocytes and intact SC with different water contents. Wideline ^{1}H NMR measurements were performed on a Bruker DMX-200 spectrometer using a Bruker DIFF-25 gradient probe at a temperature of 25 ± 0.5ºC. The ^{1}H resonance frequency for this system is 200 MHz. The probe is equipped with a home made 5 mm saddle-coil RF insert with negligible ^{1}H background signal. Free induction decays (FIDs) were recorded after a 4 µs 90º pulse using a dwell time of 1 µs and a receiver dead time of 4.5 µs. The FIDs were both analysed in the time-domain, to extract solid/liquid ratios, and Fourier transformed to obtain frequency domain NMR spectra. Transverse relaxation time (T_2) measurements were performed with the spin echo pulse sequence (90°- t_E/2-180°-t_E/2-acquire) using 64 logarithmically spaced echo times t_E between 0.1 ms and 0.5 s. For a single component the signal I decays according to $I = I_0\exp(-R_2t_E)$, where $R_2 = 1/T_2$ and I_0 is the signal at $t_E = 0$. Multicomponent signal decays can be deconvoluted to yield relaxation probability distributions $P(R_2)$ using an inverse Laplace transform algorithm [278]. 2D relaxation - chemical shift correlation spectra were obtained by Fourier transform in the chemical shift dimension, and subsequent inverse Laplace transform in the relaxation dimension in a manner analogous to the DOSY method for analysis of NMR diffusion experiments [279]. In this way overlapping peaks in the 1D NMR spectra can be separated according to their relaxation times.

2.7 Optical microscopy

The sample composed by individual corneocytes was observed with a Leica DMIL inverted microscope (Leica Microsystems, Inc., Germany) under transmitted light and the images, at 200x magnification, were captured using a Canon Power Shot S45 digital camera with a microscope adaptator.

3. Results

Three independent properties related to the hydration of the SC, extracted SC lipids and isolated corneocytes were investigated: the water sorption, the partial molar enthalpy of mixing of water, and the molecular mobility. Samples obtained from two different animals (1 & 2) were investigated, and all measurements were performed at 25ºC. Below, we first present separate descriptions of the measured physical parameters. The results are then collected into a unified discussion on the hydration of SC and its components.

3.1 Sorption measurements

The calorimetric sorption measurement provides a relation between the water content and the a_w, which can also be expressed in terms of the relative humidity ($RH=a_w \cdot 100\%$) or the osmotic pressure $\Pi_{osm} = - RT/V_w \ln(a_w)$. The sorption isotherms (water content, wt%, given as the mass of water divided by the mass of the whole system including the water, as a function of RH) are presented in **Figure 3.2**. Data from sample 1 are shown as dashed lines and data from sample 2 as solid lines.

3.1.1 Extracted SC lipids

The sorption isotherms for the samples composed of extracted SC lipids are shown in **Figure 3.2(a)**. The calorimetric measurements show a minor uptake of water until ca. 60 - 80% RH, followed by a more pronounced swelling at higher RH. In the latter region, three small steps at ca. 91%, 92% and 94% RH are visible in the isotherms. These are better shown in the magnification in **Figure 3.3** (lower curve, arrows), representing RH vs. water content. The steps, which can be interpreted as transitions in a fraction of the extracted SC lipids, are associated with a small uptake of ca. 1 wt% water at almost constant RH, where the smallest uptake is seen for the transition at 91% RH.

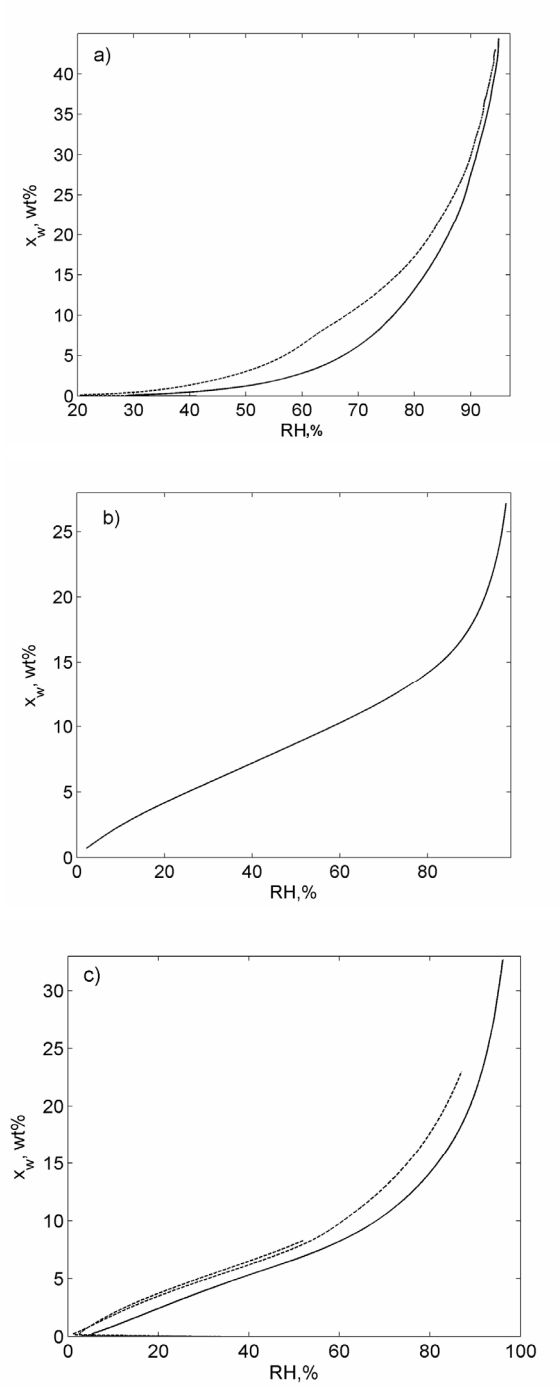

Figure 3.2 Microcalorimetric sorption data (water content [wt%] versus RH) at 25ºC for (a) extracted SC lipids, (b) isolated corneocytes and (c) SC. Key: dashed lines - sample 1; solid line - sample 2.

There is a continuously increasing rate of water uptake at RH > 60%. When comparing the sorption data from the different animals, there is a similar response at high RH, while the water uptake is slightly higher in the lipids extracted from animal 1 compared to animal 2. Furthermore, a kink at ca. 60% RH is observed in the isotherms from sample 1, although it was not observed in the sample from animal 2.

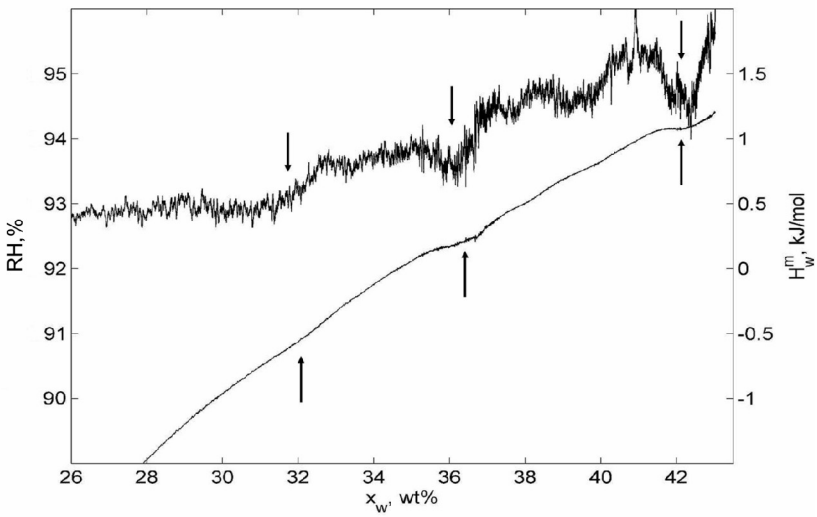

Figure 3.3 Magnifications of both the enthalpy curve (upper line, right y-axis) and the sorption isotherm (lower line, left y-axis) obtained from the extracted SC lipids from animal 1. In this regime, the sorption data suggest the presence of three phase transitions that coincide with small exothermic peaks in the enthalpy curves at the same water contents (indicated by arrows).

The extracted lipid samples were prepared by drying in vacuum and freeze-drying without special precautions taken to ensure the formation of equilibrium crystals. The discrepancy between the sorption curves at low RH might therefore be related to the presence of different amorphous states in the dry lipids, as well as normal biological variation in the lipid composition.

3.1.2 Isolated corneocytes

Isolated corneocytes with normal size and shape were recovered after the extraction of the lipids covalently linked to the cornified cell envelope as confirmed by optical microscopy (**Figure 3.4**).

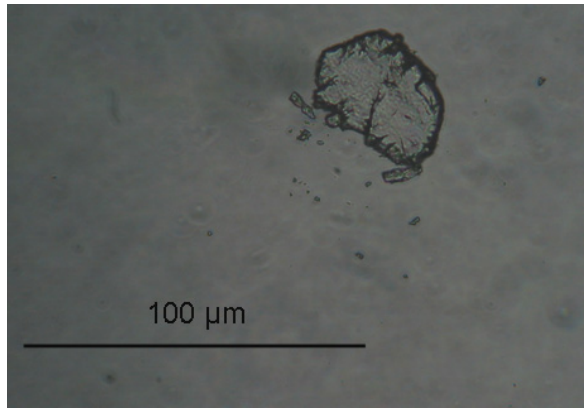

Figure 3.4 Optical microscopy image showing an isolated corneocyte, with normal size and shape. Original magnification: 200x.

The sorption curve for the isolated corneocytes [**Figure 3.2(b)**] shows a gradual swelling over the whole range of RH without pronounced steps that would indicate phase transitions. The shape of the sorption isotherm is similar to that of hen egg lysozyme studied previously using the same calorimetric method [280], although corneocytes take up slightly less water than lysozyme. The sorption isotherm of corneocytes can be roughly divided into three regimes: the initial sorption below 20% RH, the regime between 20-70% RH that features almost linear sorption isotherm, and the final regime above 70 % RH where water uptake increases.

3.1.3 *Stratum corneum*

Sorption data for SC are shown in **Figure 3.2(c)**. The isotherms show a continuous uptake of water over the entire range of RH, and no phase transitions are detected. At RH<60%, there is an almost linear relation between the water uptake and RH. At higher RH, there is an increase in the slope of the isotherm, implying a higher uptake of water. Finally, at RH>90%, there is again a large increase in water uptake. **Figure 3.2(c)** shows three data sets obtained for SC from two different animals. There is a very good agreement between the data from the two pieces of SC from animal 1, and there is a qualitative agreement between the sorption isotherms from the samples from the two different animals.

3.2 Enthalpy of sorption

A great advantage of the double twin calorimeter system is the simultaneous monitoring of the water activity and the partial molar enthalpy of mixing of water (H_w^m) during the hydration process at constant temperature [281]. The enthalpy curves obtained at 25 ºC for the three types of samples are shown in **Figure 3.5** (H_w^m as a function of water content).

3.2.1 Extracted SC lipids

The enthalpy data for the extracted SC lipids is shown in **Figure 3.5(a)**. The values of enthalpy effects measured in experiments with two samples are close to zero in almost the whole concentration range studied. At very low water contents the enthalpy effect was slightly exothermic for the sample from animal 1, and slightly endothermic for the sample from animal 2. The enthalpy data obtained at higher water contents provide further information on the transitions observed in the sorption isotherms.

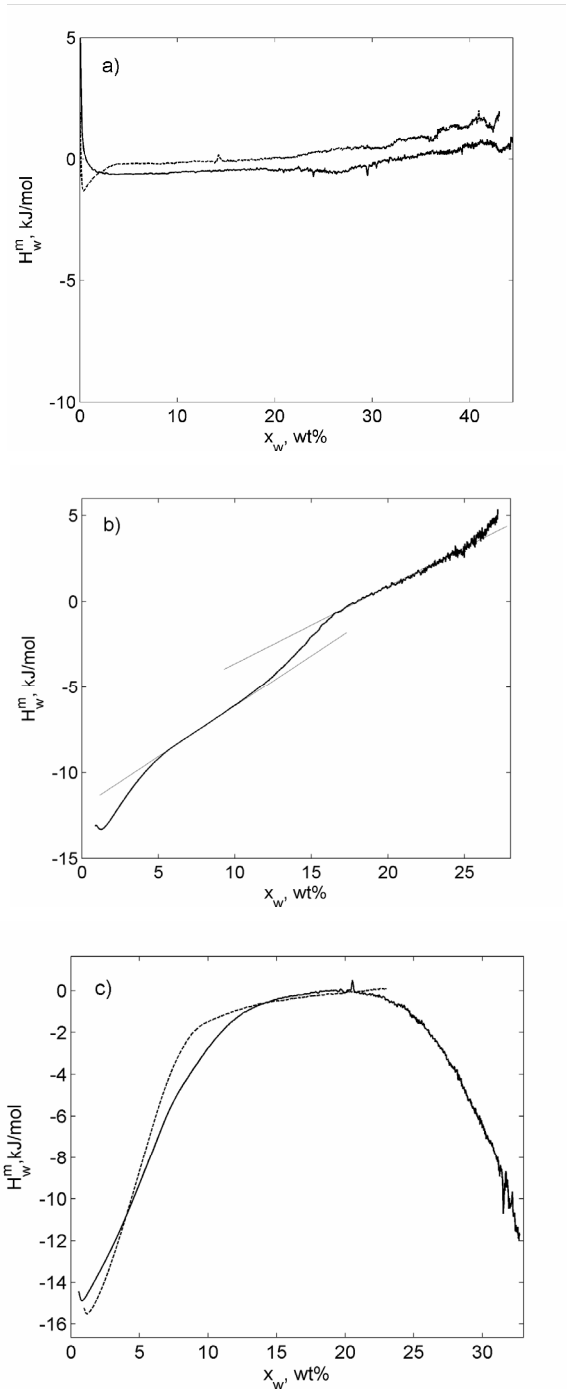

Figure 3.5 The partial molar enthalpy of mixing of water at 25ºC measured by sorption microcalorimetry. (a) Extracted SC lipids (b) Isolated corneocytes (c) SC. Key: dashed curves - sample 1; solid curves - sample 2.

Figure 3.3 shows the magnifications of the enthalpy curve (upper curve) together with the corresponding sorption isotherm (lower curve) at high water contents. In this regime, the sorption data suggest the presence of three phase transitions. We see that these are all coinciding with small exothermic peaks in the enthalpy curves at the same water contents (**Figure 3.3**, arrows). The data shown in **Figure 3.3** were obtained from animal 1. The transitions indicated by arrows in the figure were also observed for the samples from animal 2, and are therefore judged as real and reproducible effects. Due to the quasi-equilibrium conditions in the experiments and the reproducibility of these transitions, it is unlikely that they arise from, e.g., heterogeneities in the sample. The low transition energies are consistent with the involvement of just a small fraction of the lipids and low enthalpy transformations.

3.2.2 Isolated corneocytes

The enthalpy curve obtained from the isolated corneocytes from SC from animal 2 is shown in **Figure 3.5(b)**. The curve can be divided into four regimes: strongly exothermic regime with water contents 0-5 wt%, two moderately exothermic regimes with water contents 5-11 wt% and 11-17 wt% and the last regime (endothermic) with water contents above 17 wt%. The shape of the curve and the values of the enthalpy of mixing H_w^m are close to those observed in the sorption calorimetric study of hen egg lysozyme [280].

3.2.3 *Stratum corneum*

Figure 3.5(c) shows the enthalpy data obtained for the complete SC of the different animals at 25ºC. There is a very good agreement between the enthalpy curves at water contents for which comparisons can be made. At low water contents, H_w^m is negative, implying an exothermic primary hydration of the SC. At higher water contents, H_w^m is small and negative and it increases towards zero when approaching a water content of 20 wt%. Finally, when the water content exceeds 20 wt%, there is again a large exothermic enthalpy. The latter effect was only observed for SC from animal 2, as the experiment for SC from animal 1 was interrupted at lower water

contents, and therefore the reproducibility of this exothermic effect at high water contents was not studied.

3.3 NMR measurements

The mobility in different fractions of the SC as well as in the extracted lipids and the isolated corneocytes was investigated by means of relaxation and wideline ^{1}H NMR. Static dipolar interactions for molecules located in a solid environment result in fast T_2 relaxation and broad ^{1}H resonance lines - on the order of 10 kHz [282]. The dipolar interactions are averaged by molecular motions in a liquid environment leading to slow ^{1}H NMR relaxation and narrow resonance lines. Thus, NMR is a sensitive method to estimate if molecules are located in a solid or liquid environment. With sufficiently sharp resonance lines, different fluid components can be resolved in the chemical shift dimension. Even without chemical shift resolution, different components can be resolved utilizing their different relaxation rates. For microheterogeneous systems containing both solid and liquid domains, the ratio between these domains can be determined from the FID as described e.g., in ref. [283]. The terms “fluid” and “solid” used for the description of the NMR data should be interpreted in terms of the degree of averaging of the dipolar interactions. Molecular rotation and translational diffusion averages the couplings in a liquid crystal. If the system is anisotropic, such as for a hexagonal or a lamellar phase, the averaging of the intramolecular couplings is not complete, leading to the characteristic super-Lorentzian lineshape of the ^{1}H NMR spectrum [284]. The NMR data shown are all obtained for samples from animal 2.

3.3.1 Extracted SC lipids

The extracted SC lipids were studied at different water contents. **Figure 3.6** shows the ^{1}H NMR spectra for the extracted SC lipids with (a) 1.4 wt%, (b) 29.2 wt% and (c) 37.3 wt% water.

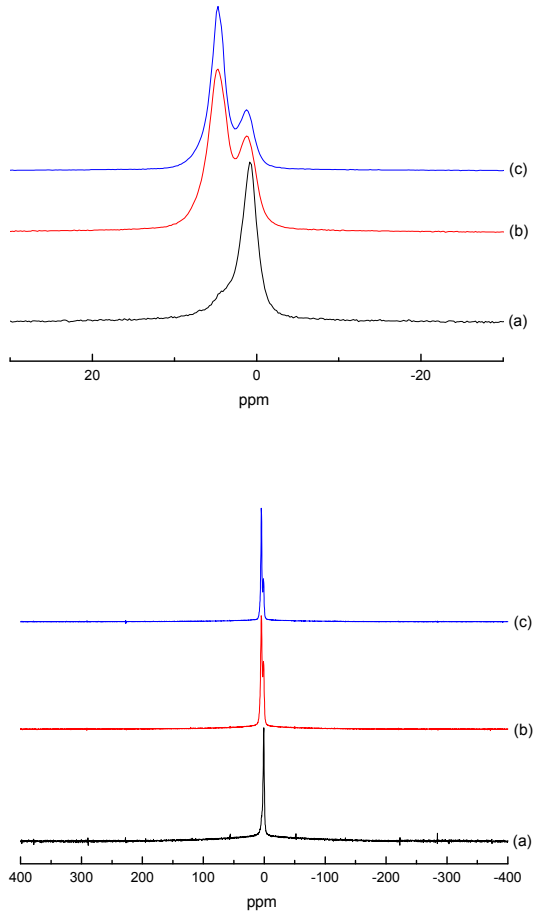

Figure 3.6 Wideline ^{1}H NMR spectra for the extracted SC lipids with (a) 1.4 wt%, (b) 29.2 wt% and (c) 37.3 wt% water at 25ºC (sample 2).

The ^{1}H NMR spectra contain two liquid-like components with chemical shifts corresponding to water and methylene groups in a hydrocarbon chain. The spectrum is too broad to observe individual peaks originating from other parts of the lipids, such as the headgroups and the methyl at the end of the hydrocarbon chain. Nevertheless, these peaks make non-resolved contributions to the liquid-like part of the spectrum. The liquid peaks are located on top of a broad peak originating from solid material. This latter component is more easily observed in the FID data (**Figure 3.7**) as a component with fast decay. The more slowly decaying part of the FID

arises from mobile protons. Extrapolation of the components to the time origin (the center of the excitation pulse) gives the ratio between the number of protons in liquid and solid environments [283]. The extrapolation was performed by fitting a bi-exponential function to the data as shown in **Figure 3.7**.

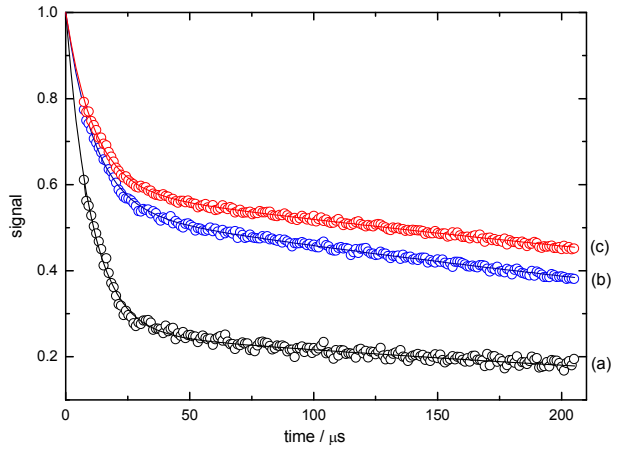

Figure 3.7 Free induction decay for the extracted SC lipids with (a) 1.4 wt%, (b) 29.2 wt% and (c) 37.3 wt% water at 25ºC (sample 2).

Monte Carlo error estimation was applied to assess the uncertainty in the analysis, including the noise contribution from the extrapolation. It is more difficult to get an estimate of the error originating from the choice of functional form for the signal decay. However, it should be noted that a sum of a Gaussian and an exponential decay produced a significantly low quality fit. Both solid and fluid lipids are detected in the lipid mixtures at all water contents investigated. T_2 relaxation experiments (log R_2=log1/T_2) were performed with the purpose of improving the resolution between the liquid components and getting further information about the environment in which the molecules are located. The T_2 distribution plot of the mobile protons in the hydrated samples is multicomponent, but it is not possible to distinguish aqueous protons from non-aqueous protons (see **Figure 3.8**, for 37.3 wt% water). If present, excess bulk water would be detected as a component with a T_2 of about 1 s. This

was not the case for any of the studied samples. Since the water contents of the samples are known, it is possible to make an estimate of the fraction of the non-aqueous protons that are mobile from the NMR FID experiments, assuming an approximate proton content in lipids of 11.9g H/100g dry weight [285]. The calculated values of the fraction of fluid lipids in the extracted SC lipids at different water contents are summarized in **Table 3.1**. For very low water content the value of the fluid lipid fraction is small. In the range 14.9-43.7 wt% water, the fraction of fluid lipids is clearly higher and no variation in fluid fraction with hydration could be detected within the resolution of the measurements.

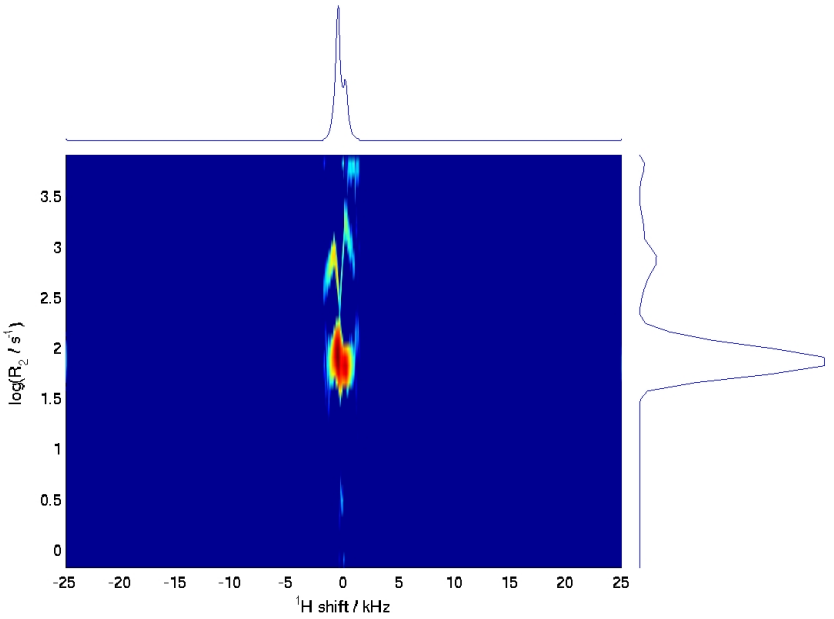

Figure 3.8 2D relaxation - chemical shift correlation spectra for extracted SC lipids with 37.3 wt% water at 25ºC (sample 2).

Finally, we note that the ^{1}H NMR spectra do not exhibit the characteristic lineshape of an anisotropic liquid crystalline phase [284]. This could be explained by molecular exchange between regions with different orientation of the lamellar director occurring on a time scale that is short with respect to the inverse NMR line width in the

absence of exchange (app. 0.1 ms). Alternatively, the environment of the fluid lipids are much more disordered and dynamic than in a typical bilayer, resulting in almost complete averaging of the anisotropic spin interactions.

Table 3.1 Estimate of the fraction of non-aqueous protons arising from lipids in the mobile state ($n_{non\text{-}aq\ mobile}/n_{non\text{-}aq\ total}$), as derived from NMR FID experiments.

Water content (%)	$n_{non\text{-}aq\ mobile}/n_{non\text{-}aq\ total}$
1.4	0.24
14.9	0.36
29.2	0.35
37.3	0.35
43.7	0.38

3.3.2 Isolated corneocytes

The isolated corneocytes were investigated at different degrees of hydration. The ^1H NMR spectra and T_2 relaxation experiments indicate the presence of only one liquid-like component while the major part of the sample is solid. With increasing water content, there is a continuous decrease in the fraction of the solid component (from 0.91 until 0.36) and a increase in the value of T_2 for the liquid component (from ca. 0.13 ms to a maximum value of 10 ms) - an indication that the mobile protons are those of water. An estimate of the fraction of mobile protons arising from the non-aqueous part of the sample based on the NMR FID experiments, assuming a proton content in keratin of 5.8 g H/100 g of dry weight [285] shows that the fraction of the fluid component in the non-aqueous part of the sample is zero and that it is not affected by the water content. The ^1H spectra shown in **Figure 3.9** further indicate that no significant change of the mobility of the solid component occurs upon hydration.

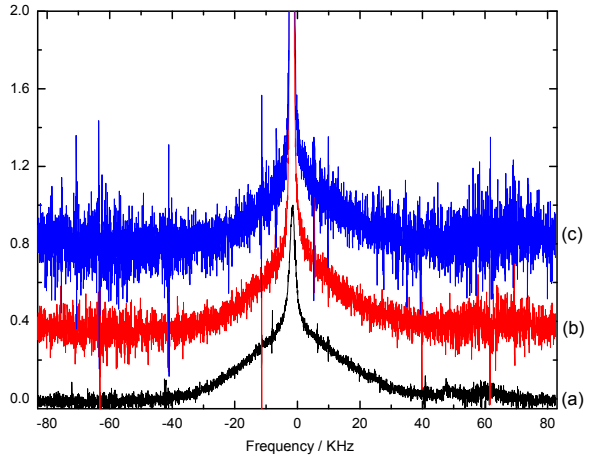

Figure 3.9 Wideline ^{1}H NMR for the isolated corneocytes with (a) 5.8 wt%, (b) 15.1 wt% and (c) 31.2 wt% at 25ºC (sample 2).

3.3.3 *Stratum corneum*

Samples of intact SC were investigated at different water contents. For all compositions, both fluid and solid material is present. Only one liquid-like peak can be observed in the chemical shift dimension. Using the relaxation-chemical shift correlation experiment, the liquid-like peak is resolved into two components as shown in **Figure 3.10** for 12.8 wt% water. In contrast to the case of extracted lipids, the aqueous and non-aqueous fluid components cannot be resolved in the chemical shift dimension (**Figure 3.8**) for the intact SC, presumably because of peak broadening originating from magnetic susceptibility differences between the different domains in the microheterogeneous system. The intensity of the peak with higher T_2 value did not change with different water contents, therefore it is probably related with the non-aqueous mobile component of the sample and the lipid hydrocarbon tails. This result shows that lipids in a fluid state are also present in the intact SC and not only in the isolated lipids. The rather fast T_2 relaxation of the water is typical for water in close proximity (<1 nm) to solid components [286]. Upon hydration the value of T_2 is continuously increasing. This fact can be explained by fast exchange

occurring between a perturbed surface layer with fast relaxation and a slowly relaxing pool of free water without direct contact with the solid surface. At 44 wt% water content a considerable part of the sample remains solid. As was also the case for the extracted SC lipids and the isolated corneocytes, excess bulk water was not detected in the investigated samples.

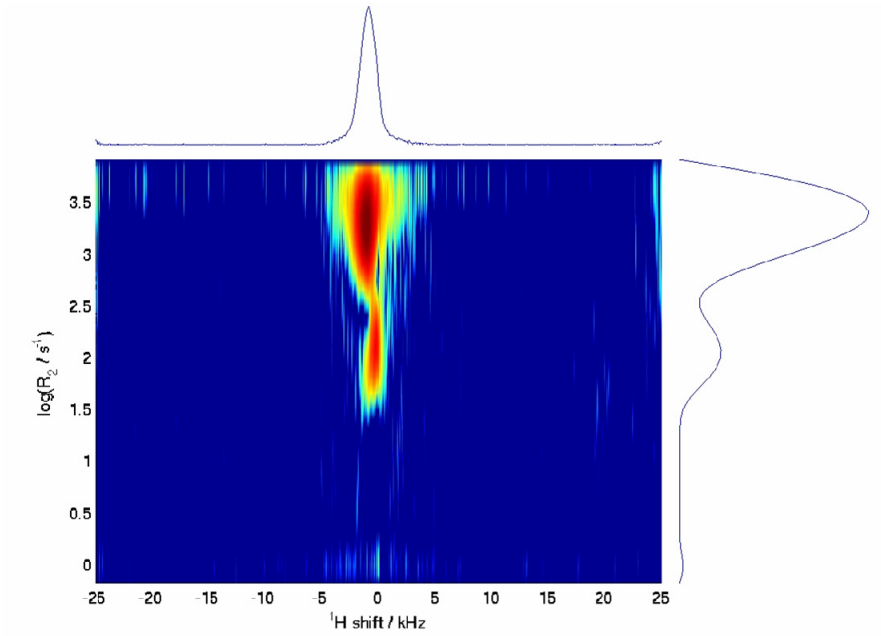

Figure 3.10 2D relaxation - chemical shift correlation spectra for SC with 12.8 wt% water at 25ºC (sample 2).

4. Discussion

The data presented in this work were obtained from measurements with two complementary techniques, NMR and sorption microcalorimetry. NMR is a very powerful tool to detect minor fractions of fluid components in complex mixtures,

which is more difficult to reach with, e.g., X-ray diffraction techniques. NMR has also some advantages over, e.g., fluorescent techniques and ESR, in that it does not require any labeling of the molecules or the presence of fluorescent probes that might affect the (local) phase equilibria. The sorption microcalorimetry measurements provide almost complete thermodynamic description of the hydration process in the different systems. By combining these techniques, the thermodynamic events can be related to the local mobility, and thereby molecular interpretations on the process of SC hydration can be made.

4.1 Solid and fluid SC lipids

It is well established that the extracellular SC lipids form a lamellar structure [55, 58, 63, 121]. Still, the molecular organization of the SC lipids within this lipid lamellar matrix is not fully understood. Several models based on large amount of experimental data have been proposed, including structures of connected bilayers [71, 233, 237] and the formation of domains within the bilayers [68]. These models take into account the coexistence of fluid and solid lipids, although the relative amounts have not been quantified experimentally. The NMR data in the present study clearly show such coexistence of fluid and solid lipids. It is also shown that a small fraction of the lipids remain in the fluid state at water contents as low as 1.4 wt% water. The existence of fluid lipids is considered crucial to the barrier properties of the SC because these are lipids likely to constitute a major transport route. Presumably, water and other small molecules that penetrate the SC diffuse through the fluid lipid regions, as the permeability is considerably higher in the fluid phase than in the solid phase.

From values of the fraction of fluid lipids estimated from the NMR FID experiments (**Table 1**), we conclude that a rather substantial fraction of the lipids are in the liquid state. This confirms previous results pointing to the existence of fluid SC lipids at ambient temperatures [59, 63, 64, 287-290], and it is the first time that a numerical value is assigned. The amount of fluid lipids is significantly lower at a water content of 1.4% than at water contents of 15% or higher. Within the resolution of our method, we are not able to demonstrate any variation within the fraction of fluid

lipids at 25ºC and water contents above 14.9 wt% of water. Previous IR studies have shown that the acyl-chain order in the intercellular lipids increases with hydration at low water contents, while it is independent of the degree of hydration at higher water contents [64, 291]. On the other hand, ESR studies have shown that, at a slightly higher temperature, there is an increase in the membrane fluidity with increasing water content up to the fully hydrated state [261, 287]. Taken together, this implies that both temperature and hydration influence the SC phase behavior. It is also likely that, e.g., pH affect the SC lipid phase behavior. The hydration process can effect the degree of ionization of the fatty acids [292] in the SC lipids, and it is possible that the proton concentration between the lamellae can vary between the swollen and the dry sample. However, it is not possible to control pH in the sorption calorimetry measurements.

From the sorption data we conclude that there is a substantial swelling of the extracted SC lipids upon hydration. At RH approaching 100%, the lipid phase contains more than 40 wt% water (**Figure 3.2**). This is consistent with the presence of liquid crystalline lipids, as solid lipids generally have a much lower ability to take up water. The sorption isotherm in **Figure 3.2(a)** can be analyzed in terms of interlamellar forces in bilayer systems because the osmotic pressure of water is equal to the interbilayer force in a lamellar system. At RH>65%, the sorption data show an exponential relation between the osmotic pressure and water content, which is typical for the swelling of lamellar lipid systems [293]. There exists a debate in the literature on whether the SC lipids are able to swell in water or not. This discussion is mainly based on data obtained from SAXS measurements on SC and SC lipid models that in fact, have shown somewhat contradictory results. In some of these studies, no swelling was detected in human and mouse SC [55, 57, 121], while minor swelling has been reported for the lipid bilayers in pig SC [54] and SC lipid models [62], and a rather pronounced swelling was shown for the short lamellar repeat distance structure in the SC of hairless mouse from 5.8 nm at 12 wt% water to 6.6 nm at 50 wt% water [58]. More recently, also neutron scattering results [294] indicated swelling of the lipid lamellar regions of human SC. An explanation for why the swelling was not observed in some of the studies might lie in the inherent limitations of the X-ray techniques, e.g. the second order peak for the long repeat distance lies very close to the first peak of the short one, which might lead to

overlapping. In fact, the most clear observation [58] of swelling in the short lamellar repeat distance was detected for SC from hairless mouse, which apparently gives sharper diffraction peaks than that from human or pig SC. The previous data displaying swelling of the short lamellar phase [54, 58], together with the present NMR and sorption data, indicate that swelling fluid lipids are present in the short lamellar structure of the SC lipids. From the present data, we cannot judge whether fluid lipids are also present in the non-swelling long repeat distance lamellar structure, which has been previously suggested [71, 237].

The NMR data show a significant increase in the fraction of fluid lipids between 1.4 wt% and 14.9 wt% water. In the calorimetric sorption measurements we did not observe pronounced phase transitions between solid and fluid lipids during the hydration process of the SC lipids at 25ºC, but the narrow endothermic regime seen for the sample from animal 2 may indicate the melting of some ordered domains at low water contents. We also note that the initial hydration of the SC lipids from animal 1 features exothermic heat effect, which is typical for the hydration of glassy materials [295]. The glassy materials are disordered like liquids but exhibit solid-like dynamic properties. The increase of the fraction of the lipids in the mobile state can thus be caused by melting or by a glass transition in a fraction of the lipids. The difference between the values of enthalpies of hydration of two samples of SC lipids at very low water contents can be explained by biological variations and by effects due to the preparation procedure. Even small differences in the drying procedure can lead to different degrees of crystallinity of the dry lipid samples. However, after the uptake of the first water molecules, the hydration process is very similar for the samples from the different animals, and the possible variations in the degree of crystallinity in the dry sample does not appear to affect the hydration process at water contents above 4 wt%.

The calorimetric data demonstrate three exothermic phase transitions in the extracted lipids at high RH (**Figure 3.3**). These transitions cannot be associated with chain melting, as that would give rise to an endothermic heat effect, and the molecular explanations for the observed transitions are not fully understood. The exothermic transition is compatible with a transition between different liquid crystalline phases, e.g. from a phase with lower curvature to a phase with a higher curvature, has been observed for other lipid systems [296]. However, there are no

evidences in the literature of non-lamellar structures in the SC at ambient temperatures, although there are indications of a reversed hexagonal phase in ceramide mixtures at high temperatures [297, 298]. The exothermic heat effect could also be related to an increase in the local curvature at the boundaries between the domains of different lamellar structures. Previous SAXS data showed that the swelling limit of the short lamellar structure coincides with the water content (ca. 50 wt%) where two repeating units seems to match the repeat unit of the long lamellar structure [58], and it was suggested that further swelling is constrained due to the structural restriction put up by the domains of the non-swelling long lamellar structure. The curvature at the domain interface would then go from a negative value to zero, which could give rise to an exothermic heat effect, in accordance to the discussion above [296]. A related explanation for the exothermic transitions at high RH lies in the reorganization of the lipid domains within the lamellar structure, e.g., fusion of fluid domains at increasing the water content. It should be noted that the domain reorganization and domain swelling are not to be considered as phase transitions from a thermodynamic point of view. Still, it could give rise to the type of enthalpy effects detected in the calorimetric measurements. The proposed explanations for the exothermic phase transition have in common that they are not expected to give rise to any large enthalpy effects. They are also consistent with the very minor uptake of water associated with the transitions, while much larger effect would be expected for a transition between a solid and a fluid phase. However, it is hard to estimate the relative amount of lipids that are involved in the transitions, which also means that we cannot judge exactly how large these effects really are.

Finally, we recall that the properties of the extracellular SC lipids are crucial to the barrier properties of the skin, as these lipids constitute the only continuous route for molecular transport. It is therefore important to relate the lipid structure to barrier properties. In fact, the exothermic transitions at RH=91-94% coincide with the region in RH where previous studies shown on a distinct change in water permeability of the SC [73, 261]. We therefore speculate that the hydration-induced lipid re-organization observed could be responsible for the alteration in SC permeability, and thereby partly explain the non-linear transport behavior of the SC.

4.2 Swelling of the isolated corneocytes

The major components of isolated corneocytes are the keratin filaments [299], and it is reasonable to assume that measured properties are related to the hydration of these. The wideline ^{1}H spectra (**Figure 3.9**) do not exhibit any changes in the mobility of the non-aqueous components of the corneocytes when increasing the water content, leading to the conclusion that the keratin filaments remains solid throughout the whole hydration process The increase in the value of T_2 for the aqueous component with hydration, and the gradually increasing component in the sorption isotherm, are both consistent with a continuous swelling of the solid keratin filament with hydration without any major structural rearrangements. There is evidence in the literature of unspecified protein conformation change induced by hydration [263], and both α and β forms have been identified as predominant secondary structures in SC proteins [300, 301]. The present measurements cannot distinguish between these different protein conformations, although the different rigid conformations are both consistent with the wideline ^{1}H NMR measurements.

According with what was pointed out above, the sorption isotherm of corneocytes has similar shape to that of lysozyme. This reflects the fact that both substances consist of aminoacid residues. Different amino acids have different hydrophilicities, the most hydrophilic ones hydrate first, the most hydrophobic ones hydrate after, which gives rise to a smooth sorption isotherm. The observation that lysozyme takes up more water, at the same RH, can reflect differences in the structures of the two protein materials (globular vs. fibrillar), as well as the difference in their aminoacid compositions. The gradual swelling profile is in good agreement with previously reported sorption data for SC samples depleted of intercellular lipids from sorption microbalance measurements [264, 302]. The enthalpy measurements show a strongly exothermic enthalpy effect at low water contents and endothermic effect at high water contents [**Figure 3.5(b)**]. The observed effects indicate that in the beginning of sorption the material is in the glassy state, which is typical for proteins at low water contents [280]. We also note that previous studies have also demonstrated a brittle to ductile transition in rat SC [299] upon hydration, which was explained by a glass transition in the keratin molecules. The exact position of the

glass transition in corneocytes is difficult to determine because in proteins this transition can be stretched over a wide range of compositions and temperatures [280]. We suggest that the glass transition occurs in the third regime on the curve of enthalpy (i.e. between 11 and 17 wt% of water). The straight lines in the **Figure 3.5(b)** correspond then to the second glassy regime (5-11 wt%) and to the elastic regime (above 17 wt%).

4.3 Hydration of *stratum corneum*

A major finding in the present study is the presence of fluid lipids in the intact SC. This is considered crucial to the barrier properties of SC as the fluid lipids likely constitute a major transport route for molecular diffusion. The fact that fluid lipids are detected in both the extracted lipids and in the intact SC further strengthens the link between the findings for the SC components to the complete SC. By reducing the complexity and studying the different components separately, it is possible to achieve more detailed information that would not be accessible for the complex system. One example of this is the transitions detected for the extracted SC lipids at high RH, which are not observed for the intact SC. The lipids constitute only a small fraction of the complete SC (ca. 15%) and the exothermic transitions are difficult to detect even in the sample composed exclusively by lipids (**Figure 3.3**). Due to the low signal we cannot expect to detect these transitions in the sorption calorimetry data for the intact SC. Still, the observed transitions might have important implications to the non-linear transport properties of the SC as discussed above.

The sorption isotherms of intact SC are similar to previous observations for human, porcine or neonatal rat SC [73, 260, 261, 263, 267], although we were able to provide a more accurate description of the SC sorption behavior, especially at high RH. The sorption data are also accompanied by the thermodynamic description of the whole hydration process. This value is higher than the swelling limit of SC previously reported for human SC (22-33 wt%) [263-267]. The enthalpy data for intact SC also show a large exothermic heat effect at the end of hydration process [**Figure 3.5(c)**]. Such exothermic heat effects at high water contents have not

previously been observed in any other materials studied by the method of sorption calorimetry. We suggest that the exothermic heat effect is a kinetic effect related to "delayed" hydration of the SC lipids and corneocytes in the glassy states due to very slow hydration (water diffusion) of the extracellular SC lipids and the protective corneocyte envelope [303]. Still, as the time of the experiment evolves and RH increases, water penetrates through the lipids and the cornified envelope, hydrates the sample which produces a "delayed" exothermic effect. Note that the beginning of the final exothermic effect also corresponds to a large increase in water uptake by SC at ca. 90 % RH [**Figure 3.2(c)**].

The capacity of SC to take up water has been attributed to swelling of the corneocytes and to the formation of water-pools in the extracellular SC lipids [54, 143] rather then swelling of the extracellular SC lipids. The formation of water-pools indicate excess solution conditions, or in other words, water contents above the swelling limit (100% RH), and this is not considered relevant to the present experiments (RH<100%). The combination of the presented calorimetric data for intact SC and its components at varying water contents can be used to further explore the different mechanisms of SC swelling.

In **Figure 3.11** we present combined data on sorption isotherms of SC and its components. This plot shows that the sorption isotherms are approximately additive, i.e., the sorption isotherm of SC lies between sorption isotherms of its components and may roughly be approximated as their sum. All three sorption isotherms cross at RH slightly higher than 80%. Below 80% RH, the hydration of corneocytes is more pronounced than that of lipids, while at high RHs, the lipids take up much more water than corneocytes do. This is also consistent with previous observations [304, 305], and this implies that the swelling and the water holding capacity of the SC lipids cannot be ignored. In this comparison one should, however, be aware that the sorption isotherm for the intact SC might include non-equilibrium effects due to a "delayed" hydration, which might complicate the analysis. Still, we believe that the results presented here reflect the general trends of hydration behavior of SC and its components.

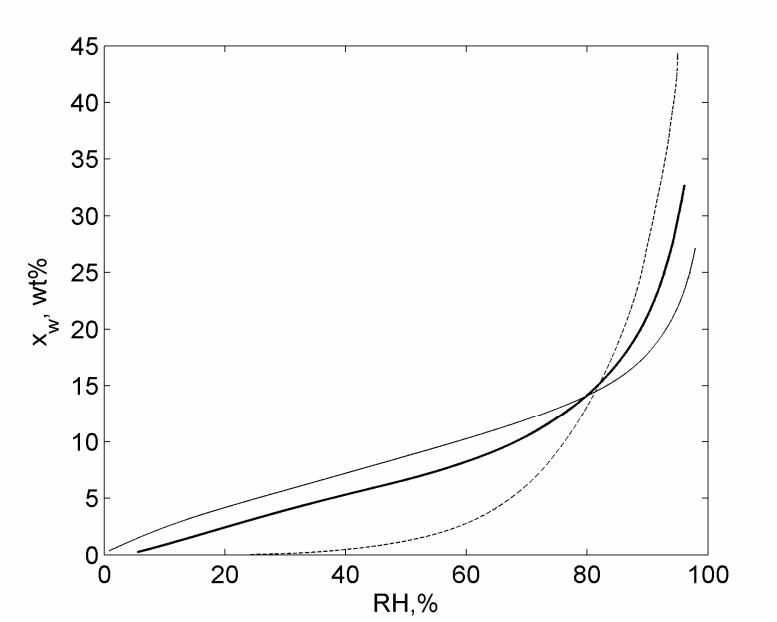

Figure 3.11 Sorption isotherms of extracted SC lipids (dashed curve), isolated corneocytes (solid curve) and *stratum corneum* (thick curve).

5. Conclusions

The SC is exposed to large variations in the chemical surroundings that can affect its structure, and thereby also its function. An important example is that the transport properties can be regulated by the water content in SC, which is related to the RH of the environment. Furthermore, the water content has profound influence on other vital functions of the SC, e.g., the mechanical properties and the enzymatic activity. In this study, we explore the process of hydration in intact SC as well as in extracted SC lipids and isolated corneocytes, and we conclude that there is a substantial swelling of SC as well as of its components at high RH. At low RHs, corneocytes take up more water than SC lipids do, while at high RHs swelling of SC lipids is more pronounced than that of corneocytes. This implies that uptake of water in SC is strongly dependent on the hydration of both the lipids and the corneocytes.
Lipids in a fluid state are present in both extracted SC lipids and in the intact SC.

At water contents ranging from 1.5-40 wt%, there is a coexistence of fluid and solid SC lipids. This coexistence is considered crucial to the barrier properties of the SC, as these phases have totally different diffusion characteristics.

There is an increase in the fraction of the fluid lipids at water contents below 15 wt%, whereas the fraction of fluid lipids remains virtually constant when the water content is further increased.

Three exothermic phase transitions are detected in the SC lipids at RH=91-94%. These transitions coincide with the region in RH where previous studies have shown a distinct change in water permeability of the intact SC, and it is possible that this hydration-induced lipid re-organization is partially responsible for non-linear transport behavior of the SC.

The hydration causes swelling of the corneocytes, while it does not affect the mobility of solid components (keratin filaments).

IV

Films based on chitosan polyelectrolyte complexes for skin drug delivery

1. Introduction

Chitosan (**Figure 4.1**) is a cationic natural copolymer consisting of β-[1→4]-linked 2-acetamido-2-deoxy-D-glucopyranose and 2-amino-2-deoxy-D-glucopyranose [201]. This linear polysaccharide is generally prepared by alkaline deacetylation of chitin, which is found in the exoskeleton of crustaceans, insects, yeasts and fungi [201, 306].

Chitosan is non-toxic, biocompatible and non-antigenic [201, 307], it is also very abundant [308], ecologically interesting and is a promising carrier for sustained drug release [309]. All these important properties make chitosan a very interesting component of hydrogels in the medical and pharmaceutical fields. In the present work, and since this formulation is intended to be applied to the skin, chitosan was selected as a starting material additionally due to its good film-forming properties, wound-healing benefits, bacteriostatic effects and bioadhesive properties [307, 309-313].

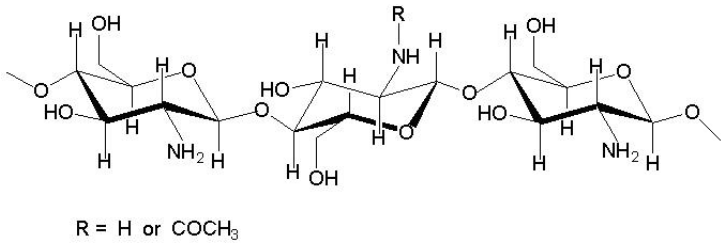

Figure 4.1 Chitosan structure.

Hydrogels composed of chitosan alone are limited by their poor tensile strength (TS), poor elasticity due to its intrinsic chain rigidity and lack of an efficient control of drug delivery [201, 202, 314]. The addition of other polymers is necessary to achieve PEC films with improved mechanical strength and elasticity while maintaining all chitosan properties after PEC formation. These systems are biocompatible, well tolerated, suitable as drug delivery systems, for wound management and tissue reconstruction [201, 315]. In this work, PEC are based on chitosan and poly(acrylic acid) polymers (PAA). Hydrogels prepared with a wide range of ratios between chitosan and PAA have been successfully prepared for different applications such as the amoxicillin site-specific delivery in stomach [310, 316] or the buccal delivery of acyclovir [309]. The PAA polymers (**Figure 4.2**) are water insoluble, have the ability to swell in water and its low glass transition temperature reflects a non rigid structure [317]. Chitosan, in combination with other polymers and molecules, has been used in several studies of PEC for the controlled delivery of drugs through different routes of administration, e.g., oral [310, 318], buccal [309], subcutaneous [319], colonic [320, 321], transmucosal [322] and ophthalmic [323].

The properties of the PEC are strongly influenced by two features: the global charge densities of the polymers involved and their relative proportion in the film that is directly related to the degree of interaction between the polymers. The suitability of a hydrogel to work as a drug delivery system and its performance also largely depends on its bulk structure. The main disadvantage of physically crosslinked

hydrogels over chemically crosslinked is the lower mechanical stability and the risk of dissolution due to highly pH-sensitive swelling.

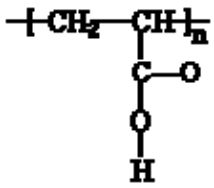

Figure 4.2 Polyacrylic acid monomer structure.

In the present work, the interaction between the oppositely charged polymers was optimized in order to circumvent this issue. In a first step, the degree of ionization of chitosan and the polyanions was determined as well as the stoichiometry of the polycation/polyanion interactions sites according to the pH by potentiometric and turbidimetric titrations. The pH and the amount of each polymer was imposed so as to obtain a ratio of one between the positively charged groups of chitosan and the negatively charged groups of the PAA and thus maximize the number of potential sites for electrostatic interaction. This value of pH was used to prepare all PEC films, considering that highly crosslinked hydrogels have a tighter structure, improving the stability of the network, which is reflected in a decreased swelling and drug release [310]. Increased crosslinking density and lower degree of swelling also tend to decrease the degree of burst release, minimizing the risk of dose dumping that can be potentially harmful to patients [324, 325].

Selection of the polymers is very important in the PEC design, since as referred earlier PEC performance will depend on its bulk structure. In this work, two different PAA polymers that have been crosslinked to different extents with allyl pentaerythritol (Carbopol 71G NF®) and divinylglycol (Noveon AA-1®) were selected to investigate the influence of the crosslinker in the PEC formation and functional properties. Further, two well known plasticizers, namely, glycerol and

PEG200, a moisturizing agent (Hydrovance®) and the additive trehalose were added to the PEC at a fixed concentration in order to study their effect on the film properties.
Glycerol and PEG200 have demonstrated in earlier studies the ability to increase the flexibility of chitosan films [326, 327], while Hydrovance® was chosen due to the higher water sorption capacity when compared with glycerol as claimed by the manufacturer. After selecting the plasticizer with the best performance, its concentration was changed in order to determine the ideal content.

In order to fulfil the therapeutic goals, films designed for skin drug delivery must assure a controlled delivery of the drug. For this purpose the delivery system is required to be bioadhesive [328, 329], to maintain an intimate and prolonged contact with the skin in the application site so as to provide a continuous drug supply; flexible and elastic to follow the movements of the skin and provide a good feel. At the same time, it must have enough strength to resist abrasion. In the absence of all or some of these physical and mechanical properties it is difficult to assure a controlled drug release to the skin.

Several key properties for the films daily use on the skin and therapeutic efficacy were evaluated: water vapor transmission rate (WVTR), tensile strength (TS), elongation to break (EB %), thickness, water sorption and *in vivo* bioadhesion. Thus, the aim of this study is the development and characterization of PEC films based on chitosan and PAA with good functional properties and cosmetic attractiveness for a potential application as a universal skin drug delivery system.

Due to the small bioadhesive properties of the formulations, an additional layer of a hydrophilic pressure-sensitive adhesive (PSA) composed of long chain polyvinylpyrrolidone (PVP) and PEG400 was applied to the film with the best functional performance and the properties of the resulting formulation were equally evaluated. This PVP-PEG400 PSA has been designed for enhanced transdermal delivery of drugs, is compatible with drugs of different physicochemical properties, does not act as a barrier to drug diffusion and is non-toxic [330-332]. We have decided to apply a hydrophilic PSA in order to keep the hydrophilic nature of the skin delivery system. Furthermore, this type of adhesives offer several advantages over

the hydrophobic ones: improved skin adhesion, compatibility with a higher variety of drugs and excipients, and expanded capability to control/manipulate adhesion-cohesive properties [333]. The PSA exhibits all the ideal properties for the development of an universal matrix for the skin delivery of drugs

The interaction between chitosan and PAA was investigated by DSC, Fourier Transform Infrared – Attenuated Total Reflectance (FTIR-ATR) and molecular dynamics simulations.

2. Materials and methods

2.1 Materials

Low molecular weight chitosan was purchased from Sigma-Aldrich. Noveon AA-1® and Carbopol 71G NF® were a gift from Noveon Inc. (Cleveland, USA) and Hydrovance® was kindly provided by the National Starch & Chemical Company (Switzerland). Trehalose, PEG200, PEG400 and polyvinylpyrrolidone K90 (PVP K90) were obtained from Fluka. All other chemical reagents were of pharmaceutical grade.

2.2 Potenciometric titration

Solutions with a concentration of 0.1% (w/v) of noveon and carbopol and a solution of 0.1% (w/v) of chitosan in 2% lactic acid were acidified by adding 2 mL of 1 M HCl. The solutions were titrated with standardized 0.5 M NaOH in a thermostatted vessel at 25.0 (± 0.1) ºC with a microburette in the presence of an inert atmosphere. Potenciometric titrations were conducted with a 665 DOSIMATE (Metrohm) microburette with minimal volume increments of 0.001 mL, recorded with a pHM 95 (Radiometer) potentiometer (± 0.1 mV). Potentiometric titration end point was

estimated by the inflection point of the titration curve [334]. Overall ionization constant was estimated using highest buffering capacity of respective solutions. The pH values were obtained via a 3 standard buffers calibration (pH 4.00, 6.86 and 10.0) under similar experimental conditions.

2.3 Turbidimetric titration

Turbidimetric measurements were carried out with a UV spectrophotometer (Shimadzu UV visible 1603) at the wavelength λ=420nm [309, 318, 335]. Solutions of 0.05% (w/v) of carbopol and noveon in distilled water and 0.1% of chitosan in 0.1 % lactic acid solution were prepared. The titrant (HCl 1M and NaOH 1M, respectively) was delivered with a microsyringe into the solution with gentle magnetic stirring at ambient temperature, until a stable reading was obtained. The pH was monitored with a digital pH meter and changes in turbidity are reported in arbitrary units as 100-%T, linearly proportional to the true turbidity for T>0.9 [318]. Turbidity values are given as a function of the pH of the solutions.

2.4 Preparation of the films based on chitosan-polyacrylic acid polyelectrolyte complexes

Chitosan solutions (1%, w/v) were prepared by dispersing chitosan in 0.5 % (w/v) aqueous lactic acid solution [336, 337] and stirring overnight. Lactic acid was used to solubilize chitosan because it has been proven to be non-irritating relative to other alternatives, such as acetic acid, on rabbit skin and has the ability to improve the flexibility of the film due to a plasticizing action [336, 337]. Low molecular weight chitosan was chosen because it has been suggested to react more completely with polyanions compared with chitosan of higher MW and originates films with smoother surfaces [338]. PAA polymers were dissolved in ultrapure water (Durapore (0.22 μm), Millipore, Bedford, MA) and the pH of the solutions was adjusted by addition of 1M HCl until the degree of ionization was less than 0.1% in order to avoid

precipitation when mixing the solutions of the polymers, and obtain a homogeneous mixture [201].

The chitosan solution is dropwise added to the PAA suspensions and mixed with a mechanical stirrer. The relative amount of both polymers was determined by the potenciometric titrations in order to obtain charge neutralization between the positively charged and negatively charged polymers at the pH where the ratio between the positive charges and negative charges is approximately one.

The concentration of each additive incorporated is given in percentage (%) and is related to the total dry weight of the polymers. **Table 4.1** summarizes the PEC compositions, and the coding used to describe the formulations.

Table 4.1 Composition, % w/w, and coding for each PEC film prepared in this work. The percentage (%) of plasticizer is given in relation to the total dry weight of the polymers.

	Chitosan	Carbopol	Noveon	Glycerol	PEG200	Hydrovance	Trehalose	PSA
F_C	67.6	32.4						
F_{CG}	67.6	32.4		20				
F_{CP}	67.6	32.4			20			
F_{CH}	67.6	32.4				20		
F_{CT}	67.6	32.4					20	
F_N	65.4		34.6					
F_{NG}	65.4		34.6	20				
F_{NP}	65.4		34.6		20			
F_{NH}	65.4		34.6			20		
F_{NT}	65.4		34.6				20	
F_{N30G}	65.4		34.6	30				
F_{N40G}	65.4		34.6		40			
F_{Na}	65.4		34.6	30				1 layer

After addition of the plasticizers, the suspension was neutralized with NaOH 1M to reach a pH of 6.1. The film forming solutions were magnetically stirred for 3 hours, cast on Petri-dishes and dried at 35 ºC for about 48 h. Dried films were conditioned at 75% RH and 25 ºC prior to testing.

An adhesive solution composed of 67 wt % PVP K90 and 33 wt % PEG400 was applied to the PEC film with the best functional performance (see **Section 3.2**) by solvent casting technique. PVP and PEG400 are miscible in a very wide composition range but only display adequate PSA properties between 30-40 wt% PEG400 [339]. PVP-PEG400 blends with 36% PEG400 showed in earlier studies the best adhesion performance [333, 339] but in pre-formulation studies in our lab for this particular type of film, the best adhesion/cohesive properties were obtained for 33 wt% PEG400.

2.5 Mechanical properties

Tensile strength (TS) and elongation to break (EB %) were measured on test strips after their equilibration for at least 72h hours in a desiccator containing a saturated solution of NaCl at 25ºC (75% RH) [340] using a TA.XTPlus Texture analyzer (Stable Micro Systems, UK) equipped with a tension grip system (**Figure 4.3**).

Figure 4.3 TA.XTPlus Texture analyzer equipped with a tension grip system for the evaluation of the TS and EB (%) of the films.

All samples were cut with scissors into bars of 15x50 mm before equilibration. In this experiment, at least four determinations were performed for each film type.
The TS is calculated by dividing de maximum breaking force (N) by the cross-sectional area (mm^2) of each film. EB (%) is the ratio between the final length at the point of rupture and the initial length of the sample and is expressed in percentage.
Film thickness was measured with a hand-held micrometer and six replicates were taken on each specimen in different places. Mean values and mean standard deviations were calculated for the film TS.

2.6 Water sorption (%)

Water sorption was assessed gravimetrically. The films were freeze-dried (Freeze-Drier Labconco FreeZone 4.5) and after drying the weight of each film was measured. The films were successively transferred to vacuum desiccators over saturated salt solutions of LiCl (11% RH), NaBr (60% RH), NaCl (75% RH) and ultrapure water (100% RH) at 25ºC [340]. All the salts were of reagent grade.
The samples were left to equilibrate for a minimum of 3 days before new weight measurement with an analytical balance and three replicates were tested for each type of film.
Water sorption of the film is given in what follows as the increase in weight, expressed as a percentage.

2.7 Water vapor transmission rate

The water vapor transmission rate (WVTR) ($g.m^{-2}.h^{-1}$) was measured using a Vapometer® (Delfin Technologies Ltd, Finland). Briefly, films specimens were mounted and sealed in the top of open specially designed cups filled with distilled water up to 1.1 cm from the film underside and left to equilibrate for one hour at room temperature (22-23ºC, 42-46% RH), see **Figure 4.4**. The Vapometer® has a closed measuring chamber not sensitive to external airflows with a humidity sensor

that enable measurements in normal room conditions [341]. Three film samples were tested for each type of film.

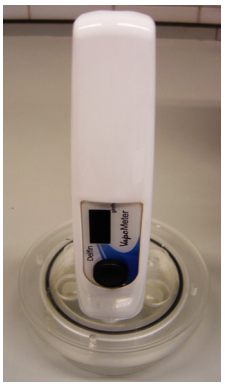

Figure 4.4 Illustration of the measurement of WVTR through the films, using the Vapometer®.

2.8 *In vivo* bioadhesive properties

The *in vivo* evaluation of the bioadhesion properties of the films, including peak adhesion force (PAF) and work of adhesion (WA), was performed using a TA.XTPlus Texture analyzer (Stable Micro Systems, UK).

The film is fixed by means of a double-sided adhesive tape on the movable carriage of the apparatus. The carriage is moved until contact between the skin of the subject forearm and the movable carriage is established (**Figure 4.5**).

A preload of 3N was applied and the contact time of the holder and the skin was 60 s. After that time, the movable carriage is moved forward at a constant speed test of 10 mm/sec until complete separation of the two surfaces. The curves of displacement (mm) versus adhesive force (mN) are recorded simultaneously. The WA is given by the integral on the range of positive force.

The force required to detach the attached film from the human forearm skin was used to represent the magnitude of bioadhesive force of the tested film specimen.

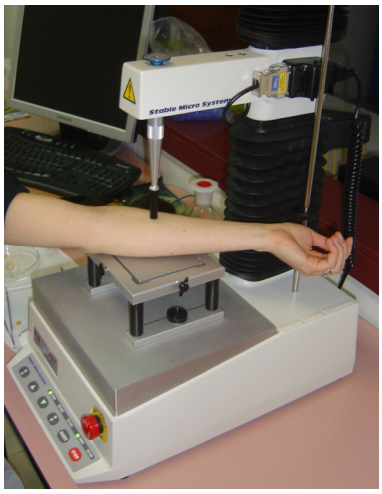

Figure 4.5 *In vivo* evaluation of the films bioadhesion to human skin using a TA.XTPlus Texture analyzer.

2.9 Differential Scanning Calorimetry (DSC) analysis

The DSC analysis was used to characterize the thermal behavior of the polymer powders and the interactions between the polymers in the films. DSC thermograms were obtained using a Shimadzu DSC-50 System (Shimadzu, Kyoto, Japan) with nitrogen at a rate of 20 mL/min as purge gas. Approximately 2-5 mg of each freeze-dried sample was accurately weighted into aluminium pans and hermetically sealed. The DSC runs were conducted from room temperature to 400ºC at a heating rate of 10ºC/min. Each sample was run in triplicate.

2.10 Fourier Transform Infrared – Attenuated Total Reflectance (FTIR-ATR) analysis

The FTIR-ATR spectra of the dried pure polymers and the films were recorded with a Magna-IR™ spectrophotometer 750 (Nicolet, USA) using the ATR sampling

technique on a ZnSe crystal. Samples were scanned 64 times over the wavenumber range of 400 to 4000 cm^{-1} with a resolution of 4 cm^{-1}.

2.11 Molecular dynamics simulations

Simulations were performed using the GROMACS software package with the standard GROMACS force field [342, 343], which is a modified version of the GROMOS87 force field [344]. Topology files were generated from initial structures, in Cartesian coordinates, resorting to the PRODRG server [345]. The polymers were added to a box and solvated with SPC (single point charge) model water [346], with the structure constrained by the SETTLE algorithm [347]. The SPC model for water considers three interaction sites centered on the atomic nuclei; the intramolecular degrees of freedom are frozen, while the intermolecular interactions are described by a conjunction of Lennard-Jones 12-6 potential and Coulombic potentials between sites with fixed point-charges.
The molecular dynamics simulation was performed with periodic boundary conditions, using the Berendsen coupling algorithm (P= 1bar, τ_p=0,5 ps; T=300K, τ_t=0,1 ps) [348] for ensuring NPT conditions (constant number of particles N, pressure P, temperature, T). The Particle Mesh Ewald method [349] was used for computation of long range electrostatic forces.

A molecular dynamics simulation was conducted with a chitosan polymer made up of 6 monomers and a polyacrylic acid polymer made up of 12 monomers, present in the simulation box with 2779 water molecules and 6 Na^+ counter-ions in order to keep the whole system neutral. Previous to each molecular dynamics (MD) simulation, an energy minimization was performed. This was followed by a MD equilibration run under position restraints for 1 ns. An unrestrained MD run was then carried out for 1 ns, as a further equilibration simulation. Finally, a MD trajectory with a total length of 12 ns was generated with a time step of 2 fs.

2.12 Statistical analysis

Results are expressed as mean ± standard error. The significance of the differences between values was assessed using a two sample t-test with a statistical significance level set at P = 0.05.

3. Results and discussion

3.1 Potenciometric and turbidimetric titrations

Potenciometric titrations were performed in order to evaluate the pH-dependent ionization degree of chitosan, noveon and carbopol, the stoichiometry of the polycation/polyanion interactions and the chitosan degree of deacetylation [334, 350].

The pK_a values obtained from the potentiometric titration curves were 6.22, 6.11 e 6.09 for chitosan, carbopol and noveon, respectively and the number of miliequivalents acids per gram of polymer ($meq.g^{-1}$) are 5.45, 12.86 and 11.48, respectively. The values determined for carbopol and noveon are very close, as could be expected since they only differ in the type of crosslinker and crosslinking extent. The degree of ionization of each polymer was calculated in order to determine the stoichiometry of the chitosan/carbopol and chitosan/noveon interactions according to the pH and is depicted in **Figure 4.6**.

It is well known that the charge densities of the polycation (chitosan) and the polyanions (carbopol and noveon) are mainly controlled by the pH. The pH value at which the ionization curve (**Figure 4.6**) of the polycation intercepts the ionization curves of the polyanions was considered the ideal pH for the preparation of the polyelectrolyte complexes due to the maximization of the number of potential electrostatic interaction sites. In both carbopol and noveon the ideal pH found for the interaction with chitosan was 6.1. With this value it is possible to calculate the

amount of the polycation and polyanion that should be mixed in order to impose a charge ratio of one, see **Table 4.1**.

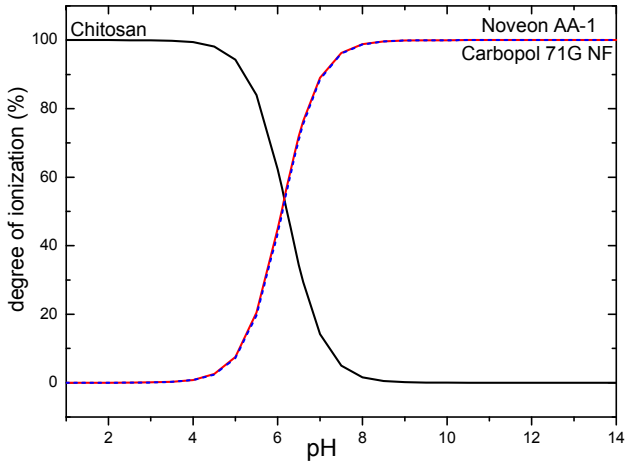

Figure 4.6 Degree of ionization of chitosan, carbopol and noveon according to pH. The ionization curves of carbopol and noveon are superimposed.

The potentiometric titration also enabled the calculation of the degree of deacetylation of chitosan. It corresponds to 88% in the polymer used in the present work.

The maximum degree of swelling in each PEC is determined by the balance between repulsion and contractile forces within the network. If there is a high degree of swelling, the complex can be dissolved. If we are maximizing the grade of network complexation we are reducing the swelling and the network exhibits properties that allow the controlled release of drugs without the need of crosslinkers [310].

Turbidimetric titrations consist in the measurement of the decrease in the intensity of a light flow passing through a solution with particles in suspension and is proportional to both molecular weight and the concentration of the particles in the

solution [351]. High turbidity indicates a high precipitation of the particles that occurs when the polymers are neutralized. In **Figure 4.7** we can see the results of the turbidimetric measurements for the three polymers. These results are in very good agreement with the degree of ionization calculated from the results of the potentiometric titrations. Turbidity of carbopol solutions is less influenced by pH when compared with the noveon solution and at pH 6.1 all three polymers exhibit a small turbidity indicating a high degree of ionization.

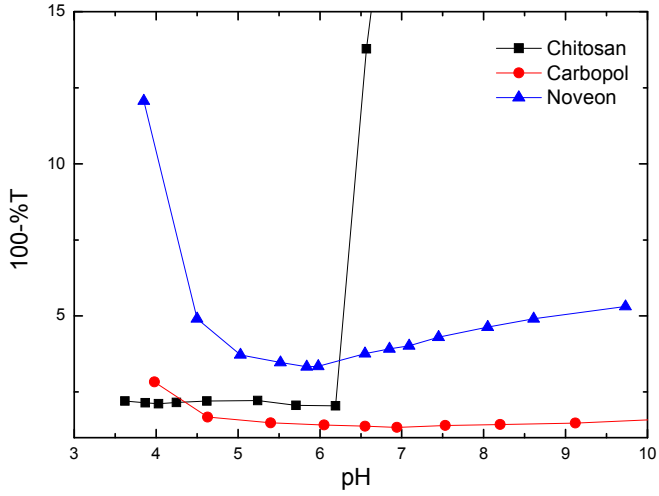

Figure 4.7 Turbidity of chitosan,carbopol and noveon as a function of pH. Values are reported in arbitrary units as 100-%T.

3.2 Characterization of the films

The PEC films prepared are thin (**Table 4.2**), smooth, transparent and slightly yellow due to the high content of chitosan, see **Figure 4.8**.

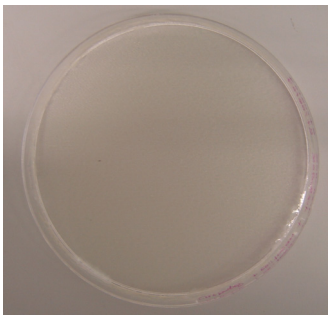

Figure 4.8 General aspect of the polyelectrolyte complex films based on chitosan and PAA after drying.

3.2.1 Mechanical properties

The TS and the EB% are important mechanical properties for the characterization of PEC films in terms of their resistance to abrasion and flexibility, respectively. Films intended for skin drug delivery must be flexible enough to follow the movements of the skin and provide a good feel, and at the same time resist the mechanical abrasion caused, for example, by clothes. For simplicity we consider that a film for skin drug delivery should be hard (high TS) and tough (high EB%) [352].
The TS values of the PEC films with 20% plasticizer are shown in **Figure 4.9(a)**. The values range from 2.7 to 5.8 N/mm^2 and are referred to films F_{CH} and F_{NG}, respectively. Comparison with the values found by other authors is difficult due to the different techniques used to determine TS and lack of standardization.

It is found that 20% PEG200 in the case of F_{NP} and 20% Hydrovance in F_{CH} films adversely affect the TS with statistical significance ($P< 0.05$) when compared with the films in the absence of plasticizer [**Figure 4.9(a)**].

The EB% values measured for the films at constant (20%) plasticizer content are shown in **Figure 4.9(b)** and range from 9.2-76.4%, being F_{CT} and F_{NG} the films with the smallest and the highest EB% values. For the case of chitosan/noveon films the values of EB% increased in the following order $\mathbf{F_{NT} < F_{NP} < F_N < F_{NH} < F_{NG}}$ while for

the case of chitosan/carbopol films the EB% values increased in the following order $F_{CT} < F_{CP} < F_C \sim F_{CH} < F_{CG}$, see **Figure 4.9(b)**. This indicates that trehalose and PEG200 always decrease the flexibility of the films and that glycerol is the plasticizer that produces the highest increase in the EB%.

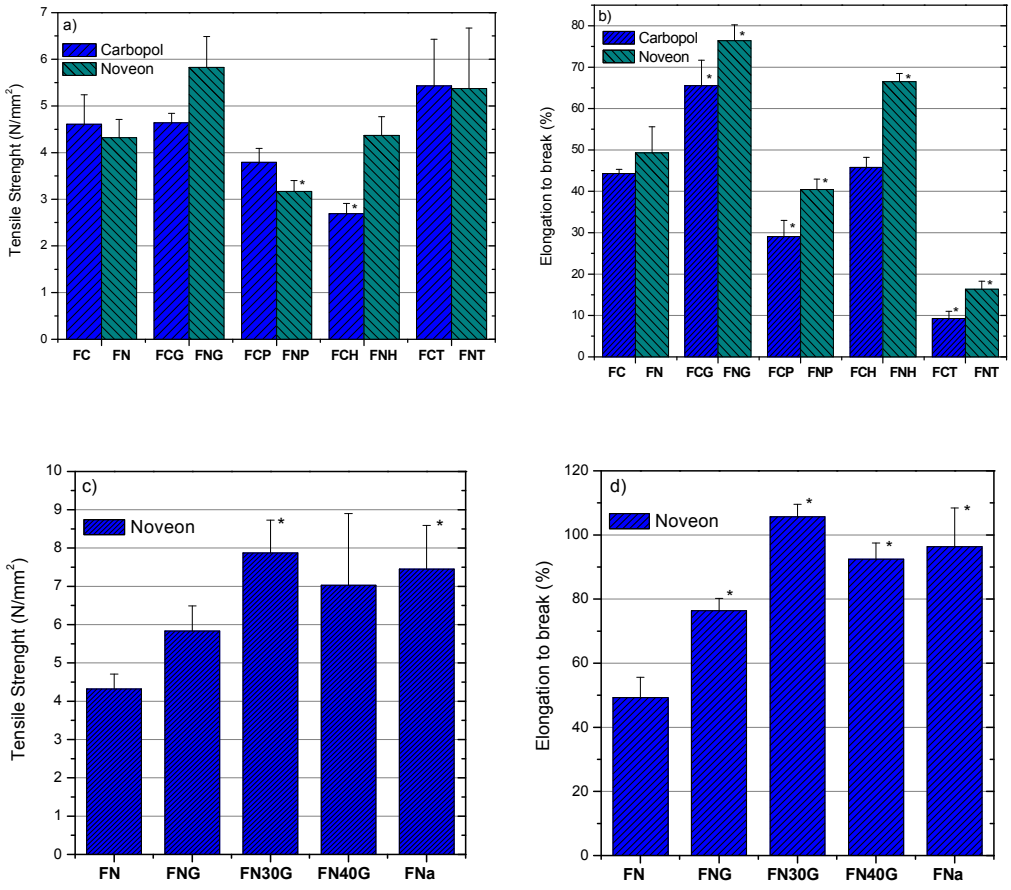

Figure 4.9 Mechanical properties of the films prepared in this work. Results of TS (a) and EB% (b) for the PEC films formed by the electrostatic interaction between chitosan/carbopol and chitosan/noveon prepared with 20% of glycerol, PEG200, Hydrovance and trehalose. Results of TS (c) and EB% (d) for the PEC films composed of chitosan and noveon prepared with different amounts of glycerol and an additional layer of the PSA. Mean (± SEM), n= 4, The symbol * signals statistically significant difference in comparison with the film in the absence of the additive ($P< 0.05$).

In the case of Hydrovance® it can be seen that only in the F_{NH} film it can significantly increase ($P< 0.05$) the EB%. It should also be noticed that chitosan/carbopol films exhibit a lower flexibility when compared with chitosan/noveon films with the same plasticizers. According with the presented results of TS and EB%, F_{NG} is the film that presents the best functional properties for the skin drug delivery because it exhibits the highest values of TS and EB%.

Glycerol was then selected to proceed the study and its concentration was further changed. **Figures 4.9(c)** and **(d)** depict the influence of the glycerol content in the TS and EB% of the films. It is clear that increasing amounts of glycerol tend to increase the mean values of both TS and EB% with the maximum effect at 30% glycerol. In other study glycerol also demonstrated the capacity to increase the TS and EB% of chitosan films [353] but in most of the studies glycerol exhibits the typical plasticizing effect (decreases TS while increases EB%) [326, 354, 355].

Glycerol reduces the rigidity of the bulk polymer network, originating films with increased polymer chain movements (increases EB%) probably due to the higher water content determined in the water sorption measurements (see below) in comparison with the films without glycerol. The increased TS may be explained by a negligible influence in the polymer-polymer interactions and possibly by the interaction with the polymers chains through the formation of hydrogen bonds.

The expected effect of a plasticizer is a decrease in the TS and an increase in the EB% [327, 352]. It is shown that trehalose exhibits an “antiplasticization” effect [327] because it increases TS and decreases EB% and none of the molecules tested acts as a true plasticizer [327, 352]. A strong interaction between trehalose and the polymers might be occurring, decreasing the molecular mobility of the polymers. Another explanation may be a reduced moisture uptake capacity of the films with trehalose that is observed in the water sorption isotherms (**Section 3.2.2**), such that we observe a reduced plasticizing effect due to a smaller amount of water present in the films.

F_{N30G} was considered the film with the best functional performance and an additional layer of a hydrophilic PSA was applied due to the small bioadhesive properties

determined for the PEC films alone (**Section 3.2.4**). The influence of this new layer in the TS and EB% of the formulation was also investigated and can be seen in **Figures 4.9(c)** and **(d)**. It is seen that the adhesive layer induces a minimum decrease of both TS and EB% when compared with F_{N30G} but the values measured in the bilayer film (F_{Na}) still show a significant improvement when compared with the film in the absence of plasticizer (F_N).

In summary, chitosan/noveon films are shown to be more flexible than the correspondent chitosan/carbopol films. PEG200 and trehalose decrease the flexibility of the films and glycerol improves both flexibility and resistance, with a maximum effect at 30% w/w. The properties of the optimized film (F_{Na}) are thus extremely adequate for application in the skin.

3.2.2 Water sorption (%)

Water sorption isotherms are important for providing some understanding in what concerns the interaction mechanism between water and film components and were also determined in order to know the water content of the films used in the tensile experiments. Considering that these films are intended to be applied on the skin for a long time, the water sorption isotherms reflect how the water content of the films changes with the ambient RH, a determinant parameter for the mechanical properties of the films. An ideal patch should keep its mechanical properties over a wide range of RH.
Water sorption in hydrophilic polymers is usually a non-linear process. PAA and chitosan are hydrophilic polymers that are able to retain a considerable amount of water that depends on the RH. In chitosan we can find at least three main sites for water absorption: hydroxyl groups, the amino group and the polymer chain end (a hydroxyl or an aldehyde group) [356].

The uptake of water increases in all films with increasing RH and is more pronounced at high RH, **Figure 4.10**.

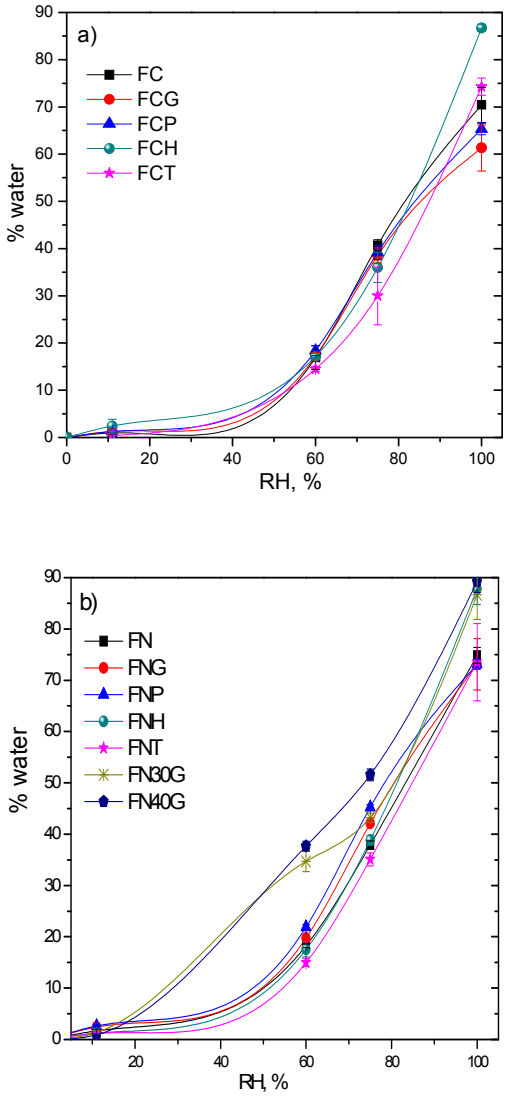

Figure 4.10 Water sorption curves of chitosan/carbopol films (a) and chitosan/noveon curves (b) according to RH and type and amount of additive incorporated. Data points are connected by spline lines.

In the case of films with or without 20 % of additives we can find two types of water sorption curves. Films F_{CH}, F_{CT}, F_{N}, F_{NH} and F_{CT} exhibit a slightly sigmoidal shape typical of polymers and films, including chitosan [355, 357, 358]. The water sorption

curve can be divided in two regimes, at low RH there is a low amount of water absorbed followed by a regime where the amount of water uptake increases exponentially. Films F_C, F_{CG}, F_{CP}, F_{NP} and F_{NG} show a different and atypical sorption curve that can be divided in three different regimes: at low RH (< 40% RH) there is a small amount of water absorbed, followed by a second regime where there is an exponential increase in the water sorption rate and finally, for RH higher than 75% RH the water sorption rate has a small decrease.
In the second type of sorption curve what is probably happening is the saturation of the surface available for water sorption at RH higher than 75% RH and higher RH produces a smaller increase in the water sorption rate. The first type of sorption curve is associated with trehalose and Hydrovance®, while the second sorption behavior is seen in films plasticized with PEG200 and glycerol at 20%.

Except for F_{CH} at 100% RH and F_{CT} at 75% RH, there is no statistical difference between the water amounts in the films composed of chitosan and carbopol, see **Figure 4.10(a)**. It is concluded that chitosan/carbopol films are less sensitive to the influence of the additives than chitosan/noveon films.

F_{CH} absorbed an amount of water significantly higher than the respective control while F_{CT} had absorbed less water than the control, a characteristic that may in part justify the decrease in the values of EB% produced by trehalose [**Figure 4.10(a)**] as discussed in **Section 3.2.1**. The decrease in the water sorption may be explained by the replacement of strongly immobilised water in the polymer chains by trehalose and is in accordance with the low hygroscopic nature of the molecule itself [359].

The exact same behavior was observed for F_{NH} and F_{NT}, suggesting that Hydrovance® has only a significant influence ($P< 0.05$) at very high RH in the increase of the water content while trehalose induces a decrease of the water content at 75% RH.

With respect to the influence of 30% and 40% glycerol content in the water sorption curves it can be seen in **Figure 4.10(b)** that there is a higher amount of water absorbed in all the range of RH ($P<0.05$). Also the shape is not typical but it is

important to emphasize that the water content is much less influenced by the RH than in the other films. This is a very important characteristic for a film that is intended to be applied on the skin and subjected to variations in the ambient humidity during application. Higher amounts of plasticizer increase the affinity of films to water, a result that can be attributed with the presence of hydroxyl groups in glycerol that are capable of strongly interact with water [357]. At low water contents glycerol interacts with the polymers via hydrogen bonds and as the amount of water is increased a higher percentage of the hydroxyl groups of glycerol became available for interacting with water [355]. Already, at 20% glycerol (F_{NG}), the films absorbed more water than F_N between 60-75% RH and the same behavior was observed for F_{NP}.

These results clearly indicate that the water sorption of the chitosan/carbopol PEC is much less influenced by the incorporation of the additives than the chitosan/noveon PEC. The incorporation of an amount of glycerol equal or higher than 30% in the chitosan/noveon PEC gives rise to films with a water uptake less affected by the RH. This implies that the mechanical properties of the optimized formulation (F_{Na}) will be relatively stable over a wide range of ambient humidity, as is desirable for such a film.

3.2.3 WVTR

As referred before, there is a normal TEWL of about 5-10 $g.m^{-2}.h^{-1}$ in healthy human skin [15, 122, 360] that is necessary to hydrate the outer layers, to maintain its flexibility, for temperature control and to allow enzymatic activity [66]. Occlusion of the skin interferes with the normal TEWL causing profound effects on the skin barrier such as increasing the percutaneous absorption of applied chemicals and the alteration of epidermal lipids, DNA synthesis, surface pH and bacterial flora [112, 139, 141]. The investigation of the permeability to moisture (WVTR) of the films to be applied in the skin is of major importance. WVTR also serves to indirectly evaluate the density of PEC and it is simultaneously dependent on the solubility coefficient and diffusion rate of water in the film [355].

WVTR of the films can be found in **Table 4.2**. Values range from 13.4 $g.m^{-2}.h^{-1}$ (F_{CH}) to 20.1 $g.m^{-2}.h^{-1}$ (F_{N30G}) and should be noticed that all the values measured are higher than the normal TEWL in healthy human skin [15, 122, 360]. These values are much higher than the values measured in crosslinked chitosan films that ranged from 0.12 to 0.42 $g.m^{-2}.h^{-1}$ [361].

Table 4.2 Bioadhesion, WVTR and thickness of the different PEC films according to the coding of Table 4.1. Results are expressed as mean (± SEM),n>3 (bioadhesion), n=9 (WVTR), n= 6 (thickness).

	***In vivo* bioadhesion**		**WVTR**	**Thickness**
	PAF (mN/cm^2)	WA (mJ/cm^2)	**($g.m^{-2}.h^{-1}$)**	**(µm)**
F_C	**71.5 ± 8.23**	**$6.4 \times 10^{-5} \pm 1.4 \times 10^{-5}$**	**14.5 ± 0.3**	**95 ± 4.5**
F_{CG}	105.8 ± 8.34*	$13.0 \times 10^{-5} \pm 1.3 \times 10^{-5}$ *	14.4 ± 0.2	92.5 ± 3.1
F_{CP}	64.1 ± 4.5	$5.2 \times 10^{-5} \pm 4.4 \times 10^{-5}$	14.5 ± 0.4	120 ± 9.7*
F_{CH}	65.2 ± 4.9	$6.4 \times 10^{-5} \pm 9.0 \times 10^{-6}$	13.4 ± 0.3 *	100 ± 5.9
F_{CT}	105.0 ± 6.6 *	$12.1 \times 10^{-5} \pm 3.7 \times 10^{-5}$	14.3 ± 0.1	102.5 ± 1.1
F_N	**68.9 ± 9.4**	**$5.7 \times 10^{-5} \pm 1.2 \times 10^{-5}$**	**14.2 ± 0.2**	**90.8 ± 2.4**
F_{NG}	127.4 ± 15.2*	$14.3 \times 10^{-5} \pm 1.8 \times 10^{-5}$*	18.1 ± 0.3 *	100.8 ± 2.7*
F_{NP}	69.1 ± 2.4	$7.8 \times 10^{-5} \pm 9.2 \times 10^{-6}$	14.8 ± 0.2	107.5 ± 6.7*
F_{NH}	62.5 ± 3.4	$5.3 \times 10^{-5} \pm 8.5 \times 10^{-6}$	15.3 ± 0.3 *	96.7 ±2.5
F_{NT}	57.9 ± 4.2	$4.9 \times 10^{-5} \pm 4.3 \times 10^{-6}$	14.2 ± 0.2	98.3 ± 3.3
F_{N30G}	64.0 ± 2.3	$6.2 \times 10^{-5} \pm 8.6 \times 10^{-7}$	20.1 ± 0.2*	105.8 ± 2.4
F_{N40G}	117.2 ± 14.4*	$13.6 \times 10^{-5} \pm 1.0 \times 10^{-5}$*	19.2 ± 0.3*	89.3 ± 1.7
F_{Na}	885.4 ± 62.2*	$311.2 \times 10^{-5} \pm 1.5 \times 10^{-4}$*	14.2 ± 0.3	102.5 ± 4.8

* Statistically significant difference in comparison with the film in the absence of the additive ($P < 0.05$)

PEG200 and trehalose do not have a significant influence ($P<0.05$) in the WVTR of the films and only Hydrovance® induces a significant decrease in the WVTR of F_{CH}. This decrease is probably due to same reduction of the film porosity since this is not related with a smaller amount of water in the films compared with the unplasticized film as depicted in **Figure 4.10(a)**.
Interestingly, Hydrovance® and glycerol increased the WVTR of chitosan/noveon films in the following order: $\mathbf{F_N<F_{NH}<F_{NG}<F_{N40G}<F_{N30G}}$. This behavior follows exactly the increase in the EB% of the same formulations and may be related with a higher amount of water sorbed in the films with Hydrovance® and glycerol, **Figure 4.10(b)**.

Films with higher water content show increased capacity to water diffusion since it contains more water. Probably, an increase in the WVTR values reflects a less compact structure, a higher mobility of the polymer chains and thus an increased flexibility. In earlier studies glycerol also induced an increase in the WVTR of films composed of N-carboxymethylchitosan and chitosan [362] and potato starch-based films [355].
With respect to the influence of the adhesive layer in the WVTR of the films, it can be seen that this layer reduces the WVTR when compared with the F_{N30G}, although there is no significant difference between F_{Na} and F_N. We can conclude that since the WVTR of the F_{Na} is 14.2 $g.m^{-2}.h^{-1}$ and higher than the normal TEWL in human skin this film is suitable for application in the skin for a long time without a significant interference in the barrier function of the skin or causing skin sensitization.

3.2.4 Bioadhesion

The adhesion to the skin is one of the most important functional properties for a skin drug delivery system [328] and should be evaluated in all formulations in development for this purpose. The *in vitro* conditions do not represent the performance of a film under *in vivo* conditions due to skin properties, such as moisture and elasticity that are not possible to reproduce in the *in vitro* test. Most of the *in vivo* bioadhesive tests are based on subjective observations resorting to scoring systems [328, 363]. We used skin *in vivo* as the substrate for testing

adhesive properties and a quantitative evaluation is made by measuring the peak adhesion force (PAF) and the work of adhesion (WA).

Acrylate polymers are well known skin adhesives [328, 329, 364]. Our films are composed of chitosan and a PAA but the amount the PAA is only approximately one third of the total polymer weight, a fact that justifies the small values measured for the PAF and WA, see **Table 4.2**.
The values of PAF in the pure films range from 57.90 mN/cm^2 (F_{NT}) to 127.43 mN/cm^2 (F_{NG}) while the values of WA range from 4.94x10^{-5} mJ/cm^2 (F_{NT}) and 14.30x10^{-5} mJ/cm^2 (F_{NG}). The plasticizers Hydrovance®, PEG200 and 30% glycerol do not significantly influence ($P>0.005$) influence the values of PAF and WA of the films. Trehalose increases the PAF ($P<0.05$) and the WA of F_{CT} film, while no difference is observed in the PAF and WA values of F_{NT} when compared with the film in the absence of plasticizer. Glycerol at 20% and 40% induced an increase in the PAF and WA in the fims. In a study performed on piroxicam-loaded Eudragit E films the plasticizer was also able to increase the adhesion strength of the films [352].

The additional layer of the hydrophilic PSA applied to a F_{N30G} film produced a dramatic increase in the values of both PAF and WA, 885.45 mN/cm^2 and 311.2x10^{-5} mJ/cm^2, respectively. These values represent approximately a 7-fold and 22-fold increase, respectively, when compared with the values measured in the film with the best bioadhesive properties (F_{NG}).

3.3 Characterization of the polymer-polymer interactions

DSC, FTIR-ATR and MD simulations were used for the examination of the interactions between the polymers in the films.

The DSC thermograms of pure chitosan, noveon, carbopol and the films prepared in this study are shown in **Figure 4.11,** while **Table 4.3** presents the endothermic and exothermic peaks detected and the values of enthalpies associated.

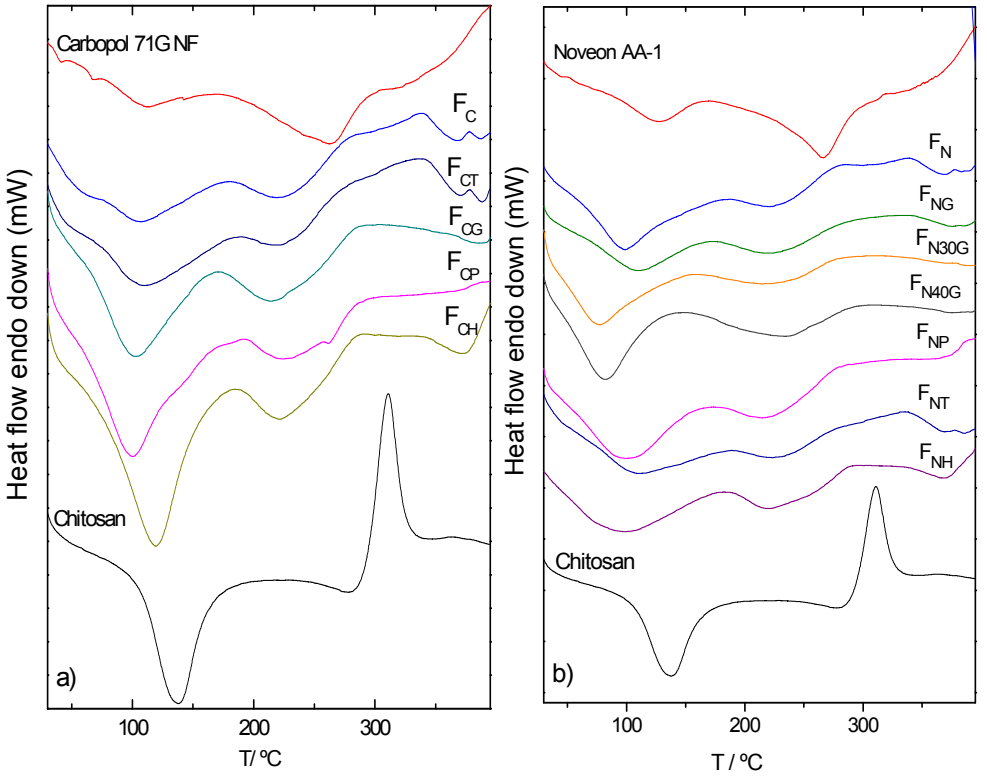

Figure 4.11 DSC thermograms of chitosan, carbopol (a), noveon (b) and PEC films determined at the same analytical condition. The coding used to designate the PEC films are in accordance with Table 4.1.

Pure chitosan exhibits one endothermic peak at 112 ºC associated to the evaporation of absorbed water, a glass transition at 243ºC and an exothermic peak at about 311ºC ascribed to the polymer degradation, including saccharide rings dehydration, depolymerization and decomposition of deacetylated and acetylated chitosan units [354, 365]. These peaks have been reported in several other studies [327, 366].

Both forms of PAA exhibit two endothermic peaks with onset temperatures at ca. 103ºC and 243ºC for noveon while for carbopol the onset temperatures are ~80ºC and ~200ºC, see **Table 4.3** and **Figure 4.11**. The first endothermic peak has been assigned to the evaporation of water from hydrophilic groups in the polymers and

the second one corresponds to a thermal degradation through intramolecular anhydride formation and water elimination [367-370]. After the second endothermic peak, the onset of a broad exothermic peak (~300 ºC) is visible in the thermograms (**Figure 4.11**). It is probably related with to a second degradation process involving the destruction of carboxylic groups with CO_2 elimination and chain scission [368, 369].
Several glass transitions (T_g) were detected in the DSC curves of the two forms of PAA at ca. 41ºC and 65ºC for noveon and ca. 37ºC, 68ºC and 140ºC for carbopol that have been also reported by other authors [317, 367-370]. The T_g detected below 100 ºC are probably related with the presence of residual amounts of solvents used in the polymer synthesis that may act as plasticizers. The glass transition of carbopol detected at ca. 140ºC may be explained by the disruption of the hydrogen bonds between carboxylic acid groups [317, 371].

The PEC films prepared in the present study exhibit two endothermic peaks. The first one is associated with the vaporization of water and the onset temperature is situated between ~53ºC (F_{N30G}) and ~82ºC (F_N) in the case of chitosan/noveon films and between ~61ºC (F_{CH}) and ~82ºC (F_{CT}) in the chitosan/carbopol films.
The second endothermic peak is probably related with the cleavage of the electrostatic interactions between the oppositely charged polymers, since it is not observed in the pure compounds [366]. The onset temperature of this new transition increases in the following order $F_{N40G} < F_{N30G} < F_{NG} < F_{NP} \sim F_N < F_{NH} < F_{NT}$ for the chitosan/noveon films and $F_{CG} < F_C \sim F_{CH} < F_{CT} < F_{CP}$ for chitosan/carbopol films, **Figure 4.11** and **Table 4.3**.

From these results, we can conclude that increasing amounts of glycerol tend to decrease the thermal stability of the polyelectrolyte complexes probably by insertion between the polymeric chains.

Hydrovance® has little influence in the thermal stability of the films and PEG200, in the other hand, does not influence the thermal stability of chitosan/noveon films, but increases the stability of chitosan/carbopol polyelectrolyte complexes. Trehalose always increases the thermal stability of the polyelectrolyte complexes as depicted in **Figure 4.11** and **Table 4.3**.

Table 4.3 Peak temperatures and enthalpy changes detected in the DSC thermograms of the pure polymers and the PEC films.

Sample	Temperature / ºC			ΔH / J.g^{-1}
	Onset	Peak	Endset	
Chitosan	85.3	112.0	133.9	-180.3
	291.8	311.0	322.6	336.3
Noveon AA-1	102.6	128.3	153.2	-54.6
	242.7	265.1	287.3	-150.6
Carbopol 71G NF	79.6	102.3	121.2	-51.1
	200.0	246.3	280.0	-239.5
F_N	82.1	95.4	122.8	-117.9
	191.8	221.0	241.3	-38.0
F_{NG}	78.3	107.6	145.6	-139.6
	186.1	219.1	248.7	-62.5
F_{30NG}	52.5	76.8	110.1	-273.9
	181.2	219.2	247.7	-126.7
F_{40NG}	62.1	88.7	114.6	-304.2
	178.8	231.6	278.1	-182.1
F_{NP}	63.6	99.0	140.1	-211.1
	191.0	216.8	240.4	-42.4
F_{NH}	59.4	84.8	134.1	-162.4
	195.7	218.8	262.6	-47.4
F_{NT}	77.4	111.1	143.8	-124.4
	196.7	223.1	252.7	-36.9
F_C	73.5	104.1	154.0	-142.4
	193.7	219.2	279.7	-35.8
F_{CG}	75.1	103.8	147.7	-187.6
	181.2	211.5	252.7	-53.6
F_{CP}	62.0	92.1	121.1	-309.4
	201.6	223.7	253.8	-32.4
F_{CH}	61.2	94.5	148.7	-249.4
	193.9	219.7	260.5	-61.4
F_{CT}	81.9	110.4	154.7	-128.4
	199.3	218.9	237.2	-19.6

The FTIR-ATR spectra of chitosan, noveon, carbopol and the PEC films are shown in **Figure 4.12**. The FTIR-ATR spectrum of chitosan shows a weak band at 2871 cm^{-1} attributed to the C-H stretching and the absorption band due to the carbonyl group stretching of the secondary amide (C=O-NHR) appears at 1651 cm^{-1} indicating that chitosan is not totally deacetylated in accordance with the results obtained in the potentiometric titration [337, 366, 372]. The peaks at 1585, 1421 and 1321 cm^{-1} correspond to the N-H bending vibration (amine I band), N-H stretching of the amide and ether bonds and the amide III band, respectively [337, 366, 372, 373]. The peaks at 1149, 1057, 1025 and 893 cm^{-1} correspond to the bridge oxygen (C-O-C) stretching bands [372]. The assignment of the main chitosan IR bands can be found in **Table 4.4**.

The FTIR-ATR spectrum of noveon in **Figure 4.12(b)** exhibits a broad band at ca 3100 cm^{-1}, a weak band at 2939 cm^{-1} and a strong band at 1697 cm^{-1} assigned to the O-H stretching (hydrogen-bonded), asymmetric CH_2 stretching and C=O stretching (hydrogen-bonded), respectively [371, 372, 374]. The weak band at 1412 cm^{-1} is due to the symmetric stretching of carboxylate anion (COO^-), bands 1228 and 1165 cm^{-1} are attributed to the C-O stretching and, finally, the bands located at 924 and 796 cm-1 are assigned to the C-O-H out-of-plane bending and CH_2 twisting, see **Figure 4.12(b)** [317, 371, 372, 374, 375]. The same bands with minor shifts and the same assignments can be observed in the FTIR-ATR spectrum of carbopol in **Figure 4.12(a)**.

When two immiscible polymers are brought together, it is expected that the resulting infrared spectrum will be the sum of the spectra the individual compounds because the polymers will have the same environment of the pure state [374]. When the polymers are by contrary miscible, intermolecular interactions may occur and will be reflected in changes on the infrared spectra of the mixture such as wavenumber shifts, band broadening and new absorption bands that are evidence of the polymers miscibility [374]. Furthermore, the films are prepared at pH 6.1 and, at this point, the degree of ionization of the polymers is approximately 50%, see **Figure 4.6**. For this reason it is expected to find the characteristic absorption bands of the NH_3^+ and COO^- groups in the FTIR-ATR spectra of the films.

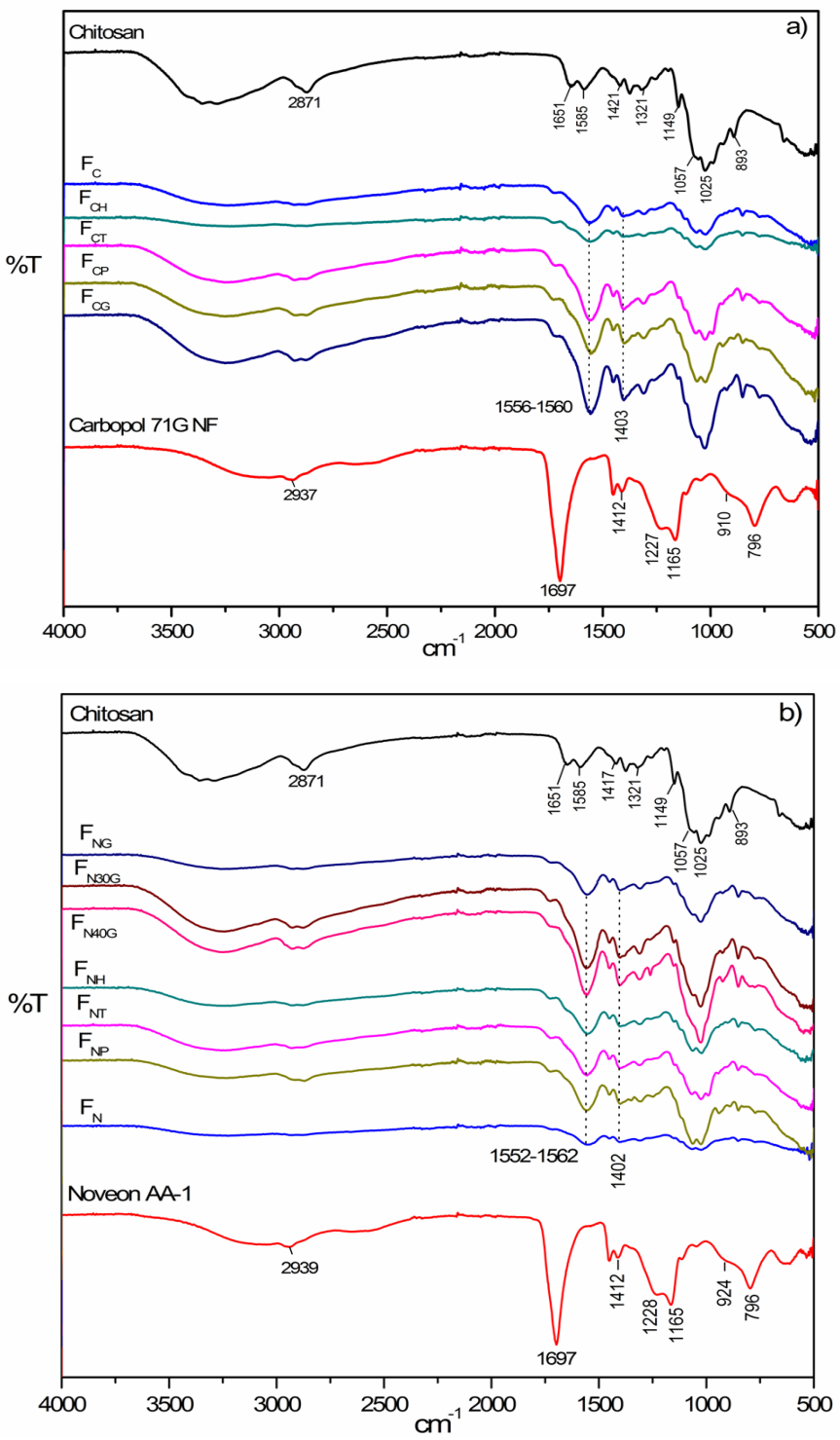

Figure 4.12. The FTIR-ATR spectra of chitosan, carbopol (a), noveon (b) and PEC films.

A new and strong peak located between 1552-1562 cm^{-1} in the chitosan/noveon films and 1556-1560 cm^{-1} in the chitosan/carbopol films can be observed in the FTIR-ATR spectra of each film in **Figure 4.12**. This band can be attributed to the overlapping of the peaks due to the asymmetric COO- stretching vibration of PAA and the NH_3^+ asymmetric bending vibration of chitosan that are reported in the literature to be located between 1550-1610 cm^{-1} and 1570-1620 cm^{-1}, respectively [372, 375, 376].

This result clearly indicates the formation of the polyelectrolyte complex between chitosan and the PAA in the absence and in the presence of additive contents as high as 40%. Another peak detected in all films at approximately 1402 cm^{-1} is a further evidence of the interaction because it is attributed to the symmetric COO^- stretching vibration [317, 372, 374, 376].

Table 4.4 Main FTIR bands of chitosan and respective assignments.

Sample	Peak position (cm^{-1})	Vibrational mode
Chitosan	893,1025, 1057, 1149	C-O-C stretching (cyclic ether)
	1321	Amide III band (chitin): N-H stretching
	1375	C-H bending
	1421	N-H stretching of the amide and ether bonds
	1585	Amine I (chitosan): N-H bending
	1651	Amide I band (chitin): C=O stretching
	2871	C-H stretching
	3280	OH stretching vibration
	3361	Amide I (chitin): NH2 asymmetric stretching

In order to obtain a better insight into the complexation behavior in these systems, a chitosan oligomer and a polyacrylic acid oligomer made up of 6 and 12 monomers, respectively were placed in a simulation box with water and 6 Na^+ counter-ions in order to keep the whole system neutral (**Figure 4.13**).

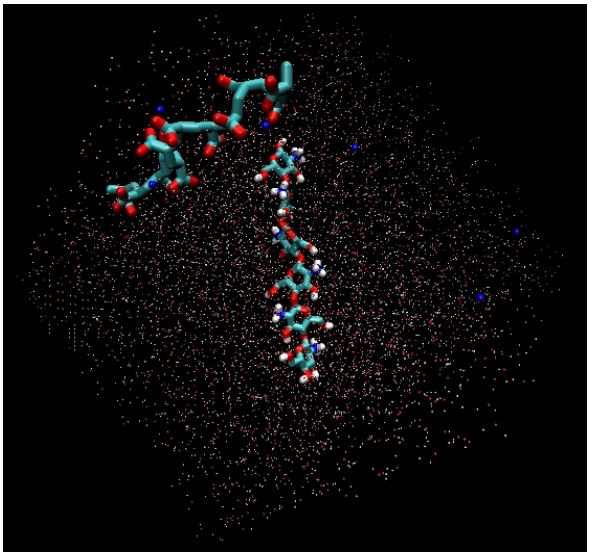

Figure 4.13 Snapshot of the initial simulation box with chitosan on the center and PAA on the left. The two polymer chains are separated from each other and are represented as sticks. The water is depicted with points and the sodium conteriuns represented as blue spheres.

There is a clear propensity for complexation between the $–NH_3^+$ in the chitosan and the $–COO^-$ groups in the PAA chain, as can be seen from the fact that they were initially placed in positions significantly separated in the simulation box (**Figure 4.13**) and they are driven together during the equilibration run (**Figure 4.14)**.

In order to obtain a general idea of the Coulombic interactions, the radial distribution function [g(r)] for the positivelly charged $–NH3^+$ group in chitosan and the negativelly charged $–COO^-$ group in the PAA is presented (**Figure 4.15)**. The g(r) gives the probability of finding a particle anywhere in the distance r of another particle. The g(r) on **Figure 4.15** presents two main peaks located at 0.33 nm and 0.55 nm. The maximum of g(r) at 0.33 nm suggests a close proximity between the oppositelly charged groups of the polymers due to strong electrostatic interactions. The attractive interchain interactions between chitosan and PAA were further confirmed by the calculation of the minimum distance between the centers of mass of both polymers. The average minimum distance is small ($0.23 \pm 2.7x10^{-4}$ nm) and tends to decrease during the MD run (**Figure 4.16**).

The results of the MD simulations confirm the electrostatic nature of polymer/polymer interactions within the network, between the cationic and anionic groups.

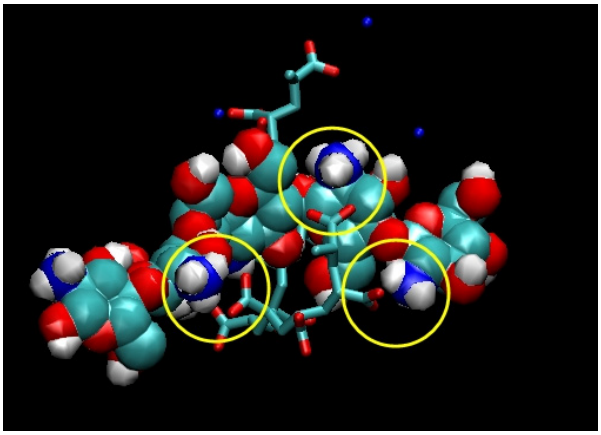

Figure 4.14 Snapshot of the molecular dynamics simulations box showing the interaction between the $–NH3^+$ groups (blue) in chitosan and the $–COO^-$ groups in the PAA marked by the yellow circles. Chitosan chain is shown using the van der Waals radii and the PAA is depicted in sticks for clarity. Sodium counterions are depicted in blue.

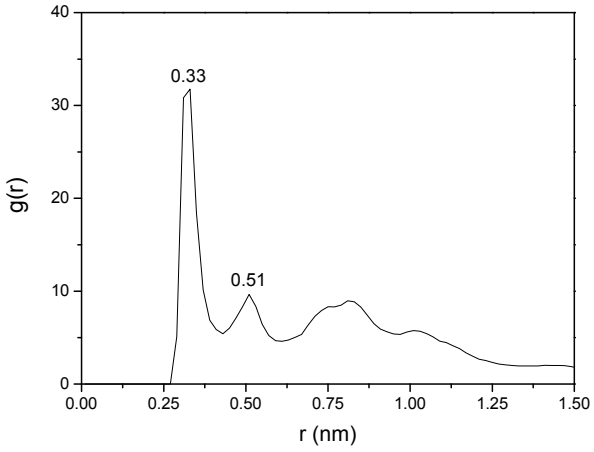

Figure 4.15 Radial distribution function for the positivelly charged $–NH3^+$ group in chitosan and the negativelly charged $–COO^-$ group in the PAA.

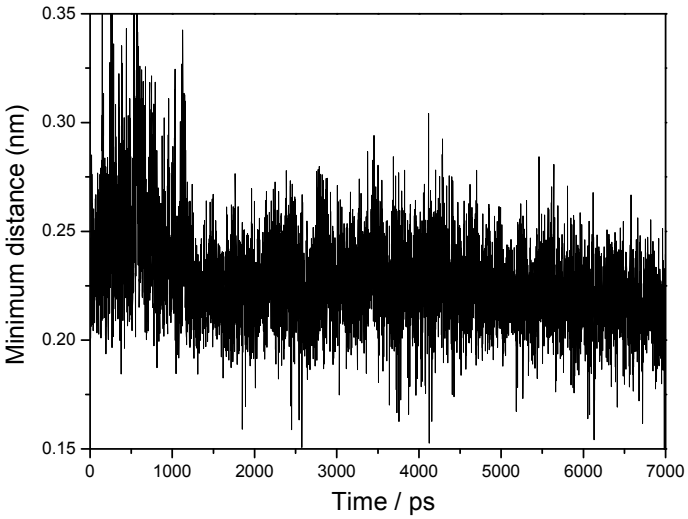

Figure 4.16 Minimum distance (nm) between the centers of mass of the two polymers during the MD run.

4. Conclusions

PEC films with maximized electrostatic interactions were successfully prepared from chitosan and two PAA polymers with different crosslinkers and crosslinking density. The formation of the PEC was confirmed by FTIR-ATR, DSC, MD simulations and it is possible to incorporate additives up to 40% of the dry polymer weight without disturbing the formation of the PEC.

Chitosan/noveon films are shown to be more flexible and more permeable to water than the correspondent chitosan/carbopol films. PEG200 and trehalose decreased the flexibility of the films and glycerol was the additive with best influence in the film properties improving the flexibility, resistance and WVTR with a maximum effect at 30%. The PSA significantly improved bioadhesion without a significant effect upon the resistance and flexibility of the films.

The optimized film (F_{Na}) has shown very good flexibility, resistance and bioadhesion which make it a very promising film for application in the skin. Also, the WVTR measured is higher than the normal TEWL so this film can be applied on skin

without the risk of a significant interference in the barrier function or causing sensitization due to occlusion.

The development of this film continues in Chapter V, with the incorporation of different drugs and by the determination of the drug release profiles and drug permeation through the skin in order to evaluate the feasibility of using these films as versatile skin delivery systems.

V

Polyelectrolyte complexes as universal skin drug delivery systems

1. Introduction

A thin, bioadhesive and transparent film based on chitosan and PAA with functional properties (e.g. tensile strength, elongation to break, water vapor transmission rate) optimized for skin drug delivery has been developed and the results were presented on Chapter IV. The aim of the present work is to test the release and delivery performance of the drug-loaded films in order to evaluate the feasibility of using these films as versatile transdermal delivery systems capable of including different drugs.

For this purpose, four drugs with different physicochemical properties were incorporated in the films: ibuprofen (IBU), galantamine free base (GB), galantamine HBr (GS) and paracetamol (PAR). The structures and physicochemical properties of the drugs [377, 378] are given in **Figure 5.1**. IBU and PAR were used as model lipophilic and hydrophilic drugs, respectively, but we note that a patch containing either of these can offer several advantages for pediatric use.

Galantamine is a therapeutically relevant cholinesterase inhibitor used in the treatment of Alzheimer's disease (AD), with a relatively short half-life (5-7 h), 88.5% oral bioavailability and doses ranging from 4-12 mg twice a day [379, 380]. The most common adverse effects reported in clinical trials include nausea, vomiting, diarrhoea and weight loss [379, 381].

Ibuprofen

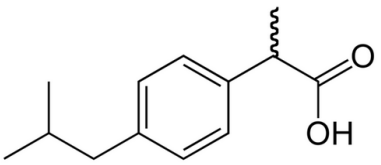

MW 206.285
MP (ºC) 75-77
Log P 3.48 [377]

Galantamine base

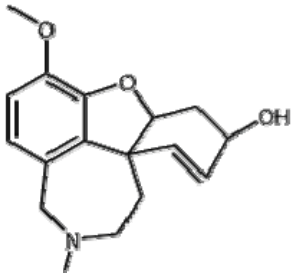

MW 287.35
MP (ºC) 127-128
Log P 2.369 [378]

Galantamine HBr

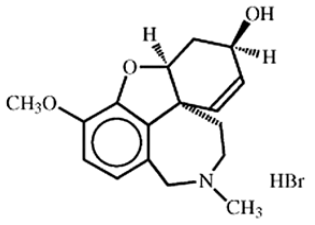

MW 368.27
MP (ºC) 269-270
Log P 1.09 [377]

Paracetamol

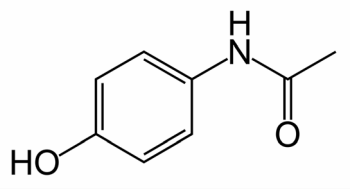

MW 151.163
MP (ºC) 169-171
Log P 0.5 [377]

Figure 5.1 Structure and physicochemical properties of the drugs used in this study, from the references [377] and [378] as indicated.

AD is a fatal and progressive neurodegenerative condition characterized by increasing cognitive deficits (e.g. memory loss) as well as progressive functional and behavioral disorders that result in the inability to perform basic activities of daily living and the need for constant caregiver assistance [379-382]. Prevalence studies indicate that the percentage of persons with AD increases with age and since it is expected a high and continuous increase in the life expectancy in the next 50 years it is urgent to find new ways to delay the onset of AD [379-382]. AD therapy involves long-term administration, and the physicochemical and pharmacokinetic characteristics of galantamine predict an effective penetration through the SC. Considering all these features, the transdermal route of drug administration seems to be a feasible option for AD treatment and more advantageous than the conventional dosage forms [4, 92]. On the basis of the above observations, galantamine is a very good candidate for transdermal drug administration.

Two forms of galantamine were used in the present study, the commercially available galantamine HBr (GS), and GB. The conversion of the hydrobromide salt to the corresponding free base increases the lipophilicity of the drug, as indicated by the increase in the log P from 1.09 to 2.369. It also decreases the respective molecular weight (MW) and reduces the melting point (MP), as shown in **Figure 5.1**. These changes in the physicochemical properties favor the permeation of the new entity through the skin and make GB a potentially more satisfactory candidate for skin drug delivery than GS [4, 92].

Another strategy, apart from chemical modification, to improve the flux of drugs through the skin is the selection of an appropriate solvent capable of permeating into the skin and improving drug partition to the SC [383, 384]. In the present study we assess the ability of the solvents PG, transcutol and glycofurol to increase the percutaneous absorption of the drugs. The structure of the solvents is depicted in **Figure 5.2**.

PG is widely used as cosolvent of drugs [385] and penetration enhancers [386, 387] in dermatological formulations and has been described to increase the permeation of drugs alone or in combination with other penetration enhancers [388-391]. PG seems to increase the uptake of drugs by the SC [388, 389] although results from other authors suggest that PG may be incorporated in the head group regions of

lipids by replacing bound water [227] or may induce a protein conformational change from α- to β-keratin [392].

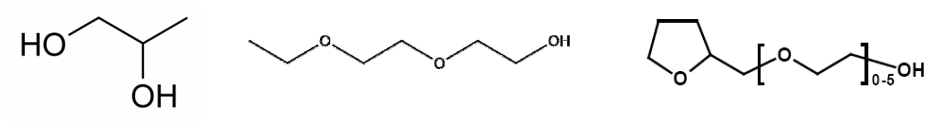

Propylene glycol **Transcutol** **Glycofurol**

Figure 5.2 Structure of the solvents used in the present study.

Transcutol is another solvent extensively used in the study of the permeation of chemicals through the skin and able to enhance the penetration of several compounds probably by altering the solubility of the permeant in the SC [393-396]. In other studies, transcutol decreased the permeation of caffeine and sumatriptan [397, 398] and appeared to be inefficacious in the permeation of testosterone [399]. Transcutol is thus a non universal penetration enhancer, and it is relevant to study its influence in the permeation of drugs with different physico-chemical properties.
Glycofurol is a widely used solvent in parenteral formulations in concentrations up to 50% v/v, nontoxic, non-irritating with a tolerability similar to propylene glycol [400]. Its potential as penetration enhancer in nasal formulations [401, 402] was studied and it does not induce irritation on nude mouse skin [403]. Its potential to increase the skin permeation of drug is also evaluated in the present work.

It should be remembered that the optimized film includes a thin layer of a hydrophilic PSA composed of long chain PVP and PEG400. PVP-PEG400 PSA has been designed for enhanced transdermal delivery of drugs. It has been demonstrated to be compatible with drugs of different physicochemical properties, does not act as a barrier to drug diffusion and it is non-toxic [330-332]. A further objective of the

present study is to evaluate the effect of the PSA in the drug release rate from the chitosan-PAA drug-loaded films.

Drug release studies and *in vitro* skin permeation where performed using Franz diffusion cells. Moreover, several functional properties important to fulfill the therapeutic goals such as WVTR, *in vivo* bioadhesion and irritation potential were also object of study [328, 329].
Finally, the polymer/polymer and polymer/drug interactions were investigated by DSC and FTIR-ATR.

2. Materials and methods

2.1 Materials

Chitosan of low molecular weight, transcutol 99% (diethylene glycol monoethyl ether) and glycofurol (tetrahydrofurfuryl alcohol polyethyleneglycol ether) were purchased from Sigma-Aldrich. Noveon AA-1® (PAA) was a gift from Noveon Inc. (Cleveland, USA) and Galantamine HBr was kindly provided by Grunenthal (Germany). PG and PVP K90 were obtained from Fluka. All other chemical reagents were of pharmaceutical grade.

2.2 Preparation of galantamine free base (GB)

Galantamine free base can be prepared from galantamine HBr (GS) by chemical treatment followed by solvent extraction. A sample composed of six grams of GS was dissolved in 200 mL of ammonia 0.1 M in an Erlenmeyer flask. The GB liberated is then extracted with successive portions of chloroform. The organic extracts are combined and the solvent is removed by rotary evaporation under reduced pressure at 35ºC [404]. The sample obtained by this procedure is then

freeze-dried and stored in the dark. The conversion of the GS to the corresponding free base was confirmed by DSC and FTIR-ATR.

2.3 DSC analysis

DSC analysis was used to confirm the conversion of GS into its free base. DSC thermograms were obtained using a Shimadzu DSC-50 System (Shimadzu, Kyoto, Japan) with nitrogen at a rate of 20 mL/min as the purge gas. Aproximatelly 2-5 mg of freeze-dried samples were accurately weighed into aluminium pans and hermetically sealed. The DSC runs were conducted from room temperature to 400ºC at a heating run of 10ºC/min. Each sample was run in triplicate.

2.4 Preparation of drug saturated solutions and solubility determination

The saturated solutions of each drug were prepared by stirring a suspension of ultrapure water, propylene glycol, transcutol or glycofurol with an excess of drug over a period of at least 24 h at 20 ± 0.1ºC. The saturated solutions were filtered through a 0.45 µm filter and were then analyzed by UV-absorption by means of calibration curves previously validated according to the reference guidelines [405-407]. For details about the validation procedures consult the Appendix. Each experiment was performed with a minimum of 3 replicates.

2.5 Preparation of drug-loaded PEC formulations

Five chitosan-PAA polyelectrolyte complexes (PEC) were prepared for each drug according to **Table 5.1**.

Table 5.1 Composition (% w/w) and coding for each film prepared in this work. Note that the percentage (%) of plasticizer and solvents is given from the corresponding ratio to the total dry weight of the polymers. All films were prepared for each drug.

	F	F_a	F_{ap}	F_{at}	F_{ag}
Chitosan	65.4	65.4	65.4	65.4	65.4
PAA	34.6	34.6	34.6	34.6	34.6
Glycerol	30	30	30	30	30
Propylene glycol			10		
Transcutol				10	
Glycofurol					10
PSA		1 layer	1 layer	1 layer	1 layer

The chitosan solution (1%, w/v) was added by dropwise addition to the PAA suspension and mixed with a mechanical stirrer. The plasticizer (glycerol) concentration was fixed at 30% of the total dry weight of the polymers according to the previous work. After the addition of the plasticizer, 6% and 10% (w/dry polymer weight) of each drug and solvent, respectively, were added prior to the neutralization of the suspension with NaOH 1M until pH of 6.1.

Film forming solutions were cast on Petri-dishes and dried at 35ºC for about 48 h. An adhesive solution composed of 67 wt % PVP K90 and 33 wt % PEG400 was applied to the films by the solvent casting technique and the solvent was evaporated again at 35ºC according to the previous work.

2.6 FTIR-ATR analysis

FTIR-ATR spectra of the dried drugs and film samples were recorded with a Magna-IR™ spectrophotometer 750 (Nicolet, USA) using the ATR sample technique on a ZnSe crystal. Samples were scanned 64 times over the wavenumber range of 400 to 4000 cm^{-1} and a resolution of 4 cm^{-1}.

2.7 Film thickness

The thickness of each film was measured at six different places using a micrometer. Mean and SEM values were calculated.

2.8 WVTR

Three film samples were tested for each type of film. The WVTR ($g/m^2.h$) was measured using a Vapometer (Delfin Technologies Ltd, Finland). Briefly, the film specimens were mounted and sealed in the top of open specially designed cups filled with distilled water up to 1.1 cm from the film underside and left to equilibrate four one hour at room temperature (22-23ºC, 42-46% RH). The Vapometer has a closed measuring chamber not sensitive to external airflows with a humidity sensor that enables measurements of the films water permeability in normal room conditions [341].

2.9 *In vivo* skin bioadhesion and irritation

Eight volunteers, 2 males and 6 females, aged 27 to 52 years old participated in this study. After being fully informed about the nature and procedures of the study, they provided their written informed consent. The volunteers had normal healthy skin and none had any earlier history of skin disease. Circular films of the placebo formulation were manually attached to the skin of different zones of the body, see **Figure 5.3**. During the 24 h of the study, all volunteers were allowed to carry out normal day activities. The *in vivo* skin bioadhesion and skin irritation potential were evaluated according to the scoring systems of the reference literature [408, 409].

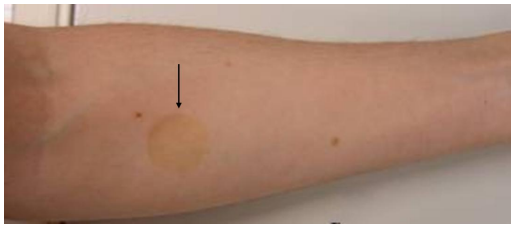

Figure 5.3 Circular placebo film attached to the arm of a volunteer.

2.10 *In vitro* drug release studies

In vitro drug release tests were performed by means of modified Franz diffusion cells with a diffusion area of 1.327 cm^2. The receptor chamber is kept at 37 ± 0.1 ºC and filled with acetate buffer pH 5.5 in order to simulate the skin surface pH. The buffer was previously filtered in vacuum through a 0.45 µm Millipore filter, followed by 15 minutes at 40ºC in ultrasounds in order to prevent the formation of air bubbles between films and receptor medium during the release experiments.

Each film is sandwiched between the donor compartment and the receptor compartment. The drug release was determined by spectrophotometric detection at 221 nm for IBU, 289 nm for GB and GS, and 243 nm for PAR. The UV/Vis spectroscopical methods for the quantification of the drugs were successfully developed and validated. For the details concerning the validation procedures consult the Appendix.

The *in vitro* drug release studies were also conducted using for the saturated solutions of each drug but in this case the donor and the receptor compartment are separated by a non-rate-limiting dialysis membrane (Visking Co., Chicago, USA) [410] and the solutions are applied in the donor compartment.

Drug release studies were conducted during 4 hours and the measurements were recorded each 5 minutes. The exact volume of the receptor chamber was measured

at the end of each experiment so as to accurately calculate the cumulative drug release of each drug.

In order to analyze the drug release mechanism, two mathematical models were tested, the zero order and Higuchi models [411, 412]:

$$Q_t = Q_0 + K_0 t \quad (\mathbf{5.1})$$

$$Q_t = Q_0 + K_H t^{1/2} \quad (\mathbf{5.2})$$

where Q_t is the amount of drug released in time t, Q_0 is the initial amount of drug in solution (e.g. as result of a burst effect), K_0 is the zero-order release constant and K_H is the Higuchi release constant. Values of the coefficient of determination (R^2) were also calculated.

2.11 *In vitro* drug permeation studies

The permeation experiments were conducted using pig epidermal membranes prepared by the heat separation technique. Pig ears were obtained from a local slaughterhouse and the skin free from hairs is separated from the ear. The whole skin is immersed in water at 60ºC for two minutes, after which the epidermis is peeled off from the underlying tissue according to the recommendations of the guidelines [184, 187, 188, 413], see **Figure 5.4**.

Epidermal membranes are stored at -20ºC in an aluminium foil until use. It was previously shown that no changes occur in the skin permeability with these conditions when compared with fresh skin [414, 415].

The epidermal membranes are mounted in Franz diffusion cells with the dermal side in contact with isotonic PBS, pH 7.4, as receptor fluid that is continuously stirred and maintained at 37 ± 0.1 ºC during the time of the study [187], see **Figure 5.5**. This is a physiologically adjusted buffer used to mimic the permeation through the skin into the systemic blood system. Sink conditions are maintained during the study.

The procedures described for the *in vitro* drug release studies to avoid the formation of air bubbles in the receptor medium and for the quantification of the drugs are also applied in these drug permeation studies.

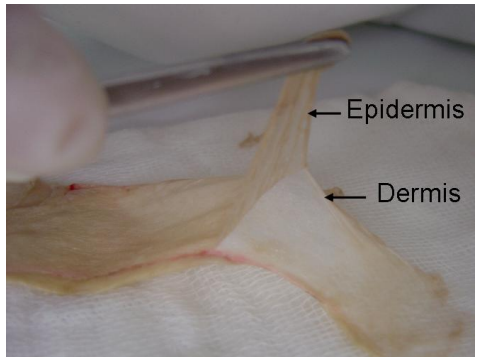

Figure 5.4 Illustration of the epidermal membranes preparation by the heat separation technique.

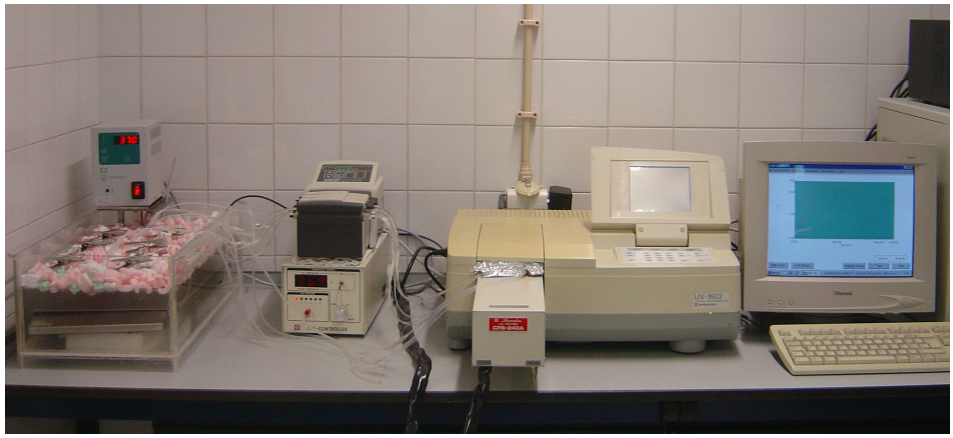

Figure 5.5 Integrated system used in the *in vitro* drug release studies and *in vitro* permeation studies.

Prior to each test, the integrity of all epidermal membranes is evaluated as required by the reference guidelines [184, 187, 188] through the measurement of the TEWL using the Vapometer described above. The measurements of TEWL are performed

under standardized conditions in order to assure the reliability of the results [416]. The epidermal membranes with high TEWL values are considered damaged and are discarded prior to the study.

The *in vitro* drug permeation studies were conducted using the saturated solutions of each drug, and the drug-loaded films. In the case of the saturated solutions the donor compartment was covered with parafilm in order to avoid the evaporation of the solvent.

The cumulative amount of drug permeated (Q) is plotted against time (t) and the flux is determined from the linear portions of the plots according to Fick's first law of diffusion [**Equation (1.1)**].

The enhancement ratio of the formulation (ER_f) is determined by dividing the flux, the cumulative drug permeated at 24 h and 48h (Q_{24h} and Q_{48h}) of each drug-loaded film by the respective value determined for the saturated solutions.

2.12 Statistical analysis

Results are expressed as mean ± standard error. The significance of the differences between values was assessed using a two sample t-test with a statistical significance level set at P = 0.05.

3. Results and Discussion

3.1 Preparation of GB

The conversion of GS to its free base form was confirmed by DSC, as can be observed in **Figure 5.6** and from the FTIR-ATR spectra of the molecules in **Figure 5.7(a)**.

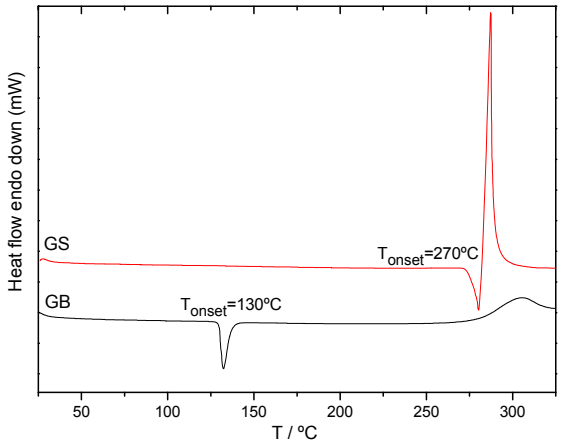

Figure 5.6 DSC thermograms of the two forms of galantamine conducted in the same analytical conditions.

In the DSC thermograms of **Figure 5.6** it is possible to observe a reduction of ca. 140ºC in the onset temperature of melting, from 270ºC in GS to 130 ºC in GB. These values are in accordance with those found in the literature for these molecules [377].

In the FTIR-ATR spectra of GS and GB [**Figure 5.7(a)**] it is possible to observe the characteristic absorption bands of galantamine at 1624/1619 cm^{-1}, 1587/1595 cm^{-1}, 1512/1508 cm^{-1}, 1437/1441 cm^{-1} and 1282/1279 cm^{-1}, respectively [417]. The FTIR-ATR spectrum of GS displays additional bands characteristic of tertiary amine salts between ~2600 and 2400 cm^{-1} [418], see **Figure 5.7(a)**.

3.2 Solubility studies

The solubilities of IBU, GB, GS and PAR in the three solvents tested are listed in **Table 5.2**. It is seen that the water solubility of the drugs does not follow the log P values of the drugs (**Figure 5.1**). Instead, it increases in the order IBU << PAR ~ GB < GS. The water solubility of IBU is much smaller than the values determined for the other drugs being PAR, GB and GS, respectively, 13, 14 and 34 times more soluble. When analyzing the relative solubility of the four drugs in propylene glycol, transcutol

and glycofurol the solubility in the three solvents increases in the same order, GS < GB < PAR < IBU.

Table 5.2 Solubility of the drugs in the different solvents under study, in (mg/ml) at 20 ± 0.1ºC (n=3).

Solvent	Solubility (mg/ml)			
	Paracetamol	Galantamine HBr	Galantamine base	Ibuprofen
Water	12.2	31.3	12.8	0.93
PG	53.1	4.7	51.4	153.1
Transcutol	180.7	1.0	146.4	364.1
Glycofurol	193.8	0.9	108.5	441.1

Table 5.3 WVTR and thickness of the different drug-loaded films according to the coding of Table 5.1. Results are expressed as mean (± SEM), n=9 (WVTR), n= 6 (thickness).

		F	F_a	F_{ap}	F_{at}	F_{ag}
WVTR	**IBU**	12.9 ± 0.3	21.5 ± 0.6	16.6 ± 0.4	12.5 ± 0.4	19.6 ± 0.7
($g/m^2.h$)	**GB**	13.1 ± 0.4	13.5 ± 0.3	13.3 ± 0.63	13.0 ± 0.7	14.4 ± 0.4
	GS	15.1 ± 0.5	13.5 ± 0.3	15.8 ± 0.6	15.1 ± 0.4	13.1 ± 0.5
	PAR	9.2 ± 0.2	11.0 ± 0.4	14.7 ± 0.3	13.7 ± 0.5	13.8 ± 0.7
Thickness	**IBU**	125.0 ± 2.2	112.5 ± 2.8	128.3 ± 3.8	115.8 ± 3.0	123.3 ± 6.1
(µm)	**GB**	148.3 ± 5.6	110.0 ± 4.8	119.2 ± 5.5	127.5 ± 2.8	128.3 ± 9.0
	GS	132.5 ± 3.3	113.3 ± 3.3	121.7 ± 4.9	134.2 ± 3.5	140.0 ± 5.2
	PAR	114.2 ± 0.8	135.8 ± 2.0	123.3 ± 4.6	123.3 ± 2.1	125.8 ± 3.3

WVTR
IBU: $p<0.05$ for F/F_a, F_a/F_{ap}, F_a/F_{at}
GB: $p>0.05$
GS: $p<0.05$ for F/F_a, F_a/F_{ap}, F_a/F_{at}
PAR: $p<0.05$ for F/F_a, F_a/F_{ap}, F_a/F_{at}, F_a/F_{ag}

Thickness
IBU: $p<0.05$ for F/F_a, F_a/F_{ap}
GB: $p<0.05$ for F/F_a, F_a/F_{at}
GS: $p<0.05$ for F/F_a, F_a/F_{at}, F_a/F_{ag}
PAR: $p<0.05$ for F/F_a, F_a/F_{ap}, F_a/F_{at}, F_a/F_{ag}

3.3 Characterization of the drug-loaded films

The drug-loaded films prepared are thin (110-140 μm of thickness, **Table 5.3**), uniform, smooth, transparent and pale yellow. Before the application of the PSA by the solvent casting technique, the films are less transparent, indicating that the drugs are not totally soluble in the polymers. After the application of the PSA the films became clear and transparent, indicating that the drugs are solubilized in a higher percentage.

A possible explanation is that the ethanolic solution of the PSA when applied to the drug-loaded films penetrates the film and dissolves part of the drug. The drug crystallization is probably inhibited by the PVP, since this polymer has shown before to be a very effective crystallization inhibitor [419-421].

The uniformity of the films can be inferred from the low standard error values in the thickness measurements (see **Table 5.3**).

The infrared spectrum of pure IBU and PAR are depicted in **Figure 5.7(a)** and exhibit the characteristic absorption peaks at 1699, 1269, 1230, 1184, 866 and 779 cm^{-1} for IBU [377], and at 3321, 3159, 1651, 1608, 1562, 1504 and 1435 cm^{-1} for PAR [377, 422].

From comparison of the ATR-FTIR spectra of the F films in **Figure 5.7(b)** in the absence and in the presence of the drugs, no interaction is detected between the polymers and PAR, GS and IBU. It is observed the strong peak located between 1556 and 1560 cm^{-1}, attributed to the overlapping of peaks due to the asymmetric COO^- stretching vibration of PAA and the NH_3^+ asymmetric bending vibration of chitosan that are reported in the literature to be located between 1550-1610 cm^{-1} and 1570-1620 cm^{-1}, respectively [372, 375, 376]. This result confirms the formation of the complex between chitosan and PAA, in spite of the incorporation of the drugs in the films. Another peak detected in all films at approximately 1402 cm^{-1} is a further evidence of the polymer/polymer interaction, since it can be attributed to the symmetric COO^- stretching vibration of PAA [317, 372, 374, 376].

In the ATR-FTIR spectrum of GB loaded-film the characteristic bands of the polyelectrolyte complex are masked by the typical infrared peaks of galantamine

[**Figure 5.7 (a)** and **(b)**]. This is probably due to the drug crystallization with formation of agglomerated crystals and a non-homogeneous distribution of GB within the film [423].

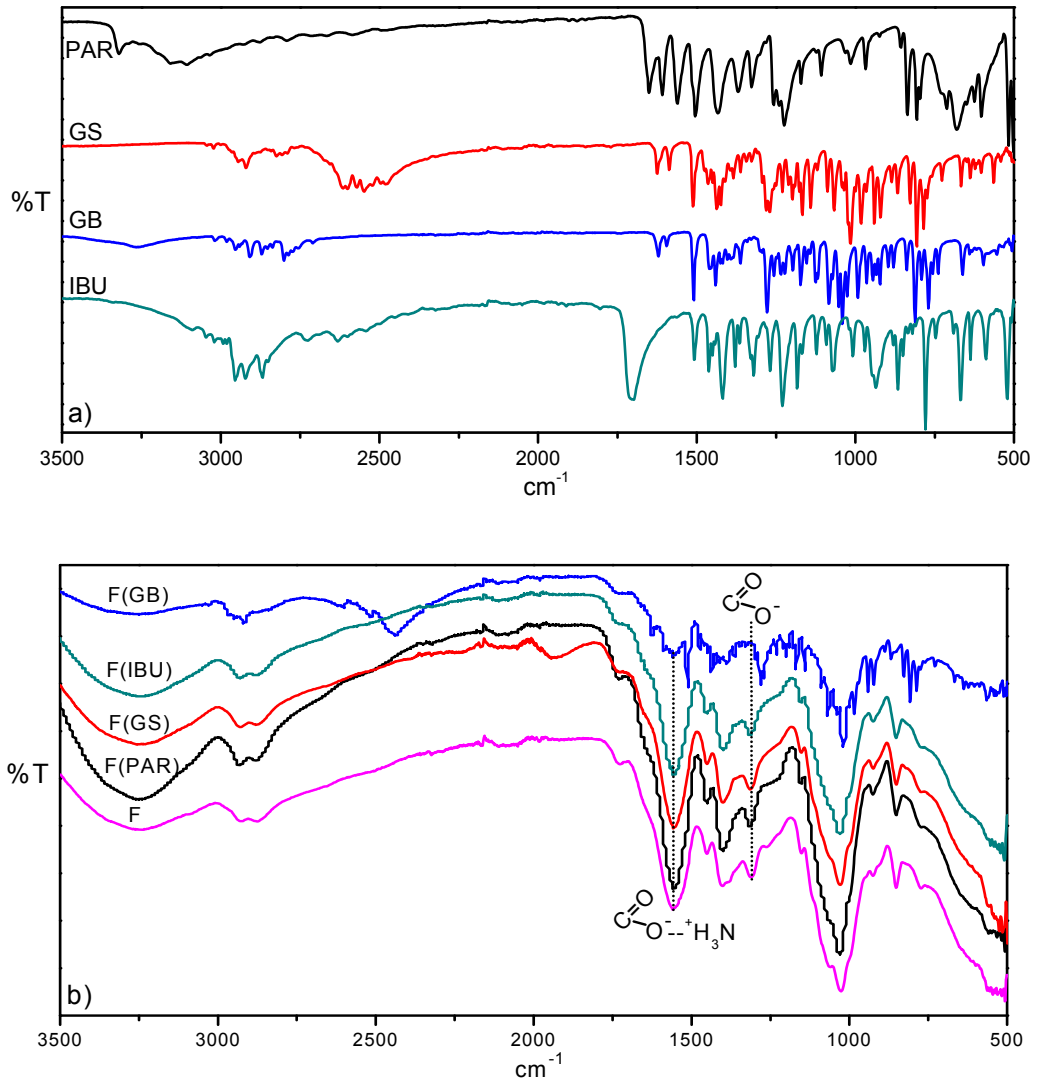

Figure 5.7 FTIR-ATR spectra of the (a) drugs and (b) drug-loaded films.

The investigation of the permeability to moisture vapour (WVTR) of films that are intended to be applied on skin is of major importance, because this property serves to assess the respective occlusive properties. Skin occlusion interferes with the normal TEWL causing profound effects on the skin barrier. These include increasing the percutaneous absorption of applied chemicals and the alteration of epidermal lipids, DNA synthesis, surface pH and bacterial flora [112, 139, 141].
WVTR also serves to indirectly evaluate the density of PEC and it is simultaneously dependent on the solubility coefficient and diffusion rate of water in the film [355].
The values of the WVTR of the films can be found in **Table 5.3**. The first observation is that no significant differences are observed between GB-loaded films.
The adhesive layer increases the WVTR of films loaded with IBU and PAR, while it decreases this value in the case of the GS-loaded films. Transcutol and PG have a similar effect and both increased the WVTR value of films loaded with GS and PAR, and decreased the permeability to water vapour in the films containing IBU. Glycofurol is the solvent with less effect in the WVTR, it only increased the value of this parameter in the films with PAR according to **Table 5.3**.

All the values measured are higher than the normal TEWL in healthy human skin [15, 122, 360], which means that the films display a low potential to interfere with TEWL and cause irritation.

3.4 *S*kin bioadhesion and skin irritation

The evaluation of bioadhesion to the skin is very important in any transdermal delivery system due to the fact that in order to provide a continuous drug supply it is necessary to maintain an intimate and prolonged contact with the skin during the entire time of application [328, 329]. The evaluation of skin irritation is equally relevant because it affects the safety and efficacy of the formulation as well as the patient compliance [409].
In vitro conditions do not allow the assessment of the performance of a film under *in vivo* conditions. Some properties of the skin, such as moisture and elasticity, cannot be accurately reproduced in the *in vitro* tests. In the previous chapter, a quantitative

evaluation of the peak adhesion force and the work of adhesion of this formulation in the absence of drugs have been carried out *in vivo*. In the present study the objective is to evaluate the bioadhesive properties and the skin irritation of the same placebo film in the normal day life activities. The scoring systems [408, 409] used to evaluate the performance of the placebo film concerning bioadhesion and irritation potential are defined in **Table 5.4**. All volunteers reported no signs of irritation (score 0) or discomfort. We conclude that the film is safe for using on the skin during the 24 h application time, and that the patient compliance is predicted to be high.

Table 5.4 Scoring system for the evaluation of skin bioadhesion and irritation of the placebo film reproduced from ref. [409].

Bioadhesion performance
0. ≥ 90% adhered (essentially no lift off from the skin)
1. ≥ 75% to < 90% adhered (some edges only lifting off from the skin)
2. ≥ 50% to < 75% adhered (less than half of the system lifting off from the skin)
3. ≤ 50% adhered but not detached (more than half the system lifting off from the skin without falling off)
4. patch detached (patch completely off the skin)
Irritation potential
0. no evidence of irritation
1. minimal erythema
2. definite erythema, readily visible; minimal edema or minimal popular response
3. erythema and papules
4. definite edema
5. erythema, edema, and papules
6. vesicular eruption
7. strong reaction spreading beyond test site

In relation to the bioadhesion performance, 6 volunteers reported that the placebo film adhered more than 90% (score 0), one subject declared that the film adhered between 75-90% (score 1) and only one volunteer stated score 2. It is thus possible to conclude that the film will be able to assure the fixation of the system during the 24 h application time without lifting off and will be able to provide the desired continuous drug supply.

3.5 Drug release studies

In hydrogels formed by ionic interactions the pH of the release medium influences the crosslinking density and by consequence the degree of swelling [201, 202, 424]. For this reason, it is very important to conduct the release studies in the normal pH of the skin. In the present study, the drug release studies were performed in acetate buffer at pH 5.5, reflecting the physiological skin conditions as advised by reference guidelines [425]. Moreover, drug release from polymer films is also influenced by the physicochemical properties of the drug such as the MW, solubility [318] and by the drug concentration within the polymer network [426, 427].

Figure 5.8 shows the cumulative drug release profiles of PAR, GS, GB and IBU from the saturated solutions, and films F, F_a, F_{ap}, F_{at} and F_{ag}.
The first observation is that the films of all drugs exhibit an initial quick release (burst effect) that is followed by a linear portion indicating a region of constant drug release. The burst effect may be produced by two different effects, the rapid swelling of the films in contact with the release medium and the presence of a high concentration of drug in the surface of the films.
A comparable burst release has been reported in other PEC based on chitosan and PAA [310]. The initial burst release can be beneficial in the sense that it helps to rapidly achieve the therapeutic plasma concentration, and the constant drug release that follows would then provide a sustained and controlled drug release.
The drug release profile of the saturated solutions is clearly related with the lipophilicity of each drug, i. e. the amount of drug released increases as the log P decreases. Except for the case of IBU that is very slightly soluble in water, the

cumulative drug released from the saturated solutions is higher than those determined for the drug-loaded PECs.

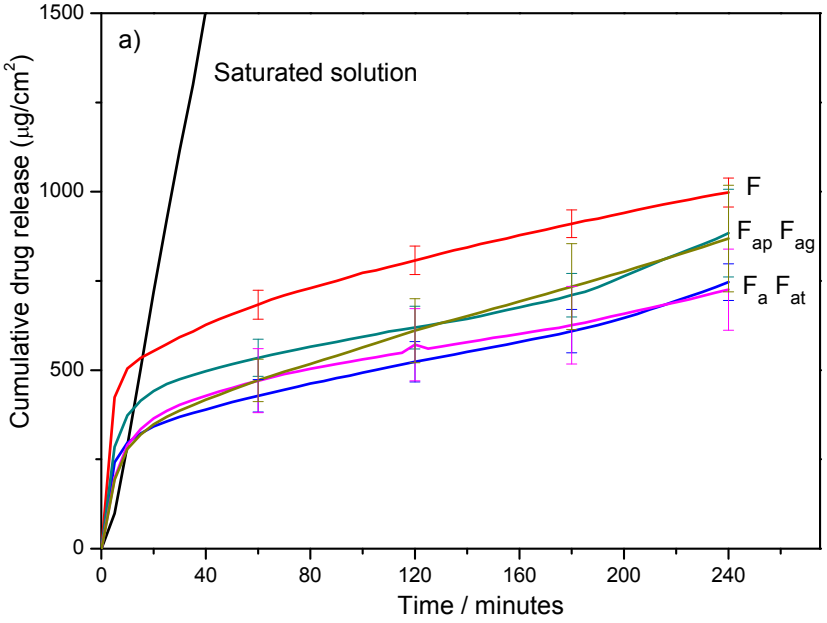

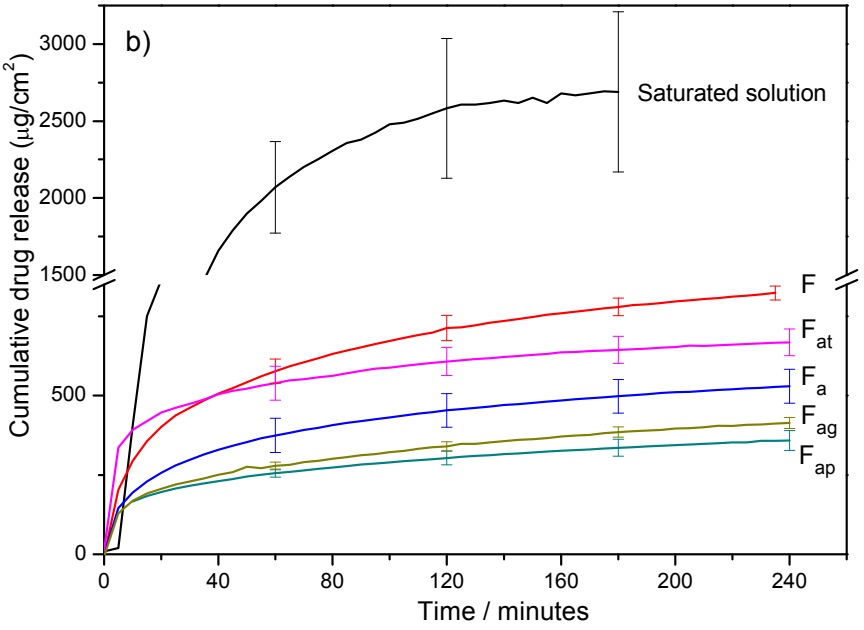

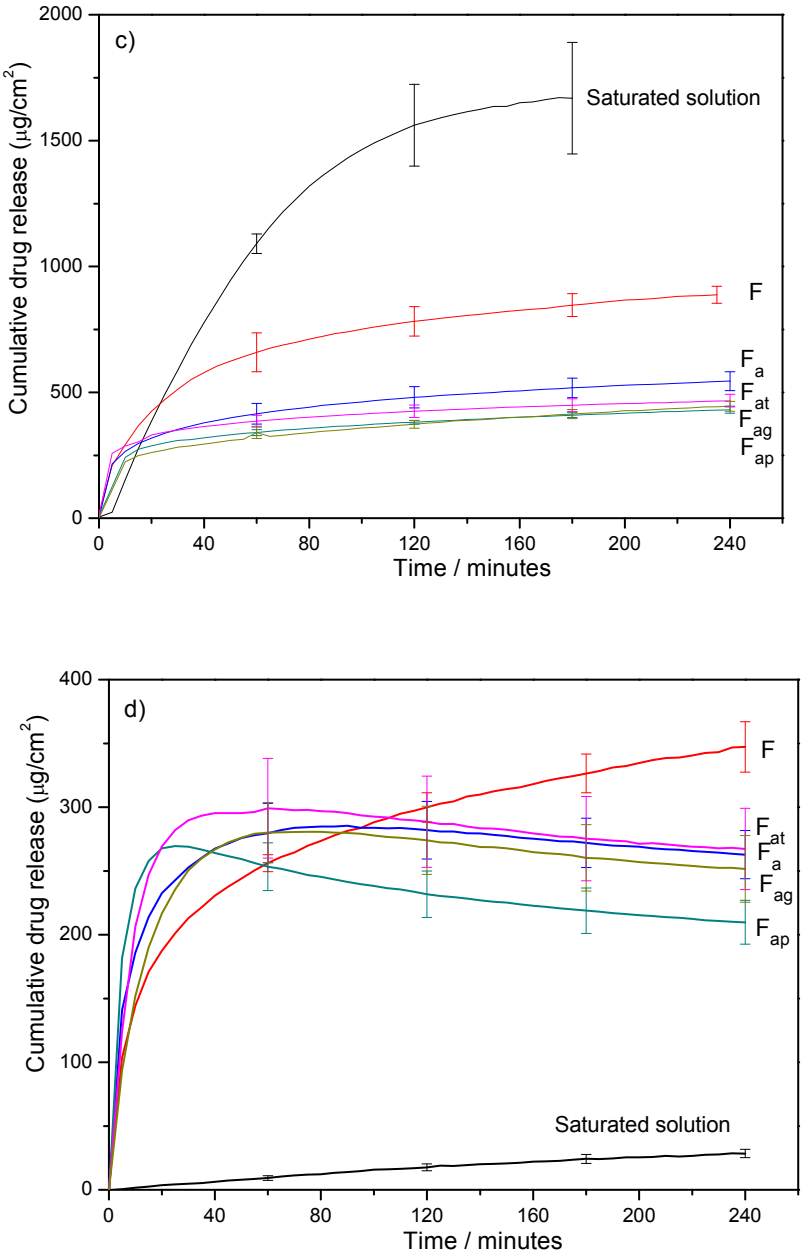

Figure 5.8 Drug release profiles from the saturated solutions and drug-loaded films of (a) paracetamol, (b) galantamine HBr, (c) galantamine free base and (d) ibuprofen. All films are loaded with 6% of drug. Mean (± SEM); n ≥ 3.

3.5.1 Ibuprofen release

The cumulative drug release profile of IBU in the films with adhesive is very unusual, **Figure 5.8(d)**. After an initial burst release that is higher than in the F film, there is a decrease in the total amount of drug in the receptor solution. This effect is more marked in the films with solvents, particularly propylene glycol, as shown in **Figure 5.8(d)**. Although IBU is very slightly soluble in water, the sink conditions are maintained during the entire time of the drug release study so this behavior is not induced by a saturation of the receptor medium.

We believe that the fraction of IBU that is dissolved in the PSA is rapidly released to the receptor medium due to the water solubility of the adhesive, producing the observed burst effect. A decrease in the hydrophilic nature of the films by the inclusion of the solvents and PEG400 from the PSA could explain a higher affinity of the drug to the film partially devoided of PSA in comparison with the release medium. This increased affinity could produce the migration of the drug from the receptor medium to the film. A similar drug release profile has also been observed in our laboratory, from gel formulations loaded with another very lipophilic drug, metronidazole (unpublished data).

3.5.2 Drug release kinetics

The drug release mechanism of hydrogels prepared by mixing the polymer solutions and the drug before the network formation, such as those in the present study, can be influenced by one or more of the following factors: drug diffusion, swelling, reversible drug-polymer interactions and degradation [428]. In order to understand the release mechanism of the films, the released data was fitted to the zero-order release kinetics and Higuchi's square root of time [411, 412, 429]. The *in vitro* kinetic release parameters are presented in **Table 5.5**. Due to the atypical IBU release profile from the films with the PSA layer, only the IBU release data from the F films was adjusted to the mathematical models.

Table 5.5 *In vitro* release kinetic parameters of drug-loaded films.

Code	Drugs	Kinetic models					
		Zero-order kinetics			Higuchi model		
		Q_0	K_0 (μg/h)	R^2	Q_0	K_H (μg/h$^{1/2}$)	R^2
F	IBU	246.8 ± 1.1	26.1 ± 4.9	0.985	**166.0 ± 10.6**	**92.6 ± 15.2**	**0.992**
	GB	640.8 ± 102.0	67.0 ± 19.4	0.974	**451.6 ± 152.0**	**227.4 ± 63.7**	**0.988**
	GS	579.7 ± 56.2	64.8 ± 9.5	0.973	**356.6 ± 59.9**	**242.3 ± 18.6**	**0.982**
	PAR	580.7 ± 42.6	108.7 ± 1.8	0.991	**368.1 ± 38.3**	**313.3 ± 14.7**	**0.998**
F_a	IBU	n.d.	n.d.	n.d.	n.d.	n.d.	n.d.
	GB	402.8 ± 48.0	37.2 ± 2.9	0.980	**292.5 ± 52.6**	**129.3 ± 8.3**	**0.989**
	GS	371.2 ± 55.9	41.2 ± 8.7	0.973	**232.0 ± 66.9**	**152.6 ± 28.1**	**0.989**
	PAR	**326.1 ± 42.8**	**98.4 ± 5.5**	**0.988**	185.4 ± 18.3	245.8 ± 25.8	0.983
F_{ap}	IBU	n.d.	n.d.	n.d.	n.d.	n.d.	n.d.
	GB	321.4 ± 17.4	28.7 ± 7.2	0.982	**250.1 ± 31.1**	**91.8 ± 20.6**	**0.994**
	GS	241.7 ± 11.2	30.5 ± 5.5	0.983	**149.0 ± 11.2**	**107.2 ± 21.0**	**0.995**
	PAR	**469.0 ± 40.4**	**75.5 ± 18.3**	**0.984**	341.2 ± 49.2	202.0 ± 36.5	0.974
F_{at}	IBU	n.d.	n.d.	n.d.	n.d.	n.d.	n.d.
	GB	376.4 ± 26.1	23.5 ± 0.5	0.980	**308.8 ± 23.6**	**80.4 ± 3.2**	**0.993**
	GS	543.5 ± 45.7	32.5 ± 1.0	0.973	**414.7 ± 69.5**	**131.5 ± 15.6**	**0.981**
	PAR	**332.7 ± 46.6**	**82.3 ± 10.4**	**0.988**	172.2 ± 26.8	230.5 ± 35.5	0.983
F_{ag}	IBU	n.d.	n.d.	n.d.	n.d.	n.d.	n.d.
	GB	287.8 ± 8.0	41.1 ± 3.0	0.987	**187.9 ± 6.9**	**130.3 ± 11.2**	**0.998**
	GS	245.3 ± 9.0	44.9 ± 3.6	0.979	**131.4 ± 6.1**	**145.3 ± 7.4**	**0.993**
	PAR	311.6 ± 33.4	110.9 ± 16.3	0.989	**51.4 ± 46.0**	**343.0 ± 67.2**	**0.992**

The zero order (K_0) and Higuchi (K_H) rate constants are established from a linear least square procedure. Points pertaining to the burst release are discarded through direct inspection of the plots. In **Figure 5.9** it can be seen the data points of the GB release from F_{ag} films and the zero order and Higuchi's fit as illustration of the procedure. The drug release data from the films show a good fit to both

mathematical models (high R^2) although in most cases the mathematical expression best describing the drug release after the initial burst release is Higuchi's profile (**Table 5.5**).

Residual analysis confirms this conclusion. In fact, the zero order model does not display a frequent alternation of the sign of residuals [**Figure 5.9**]. Analyzing the values determined both for K_H and $K_{0,}$ we observe that the drug release rates always increases in the order IBU < GB < GS < PAR. The increase of drug release constants are in accordance with the decrease of the log P values of the drugs (**Figure 5.1**).

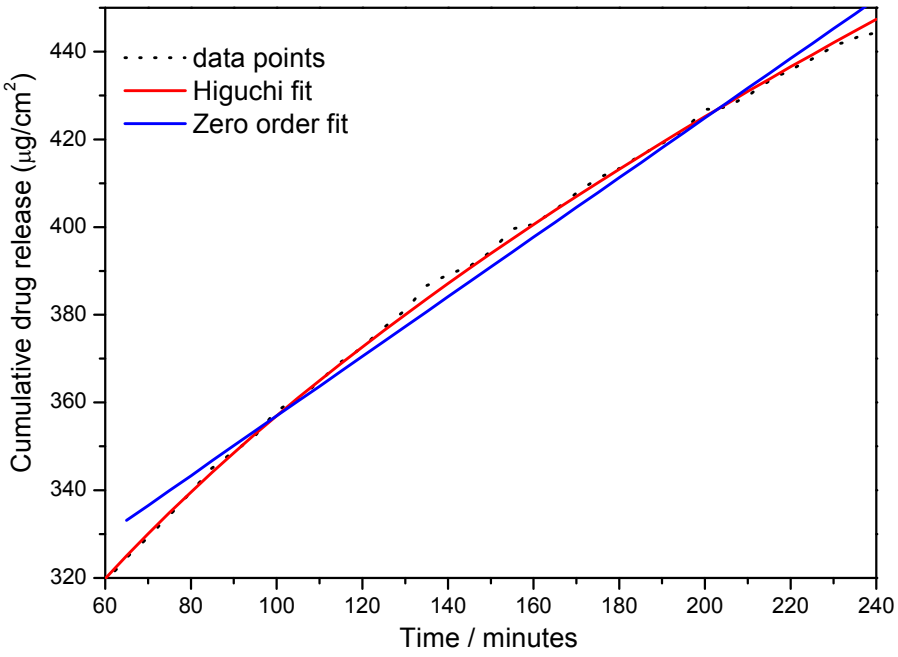

Figure 5.9 Cumulative GB release from F_{ag} films and zero order as well as Higuchi's fitted models.

Analyzing the effect of the adhesive layer and the three solvents tested in the drug release mechanism it is clear that the drug release mechanism is not changed.

Furthermore, the main effect induced by the PSA and the solvents consists of a decrease in the values of the drugs release constants. Note that this is a very beneficial feature, since the main objective is to obtain a formulation with prolonged and sustained drug release over time.

These results indicate that the drug release from the films is mainly controlled by diffusion and follows a quasi-zero order release kinetics. Moreover, the PEC films with maximized electrostatic interactions between chitosan and PAA are able to assure the release of both hydrophilic and lipophilic drugs in a reliable, reproducible and sustained manner.

3.6 *In vitro* drug permeation across pig ear skin

The permeation profiles obtained for each drug are presented in **Figure 5.10** and the calculated parameters are shown in **Table 5.6**.

From **Figure 5.10** it is clear that the drug permeation profiles from the films do not exhibit the typical profile with an initial lag time. Instead, in the early stages of the permeation studies there is an unusually fast permeation followed by a region of constant flux. This effect is maximal in the case of IBU films.

In the evaluation of the film with the best performance, the initial burst effect has to be taken into account. The cumulative drug release at 24 h (Q_{24h}) will be a result of the flux determined in the steady-state and the amount of drug permeated in the early stages of the permeation. The burst effect becomes obviously less important when analyzing, for example, the values of Q_{48h} (see **Table 5.6**, and **Figures 5.10** and **5.11**).
Another important observation is that the IBU permeation from all formulations is much higher than the permeation of the other three molecules under study. Despite the different physicochemical properties of PAR, GS and GB illustrated in **Figure 5.1**, the flux values determined for the three drugs are very similar, as shown in **Table 5.6** and **Figure 5.11**.

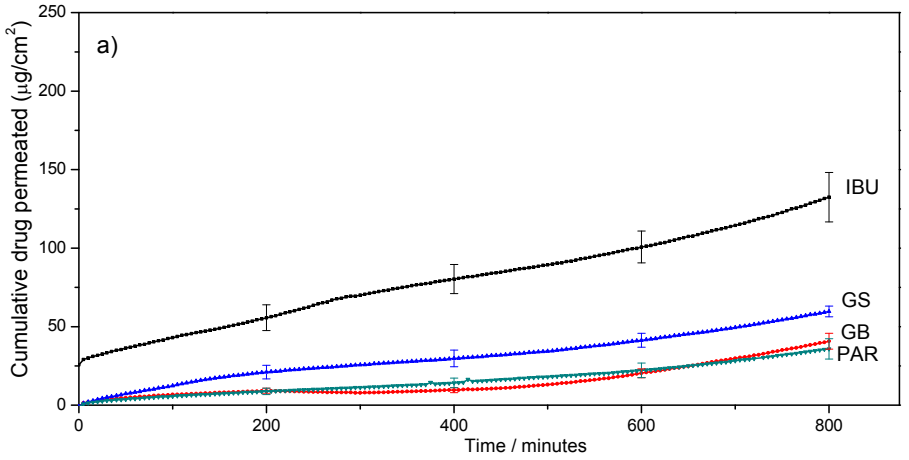
a)
Cumulative drug permeated (μg/cm²)
Time / minutes
IBU
GS
GB
PAR

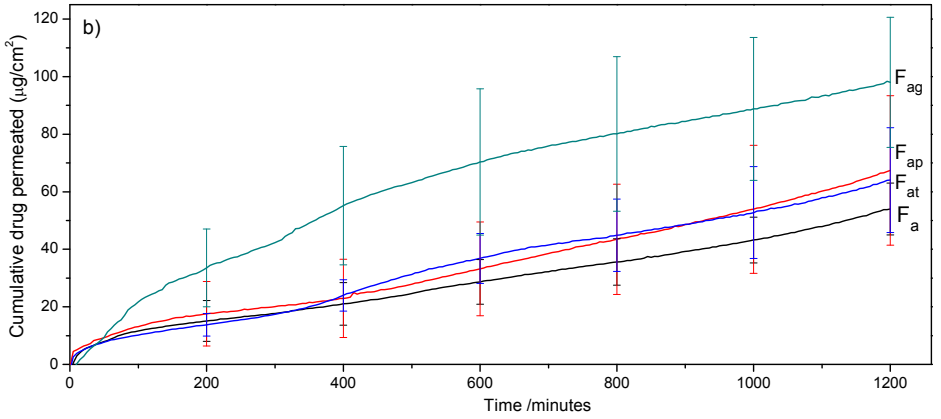
b)
Cumulative drug permeated (μg/cm²)
Time /minutes
F ag
F ap
F at
F a

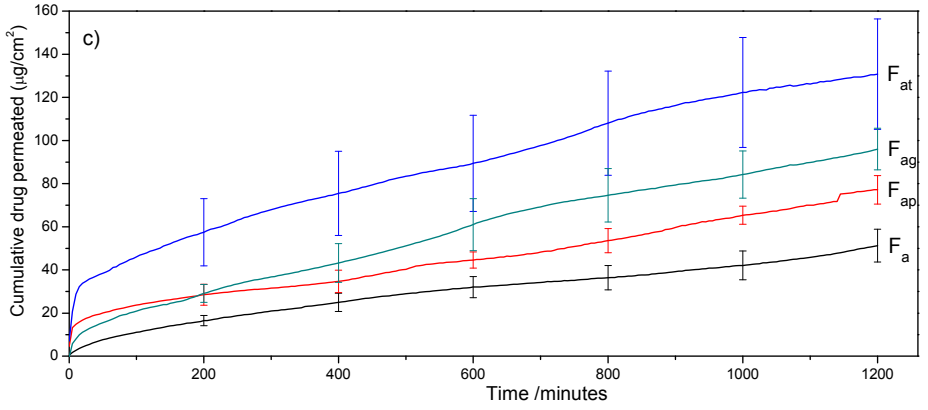
c)
Cumulative drug permeated (μg/cm²)
Time /minutes
F at
F ag
F ap
F a

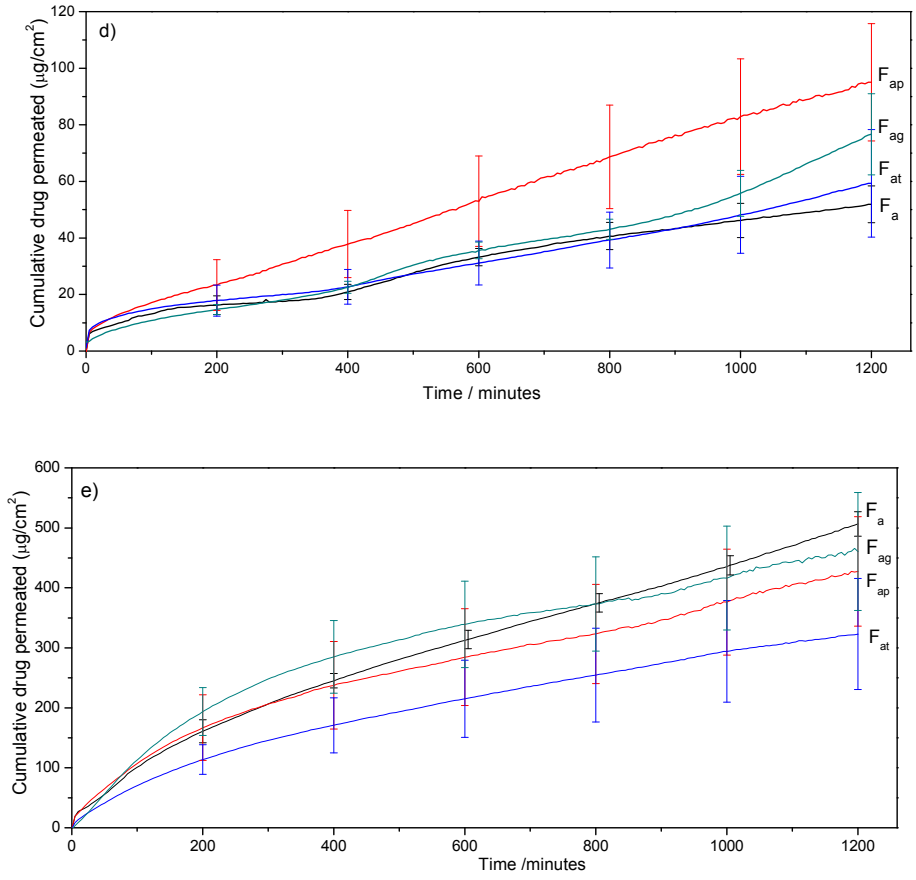

Figure 5.10 Permeation profiles of the drugs from (a) saturated solutions and from the drug-loaded films for (b) paracetamol, (c) galantamine HBr, (d) galantamine base and (e) ibuprofen. All films are loaded with 6% of drug. Mean (± SEM); n ≥ 3.

The cumulative amount of each drug released over time, **Figure 5.8**, is always higher than the amount of drug permeation which indicates that drug release is not a rate-limiting step. The initial "burst" effect in permeation is most probably a consequence of the initial higher drug release rate depicted in **Figure 5.8**. Although unusual, this type of drug permeation profile has been observed before, especially in film formulations [390, 426, 427, 430, 431] but also in HPMC gels [432].

3.6.1 Galantamine HBr and paracetamol

In order to evaluate the drug delivery potential of the films, the permeation of each drug from the respective saturated solutions was considered as reference due to the fact that an equivalent commercial formulation is absent for some of the drug molecules.
The results indicate that there is no significant improvement in the drug permeation in the F_a films of the most hydrophilic drugs (PAR and GS, **Figure 5.1**) when compared to the respective saturated solutions, see **Table 5.6.**

In the case of PAR the drug with the lower log P, glycofurol was the only solvent that produced a significant improvement ($P<0.05$) of the flux and Q_{48h} both in relation to the values determined for the saturated solutions and F_a film [see **Table 5.6** and **Figure 5.11(a)** and **(b)**]. Although PG and transcutol did not produce a significant improvement in PAR permeation some degree of increase is visible for the flux, Q_{24h} and Q_{48h}.
In the case of GS, the flux of the drug in F_a films displayed, rather than an increase, a significant decrease ($P<0.05$). Analyzing the effect of the solvents in comparison with the F_a films, we can see that glycofurol and transcutol induce a significant ($P<0.05$) increase in the flux, Q_{24h} and Q_{48h} while PG produces only a significant increase of Q_{24h} and Q_{48h} (see **Table 5.6** and **Figure 5.11**). The PG result is explained by a higher amount of the drug permeated in the early stages from F_{ap} films, that is reflected in the higher values of Q_{24h} and Q_{48h} [**Figure 5.10(c)**] rather than a significant increase of the flux. Transcutol is the solvent with the best performance, followed by glycofurol.

The results from the films loaded with PAR and GS confirm that glycofurol can act as a skin penetration enhancer, and we believe that the respective mechanism of action should be the object of further research. This result is even more important when taking into consideration that glycofurol produces a better result than PG, a reference molecule known to act as a “universal” skin penetration enhancer [388-391].

Table. 5.6. Permeation parameters of the drugs across pig ear skin. Results are expressed as mean (± SEM), n ≥ 3.

Code	Parameter	Ibuprofen	ER_f	GB	ER_f	GS	ER_f	Paracetamol	ER_f
Saturated solutions	Flux (µg/cm^2.h)	7.1 ± 0.7		1.3 ± 0.1		3.4 ± 0.5		2.4 ± 0.5	
	Q_{24h} (µg)	201.2 ± 19.5		35.2 ± 1.4		88.4 ± 12.6		56.9 ± 11.9	
	Q_{48h} (µg)	370.5 ± 36.0		69.0 ± 4.0		169.4 ± 23.5		113.8 ± 24.2	
F_a	Flux (µg/cm^2.h)	21.5 ± 1.1*	3.1	2.5 ± 0.1*	1.9	2.0 ± 0.3	1.9	2.2 ± 0.4	0.9
	Q_{24h} (µg)	601.9 ± 19.0*	3.0	63.4 ± 7.1*	1.8	58.5 ± 9.1	1.8	60.0 ± 9.7	1.1
	Q_{48h} (µg)	1117.9 ± 41.3*	3.0	118.6 ± 12.5*	1.7	107.3 ± 17.0	1.7	113.2 ± 17.7	1.0
F_{ap}	Flux (µg/cm^2.h)	14.0 ± 2.4*	2.0	4.4 ± 0.9*	3.4	2.5 ± 0.7	0.7	2.9 ± 1.0	1.2
	Q_{24h} (µg)	410.4 ± 91.5*	2.0	114.6 ± 27.8*	3.3	84.3 ± 5.5#	1.0	75.2 ± 29.6	1.3
	Q_{48h} (µg)	746.4 ± 146.7*	2.0	220.2 ± 53.3*	3.3	151.0 ± 32.4*#	0.9	144.6 ± 52.6	1.3
F_{at}	Flux (µg/cm^2.h)	9.2 ± 1.4	1.3	2.4 ± 0.8	1.8	4.8 ± 1.0#	1.4	3.0 ± 1.0	1.3
	Q_{24h} (µg)	280.2 ± 47.4	1.4	65.3 ± 18.7	1.9	157.0 ± 32.4*#	1.8	75.8 ± 22.5	1.3
	Q_{48h} (µg)	501.8 ± 81.7*	1.4	122.0 ± 36.9	1.8	272.9 ± 54.4#	1.6	146.8 ± 45.7	1.3
F_{ag}	Flux (ug/cm^2.h)	14.3 ± 3.4	2.0	3.3 ± 0.6*	2.5	4.2 ± 0.5	2.5	4.2 ± 0.8*#	1.8
	Q_{24h} (µg)	463.0 ± 103.3	2.3	81.2 ± 11.6*	2.3	117.0 ± 15.7#	2.3	122.5 ± 32.5*	2.2
	Q_{48h} (µg)	805.4 ± 183.5	2.2	159.8 ± 25.6*	2.3	218.5 ± 27.5#	2.3	223.1 ± 52.0*#	2.0

***** Statistically significant difference in comparison with the saturated solution (P< 0.05)

Statistically significant difference in comparison with the film F_a (P< 0.05)

3.6.2 Galantamine base and Ibuprofen

The results indicate that there is a significant improvement ($P<0.05$) in the drug permeation in the F_a films of the most lipophilic drugs (IBU and GB, **Figure 5.1**), see **Table 5.6**.

The results of the GB permeation from F_a, F_{ap} and F_{ag} films were significantly higher than the results from the saturated solutions; see **Table 5.6** and **Figures 5.10(d)** and **5.11**. The solvents do not induce a significant increase in the permeation of GB comparing with the F_a films, although PG and glycofurol exhibit a tendency to induce some degree of improvement of permeation with the highest value observed for F_{ap} films.

Comparing the results of the two forms of galantamine (GB and GS) we can conclude that the conversion of the hydrobromide salt to the free base generates a molecule with a higher potential for skin permeation, as expected. Although when analyzing the results for the two molecules in **Table 5.6**, it may seem that the permeation of GS from F_{at} and F_{ag} is higher, if we convert the values obtained to galantamine equivalents, we realize that GB still permeates more easily through the skin in these films.

From the analysis of the permeation profiles from the IBU-loaded films we conclude that, although the drug release from the films show an atypical behavior this fact does not seem to affect the permeation of the drug through the skin. Moreover, the permeation results indicate that transcutol, PG and glycofurol produce a significant decrease in the drug flux, when comparing with values obtained for F_a films, see **Table 5.6** and **Figure 5.11**.

3.6.3 “Supersaturation” effect

It is important to note that, although the concentration of the four drugs is the same in all films (6%), the respective degree of saturation is not, due to the different physicochemical properties of each molecule (**Figure 5.1**).

In the saturated solution, the ratio $C_v / C_{s,m}$ [**Equation (1.2)**] is equal to one; in situations of supersaturation in the films this ratio will exceed one and, as a consequence, the value of the flux increases. The flux is directly proportional to the degree of saturation and this means that the flux of a permeant will be, in principle, the same from different vehicles which do not alter the barrier of the skin, at the same degree of saturation. Moreover, the flux is also determined by the physicochemical properties of the permeant, influencing both D and $C_{s,m}$.

In the present work, the films have a hydrophilic nature. As a consequence, more lipophilic drugs will have a smaller solubility in the films, and consequently, a higher degree of saturation. Moreover, in order to be able to make a direct comparison between the permeation of the different drugs they should be in the same saturation degree on each film. Since this is a very difficult parameter to correctly determine in solid formulations, we prepared films with the same drug concentration.

A “supersaturation” effect could explain the statistically significant improvement of the flux from F_a films of the most lipophilic drugs (IBU and GB) in comparison with the saturated solutions. Furthermore, the higher ER_f observed in the case of the F_a films of IBU, than the corresponding value for the GB case (**Table 5.6**) could also be justified by the same effect.

In fact, not only the log P of IBU is higher than GB, also the major difference is observed in the water solubility, that increases by ~14 times from IBU to GB as discussed earlier (see **Table 5.2**). The water solubility rather than the log P may also explain the approximate ten-fold difference between the IBU flux from F_a films, and the very similar values of the flux of GB, GS and PAR in the corresponding films.

Glycofurol and PG produce a significant decrease ($P<0.05$) of the IBU flux when comparing with values obtained from the F_a film (see **Table 5.6** and **Figure 5.11**). The three solvents dramatically increase the solubility of IBU, as discussed earlier, in the following order: PG < transcutol < glycofurol (**Table 5.2**). The incorporation of these solvents in the films loaded with IBU, most probably reduces the supersaturation degree of the drug in the formulation (**Equation 1.2**), which in turn

reduces the amount of drug permeated over time. This is probably the major effect accounting for the results but is not the only one because the reduction in permeation does not follow the increase in the IBU solubility discussed before. Instead, the IBU permeation increases in the order $F_{at} < F_{ap} < F_{ag}$, according to **Table 5.6** and **Figure 5.11**. This leads us to conclude that the solvents may be also interfering with the skin barrier and influencing the drug diffusion coefficient (*D* in **Equation 1.2**) within the SC.

On the contrary, it seems that the supersaturation effect is not the most important factor influencing the drug permeation of the most hydrophilic drugs (GS and PAR). In fact, not only there is no improvement of the permeation of PAR and GS from the F_a films, in comparison with the saturated solutions, but also in the case of GS it was verified a significant decrease (see **Table 5.6**). This may indicate that the degree of the saturation in F_a films loaded with GS can be smaller than the unity, explaining this reduction. This explanation is also in accordance with the results of the drugs water solubility that indicate that GS is the drug more soluble in water (see **Table 5.2**).

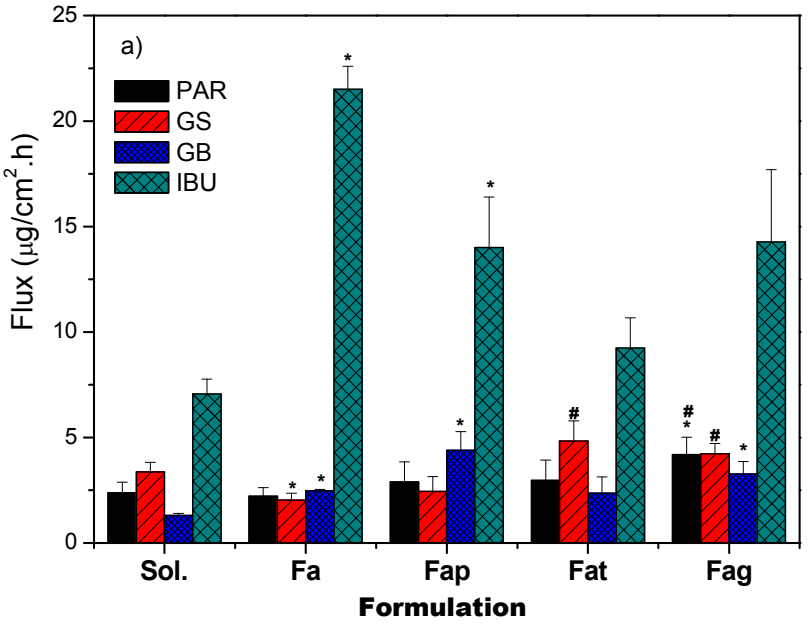

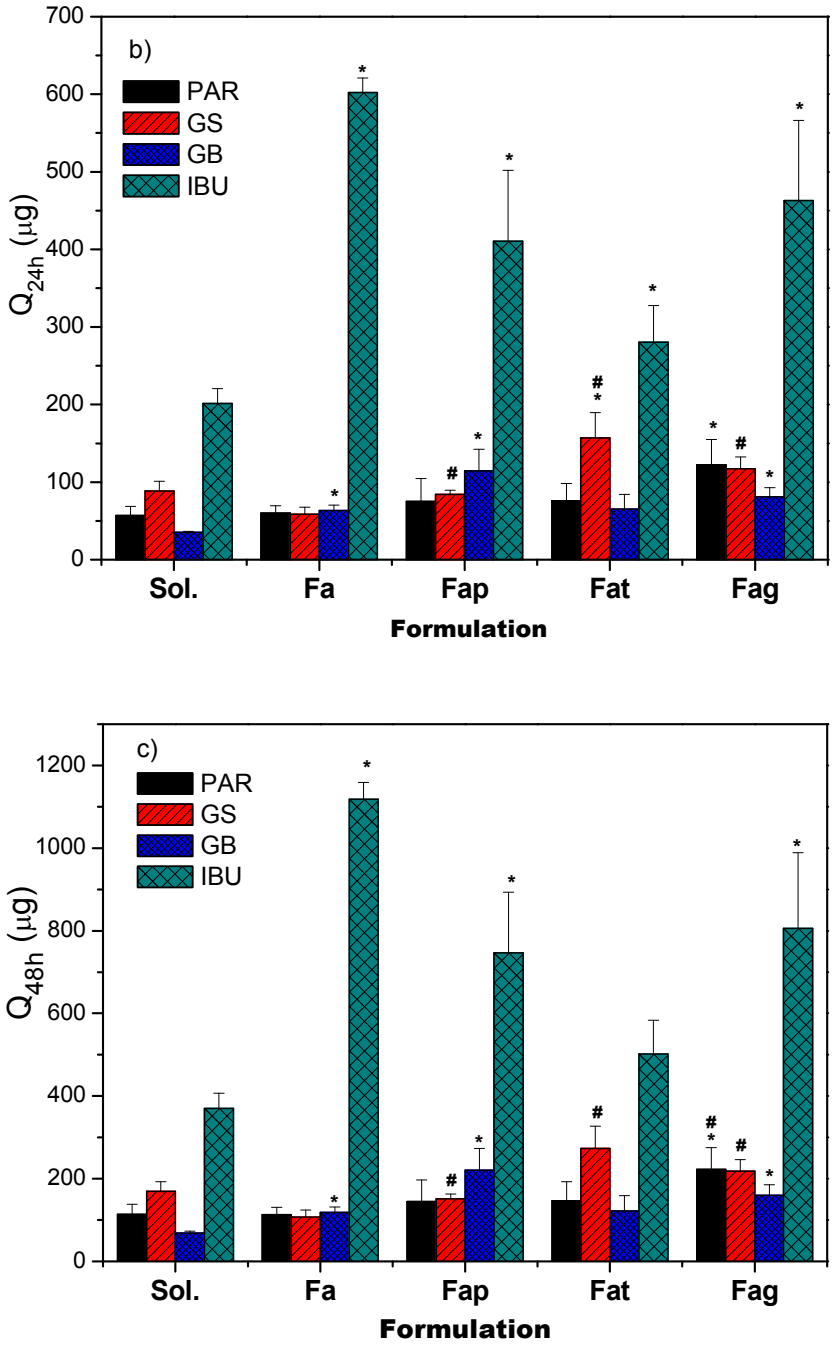

Figure 5.11 Permeation parameters of the drugs calculated from the results of the *in vitro* permeation studies. (a) Flux (µg/cm^2.h), (b) Q_{24h} (µg) and (c) Q_{48h} (µg). The symbol * signals statistically significant difference in comparison with the saturated solution ($P< 0.05$) while the symbol # signals statistically significant difference in comparison with the F_a films. Mean (± SEM).

4. Conclusions

From the data obtained we have demonstrated that the bioadhesive film is water permeable, safe, non-irritating and capable of firmly adhere to the skin for at least 24h. The PEC films with maximized electrostatic interactions between chitosan and PAA are able to assure the release of both hydrophilic and lipophilic drugs in a reliable, reproducible and sustained manner. The PSA decreases the release rate constant that is very advantageous in formulations for sustained drug delivery.

Furthermore, the drug release from the drug-loaded films is mainly controlled by diffusion and follows a quasi-zero order release kinetics.

The shape of the permeation profiles reveals in the early stages an unusually fast permeation followed by a region of constant flux. This behaviour is most beneficial because it enables to rapidly attain the pharmacological action.

Glycofurol can work as a skin penetration enhancer and, in some cases, produces a better result than PG, a reference molecule known to act as a “universal” skin penetration enhancer [388-391].

On the basis of the in vitro permeation results of four molecules with different lipophilicity the film developed is a viable option for the effective delivery of drugs through the skin. Finally, it was shown that it is possible to modulate the drug permeation from the films by adding different solvents.

VI

Optimization of an anti-Alzheimer's transdermal film

1. Introduction

In the previous chapter, two forms of galantamine were tested in order to evaluate the molecule with the higher potential for skin permeation: the commercially available galantamine HBr (GS) and galantamine free base (GB). GB demonstrated a higher capacity to permeate the skin and will be used in the present study.

The selection of an appropriate vehicle is very important for the percutaneous absorption of drugs, along with a proper choice of the physicochemical properties of the permeant. The screening study previously carried out to evaluate the ability of different solvents (PG, transcutol and glycofurol) to enhance the permeation of galantamine showed that PG is, among the solvents tested, the one that induced the maximum GB flux. PG is widely used as cosolvent of drugs [385] and penetration enhancers [386, 387] in dermatological formulations, and has been described to increase the permeation of drugs alone or in combination with other penetration enhancers [388-391]. PG seems to increase the uptake of drugs by the SC [388, 389], although it is also suggested that it may be incorporated in the head group

regions of lipids by replacing bound water [227], or may induce a protein conformational change from α- to β-keratin [392].

The aim of the present work is to determine the ability of Azone and NMP (N-methyl pyrrolidone), alone and in combination with PG, to improve the *in vitro* skin permeation of GB. Azone and NMP were selected on the basis of their penetration enhancing properties, different mechanism of action and the synergistic effect demonstrated in other studies with PG [138, 433-435].
Azone has the ability to partition into the lipid lamellae of SC, where it produces a fluidizing effect responsible for the enhancement of drug permeation [219, 436]. NMP acts directly on the aqueous regions of the SC, altering the solubilizing ability of these regions to the drugs. This action favours skin permeation by increasing the partition coefficient of the drugs into the SC [130, 389, 434]. The structure as well as some physicochemical properties of PG, Azone and NMP can be found in **Figure 6.1**.

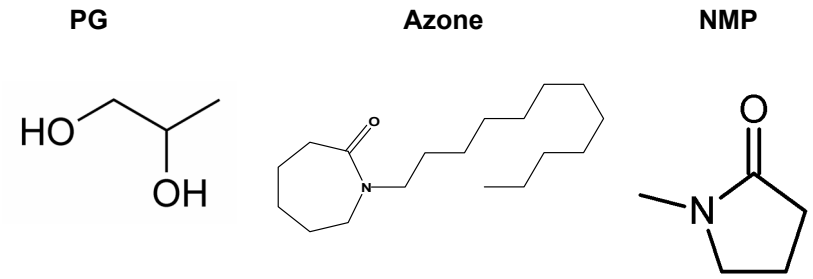

	PG	Azone	NMP
MW	76.09	281.48	99.13
MP (ºC)	-42.4	-7 ºC	-24ºC
Log P	-0.47	6.21	-0.38

Figure 6.1 Structure and physicochemical properties of the penetration enhancers.

In the present study, the effect of Azone, NMP, PG and their interaction effects were evaluated using experimental design techniques, namely factorial design and

surface response methodology [437, 438], in order to optimize the GB permeation through the skin. The application of factorial design to the optimization of pharmaceutical formulations enables the simultaneous evaluation of the relative importance of several factors and the respective interactions [439, 440]. A simple mathematical model is derived from the experimental results, and it can be used to predict the response to a combination of factors not tested experimentally, inside the experimental domain [439]. This model is also used to build response surfaces that enable the visualization of the influence of the variables in the response [439-441]. In a first step, nine drug-loaded films were prepared with different penetration enhancers and different levels, one enhancer at a time or in combinations of two. The GB flux and the Q_{24h} were used as responses to evaluate the penetration enhancers performance. After assessing the effect of the independent variables on the responses and the formulation limitation in terms of the amount of additives that can be incorporated, a new optimized film was prepared. The GB flux and Q_{24h} were also evaluated for this new film in pig epidermal membranes as well as in human epidermis.

GB release profiles from all the films are determined using modified Franz diffusion cells. The influence of the incorporation of penetration enhancers in the films on the GB release kinetics release is also evaluated. Moreover, several functional properties important to fulfil the therapeutic goals such as water vapor transmission rate (WVTR) and bioadhesion of the films are equally examined [328, 329].

2. Materials and methods

2.1 Materials

Chitosan of low molecular weight and NMP (N-methyl pyrrolidone) were purchased from Sigma-Aldrich. Noveon AA-1® (PAA), GS and Azone (1-dodecylazacycloheptan-2-one) were kindly provided by Noveon Inc. (Cleveland, USA), Grunenthal (Germany) and Bluepharma (Portugal), respectively. PG and polyvinylpyrrolidone K90 (PVP K90) were obtained from Fluka. All other chemical reagents were of pharmaceutical grade.

2.2 Preparation of the GB-loaded film formulations

The films consist of chitosan-PAA polyelectrolyte complexes (PEC), and were prepared according to a description given in the last chapters. Briefly, a chitosan solution (1.5 %, w/v) in 0.75 % (w/v) aqueous lactic acid is dropwise added to the PAA suspension, and mixed with a mechanical stirrer. The plasticizer (glycerol) concentration is fixed at 30% of the total dry weight of the polymers according to the work of Chapter IV. After the addition of the plasticizer, 10% of GB (w/dry polymer weight) and the appropriate amount of each penetration enhancer (PG, Azone and NMP) are added prior to the suspension neutralization with NaOH 1M. The latter allows to obtain a pH of 6.1.

Film forming solutions are cast on Petri-dishes and dried at 35ºC for about 48 h. An adhesive solution composed of 67 wt % PVP K90 and 33 wt % PEG400 is applied to the films by solvent casting technique, and the solvent is evaporated again at 35ºC as previously described in previous chapters.

2.3 *In vitro* drug permeation studies

Permeation experiments were conducted using pig epidermal membranes prepared by heat separation technique and human epidermis in the final optimized film. Pig ears were obtained from a local slaughterhouse and the areas of skin free from hairs are separated from the ear. The human skin was obtained from post-mortem collection. The whole skin is immersed in water at 60ºC for two minutes, after which the epidermis is peeled off from the underlying tissue according to the guidelines recommendations [184, 187, 188, 413]. Epidermal membranes are stored at -20ºC in an aluminium foil until use. It was demonstrated that no changes occur in the skin permeability kept in these conditions when compared to fresh skin [414, 415].

The epidermal membranes are mounted in modified Franz diffusion cells with the dermal side in contact with a PBS, pH 7.4, as receptor fluid that is continuously stirred and maintained at 37 ± 0.1 ºC during the time of the study [187]. This is a physiologically adjusted buffer used to mimic the permeation through the skin into

the systemic bloodstream. The amount of GB permeated at each time is determined by spectrophotometric detection at 289 nm, using a previously validated calibration curve, in agreement with the reference guidelines, see Appendix [405-407]. Sink conditions are maintained during the study.
The buffer is previously filtered in vacuum through a 0.45 μm Millipore filter, followed by 15 minutes at 40ºC in ultrasounds in order to prevent the formation of air bubbles between the skin and the receptor medium during the GB permeation experiments.
Prior to each test, the integrity of all epidermal membranes is evaluated as required by the reference guidelines [184, 187, 188] through the measurement of the TEWL using a Vapometer (Delfin Technologies Ltd, Finland). The measurements of the TEWL are conducted under standardized conditions in order to assure the reliability of the results [416]. Epidermal membranes with high TEWL values are considered damaged and discarded prior to the study.

The *in vitro* drug permeation studies were conducted for the drug-loaded films during 20h. The cumulative amount of drug permeated per cm^2 of skin (Q) is plotted against time (t) and the flux is determined from the linear portions of the plots according to the **Equation (1.1)**.

2.4 *In vitro* drug release studies

In vitro drug release tests were performed by means of modified Franz diffusion cells with a diffusion area of 1.327 cm^2. The receptor chamber is kept at 37 ± 0.1 ºC and filled with acetate buffer, pH 5.5, in order to simulate the pH of the skin surface and the sink conditions are maintained during the time of the study. All precautions were taken in order to avoid the formation of air bubbles between the films and the receptor medium during the release experiments.
Each film is sandwiched between the donor compartment and the receptor compartment. The GB release is determined by spectrophotometric detection at 289 nm.
Studies were conducted during 6 hours and the measurements were recorded each 5 minutes. The exact volume of the receptor chamber was measured at the end of

each experiment, in order to accurately calculate the cumulative drug release of each drug.

2.5 Drug release kinetics

In order to analyze the drug release mechanism three mathematical models were used, the zero order, Higuchi and Korsmeyer-Peppas models [411, 412, 442], respectively given by:

$$\frac{Q_t}{Q_\infty} = \frac{Q_0}{Q_\infty} + K_0 t \qquad (\mathbf{6.1})$$

$$\frac{Q_t}{Q_\infty} = \frac{Q_0}{Q_\infty} + K_H \sqrt{t} \qquad (\mathbf{6.2})$$

$$\frac{Q_t}{Q_\infty} = \frac{Q_0}{Q_\infty} + K_{KP} t^n \qquad (\mathbf{6.3})$$

where Q_t/Q_∞ is the fraction of drug released at time t and Q_0/Q_∞ the initial fraction of drug in the release medium as a result of burst effects. K_0, K_H and K_{KP} are the zero-order, the Higuchi and the Korsmeyer-Peppas release constants, respectively.

In the Korsmeyer-Peppas model, K_{KP} is a constant related with the structural and geometric properties of the formulation, while the n value depends on the drug release mechanism from the formulation and the shape of the matrix tested [412, 442]. In the case of a slab, n=0.5 indicates a Fickian diffusion, while 0.5<n<1 when there is a superposition of diffusion-controlled and swelling-controlled drug release and, finally, n=1 for zero-order release kinetics [412, 442]. For the determination of the n exponent only the data points of the release curves up to 60% of drug release are considered [412, 442].

The models were analyzed according to a previous work employing a least squares procedure based on the Marquardt algorithm [429].

2.6 Comparison of GB release profiles

A model-independent method that includes the calculation of the difference factor (f_1) and the similarity factor (f_2) is used to compare the GB release profiles from the different drug-loaded films. The f_1 is a measure of the relative error between the two curves, while the f_2 is a measurement of the similarity in the percent release between the two release profiles [412, 443]:

$$f_1 = \frac{\sum_{j=1}^{n} \left| R_j - T_j \right|}{\sum_{j=1}^{n} R_j} \times 100 \qquad (\mathbf{6.4})$$

$$f_2 = 50 \times \log\left\{ \left[1 + 1/n \sum_{j=1}^{n} w_j \left| R_j - T_j \right|^2 \right]^{-0.5} \times 100 \right\} \qquad (\mathbf{6.5})$$

being n is the sampling number, R_j and T_j the percentage (%) of drug release from the reference and from the test formulations at each time point j,and w_j is an optional weight factor.

The f_1 and f_2 are recommended by the FDA and EMEA as a valid method to assess the similarity of in vitro drug release profiles [412, 444, 445]. Two *in vitro* drug release curves are considered similar when f_1 values are lower than 15 and f_2 values are higher than 50 which corresponds to an average difference of no more than 15% and 10%, respectively [412, 443, 446].

2.7 Film thickness

The thickness of each film was measured at six different sites using a micrometer. Mean and standard error values are calculated.

2.8 Surface morphology

The film surfaces were observed with a Leica DMIL inverted microscope (Leica Microsystems, Inc., Germany) under transmitted light and the images at 400x magnification were captured using a Canon Power Shot S45 digital camera with a microscope adaptator.

2.9 WVTR

Three samples were tested for each type of film. The WVTR ($g/m^2.h$) is measured using a Vapometer (Delfin Technologies Ltd, Finland). Briefly, film specimens are mounted and sealed in the top of open specially designed cups, filled with distilled water up to 1.1 cm from the film underside and left to equilibrate for one hour at room temperature (22-23ºC, 42-46% RH). The vapometer is equipped with a humidity sensor, inside a closed measuring chamber not sensitive to external airflows that enables measurements of the films water permeability in normal room conditions [341].

2.10 *In vitro* bioadhesive properties

The *in vitro* evaluation of the bioadhesion properties of the films, including peak adhesion force (PAF) and work of adhesion (WA) is performed using a TA.XTPlus Texture analyzer (Stable Micro Systems, UK). The film is fixed by means of a double-sided adhesive tape on the movable carriage of the apparatus, while the pig

skin is fixed in the test rig. The carriage is moved until the contact between pig skin and the movable carriage is established. A preload of 3N is applied and the contact time of the holder and the skin was 60s. After that time, the movable carriage is moved forward at a constant speed test of 10 mm/sec until complete separation of the two surfaces. The curves of displacement (mm) versus adhesive force (mN) are recorded simultaneously. The WA is given by integration on the range of positive force.The force required to detach the film from the pig skin is used to represent the magnitude of bioadhesive force of the tested film specimen.

2.11 Experimental design

In the present study, two experimental designs were performed, each with two factors at three levels: PG/azone and PG/NMP. The penetration enhancers (independent variables) and the respective levels, coded and in absolute values are shown in **Tables 6.1** and **6.2**. The flux and the Q_{24h} of GB were considered the responses or dependent variables. From the response surface of a partial 3^2 factorial design, a non-linear quadratic model can be extracted and calculated according to:

$$Z = a + a_X X + a_Y Y + a_{X^2} X^2 + a_{Y^2} Y^2 + a_{XY} XY \qquad (\mathbf{6.6})$$

where *Z* is the response variable, *X* and *Y* are the independent variables, and a, a_X, a_Y, a_{X2}, a_{Y2} and a_{XY}, the regression coefficients corresponding to the constant, the main effects, quadratic terms and interaction, respectively.

2.12 Statistical analysis

Results are expressed as mean ± standard error (SEM). The significance of the differences between values is assessed using a two sample t-test with a statistical significance level set at P = 0.05.

In order to evaluate the validity of the quadratic models of the partial factorial designs, the analysis of variance (ANOVA) was used. F-ratios and the correlation coefficients were the criteria for validation.

3. Results and discussion

3.1 *In vitro* skin permeation studies

Two different partial 3^2 factorial designs were used in order to evaluate the effect of PG, Azone, NMP and the combination of PG/Azone and PG/NMP in the permeation of GB through pig epidermis. Based on **Table 6.1**, the first nine drug-loaded films in **Table 6.2** were initially prepared by varying each factor individually and using combinations of two factors at the respective levels.

Table 6.1 Dependent and independent variables and respective levels used in the construction of a partial 3^2 factorial design.

Variables	Levels		
	Low (-1)	Medium (0)	High (1)
Concentration of PG (%)	0	20	40
Concentration of Azone (%)	0	5	10
Concentration of NMP (%)	0	5	10
Responses		Flux and Q_{24h}	

After conducting the *in vitro* permeation studies, the GB flux and the Q_{24h} were calculated and are also included in **Table 6.2**. The GB permeation profiles are presented in **Figure 6.2**, and the enhancement ratios (ER) obtained from the

incorporation of penetration enhancers in the GB-loaded films are depicted in **Figure 6.3**.

Table 6.2 Formulations prepared in the present work, and the respective flux and amount of GB permeated per unit of area of pig skin at 24h (Q_{24h}). Results are expressed as mean (± SEM), n ≥ 3.

Formulation	Concentration (%)			Responses	
	PG	Azone	NMP	Flux (μg/cm^2.h)	Q_{24h} (μg)
F	0	0	0	2.8 ± 0.6	73.6 ± 13.5
F_{20P}	20	0	0	3.7 ± 0.4	95.0 ± 7.8
F_{40P}	40	0	0	3.7 ± 0.5	97.3 ± 13.6
F_{5A}	0	5	0	2.1 ± 0.7	66.3 ± 12.8
F_{10A}	0	10	0	2.0 ± 0.1	72.3 ± 3.0
F_{20P10A}	20	10	0	3.0 ± 0.4	80.0 ± 14.7
F_{5N}	0	0	5	4.1 ± 0.6	98.3 ± 10.0
F_{10N}	0	0	10	7.3 ± 1.2*	197.7 ± 23.8*
F_{20P10N}	20	0	10	7.9 ± 0.6*	223.7 ± 27.1*
F_{20N}	0	0	20	9.0 ± 0.8*	216.9 ± 17.0*

* Statistically significant difference in comparison with the film F ($P < 0.05$)

The GB permeation profiles from the films do not exhibit the typical profile with an initial lag time. Instead, in the early stages of the permeation studies there is an unusually fast permeation followed by a region of constant flux. This initial "burst" effect is most probably a consequence of an initially higher GB release rate from the films, probably as a result of the film swelling and a "supersaturation" of the drug in the film surface. Although unusual, this type of drug permeation profiles have been observed before, mostly in film formulations [390, 426, 427, 430, 431] but also in HPMC gels [432]. This initially higher permeation rate of the drug is advantageous because it enables to rapidly attain the pharmacological action, contrary to the usual lag-time that delays the onset of the therapeutic effect. The magnitude of this burst effect also depends on the amount and type of penetration enhancer incorporated in

the formulations, as it is clear from **Figure 6.2** and from the ER of Q_{24h} on **Figure 6.3**.

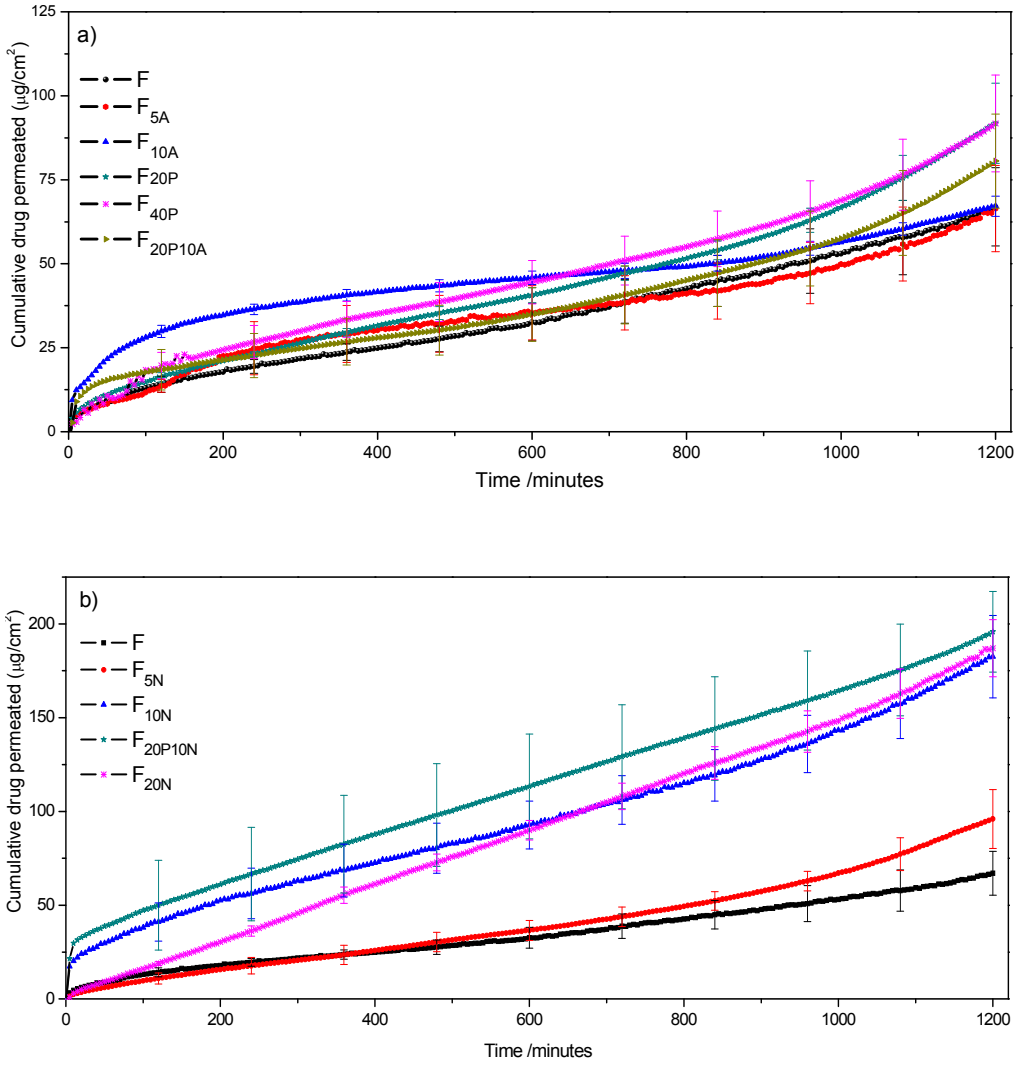

Figure 6.2 The *in vitro* permeation profiles of the GB from the drug-loaded films in the absence and after the incorporation of the penetration enhancers. All films are loaded with 10% of GB. Mean (± SEM); n ≥ 3.

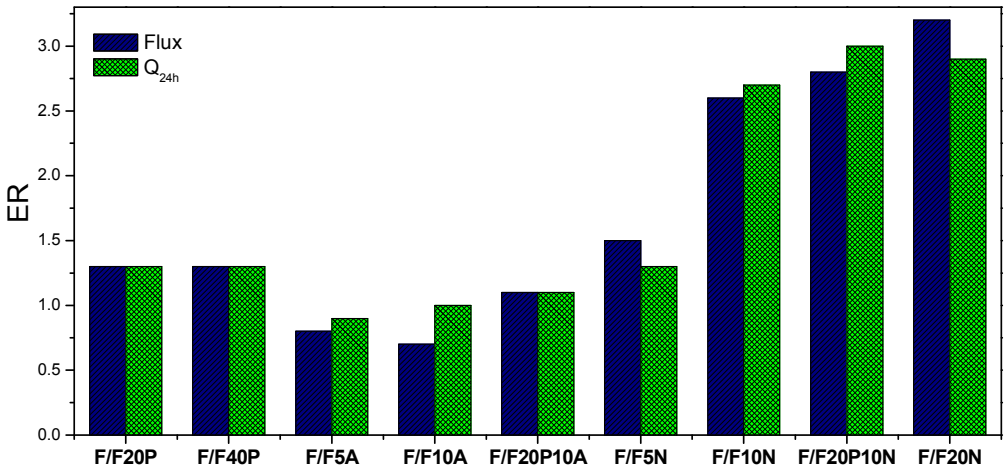

Figure 6.3 Enhancement ratio of the flux and Q_{24h} of GB produced by the incorporation of the penetration enhancers in the drug-loaded films.

The flux and Q_{24h} results allowed the calculation of the response surface models that are depicted in **Figures 6.4** and **6.5** for the combinations of PG/NMP and PG/Azone, respectively. They were obtained, using a standard approach [447], as a function of the concentrations of PG and NMP, and as a function of the PG and Azone concentrations, respectively:

$$Z_{flux}=4.9+2.1[NMP]+0.3[PG]+0.9[NMP]^2 -0.5\,[PG]^2-0.1[NMP][PG] \quad (6.7)$$

$$Z_{Q24h}=122.0+64.4[NMP]+14.2[PG]+37.7[NMP]^2-9.5[PG]^2+2.3[NMP][PG] \quad (6.8)$$

$$Z_{flux}=3.1–0.4[Azone]+0.5[PG]+0.3[Azone]^2 -0.5[PG]^2+0.1[Azone][PG] \quad (6.9)$$

$$Z_{Q24h}=80.9-7.5[Azone]+5.0[PG]+6.7[Azone]^2-9.5[PG]^2-6.8[Azone][PG] \quad (6.10)$$

In the regression we used coded (-1 for the lower and +1 for the higher) levels of the independent variables, in order to obtain regression coefficients that can be directly compared with each other [439]. Also, the use of coded data facilitates the interpretation of the relative importance, avoiding potential misleading deductions from raw data [448].

.

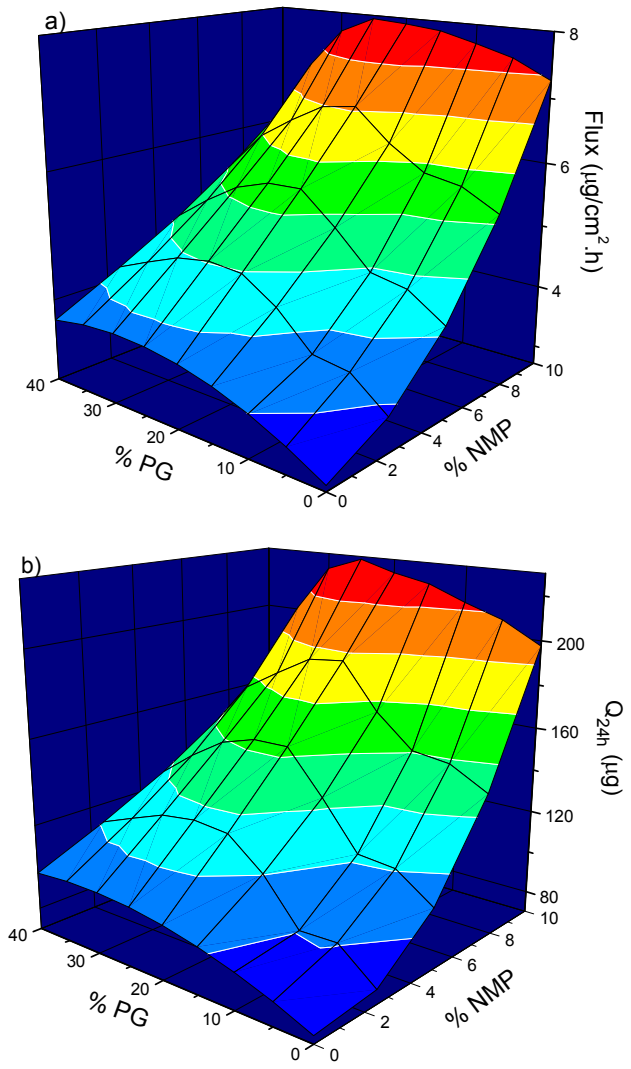

Figure 6.4 Estimated response surface plot illustrating the effect of the concentration of NMP and the concentration of PG in the (a) GB flux and (b) GB Q_{24h}.

The polynomial equations display the quantitative effect of the process variables (NMP, Azone and PG) and indicate how their interactions affect the responses (Flux and Q_{24h}). The coefficients with only one independent variable represent the main effect of that variable; the regression coefficients with more than one process variable and those with second order terms are related with the interaction effects and the quadratic contribution to the response, respectively. A positive sign indicates

an increase in the response produced by that independent variable or a synergistic effect produced by the combination of the two independent variables. A negative sign indicates the opposite. A larger regression coefficient is an indication of a higher importance of the independent variable on the response [448].

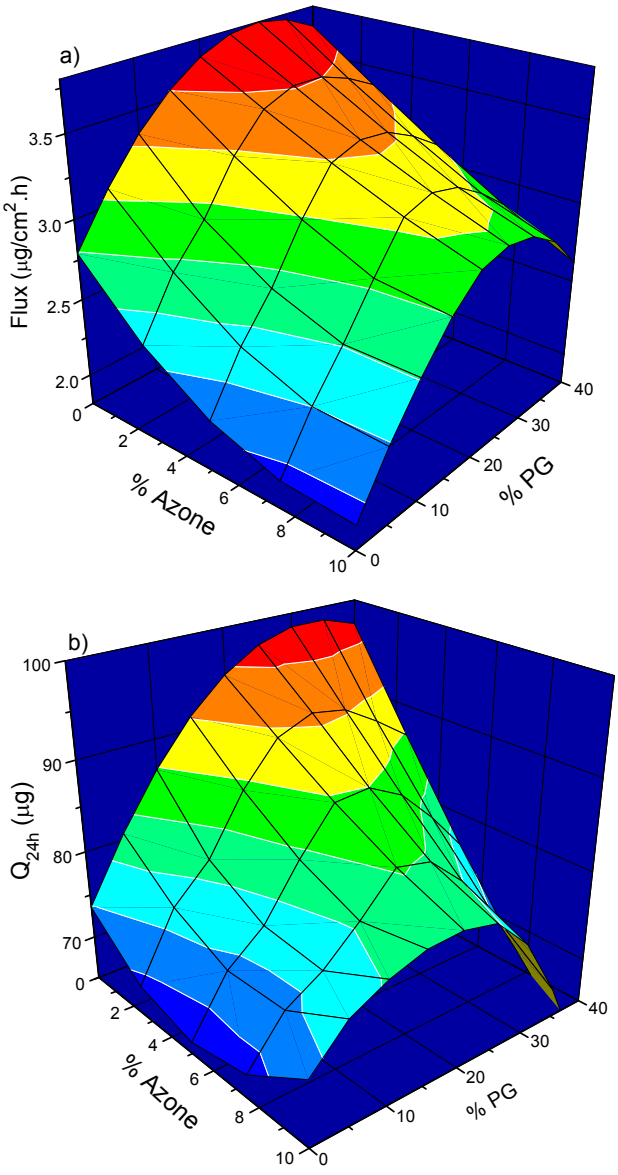

Figure 6.5 Estimated response surface plot illustrating the effect of the concentration of Azone and the concentration of PG in the (a) GB flux and (b) GB Q_{24h}.

A standard analysis using ANOVA [441] was also carried out on the designs and the statistical parameters for each response variable can be found in **Table 6.3**.

The results show that $F_{calculated}$ is higher than the critical value of F, for a probability of 99%, indicating that the responses (flux and Q_{24h}) are significantly affected by the independent variables of **Equations 6.7** and **6.8** [441, 449]. On the contrary, $F_{calculated}$ is smaller than $F_{critical,}$ for a probability of 95%, in **Equations 6.9** and **6.10**, indicating that the independent variables (Azone and PG) do not significantly affect the flux and Q_{24h} of GB [441, 449]. These findings are in accordance with the results of the statistical analysis of the flux and Q_{24h} data obtained from the permeation studies, which indicate a statistically significant difference only in the films with 10% NMP or more.

Table 6.3 Statistical parameters of the responses variables studied in this work.

ANOVA	DF	SS	MS	F-ratio
Z_{flux} (NMP)				
Total	17	125.5		
Regression	5	91.8	18.4	
Residual	17	33.7	2.0	9.4[#]
Z_{Q24h} (NMP)				
Total	17	1.1×10^5		
Regression	5	8.2×10^4	1.6×10^4	
Residual	17	2.5×10^4	1.5×10^3	10.9[#]
Z_{flux} (Azone)				
Total	14	21.0		
Regression	5	9.4	1.9	
Residual	14	11.6	0.8	2.3[&]
Z_{Q24h} (Azone)				
Total	14	9.1×10^3		
Regression	5	2.8×10^3	5.7×10^2	
Residual	14	6.2×10^3	4.4×10^2	1.3[&]

[#] Fcalculated > Fcritical (probability of 99%)

[&] Fcalculated < Fcritical (probability of 95%)

Table 6.4 Values of the regression coefficients, and the respective t and probability, in percentage, for a Student's t-test.

Coefficient	Value	t	Probability (%)
Z_{flux} (NMP)			
a	4.9	4.9	99.99
a_N	2.1	4.5	99.97
a_P	0.3	0.4	32.90
a_{N2}	0.9	1.0	67.32
a_{P2}	-0.5	-0.5	38.26
a_{NP}	-0.1	-0.2	14.32
Z_{Q24h} (NMP)			
a	122.0	4.4	99.96
a_N	64.4	4.9	99.99
a_P	14.2	0.7	51.74
a_{N2}	37.4	1.5	85.54
a_{P2}	-9.5	-0.4	29.10
a_{NP}	2.3	0.1	9.14
Z_{flux} (Azone)			
a	3.1	4.5	99.95
a_A	-0.4	-1.1	68.86
a_P	0.5	1.0	65.02
a_{A2}	0.3	0.4	32.57
a_{P2}	-0.5	-0.8	55.57
a_{AP}	0.1	0.1	7.95
Z_{Q24h} (Azone)			
a	80.9	5.1	99.98
a_A	-7.5	-0.9	63.06
a_P	5.0	0.4	32.48
a_{A2}	6.7	0.5	36.76
a_{P2}	-9.5	-0.7	50.42
a_{AP}	-6.8	-0.6	42.83

The values of the regression coefficients of the models, as well as the values of t and the percent probability for the significance of each coefficient in a Student's t-test [448] are gathered in **Table 6.4**. The higher the probability associated with the regression coefficient, the greater is the confidence that the independent variable has a significant effect on the response [448].

Analyzing all the polynomial equations and **Table 6.4**, it is clear that the regression coefficients of NMP are higher than the regression coefficients of any other independent variable determined. Also, their percent probability for the significance is greater than the observed for the other regression coefficients (**Table 6.4**). Therefore, NMP is the penetration enhancer with the largest impact in the increase of both flux of GB through the skin and respective Q_{24h}. This observation is clearly depicted in **Figures 6.2**, **6.3** and **6.4**.

It can also be concluded that in order to obtain a statistical significant ($P<0.05$) improvement of the GB flux and Q_{24h}, it is necessary to incorporate more than 5% of NMP in the films according to **Table 6.2**. The ER obtained by the incorporation of 5% NMP and 10% NMP in comparison with the control film (F) was 1.5 and 2.6 for the flux and 1.3 and 2.7 for the Q_{24h}, respectively.
The improvement of the GB permeation can be due to the NMP action on the aqueous regions of the SC [130, 389, 434], producing an increase in the GB partitioning coefficient into the SC. Our results confirm the NMP ability to increase the percutaneous permeation of drugs as demonstrated in several other works [389, 434, 435, 450].

On the contrary, by the analysis of **Figures 6.2**, **6.3**, **6.5** and **Equations 6.9** and **6.10**, we see that Azone causes a decrease of the transdermal permeation of GB. Although the values of the flux and Q_{24h} of films with Azone cannot be considered statistically significant when compared with the reference film (**Table 6.2**), there is a consistent decrease of these responses when Azone is incorporated in the films. Also, the regression coefficients pertaining to the Azone concentration are associated with a small probability for the significance (**Table 6.4**), which also indicates that Azone has not a significant effect on the responses, in agreement with the results on **Table 6.2**.

The regression coefficients associated with the main effect of Azone have a negative sign, reflecting the tendency to decrease of the GB flux and Q_{24h} with the incorporation of this compound in the films, see **Tables 6.2** and **6.4**. In fact, the ER of films with 5% and 10% Azone are smaller than unity, as shown in **Figure 6.3**.

Despite of its well known ability to fluidize the lipid lamellae of SC [219, 436] and, in that way, increase the drugs permeation through the skin [393, 433, 440, 451], the incorporation of Azone in our films has a detrimental effect on the percutaneous permeation of GB.

In a recent work, Azone also reduced the amount of ethinylestradiol permeated through human epidermis from polymeric films [390], and it was also shown that Azone has an unfavourable effect on the permeation of highly lipophilic compounds (log P>3) [452]. Probably, the partition of Azone from the films to the SC is very small, which prevents its fluidizing effect on the SC and the consequent increase in the permeation of GB. The decrease in the permeation may also be explained by a solubilizing effect of GB in the film.

From the analysis of **Equations 6.7**-**6.9** and **Figures 6.3** and **6.4** the results of previous works in which PG has the capacity to increase the transdermal delivery of drugs are confirmed [138, 388, 389, 435, 453]. In fact, the regression coefficients associated with PG have a positive sign, although the effect of PG in the GB flux and Q_{24h} is not statistically significant (P>0.05) and can thus be considered only moderate, see **Table 6.2**. The small % probability for the significance associated with the regression coefficients of PG confirms this result (**Table 6.4**). It can also be observed that increasing the concentration of PG in the films from 20% to 40% does not further increase the GB transdermal permeation (**Table 6.2** and **Figure 6.3**). Probably, this beneficial effect of PG is related with an increase of the uptake of GB by the SC as suggested by other authors [388, 389].

Analyzing the effect of combining PG with NMP and Azone, it is realized that it is not more beneficial to the GB permeation than the effect of PG or NMP alone. These findings contradict some results that indicate a synergistic action of the associations PG/Azone [138, 391, 433] and PG/NMP [138]. In fact, the regression coefficients of the combinations are very small as well as their % probability for significance depicted in **Equations 6.7**, **6.8** and **6.9**, while for the response of **Equation 6.10** the

negative value of the regression coefficient of the PG/Azone combination indicates an unfavourable effect of this association in the Q_{24h} of GB. The association of PG/Azone is disadvantageous in relation to the GB Q_{24h} due to the fact that the burst effect in the permeation profile of the films with Azone is high, but the addition of PG decreases its magnitude and by consequence, reduces Q_{24h} [**Figure 6.2**].

After taking into consideration all the results discussed before and the limitation of the amount of additives that can be included in the polymer matrix, it was decided that the best option to further improve the permeation of GB was the increase of NMP concentration up to 20%. Since 20% of NMP is well beyond the experimental domain evaluated in the present work, the response surface methodology and the polynomial equations may not accurately predict the value of the responses of this new formulation [439].

The flux and Q_{24h} of GB that resulted from this new film can be found on **Table 6.2**, and the permeation profile of the formulation is depicted in **Figure 6.2(b)**. The F_{20N} film improved the GB flux about 3.2 times and the Q_{24h} 2.9 times when compared with the control (F film), see **Figure 6.3**. The ER of the Q_{24h} is not so high when compared with the ER of the flux due to a significant reduction of the initial burst effect. If we compare the values of the GB flux (1.30 μg/cm^2.h) and Q_{24h} (35.2 μg) from saturated solutions of the drug obtained in the previous study, we realize that the F_{20N} film represents an improvement of GB percutaneous permeation of 6.9 fold and 6.2 fold for flux and Q_{24h}, respectively.

In order to do a more accurate determination of the film size necessary to produce *in vivo* the pharmacological action in humans, the GB permeation from the F_{20N} film was also evaluated in human epidermal membranes. The GB permeation profiles from the F_{20N} film through human and pig epidermal membranes are depicted in **Figure 6.6**. The values of the GB flux and Q_{24h} determined using human epidermal membranes were 4.10 ± 0.20 μg/cm^2.h and 97.73 ± 4.58 μg, respectivelly. This values have the same order of magnitude that the values determined in pig epidermal membranes (**Table 6.2**) although ca. 2 times smaller. These values indicate that pig epidermal membranes are a reasonable model when human epidermal membranes are not readilly available, specially if we compare with other

studies that indicate that, e.g. rat skin can be 10 times more permeable than human skin [454].

Considering an initial dose of 4 mg twice a day and a oral bioavalability of 88.5%, it is necessary that ca 7.08 mg/24h of GB passes through the skin in order to produce the therapeutic effect *in vivo* [377]. Since the determined GB Q_{24h} value through human epidermal membranes was 97.73 µg, it is necessary a film size of ca. 72 cm^2 to deliver 7.08 mg of GB in 24h.

The optimized formulation constitutes thus a very promising option for the effective delivery of GB through the skin and the transdermal drug delivery is a promising option for the effective treatment of the Alzheimer's disease.

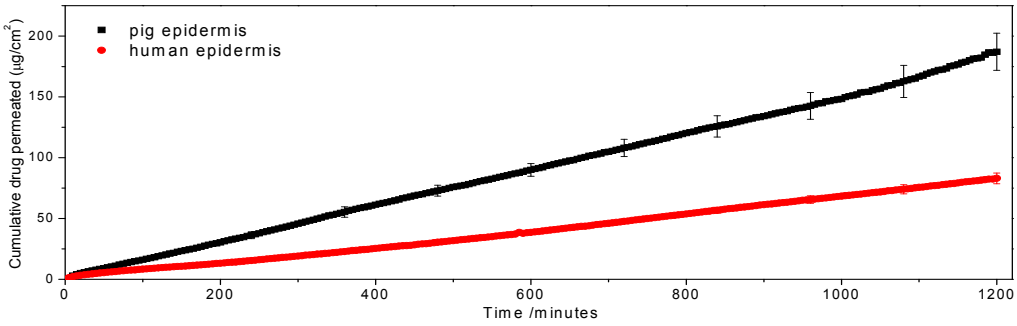

Figure 6.6 The *in vitro* permeation profiles of the GB from the F_{20N} films through pig and human epidermis. The films are loaded with 10% of GB. Mean (± SEM); n ≥ 3**.**

3.2 Evaluation of GB release from the films

The films prepared in the present study are composed by a hydrogel formed due to electrostatic interactions between chitosan and PAA, and also comprise a PSA layer. In this type of PEC, the pH of the release medium influences the crosslinking density and by consequence the degree of swelling [201, 202, 424]. For this reason, the GB release studies were performed in acetate buffer at pH 5.5 in order to reflect

the physiological pH of the skin as advised by reference guidelines [425]. Likewise, the drug release from polymer films is also influenced by the physicochemical properties of the drug such as the molecular weight (MW), solubility [318] and by the drug concentration within the polymer network [426, 427].

Figure 6.7 shows the cumulative GB release profiles from all drug-loaded films prepared. All the films exhibit an initial burst effect that is followed by a region of constant drug release. Two different mechanisms may be accounting for this initially fast GB release: a rapid swelling of the films when they enter in contact with the release medium, and a high concentration of the drug in the surface of the films. This effect was previously described, in systems with the same films loaded with different drugs on Chapter V. Comparable burst releases have been reported in a different PEC [310].
The direct comparison of the burst effect observed in the F films and other chitosan/PAA films described in the literature is not possible, due to the different pH and composition of the release media [310, 424, 455] as well as the different ionic strength of the hydrogel forming medium [316]. The incorporation of the penetration enhancers always increases the initial burst effect, probably due to a reduction of the percentage of the polymer matrix in the films that in turn reduces the ability to control the release of the drug.

The initially higher drug releases have been proved to be very beneficial, because a related effect can be discerned in the drug permeation profiles through the skin. This enables to rapidly achieve the therapeutic plasma concentration of the drug, and the constant drug release that follows then provides a sustained and controlled drug release. However, as we cannot find a correlation between an increase in the magnitude of the burst effect in the drug release and a concomitant increase of the burst effect on the GB permeation, we conclude that also the type and concentration of the additives incorporated in the film play an important role. Additionally, the GB release from the films is always higher than the amount of drug that permeates the skin, so the drug release is not the limiting step of the percutaneous penetration of the drug through the epidermal membranes.

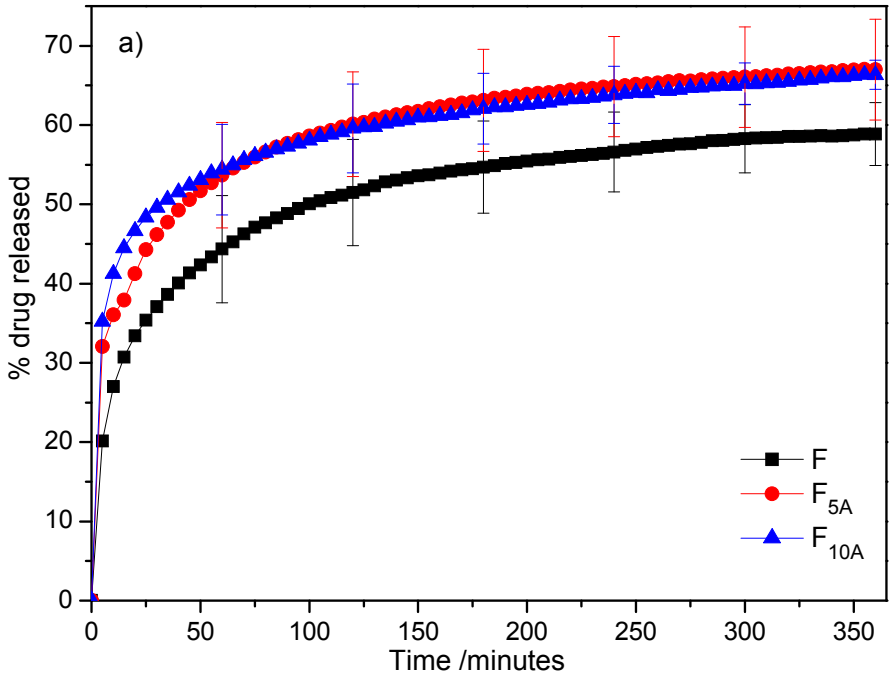
a)
% drug released
Time /minutes
F
F5A
F10A

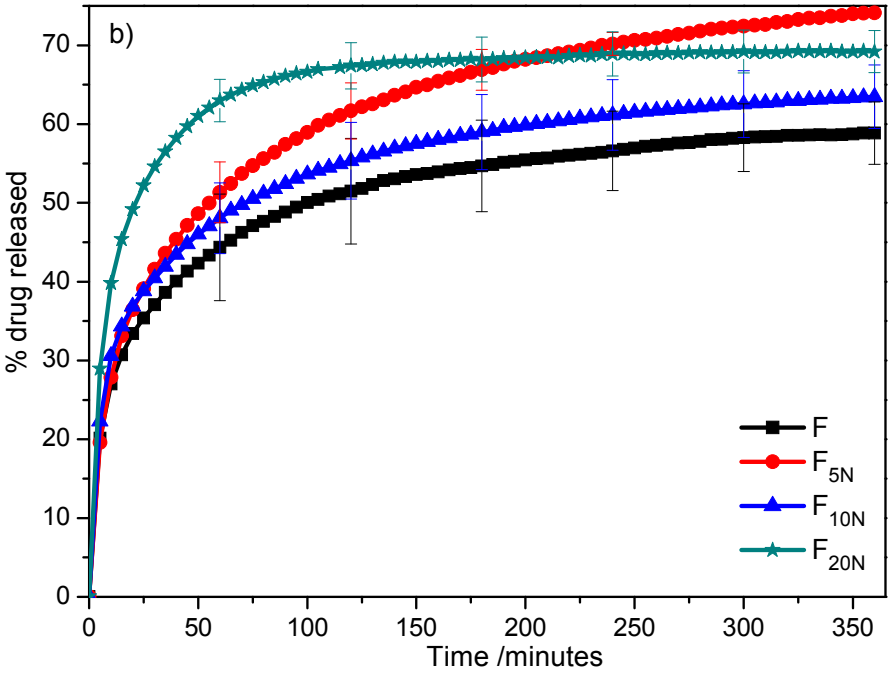
b)
% drug released
Time /minutes
F
F5N
F10N
F20N

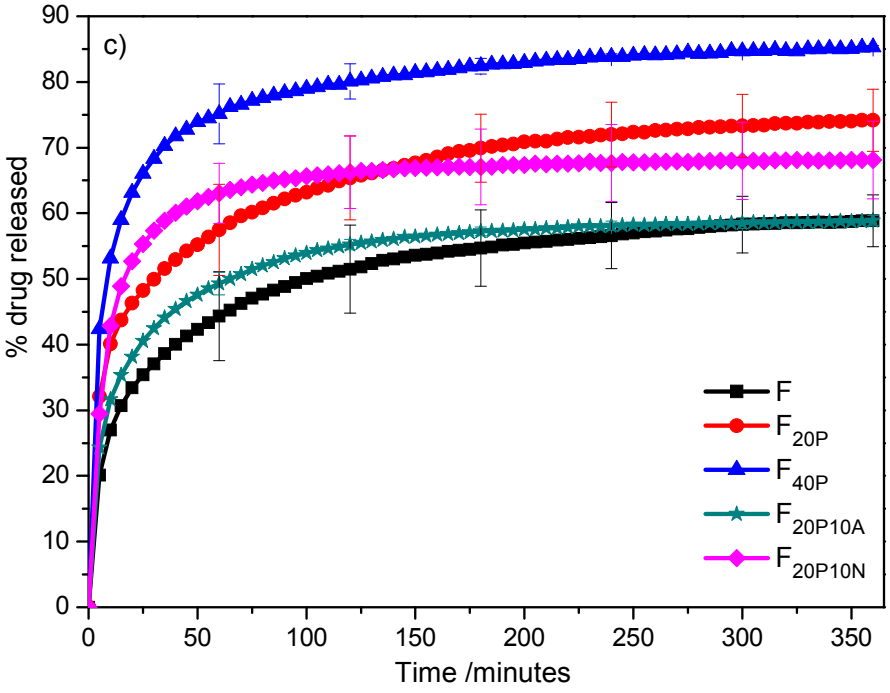

Figure 6.7 The *in vitro* drug release profiles from GB-loaded films. All films are loaded with 10% of drug. Mean (± SEM); n ≥ 3.

The drug release mechanism from the hydrogels of the type evaluated in the present work, prepared by mixing the polymer solutions and the drug before the network formation, can be established by one or more of the following factors: drug diffusion, swelling, reversible drug-polymer interactions and degradation [428]. In order to clarify the GB release kinetics from the films, the release data were fitted to the zero-order release kinetics [**Equation (6.1)**], Higuchi's square root of time [**Equation (6.2)**] and Korsmeyer-Peppas models [**Equation (6.3)**] [411, 412, 429, 442]. The *in vitro* kinetic release parameters calculated, and the standard deviations of the regressions, are presented in **Table 6.5**.

For the fit to the zero order and Higuchi models the points pertaining to the burst release are discarded through direct inspection of the plots. The zero order (K_0) and Higuchi (K_H) rate constants as well as the Q_0/Q_∞ of both models are established according to previous work [429].

Table 6.5 *In vitro* release kinetic parameters of GB-loaded films.

Film	Kinetic models							
	Zero-order kinetics			Higuchi			Korsmeyer-Peppas	
	Q_0/Q_∞ (%)	K_0 (%/h)	StdFit	Q_0/Q_∞(%)	K_H (%/h$^{1/2}$)	StdFit	n	StdFit
F	48.7 ± 0.3	1.9 ± 6.4x10^{-2}	0.6	41.8 ± 0.3	7.3 ± 0.2	0.4	0.19 ± 5.2x10^{-3}	1.6
F_{20P}	61.4 ± 0.5	2.4 ± 0.1	1.1	52.7 ± 0.6	9.3 ± 0.3	0.9	0.21 ± 5.0x10^{-3}	0.6
F_{40P}	76.4 ± 0.3	1.7 ± 7.8x10^{-2}	0.9	71.1 ± 0.4	6.2 ± 0.2	0.6	0.28 ± 1.3x10^{-2}	0.7
F_{5A}	56.6 ± 0.3	1.9 ± 6.9x10^{-2}	0.7	50.0 ± 0.3	7.2 ± 0.2	0.4	0.21 ± 4.1x10^{-3}	0.7
F_{10A}	54.7 ± 0.3	2.1 ± 6.7x10^{-2}	0.8	48.2 ± 0.2	7.6 ± 0.1	0.4	0.15 ± 3.2x10^{-3}	0.6
F_{20P10A}	53.5 ± 0.2	1.0 ± 6.2x10^{-2}	0.6	49.8 ± 0.4	4.0 ± 0.2	0.5	0.14 ± 6.2x10^{-3}	2.1
F_{5N}	56.7 ± 0.4	3.2 ± 0.1	0.9	45.2 ± 0.5	12.2 ± 0.2	0.6	0.32 ± 7.4x10^{-3}	1.0
F_{10N}	52.3 ± 0.3	2.0 ± 7.6x10^{-2}	0.7	44.8 ± 0.4	8.0 ± 0.2	0.5	0.22 ± 5.1x10^{-3}	1.1
F_{20N}	66.4 ± 0.1	0.6 ± 3.2x10^{-2}	0.3	64.4 ± 0.2	2.1 ± 9.5x10^{-2}	0.2	0.30 ±1.6x10^{-2}	1.4
F_{20P10N}	64.4 ± 0.2	0.7 ± 5.2x10^{-2}	0.6	62.0 ± 0.3	2.8 ± 0.1	0.5	0.30 ± 2.9x10^{-2}	2.3

The drug release data from the films show a good fit to both mathematical models according to the values of the standard deviation of the fit (StdFit) on **Table 6.5**. However, the function best describing the drug release after the initial burst release is Higuchi's profile (**Table 6.5**). Residual analysis confirms this conclusion.
The values of K_H vary between 2.1 and 12.2 (% drug release per $\sqrt{t}$) in F_{20N} film and in the F_{5N} film, respectively. Simultaneously, the percentage of GB released in the initial burst effect (Q_0/Q_∞) ranged from ca. 42% in the F films to ca. 71% in the case of F_{40P} formulation (see **Table 6.5**) which indicates that the incorporation of additives in the films always increases the magnitude of the burst effect.

The release exponent (*n*) of the Korsmeyer-Peppas model ranged from 0.14 (F_{20P10A} film) and 0.32 (F_{5N}) as can be seen in **Table 6.5**. All the values determined for the n parameter are lower than 0.5, which is consistent with GB release from the films mainly determined by a Fickian diffusion mechanism [412, 442]. The small *n* values eliminate the possibility of erosion and solubilization of the polymer matrix as the

main mechanism of drug release, and reinforces the idea of the stability of the complexes formed by maximizing the electrostatic interactions between chitosan and poly(acrylic acid). Other films based on PEC of chitosan and PAA have previously exhibited the same type of release kinetics [310, 316, 424].

The GB release profiles of the films with penetration enhancers were further compared with the GB release profile from the film in the absence of any of these additives (F film). The comparison between drug release profiles of different formulations can be performed by several methods, including model dependent, statistical analysis and model independent methods. We used a model independent method (fit factors) that has the advantage of providing a single number to describe curves that consist of several data points [443, 446]. Moreover, f_1 and f_2 factors are also recommended by several FDA and EMEA guidance documents as a valid method to assess the similarity of in vitro drug release profiles [412, 444, 445]. We recall that, two *in vitro* drug release curves are considered similar when f_1 values are lower than 15 and f_2 values are higher than 50, which corresponds to an average difference of no more than 15% and 10%, respectively [412, 443, 446].
The values of the fit factors obtained from our drug-loaded films are shown on **Table 6.6**.

Table 6.6 Fit factors values determined for the formulations with penetration enhancers in comparison with the control film.

Formulation	Fit factors	
	f_1	f_2
F/F_{20P}	27.8	42.0
F/F_{40P}	53.9	27.7
F/F_{5A}	16.3	53.5
F/F_{10A}	16.0	53.4
F/F_{20P10A}	4.8	74.7
F/F_{5N}	21.1	46.8
F/F_{10N}	7.8	68.8
F/F_{20N}	26.6	42.5
F/F_{20P10N}	25.5	43.3

From the results presented we can conclude that the GB release from the films F_{10N} and F_{20P10A} can be considered equivalent to the GB drug release from F films (f_1<15 and f_2>50). This is in accordance with our previous findings that demonstrate that these two films possess burst release effects most similar to the F films. The results in **Table 6.6** also show clear differences between the reference formulation (F film) and the films F_{20P}, F_{40P}, F_{5N}, F_{20N} and F_{20P10N} (f_1>15 and f_2<50).

We also observe that the difference factor f_1 was more sensitive in finding dissimilarity between drug release profiles, than the similarity factor f_2 for the present systems. This result contrasts with other studies, that indicate that f_2 is more sensitive in finding dissimilitude between dissolution curves than f_1 [429, 456]. In fact, the f_1 factor show that the drug release profile of the films F_{5A} and F_{10A} are not equivalent to the reference film.

3.3 Characterization of the drug-loaded films

The thickness of the drug-loaded films ranged from 193 to 240 μm, as depicted in **Table 6.7**. Moreover, they are uniform, smooth, transparent and pale yellow due to the high chitosan content. The uniformity of the films can be confirmed by the low SEM values in the thickness measurements in **Table 6.7**.

Before the application of the PSA, the films are less transparent indicating that GB is not totally solubilized in the polymers. After the application of the PSA, the films become clear and transparent indicating that the drug is solubilized in a higher percentage. We believe that when the ethanolic solution of the PSA is applied to the drug-loaded films, it penetrates the film and dissolves part of the drug, and then the drug crystallization is probably inhibited by the PVP, which has proved to be a very effective crystallization inhibitor [419-421]. This hypothesis can be supported by the images of optical microscopy, shown in **Figure 6.8**. In **Figure 6.8(a)** we can see the F film before the application of the adhesive layer. In fact, the presence of large GB crystals within the polymer network is visible, in agreement with the suggestion that the higher opacity of the films is due to the drug crystallization. In **Figure 6.8(b)**, we can see an image of the adhesive layer of the F film, where we can find several GB crystals much smaller than the ones observed in **Figure 6.8(a)**. This fact

substantiates the solubilizing effect of the PSA on the GB crystals present within the polymer matrix. The small size of the crystals is probably due to the crystallization inhibition produced by PVP. Furthermore, this concentration of small GB crystals on the PSA layer may be in part responsible for the burst effect observed in the drug release and permeation profiles.

Table 6.7 Water vapor transmission rate (WVTR), thickness and bioadhesion of the different GB-loaded films. Results are expressed as mean (± SEM), n=9 (WVTR), n= 6 (thickness), n=4 (bioadhesion).

Formulation	WVTR (g/m^2.h)	Thickness (µm)	*In vitro* bioadhesion	
			PAF (mN/cm^2)	WA (mJ/cm^2)
F	14.0 ± 0.5	200.0 ± 7.9	1164.6 ± 196.4	3.7 ± 0.3
F_{20P}	11.3 ± 0.5*	220.6 ± 5.9	1026.4 ± 199.1	1.0 ± 0.1*
F_{40P}	12.0 ± 0.4*	211.7 ± 4.8	1487.6 ± 227.5	1.1 ± 0.2*
F_{5A}	11.6 ± 0.5*	201.7 ± 10.1	629.5 ± 48.4	1.5 ± 0.2*
F_{10A}	13.1 ± 0.4	206.7 ± 3.1	799.5 ± 54.8	1.8 ± 0.3*
F_{20P10A}	11.4 ± 0.3*	201.7 ± 5.6	1272.3 ± 190.6	1.5 ± 0.2*
F_{5N}	15.4 ± 0.6	193.3 ± 4.2	2032.7 ± 209.8*	2.3 ± 0.1*
F_{10N}	13.6 ± 0.5	197.5 ± 7.0	3304.5 ± 500.6*	3.5 ± 0.2
F_{20P10N}	14.9 ± 0.4	210.0 ± 9.8	1428.5 ± 162.5	1.4 ± 0.1*
F_{20N}	14.6 ± 1.0	240.8 ± 8.3*	1197.2 ± 101.4	2.6 ± 0.4

*Statistically significant difference in comparison with the film F (P< 0.05)

The determination of the permeability to water (WVTR) of films that are intended to be applied on skin is of uppermost importance because this property serves to evaluate their occlusive properties. The WVTR also provides an indirect evaluation of the density of PEC and it is simultaneously dependent on the solubility coefficient and diffusion rate of water in the film [355].

The WVTR of the drug-loaded films can be found in **Table 6.7**. The values range from 11.3 to 15.4 g/cm^2.h, with the lower and upper limits pertaining to films F_{20P} and

F_{5N}, respectively. The values of WVTR are in the same range of those previously described in Chapters IV and V.

It was found that 5% Azone (F_{5N}), 20% PG (F_{20P}), 40% PG (F_{40P}) and 10% Azone in combination with 20% PG (F_{10A20P}) adversely affect the WVTR with statistical significance ($P< 0.05$) when compared with the films in the absence of any penetration enhancer, see **Table 6.7**. Despite of this decrease, they all exhibit a higher value for the permeability to water than the normal TEWL in healthy human skin [15, 122, 360]. This characteristic indicates that the drug-loaded films have a low potential to interfere with the skin TEWL and cause sensitization when applied o the skin.

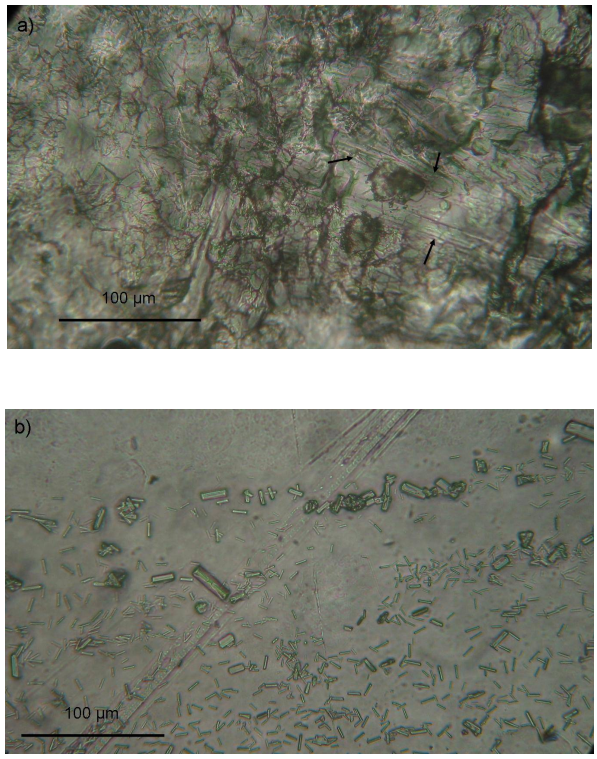

Figure 6.8 Optical microscopy images of the F film loaded with 10% GB (a) before the application of the PSA and (b) PSA layer. The arrows indicate the GB crystals. Original magnification: 400x.

3.4 Bioadhesive properties

Any transdermal drug delivery system must maintain an intimate and prolonged contact with the skin during the entire time of application in order to be able provide a continuous drug supply [328, 329]. There is no doubt that the adhesion to the skin is one of the most important functional properties that should be evaluated in all formulations designed to be applied on the skin [328].

In the previous chapter it was shown, from results in human volunteers that the placebo film is safe, non-sensitizing and capable of firmly adhere to the skin for at least 24h. In the present work, the objective is to make a quantitative evaluation of the bioadhesive properties of the drug-loaded films using excised pig ears skin. Due to the fact that the films have a drug incorporated, it is not advisable to perform these studies directly in human volunteers.

The results of the PAF and the WA can be found in **Table 6.7**. The values of PAF range from 629.5 mN/cm^2 (F_{5A}) to 3304.5 mN/cm^2 (F_{10N}), while the values of WA range from 0.95 mJ/cm^2 (F_{20P}) to 3.66 mJ/cm^2 (F). The values of the PAF are in the same order of the results described for hydroxypropylcellulose topical films in human volunteers [457].

The NMP at 5% and 10% was able to significant increase ($P<0.05$) the PAF of the drug-loaded films and no statistical difference was found for the other films. Although Azone did not produce a significant alteration in the values of the PAF, the values of the PAF of the films F_{5A} and F_{10A} display a tendency to decrease the adhesion force of the drug-loaded films.

In what concerns WA, and except for the case of NMP in concentrations ranging from 5-20%, all other drug-loaded films display a significant decrease ($P<0.05$) in comparison with the situation in the absence of the drug.

From all the above results, we conclude that NMP seems to improve the bioadhesive properties of the drug-loaded films, while PG and Azone adversely affect bioadhesion to the skin.

4. Conclusions

In this work we have shown that the shape of the permeation profiles reveals, in the early stages, an unusually fast permeation followed by a region of constant flux. This sequence is most beneficial because it enables to rapidly attain pharmacological action. The fast initial permeation is a result of the GB initial burst release, but is also affected by the type and concentration of the additive incorporated in the films.
NMP is the penetration enhancer that produces the largest improvement on the permeation rate of GB, while PG induces only a moderate increase. Furthermore, the incorporation of 5% and 10% Azone in the films results in a decrease of flux and cumulative amount of GB permeated. The association between PG and Azone or NMP is not beneficial, contradicting some previous results.
The optimized F_{20N} film represents a significant improvement of the percutaneous penetration of GB. It amounts to about 6.9 fold when compared with saturated solution of GB. On the basis of the *in vitro* permeation results, the F_{20N} film is a very promising option for the effective delivery of GB through the skin.

The analysis of the GB release profiles revealed that the drug release kinetics from the films is mainly determined by a Fickian diffusion mechanism. It is also concluded, from inspection of fit factors, that except for the films F_{10N} and F_{20P10A}, the GB release profiles are not equivalent to the drug release profile from the film in the absence of penetration enhancers. These dissimilarities can also be found in the analysis of the magnitude of the burst release. In fact, the incorporation of the additives always increases burst release.

Finally, GB-loaded films, both in the presence and absence of penetration enhancers, are water permeable and have the ability to firmly adhere to the skin.

VII

Concluding remarks

1. Thesis highlights

The complexity of the skin structure and functions, as well as the many factors that govern the successful transdermal delivery of drugs was clearly illustrated in this thesis. In fact, the research carried out in this work aimed to embrace the most important aspects that are required for the design, development and therapeutic efficacy of pharmaceutical products intended for transdermal drug administration.

In a first step, the efforts were directed towards a further understanding of the physicochemical and biological nature of the skin, which holds an intimate relationship with the drug percutaneous permeation. The SC barrier function and its phase behavior are essentially determined by the lipid composition and physical conditions such as temperature and hydration. Focus was given on the investigation of phase transitions induced both by temperature and water in the SC and SC components (e.g. lipids and proteins), and their role in the selective permeability of skin. Apart from the contributions extensively discussed in Chapters II and III, these

studies have determined an acute consciousness of the complexity of the skin biology and microanatomy, which clearly influenced the subsequent steps, including the formulation studies. This influence was determinant in terms of selecting a film as the transdermal device, in the choice of the type of film, the specific polymers and other excipients used, and it led to an identification of the properties relevant to the study.

The main objectives in the first step of the development of the transdermal film were to create a non-occlusive film, in order to have the minimum influence in the normal functions of the skin (e.g. TEWL), and with good functional properties, so as to be comfortable and efficient when applied on the skin (Chapter IV). It should be stressed that these two aspects are critical for patient compliance. In fact, there are many factors that influence the effectiveness of a transdermal therapeutic system. The rate of drug permeation through the skin is crucial, since it determines whether or not the right amount of drug reaches the site of action within the body, in order to produce the pharmacological action. The system must be also bioadhesive in order to maintain an intimate and prolonged contact with the skin during the entire time of application. Finally, the potential for localized irritant and allergic cutaneous reactions must be negligible. As such, a major effort was made to reduce these adverse effects by the choice of non-irritant and non-allergenic excipients, gathered in a comfortable and non-occlusive film.

After the development of the transdermal film, four drugs with different physicochemical properties where incorporated in the film. The objective was to assess the possibility of using these films as the basis for universal transdermal delivery systems, capable of including different drugs. Emphasis was, however, given to the optimization of a galantamine containing trandermal device. Galantamine is a therapeutically relevant cholinesterase inhibitor used in the treatment of Alzheimer's disease, the most common form of dementia among older people that is progressive and fatal. The treatment of its symptoms can delay its progression, improving the quality of life both for the patients and their families. Chapters V and VI contain the contributions from this work to those goals.

2. Future work

Chapter IV contains the description of a systematic approach for obtaining films based on polyelectrolyte complexes with maximized interactions between oppositely charged polymers. The films obtained were able to release both hydrophilic and lipophilic drugs in a reliable, reproducible and sustained manner. The respective release profiles follow a quasi-zero order kinetics, and the permeation profile is such that the pharmacological response is rapidly attained. It would be interesting in the future to test this approach for polyelectrolyte complexes composed by other polymers, e.g. with different linear charge densities and backbone rigidities, and to assess the type of release profile obtained. These new polyelectrolyte complexes could be tested as drug delivery systems not only for transdermal drug administration, but also for more conventional routes.

It was also shown that the PSA applied on the PEC films has very good bioadhesive properties, does not induce irritation, is very easily applied onto the surface of the films and contributes for the prolonged drug release. Any future work involving the development of non self-adhesive transdermal delivery systems should further analyse the benefits of the use of this hydrophilic PSA, in alternative to the silicone based adhesives, that are costly, difficult to handle and occlusive.

The study of the drug delivery potential of the PEC films and the ability of PG, transcutol and glycofurol to increase the percutaneous permeation of the four drugs tested was analyzed in Chapter V. PG is considered an almost universal skin penetration enhancer, while transcutol acts as a penetration enhancer only in some molecules. Glycofurol is a widely used solvent in parenteral formulations, non-toxic, non-irritating, with a tolerability similar to PG and acted as a penetration enhancer in nasal formulations. Due to their good properties and structure it was considered relevant to test its ability to act also as a penetration enhancer in the skin. Our results indicate that glycofurol is able to increase the percutaneous permeation of drugs and, in some cases, the enhancing effect is higher than with PG. It would be very interesting and relevant to perform, in the future, a deep investigation about the

penetration enhancement ability of glycofurol, its mechanism of action and sensitization potential.

The results described on Chapter VI concern the percutaneous permeation of GB, from the optimized film. They indicate that this formulation, per se, represents a very significant improvement when compared with the saturated solution. In future work, the GB flux should be further optimized by the addition of other penetration enhancers, in order to allow a reduction in the size of the film. Furthermore, the impact of the procedures used to obtain the films on the quality and stability of the drug should be carefully investigated.

VIII

Appendix

1. Validation of the method for the quantification of drugs

The quantification methods used for IBU, PAR, GS and GB in the studies presented on Chapters V and VI, were validated according to the reference guidelines [405-407]. This validation is required in order to demonstrate that the method of choice is suitable for the intended use in terms of reliability and reproducibility of the results [458]. Linearity, sensitivity, accuracy, precision and the limit of detection and quantification were some of the determined parameters.

The validation begins by establishing the preliminary working range, for each drug, in acetate buffer pH 5.5 and PBS pH 7.4. Six standard samples were prepared in three different days from a freshly prepared stock solution of each drug in the two buffers. The absorbance of the standard samples is measured at least three times and the values recorded.

1.1 Test for homogeneity of the variances

The variance of the absorbance values determined for the drugs standard samples must be homogeneous and independent of the concentration, within the working range.

The data sets of the concentrations x_1 and x_6 were used to calculate variances $(s_1)^2$ and $(s_6)^2$. The F-test was performed in order to test if the variances have significant differences at the limits of the working range [406, 407]. The test value PW is determined from:

$$PW = (s_1)^2 / (s_6)^2, \quad \text{if} \quad (s_1)^2 > (s_6)^2$$
$$PW = (s_6)^2 / (s_1)^2, \quad \text{if} \quad (s_6)^2 > (s_1)^2 \qquad (\mathbf{7.1})$$

The value of PW is then compared to the values of the F-distribution.

All the values determined for PW were smaller than F critical (99%) which means that the difference between the variances is not significant. The variances are homogeneous and a simple regression analysis may be performed.

1.2 Linearity

The linearity of an analytical method can be defined as its ability to obtain test results that are directly or, by means of well-defined mathematical transformations, proportional to the analyte concentration in the samples within a certain range [458].

The linearity was evaluated by the regression with least squares estimation [405], followed by graphic representation, determination of the R^2 and inspection of the residuals.

The linear calibration function is given by:

$$y = a + bx \qquad (\mathbf{7.2})$$

where *y* is the signal (absorbance), *x* is the amount of analyte, *a* is the y-intercept and *b* the slope of the calibration curve.

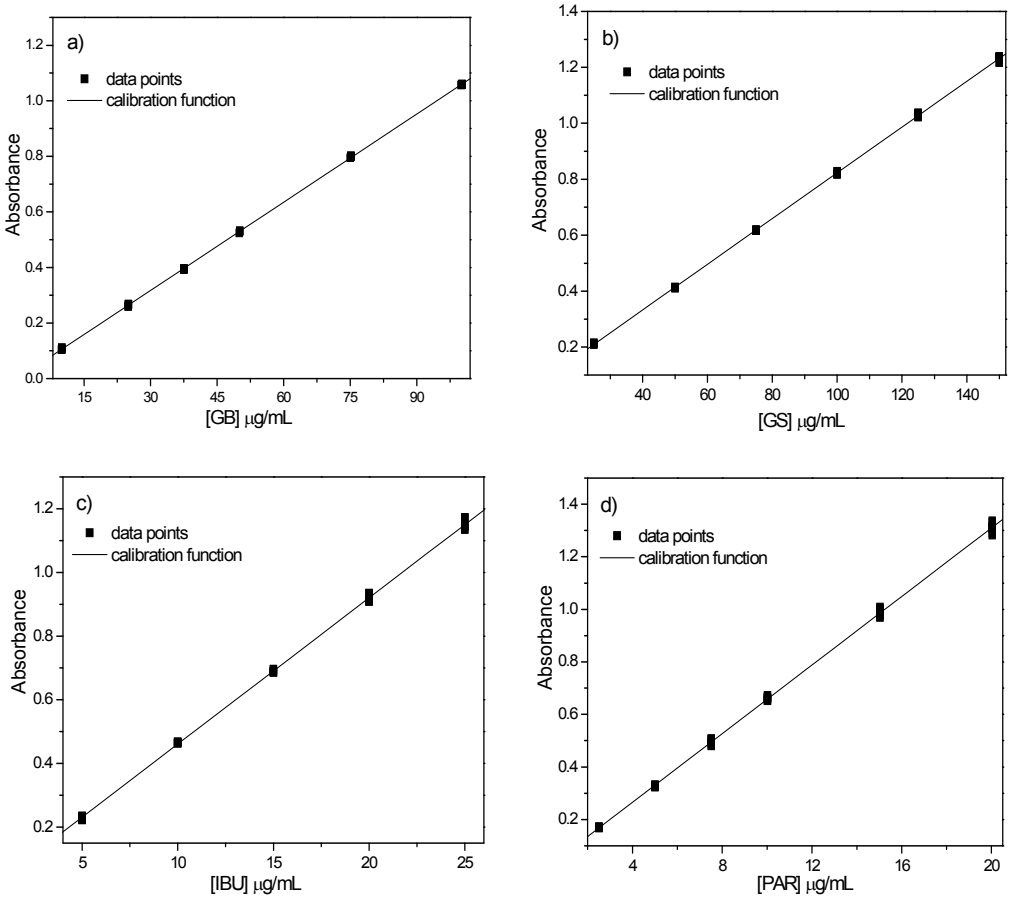

Figure 7.1 Data points and linear calibration functions for (a) GB, (b) GS, (c) ibuprofen and (d) paracetamol, in acetate buffer, pH=5.5.

The coefficients *a* and *b* provide an estimate of the true function. The slope (*b*) of the calibration functions is a measure of sensitivity and the ordinate intercept (*a*) is the calculated blank signal. The sensitivity is the ability of the analytical procedure to detect small changes of analyte concentration in the sample [458]. The quality of the

analytical procedures increases with sensitivity [406] and the standard error of the coefficients (*a* and *b)* is a measure of the method uncertainty due to indeterminate errors [459].

The linear calibration functions obtained from the measurement of the absorbance of standard samples of each drug in the buffers are depicted in **Figures 7.1** and **7.2** and the values are summarized in **Table 1**.

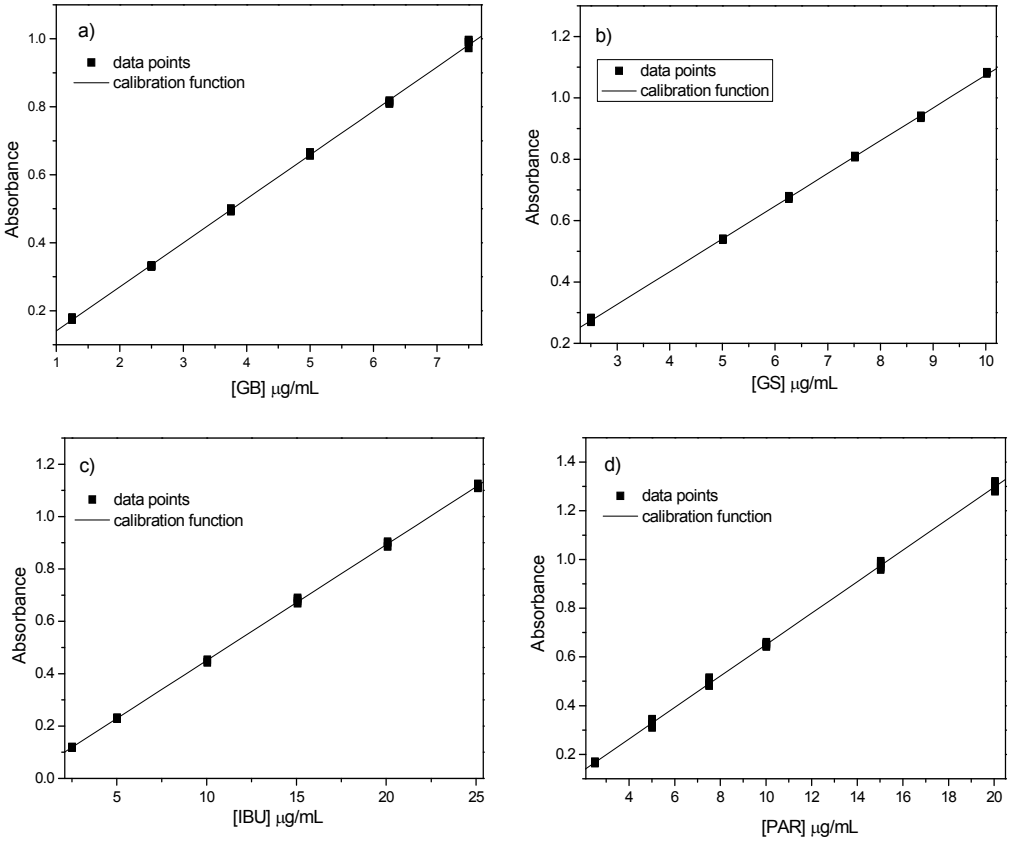

Figure 7.2 Data points and linear calibration functions for (a) GB, (b) GS, (c) IBU and (d) PAR, in PBS, pH=7.4.

Table 7.1 Example of linear calibration functions for the drugs in the two buffers used and respective UV absorption maxima and R^2. Value ± standard error.

	Acetate buffer, pH 5.5	PBS, pH 7.4
Galantamine base		
λ (nm)	289	212
a	-0.00043 ± 0.00082	0.01170 ± 0.00194
b	0.01058 ± 0.00001	0.129385 ± 0.00040
R^2	>0.999	0.999
Galantamine HBr		
λ (nm)	289	210
a	0.00554 ± 0.00178	0.00675 ± 0.00158
b	0.00817 ± 0.00001	0.10673 ± 0.00022
R^2	0.999	>0.999
Ibuprofen		
λ (nm)	221	221
a	0.00171 ± 0.00247	0.00785 ± 0.00157
b	0.04593 ± 0.00016	0.04423 ± 0.00010
R^2	0.999	>0.999
Paracetamol		
λ (nm)	243	243
a	0.00451 ± 0.00240	0.00472 ± 0.00265
b	0.06528 ± 0.00021	0.064591 ± 0.00028
R^2	0.999	0.999

The residual errors for each drug standard solution were evaluated and it was verified that they were randomly distributed about an average residual error of 0, with no apparent trend toward either smaller or larger residual errors and with frequent alternation of signal. These features indicate that the regression models are valid [459]. An example of a residual plot is shown on **Figure 7.3**.

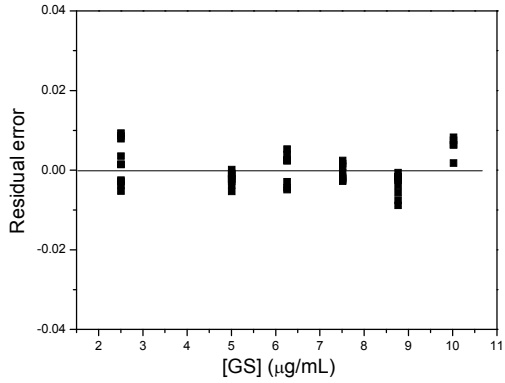

Figure 7.3 Typical plot of the residual errors for the values of absorbance determined as a function of GS concentration in PBS, pH 7.4.

1.3 Performance characteristics

The performance characteristics of the analytical methods used in the quantification of GB, GS, IBU and PAR were evaluated and the definitions are discussed in the next sections. The results are compiled in **Tables 7.2-7.5**.

1.3.1 Residual standard deviation

The residual standard deviation (S_y) is a measure of the scatter of the data values about the calibration function, and is a figure of merit to describe the precision of the calibration [406]. The quality of the analytical procedure increases as S_y decreases. The value of S_y is given by:

$$S_y = \sqrt{\frac{\sum_{i=1}^{N}(y_i - y_i^*)^2}{N-2}} \qquad (\mathbf{7.3})$$

where y_i corresponds to the signal at the i^{th} replicate for the concentration x_i, y_i* is the predictive absorbance value calculated from the calibrated function for the standard concentration x_i and N is the number of data points.

Table 7.2 Example of the performance characteristics of the spectrophotometric method used for the quantification of GB, in acetate buffer and PBS.

		Acetate buffer, pH 5.5	PBS, pH 7.4
	S_y	0.00315	0.00655
	S_{xo}	0.29733	0.05066
	V_{xo}	0.00599	0.01175
	DL	0.98119 µg/mL	0.16718 µg/mL
	QL	2.97333 µg/mL	0.50659 µg/mL
Accuracy (%)	Standard 1	101.4	101.9
	Standard 2	100.0	98.9
	Standard 3	99.3	99.8
	Standard 4	99.8	100.6
	Standard 5	100.5	99.1
	Standard 6	99.9	100.5
RSD (%)	Standard 1	0.89	0.03
	Standard 2	0.45	0.01
	Standard 3	0.03	0.02
	Standard 4	0.18	0.02
	Standard 5	0.10	0.01
	Standard 6	0.02	0.09

1.3.2 Standard deviation of the method

The standard deviation of the method (S_{xo}) is the figure of merit for the performance of the analytical method [406]. It is given by:

$$S_{xo} = \frac{S_y}{b} \qquad (7.4)$$

Table 7.3 Same as Table 7.2 relatively to the quantification of GS, in acetate buffer and PBS.

		Acetate buffer, pH 5.5	PBS, pH 7.4
	S_y	0.00573	0.00416
	S_{xo}	0.70148	0.03900
	V_{xo}	0.00802	0.00587
	DL	2.31487 µg/mL	0.128716 µg/mL
	QL	7.01477 µg/mL	0.39005 µg/mL
Accuracy (%)	Standard 1	100.9	100.7
	Standard 2	99.5	99.6
	Standard 3	99.8	100.1
	Standard 4	99.8	99.9
	Standard 5	100.4	99.6
	Standard 6	99.9	100.4
RSD (%)	Standard 1	0.42	0.10
	Standard 2	0.09	0.01
	Standard 3	0.07	0.02
	Standard 4	0.40	0.01
	Standard 5	0.49	0.01
	Standard 6	1.01	0.01

1.3.3 Coefficient of variation of the method

The coefficient of variation of the method (V_{xo}) is used for the comparison of different standardized analytical methods [406] and is given by:

$$V_{xo} = \frac{S_{xo}}{\bar{x}} \qquad (\mathbf{7.5})$$

where $\bar{x}$ is the mean value of *x*.

Table 7.4 Same as Table 7.2 relatively to the quantification of IBU, in acetate buffer and PBS.

		Acetate buffer, pH 5.5	PBS, pH 7.4
	S_y	0.00951	0.00607
	S_{xo}	0.20714	0.13724
	V_{xo}	0.01604	0.01058
	DL	0.68357 µg/mL	0.45289 µg/mL
	QL	2.07143 µg/mL	1.37238 µg/mL
Accuracy (%)	Standard 1	99.8	99.8
	Standard 2	99.1	100.0
	Standard 3	100.9	99.5
	Standard 4	99.9	100.6
	Standard 5	99.8	100.0
	Standard 6	100.1	99.9
RSD (%)	Standard 1	1.60	0.03
	Standard 2	0.22	0.04
	Standard 3	0.02	0.13
	Standard 4	0.05	0.25
	Standard 5	0.37	0.15
	Standard 6	0.52	0.10

Table 7.5 Same as Table 7.2 relatively to the quantification of PAR, in acetate buffer and PBS.

		Acetate buffer, pH 5.5	PBS, pH 7.4
S_y		0.01044	0.01150
S_{xo}		0.15987	0.17803
V_{xo}		0.01595	0.01777
DL		0.52758 µg/mL	0.58748 µg/mL
QL		1.59873 µg/mL	1.78026 µg/mL
Accuracy (%)	Standard 1	101.1	100.1
	Standard 2	98.8	98.8
	Standard 3	99.9	101.0
	Standard 4	100.4	99.9
	Standard 5	100.2	100.1
	Standard 6	99.8	99.9
RSD (%)	Standard 1	0.03	0.06
	Standard 2	0.04	0.47
	Standard 3	0.29	0.62
	Standard 4	0.11	0.11
	Standard 5	0.30	0.28
	Standard 6	0.37	0.25

1.3.4 Detection and quantification limit

The detection limit (*DL*) of an analytical method can be defined as the lowest concentration of analyte that produces a signal detectable above the noise level of the equipment [460] and is usually given by [405]:

$$DL = \frac{3.3 S_y}{b} \quad (\mathbf{7.6})$$

The quantification limit (*QL*) can be defined as the lowest concentration of analyte that can be precisely and accurately measured [460] and can be written as [405]:

$$QL = \frac{10S_y}{b} \quad (\mathbf{7.7})$$

1.3.5 Accuracy and precision

The accuracy of the method can be assessed by recovery of the analyte from a given sample [461]. The accuracy of any analytical procedure expresses its ability to give results as close as possible to the theoretical value [458] and can be calculated according to [461]:

$$accuracy = \frac{\bar{x}}{x_t} * 100 \quad (\mathbf{7.8})$$

where x_t is the value of x accepted as the true mean.

The precision of an analytical procedure is defined as the degree of dispersion of the results around the mean value, and is considered an estimate of the random error of the method [458]. The precision varies according to the sources of variation. The repeatability is the designation of the precision when the method is carried out under the same conditions (e.g. same analyst, laboratory, instruments and reagents), like in the case of the present work [458]. The relative standard deviation (*RSD*) is the relative error term used to describe precision and can be given by:

$$RSD = \frac{S_x}{\bar{x}} * 100 \quad (\mathbf{7.9})$$

where S_x is the standard deviation of the sample.

Values of S_y, S_{xo}, V_{xo}, *DL*, *QL*, accuracy and precision for each drug in the two buffers can be found in **Tables 7.2-7.5**.

IX

References

[1] B. Idson, Percutaneous absorption. J. Pharm. Sci. 64(6) (1975) 901-924.

[2] R.D. Gordon, T.A. Peterson, Four myths about transdermal drug delivery. Drug Delivery Technol. 3(4) (2003) 1-7.

[3] H.A.E. Benson, Transdermal drug delivery: penetration enhancement techniques. Curr. Drug Deliv. 2 (2005) 23-33.

[4] B.C. Finnin, T.M. Morgan, Transdermal penetration enhancers: applications, limitations, and potential. J. Pharm. Sci. 88(10) (1999) 955-957.

[5] S. Singh, An overview of transdermal drug delivery. Drug Delivery Report (2005) 35-40.

[6] B.W. Barry, Novel mechanisms and devices to enable successful transdermal drug delivery. Eur. J. Pharm. Sci. 14(2) (2001) 101-114.

[7] R. Wickett, M. Visscher, Structure and function of the epidermal barrier. Am. J. Infect. Control 34(10) (2006) S98-S110.

[8] M. Foldvari, Non-invasive administration of drugs through the skin: challenges in delivery system design. PSTT 3(12) (2000) 417-425.

[9] R. Paus, What is the 'true' function of the skin? Exp. Dermatol. 11 (2002) 159-187.

[10] G.S. Banker, C.T. Rhodes, Modern Pharmaceutics, Marcel Dekker, New York, 2002.

[11] K.C. Madison, Barrier function of the skin: "la raison d'Être" of the epidermis. J. Invest. Dermatol. 121 (2003) 231-241.

[12] K.A. Walters, Dermatological and transdermal formulations, Marcel Dekker, New York, 2002.

[13] M. Brown, G. Martin, S. Jones, F. Akomeah, Dermal and transdermal drug delivery systems: Current and future prospects. Drug Delivery 13(3) (2006) 175-187.

[14] J.E. Riviere, Dermal absorption models in toxicology and pharmacology, CRC Press, Boca Raton, 2006.

[15] R. Marks, The stratum corneum barrier: the final frontier. J. Nutr. 134 (2004) 2017S-2021S.

[16] P.M. Elias, Stratum corneum defensive functions: an integrated view. J. Invest. Dermatol. 125 (2005) 183-200.

[17] http://www.skiniworld.com/, (14/11/2007).

[18] V.C. Scanlon, T. Sanders, Essentials of Anatomy and Physiology, F. A. Davies company, Philadelphia, 2007.

[19] G.K. Menon, New insights into skin structure: scratching the surface. Adv. Drug Deliv. Rev. 54(Suppl. 1) (2002) S3-S17.

[20] A.V. Rawlings, P.J. Matts, Stratum corneum moisturization at the molecular level: an update in relation to the dry skin cycle. J. Invest. Dermatol. 124 (2005) 1099-1110.

[21] E. Berardesca, Disorders of skin barriers: clinical implications. J. Eur. Acad. Dermatol. Venereol. 16 (2002) 559-561.

[22] J.C.R. Jones, S.B. Hopkinson, L.E. Goldfinger, Structure and assembly of hemidesmosomes. BioEssays 20 (1998) 488-494.

[23] D.T. Woodley, Importance of the dermal-epidermal junction and recent advances. Dermatologica 174 (1987) 1-10.

[24] L. Norlén, Skin structure, function and formation - learning from cryo-electron microscopy of vitreous, fully hydrated native human epidermis. Int. J. Cosm. Sci. 25 (2003) 209-226.

[25] http://www.usccompany.com/index.asp?PageAction=Custom&ID=1, (2007).

[26] B. Sondell, L.-E. Thornell, T. Egelrud, Evidence that stratum corneum chymotryptic enzyme is transported to the stratum corneum extracellular space via lamellar bodies. J Invest. Dermatol. 104(5) (1995) 819-823.

[27] L. Norlén, A. Al-Amoudi, J. Dubochet, A cryotransmission electron microscopy study of skin barrier formation. J. Invest. Dermatol. 120 (2003) 555-560.

[28] L. Norlén, Skin barrier formation: the membrane folding model. J. Invest. Dermatol. 117 (2001) 823-829.

[29] J. van der Meulen, B.A.I. van den Bergh, A.A. Mulder, A.M. Mommaas, J.A. Bouwstra, H.K. Koerten, The use of vibratome sections for the ruthenium tetroxide protocol: a

key for optimal visualization of epidermal lipid bilayers of the entire human stratum corneum in transmission electron microscopy. J. Microsc. 184(1) (1996) 67-70.

[30] L. Landmann, Epidermal permeability barrier: transformation of lamellar granule disks into intercellular sheets by a membrane fusion process. J. Invest. Dermatol. 87 (1986) 202-206.

[31] C.R. Harding, The stratum corneum: structure and function in health and disease. Dermatol. Therapy 17 (2004) 6-15.

[32] P. Elias, Epidermal lipids, barrier function, and desquamation. J. Invest. Dermatol. 80 (1983) 44-49.

[33] H. Boddé, M. Kruithof, J. Brussee, H. Koerten, Visualisation of normal and enhanced $HgCl_2$ transport through human skin in vitro. Int. J. Pharm. 53 (1989) 13–24.

[34] J.A. Bouwstra, P.L. Honeywell-Nguyen, G.S. Gooris, M. Ponec, Structure of the skin barrier and its modulation by vesicular formulations. Prog. Lipid Res. 42 (2003) 1-36.

[35] R.O. Potts, M.L. Francoeur, Lipid biophysics of water loss through the skin. Proc. Natl. Acad. Sci. USA 87 (1990) 3871–3873.

[36] D.S. Rubenstein, A hard core look at rod packing in the skin. J. Invest. Dermatol. 123 (2004) ix–x.

[37] N.D. Lazo, J.G. Meine, D.T. Downing, Lipids are covalently attached to rigid corneocyte protein envelopes existing predominantly as β-sheets: a solid-state Nuclear Magnetic Resonance study. J. Invest. Dermatol. 105(2) (1995) 296-300.

[38] J. Swarbrick, J.C. Boylan, Encyclopedia of Pharmaceutical Technology, Marcel Dekker New York, 2002.

[39] A.E. Kalinin, A.V. Kajava, P.M. Steinert, Epithelial barrier function: assembly and structural features of the cornified cell envelope. BioEssays 24 (2002) 789-800.

[40] F. Chang, D.C. Swartzendruber, P.W. Wertz, C.A. Squier, Covalently bound lipids in keratinizing epithelia. Biochim. Biophys. Acta 1150 (1993) 98-102.

[41] O. Lopez, M. Cocera, P.W. Wertz, C. Lopez-Iglesias, A. de la Maza, New arrangement of proteins and lipids in the stratum corneum cornified envelope. Biochim. Biophys. Acta - Biomembranes 1768(3) (2007) 521-529.

[42] K.J. Robson, M.E. Stewart, S. Michelsen, N.D. Lazo, D.T. Downing, 6-Hydroxy-4-sphingenine in human epidermal ceramides. J. Lipid Res. 35 (1994) 2060-2068.

[43] P.W. Wertz, D.T. Downing, Covalently bound w-hydroxiacylsphingosine in the stratum corneum. Biochim. Biophys. Acta 917 (1987) 108-111.

[44] S. Meguro, Y. Arai, Y. Masukawa, K. Uie, I. Tokimitsu, Relationship between covalently bound ceramides and transepidermal water loss (TEWL). Arch. Dermatol. Res. 292 (2000) 463-468.

[45] P.W. Wertz, D.C. Swartzendruber, D.J. Kitko, K.C. Madison, D.T. Downing, The role of the corneocyte lipid envelopes in cohesion of the stratum corneum. J. Invest. Dermatol. 93 (1989) 169-172.

[46] P.W. Wertz, K.C. Madison, D.T. Downing, Covalently bound lipids of Human stratum corneum. J. Invest. Dermatol. 92 (1989) 109-111.

[47] M. Jarnik, M.N. Simon, A.C. Steven, Cornified cell envelope assembly: a model based on electron microscopic determinations of thickness and projected density. J. Cell Sci. 111(8) (1998) 1051-1060.

[48] M.A. Lampe, A.L. Burlingame, J. Whitney, M.L. Williams, B.E. Brown, E. Roitman, P.M. Elias, Human stratum corneum lipids: characterization and regional variations. J. Lipid Res. 24(2) (1983) 120-130.

[49] A. Weerheim, M. Ponec, Determination of stratum corneum lipid profile by tape stripping in combination with high-performance thin-layer chromatography. Arch. Dermatol. Res. 293(4) (2001) 191-199

[50] F. Bonté, A. Saunois, P. Pinguet, A. Meybeck, Existence of a lipid gradient in the upper stratum corneum and its possible biological significance. Arch. Dermatol. Res. 289 (1997) 78-82.

[51] M. Ponec, A. Weeheim, P. Lankhorst, P. Wertz, New acylceramide in native and reconstructed epidermis. J. Invest. Dermatol. 120 (2003) 581–588.

[52] S.M. Motta, M. Monti, S. Sesana, Ceramide composition of psoriatic scale. Biochim. Biophys. Acta 1182 (1993) 147-151.

[53] A. Al-Amoudi, J. Dubochet, L. Norlén, Nanostructure of epidermal extracellular space as observed by cryo-electron microscopy of vitreous sections of human skin. J. Invest. Dermatol. 124 (2005) 764-777.

[54] J.A. Bouwstra, G. Gooris, W. Bras, D. Downing, Lipid organization in pig stratum corneum. J. Lipid Res. 36 (1995) 685-695.

[55] J.A. Bouwstra, G.S. Gooris, J.A.V.D. Spek, W. Bras, Structural investigations of human stratum corneum by small-angle X-ray scattering. J. Invest. Dermatol. 97 (1991) 1005-1012.

[56] I. Hatta, N. Ohta, S. Ban, H. Tanaka, S. Nakata, X-ray diffraction study on ordered, disordered and reconstituted intercellular lipid lamellar structure in stratum corneum. Biophys. Chem. 89 (2001) 239-242.

[57] J. Bouwstra, G. Gooris, J.v.d. Spek, S. Lavrijsen, W. Bras, The lipid and protein structure of mouse stratum corneum: a wide and small angle diffraction study. Biochim. Biophys. Acta 1212 (1994) 183–192.

[58] N. Ohta, S. Ban, H. Tanaka, S. Nakata, I. Hatta, Swelling of intercellular lipid lamellar structure with short repeat distance in hairless mouse stratum corneum as studied by X-ray diffraction. Chem. Phys. Lipids 123 (2003) 1–8.

[59] J.A. Bouwstra, G.S. Gooris, F.E.R. Dubbelaar, M. Ponec, Phase behaviour of lipid mixtures based on human ceramides: coexistence of crystalline and liquid phases. J. Lipid Res. 42 (2001) 1759-1770.

[60] J.A. Bouwstra, G.S. Gooris, F.E.R. Dubbelaar, M. Ponec, Phase behaviour of stratum corneum lipid mixtures based on human ceramides: the role of natural and synthetic ceramide 1. J. Invest. Dermatol. 118 (2002) 606-617.

[61] J.A. Bouwstra, G.S. Gooris, F.E.R. Dubbelaar, A.M. Weerheim, A.P. Ijzerman, M. Ponec, Role of ceramide 1 in the molecular organization of stratum corneum lipids. J. Lipid Res. 39 (1998) 186–196.

[62] T.J. McIntosh, M.E. Stewart, D.T. Downing, X-ray diffraction analysis of isolated skin lipids: reconstitution of intercellular lipid domains. Biochemistry 35 (1996) 3649-3653.

[63] S.H. White, D. Mirejovsky, G.I. King, Structure of lamellar lipid domains and corneocyte envelopes of murine stratum corneum. An X-ray diffraction study. Biochemistry 27 (1988) 3725–3732.

[64] C.L. Gay, R.H. Guy, G.M. Golden, V.H.W. Mak, M.L. Francoeur, Characterization of low-temperature (i.e.< 65ºc) lipid transitions in human stratum corneum. J. Invest. Dermatol. 103 (1994) 233–239.

[65] A.V. Rawlings, Trends in stratum corneum research and the management of dry skin conditions. Int. J. Cosm. Sci. 25 (2003) 63-95.

[66] A.V. Rawlings, C.R. Harding, Moisturization and skin barrier function. Dermatol. Therapy 17 (2004) 43-48.

[67] G. Grubauer, P.M. Elias, K.R. Feingold, Transepidermal water loss: the signal for recovery of barrier structure and function. J. Lipid Res. 30 (1989) 323-333.

[68] B. Forslind, A domain mosaic model of the skin barrier. Acta Derm. Venereol. 74 (1994) 1-6.

[69] B. Forslind, S. Engström, J. Engblom, L. Norlén, A novel approach to the understanding of human skin barrier function. J. Dermatol. Sci. 14(2) (1997) 115-125.

[70] L. Norlén, Skin barrier structure and function: the single gel phase model. J. Invest. Dermatol. 117 (2001) 830-836.

[71] J.A. Bouwstra, F.E.R. Dubbelaar, G.S. Gooris, M. Ponec, The lipid organisation in the skin barrier. Acta Derm. Venereol. Suppl. 208 (2000) 23-30.

[72] J. Bouwstra, G. Pilgram, G. Gooris, H. Koerten, M. Ponec, New aspects of the skin barrier organization. Skin Pharmacol. Appl. Skin Physiol. 14 (2001) 52-62.

[73] I.H. Blank, J. Moloney, A.G.E.I. Simon, C. Apt, The diffusion of water across the stratum corneum as a function of its water content. J. Invest. Dermatol. 82 (1984) 188-194.

[74] M. Denda, J. Sato, Y. Masuda, T. Tsuchiya, J. Koyama, M. Kuramoto, P.M. Elias, K.R. Feingold, Exposure to a dry environment enhances epidermal permeability barrier function. J. Invest. Dermatol. 111 (1998) 858–863.

[75] C.R. Harding, A. Watkinson, A.V. Rawlings, Dry skin, moisturization and corneodesmolysis. Int. J. Cosm. Sci. 22 (2000) 21-52.

[76] P.J. Caspers, G.W. Lucassen, E.A. Carter, H.A. Bruining, G.J. Puppels, In Vivo confocal Raman microspectroscopy of the skin: noninvasive determination of molecular concentration profiles. J. Invest. Dermatol. 116(3) (2001) 434-442.

[77] P.W. Wertz, Stratum corneum lipids and water. Exog. Dermatol. 3 (2004) 53-56.

[78] M. Hara, A. Verkman, Glycerol replacement corrects defective skin hydration, elasticity, and barrier function in aquaporin-3-deficient mice. Proc. Natl. Acad. Sci. USA 100 (2003) 7360–7365.

[79] T. Ma, M. Hara, R. Sougrat, J. Verbavatz, A. Verkman, Impaired stratum corneum hydration in mice lacking epidermal water channel aquaporin-3. J. Biol. Chem. 277 (2002) 17147–17153.

[80] R. Panchagnula, Transdermal delivery of drugs. Ind. J. Pharmacol. 29 (1997) 140-156.

[81] B.J. Thomas, B.C. Finnin, The transdermal revolution. Drug Discovery Today 9(16) (2004) 697-703.

[82] M. Grob, P. Scheidegger, B. Wüthrich, Allergic skin reaction to celecoxib. Dermatology 201 (2000) 383-383.

[83] V.M. Meidan, M. Docker, A.D. Walmsley, W.J. Irwin, Low intensity ultrasound as a probe to elucidate the relative follicular contribution to total transdermal absorption. Pharm. Res. 15(1) (1998) 85-92.

[84] C. Ramachandran, D. Fleisher, Transdermal delivery of drugs for the treatment of bone diseases. Ad. Drug Deliv. Rev. 42 (2000) 197-223.

[85] T. Ogiso, T. Tanino, M. Iwaki, T. Shiraki, K. Okajima, T. Wada, Transfollicular drug delivery: penetration of drugs through human scalp skin and comparison of penetration between scalp and abdominal skins in vitro. J. Drug Target. 10(5) (2002) 369-378.

[86] N. Otberg, H. Richter, H. Schaefer, U. Blume-Peytavi, W. Sterry, J. Lademann, Variations of hair follicle size and distribution in different body sites. J. Invest. Dermatol. 122 (2004) 14-19.

[87] T. Serizawa, T. Onodera, K. Oba, Percutaneous absorption of a drug into hair follicles. Exog. Dermatol. 22 (1995) 195-200.

[88] L.M. Lieb, B.D. Brown, G.G. Krueger, A.P. Liimatta, R.N. Bryan, Description of the intrafollicular delivery of large molecular weight molecules to follicles of human scalp skin in vitro. J. Pharm. Sci. 86(9) (1997) 1022-1029.

[89] S. Mura, F. Pirot, M. Manconi, F. Falson, A.M. Fadda, Liposomes and niosomes as potential carriers for dermal delivery of minoxidil. J. Drug Targeting 15(2) (2007) 101-108.

[90] R.H. Guy, J. Hadgraft, Transdermal drug delivery, Marcel Dekker, New York, 2003.

[91] G.P. Moss, J.C. Dearden, H. Patel, M.T.D. Cronin, Quantitative structure-permeability relationships (QSPRs) for percutaneous absorption. Toxicol. in Vitro 16 (2002) 299-317.

[92] J. Hadgraft, Skin deep. Eur. J. Pharm. Biopharm. 58 (2004) 291-299.

[93] J.D. Bos, M.M.H.M. Meinardi, The 500 dalton rule for the skin penetration of chemical compounds and drugs. Exp. Dermatol. 9(3) (2000) 165-169.

[94] B.M. Magnusson, Y.G. Anissimov, S.E. Cross, M.S. Roberts, Molecular size as the main determinant of solute maximum flux across the skin. J. Invest. Dermatol. 122(4) (2004) 993-999.

[95] R.O. Potts, R.H. Guy, Prediction skin permeability. Pharm. Res. 9(5) (1992) 663-669.

[96] J. du Plessis, W.J. Pugh, A. Judefeind, J. Hadgraft, Physico-chemical determinants of dermal drug delivery: effects of the number and substitution pattern of polar groups. Eur. J. Pharm. Sci. 16 (2002) 107-112.

[97] A. Naik, Y.N. Kalia, R.H. Guy, Transdermal drug delivery: overcoming the skin's barrier function. PSST 3(9) (2000) 318-326.

[98] L. Cole, C. Heard, Skin permeation enhancement potential of Aloe Vera and a proposed mechanism of action based upon size exclusion and pull effect. Int. J. Pharm. 333(1-2) (2007) 10-16.

[99] D.D. Kim, Y.W. Chien, Transdermal delivery of dideoxynucleoside-type anti-HIV drugs. 2. The effect of vehicle and enhancer on skin permeation. J. Pharm. Sci. 85(2) (1996) 214-219.

[100] J.S. Ross, J.C. Shah, Reduction in skin permeation of N,N-diethyl-m-toluamide (DEET) by altering the skin/vehicle partition coefficient. J. Control. Release 67(2-3) (2000) 211-221.

[101] A.C. Williams, Transdermal and topical drug delivery; from theory to clinical practice, Pharmaceutical Press, London, 2003.

[102] R.C. Wester, H.I. Maibach, Percutaneous absorption of drugs. Clin. Pharmacokinet. 23(4) (1992) 253-266.

[103] K.V. Roskos, H.I. Maibach, R.H. Guy, The effect of aging on percutaneous absorption in man. J. Pharmacokinet. Biopharm. 17(6) (1989) 617-630.

[104] K.P. Wilhelm, A.B. Cua, H.I. Maibach, Skin aging. Effect on transepidermal water loss, stratum corneum hydration, skin surface pH, and casual sebum content. Arch. Dermatol. 127(12) (1991) 1806-1809.

[105] R.O. Potts, E.M. Buras, D.A. Chrisman, Changes with age in moisture content of human skin. J. Invest. Dermatol. 82 (1984) 97-100.

[106] R. Ghadially, B.E. Brown, S.M. Sequeira-Martin, K.R. Feingold, P.M. Elias, The aged epidermal permeability barrier. Structural, functional, and lipid biochemical abnormalities in humans and a senescent murine model. J. Clin. Invest. 95(5) (1995) 2281-2290.

[107] P. Buck, Skin barrier function: effect of age, race and inflammatory disease. Int. J. Aromat. 14(2) (2004) 70-76.

[108] G. Yosipovitch, A. Maayan-Metzger, P. Merlob, L. Sirota, Skin barrier properties in different body areas in neonates. Pediatrics 106(1) (2000) 105-108.

[109] J.-C. Tsai, Y.-L. Lo, Y.-H. Huang, C.-Y. Lin, H.-M. Sheu, Noninvasive characterization of regional variation in drug transport into human stratum corneum in vivo. Pharm. Res. 20(4) (2003) 632-638.

[110] A. Fullerton, J.R. Andersen, A. Hoelgaard, Permeation of nickel through human skin in vitro—effect of vehicles. Br. J. Dermatol. 118(4) (1988) 509-516.

[111] H. Zhai, H.I. Maibach, Skin occlusion and irritant and allergic contact dermatitis: an overview. Contact Dermatitis 44(4) (2001) 201-206.

[112] H. Zhai, H.I. Maibach, Occlusion vs. skin barrier functions. Skin Res. Technol. 8 (2002) 1-6.

[113] N. Ohara, K. Takayama, T. Nagai, Combined effect of d-limonene pretreatment and temperature on the rat skin permeation of lipophilic and hydrophilic drugs. Biol. Pharm. Bull. 18(3) (1995) 439-442.

[114] N. Ohara, K. Takayama, Y. Machida, T. Nagai, Combined effect of d-limonene and temperature on the skin permeation of ketoprofen. Int. J. Pharm. 105(1) (1994) 31-38.

[115] K.D. Peck, A.H. Ghanem, W.I. Higuchi, The effect of temperature upon the permeation of polar and ionic solutes through human epidermal membrane. J. Pharm. Sci. 84(8) (1995) 975-982.

[116] G.M. Golden, D.B. Guzek, R.R. Harris, J.E. Mckie, R.O. Potts, Stratum corneum lipid phase transitions and water barrier properties. Biochemistry 26 (1987) 2382-2388.

[117] W. Hull, Heat-enhanced transdermal drug delivery: a survey paper. J. App. Res. 2(1) (2002) 1-9.

[118] F. Akomeah, T. Nazir, G.P. Martin, M.B. Brown, Effect of heat on the percutaneous absorption and skin retention of three model penetrants. Eur. J. Pharm. Sci. 21(2-3) (2004) 337-345.

[119] C.L. Silva, S.C.C. Nunes, M.E.S. Eusébio, A.A.C.C. Pais, J.J.S. Sousa, Study of human stratum corneum and extracted lipids by thermomicroscopy and DSC. Chem. Phys. Lipids 140 (2006) 36–47.

[120] C.L. Silva, S.C.C. Nunes, M.E.S. Eusébio, A.A.C.C. Pais, J.J.S. Sousa, Thermal behavior of human stratum corneum. A differential scanning calorimetry study at high scanning rates. Skin Pharmacol. Physiol. 19 (2006) 132-139.

[121] J.A. Bouwstra, G.S. Gooris, M.A.S. Vries, J.A.V. Spek, W. Bras, Structure of human stratum corneum as a function of temperature and hydration: A wide-angle X-ray diffraction study. Int. J. Pharm. 84 (1992) 205–216.

[122] Y. Kalia, F. Pirot, R. Guy, Homogeneous transport in a heterogeneous membrane: water diffusion across human stratum corneum in vivo. Biophys. J. 71 (1996) 2692–2700.

[123] G. Grubauer, K.R. Feingold, R.M. Harris, P.M. Elias, Lipid content and lipid type as determinants of epidermal permeability barrier. J. Lipid Res. 30 (1989) 89-96.

[124] M.P. Schon, Animal models of psoriasis - What can we learn from them? J. Invest. Dermatol. 112(4) (1999) 405-410.

[125] F. Manigé, Epidermal barrier in disorders of the skin. Microsc. Res. Techn. 38(4) (1997) 361-372.

[126] J.A. Segre, Epidermal barrier formation and recovery in skin disorders. J. Clin. Invest. 116(5) (2006) 1150-1158.

[127] S.J. Rehfeld, W.Z. Plachy, M.L. Williams, P.M. Elias, Calorimetric and electron spin resonance examination of lipid phase transitions in human stratum corneum: molecular basis for normal cohesion and abnormal desquamation in recessive X-linked ichthyosis. J. Invest. Dermatol. 91 (1988) 499-505.

[128] B.W. Barry, Drug delivery routes in skin: a novel approach. Adv. Drug Deliv. Rev. 54 Suppl.(1) (2002) S31-S40.

[129] K. Moser, K. Kriwet, Y.N. Kalia, R.H. Guy, Enhanced skin permeation of a lipophilic drug using supersaturated formulations. J. Control. Release 73(2-3) (2001) 245-253.

[130] A.C. Williams, B.W. Barry, Penetration enhancers. Ad. Drug Delivery Rev. 56 (2004) 603-618.

[131] B.W. Barry, Is transdermal drug delivery research still important today? Drug Discovery Today 6(19) (2001) 967-971.

[132] J. Hadgraft, Passive enhancement strategies in topical and transdermal drug delivery. Int. J. Pharm. 184 (1999) 1-6.

[133] B.W. Barry, Lipid-protein-partitioning theory of skin penetration enhancement. J. Control. Release 15 (1991) 237-248.

[134] B.W. Barry, Breaching the skin's barrier to drugs. Nature Biotechnol. 22 (2004) 165-167.

[135] K. Takahashi, H. Sakano, M. Yoshida, N. Numata, N. Mizuno, Characterization of the influence of polyol fatty acid esters on the permeation of diclofenac through rat skin. J. Control. Release 73 (2001) 351-358.

[136] A. Naik, L.A.R.M. Pechtold, R.O. Potts, R.H. Guy, Mechanism of oleic acid-induced skin penetration enhancement in vivo in humans. J. Control. Release 37(3) (1995) 299-306.

[137] J.-C. Tsai, H.-M. Sheu, P.-L. Hung, C.-L. Cheng, Effect of barrier disruption by acetone treatment on the permeability of compounds with various lipophilicities: implications for the permeability of compromised skin. J. Pharm. Sci. 90 (2001) 1242-1254.

[138] K.A. Walters, J. Hadgraft, Pharmaceutical skin penetration enhancement, Marcel Dekker, NewYork, 1993.

[139] R. Aly, C. Shirley, B. Cunico, H.I. Maibach, Effect of prolonged occlusion on the microbial flora, pH, carbon dioxide and transepidermal water loss on Human skin. J. Invest. Dermatol. 71(6) (1978) 378-381.

[140] H. Zhai, J.P. Ebel, R. Chatterjee, K.J. Stone, V. Gartstein, K.D. Juhlin, A. Pelosi, H.I. Maibach, Hydration vs. skin permeability to nicotinates in man. Skin Res. Technol. 8(1) (2002) 13-18.

[141] H. Zhai, H.I. Maibach, Effects of skin occlusion on percutaneous absorption: an overview. Skin Pharmacol. Appl. Skin Physiol. 14 (2001) 1-10.

[142] C.R. Behl, G.L. Flynn, T. Kurihara, N. Harper, W. Smith, W.I. Higuchi, N.F.H. Ho, C.L. Pierson, Hydration and percutaneous absorption: 1. Influence of hydration on alkanol permeation through hairless mouse skin. J. Invest. Dermatol. 75(4) (1980) 346-352.

[143] J.A. Bouwstra, A. Graaff, G.S. Gooris, J. Nijsse, J.W. Wiechers, A.C. Aelst, Water distribution and related morphology in Human stratum corneum at different hydration levels. J. Invest. Dermatol. 120 (2003) 750-758.

[144] R.R. Warner, K.J. Stone, Y.L. Boissy, Hydration disrupts human stratum corneum ultrastructure. J. Invest. Dermatol. 120(2) (2003) 275-284.

[145] K.B. Sloan, S. Wasdo, Designing for topical delivery: prodrugs can make the difference. Med. Res. Reviews 23(6) (2003) 763-793.

[146] S. Bracht, Transdermal therapeutic system: a review. Innov. Pharm. Technol. (2000) 92-98.

[147] B.-Y. Kim, H.-J. Doh, T.N. Le, W.-J. Cho, C.-S. Yong, H.-G. Choi, J.S. Kim, C.-H. Lee, D.-D. Kim, Ketorolac amide prodrugs for transdermal delivery: stability and in vitro rat skin permeation studies. Int. J. Pharm. 293(1-2) (2005) 193-202.

[148] H. Imoto, Z. Zhou, A.L. Stinchcomb, G.L. Flynn, Transdermal prodrug concepts: permeation of buprenorphine and its alkyl esters through hairless mouse skin and influence of vehicles. Biol. Pharm. Bull. 19 (2) (1996) 263-267.

[149] C. Udata, G. Tirucherai, A.K. Mitra, Synthesis, stereoselective enzymatic hydrolysis, and skin permeation of diastereomeric propranolol ester prodrugs. J. Pharm. Sci. 88(5) (1999) 544-550.

[150] F.S.D. Rosa, A.C. Tedesco, R.F.V. Lopez, M.B.R. Pierre, N. Lange, J.M. Marchetti, J.C.G. Rotta, M.V.L.B. Bentley, In vitro skin permeation and retention of 5-aminolevulinic acid ester derivatives for photodynamic therapy. J. Control. Release 89(2) (2003) 261-269.

[151] J.J. Wang, K.C. Sung, J.F. Huang, C.H. Yeh, J.Y. Fang, Ester prodrugs of morphine improve transdermal drug delivery: a mechanistic study. J. Pharm. Pharmacol. 59(7) (2007) 917-925.

[152] S.R. Gorukanti, L. Li, K.H. Kim, Transdermal delivery of antiparkinsonian agent, benztropine. I. Effect of vehicles on skin permeation. Int. J. Pharm. 192(2) (1999) 159-172.

[153] R. Aboofazeli, H. Zia, T.E. Needham, Transdermal delivery of Nicardipine: an approach to in vitro permeation enhancement. Drug Delivery 9(4) (2002) 239-247.

[154] M.A.H.M. Kamal, N. Iimura, T. Nabekura, S. Kitagawa, Enhanced skin permeation of diclofenac by ion-pair formation and further enhancement by microemulsion. Chem. Pharm. Bull. 55(3) (2007) 368-371.

[155] M.A.H.M. Kamal, N. Iimura, T. Nabekura, S. Kitagawa, Enhanced skin permeation of salicylate by ion-pair formation in non-aqueous vehicle and further enhancement by ethanol and l-menthol. Chem. Pharm. Bull. 54(4) (2006) 481-484.

[156] P. Mayorga, F. Puisieux, G. Couarraze, Formulation study of a transdermal delivery system of primaquine. Int. J. Pharm. 132(1-2) (1996) 71-79.

[157] K. Moser, K. Kriwet, C. Froehlich, Y.N. Kalia, R.H. Guy, Supersaturation: enhancement of skin penetration and permeation of a lipophilic drug. Pharm. Res. 18(7) (2001) 1006-1011.

[158] K. Moser, K. Kriwet, Y.N. Kalia, R.H. Guy, Stabilization of supersaturated solutions of a lipophilic drug for dermal delivery. Int. J. Pharm. 224(1-2) (2001) 169-176.

[159] M. Iervolino, S.L. Raghavan, J. Hadgraft, Membrane penetration enhancement of ibuprofen using supersaturation. Int. J. Pharm. 198(2) (2000) 229-238.

[160] U. Kumprakob, J. Kawakami, I. Adachi, Permeation enhancement of ketoprofen using a supersaturated system with antinucleant polymers. Biol. Pharm. Bull. 28(9) (2005) 1684-1688.

[161] P.W. Stott, A.C. Williams, B.W. Barry, Transdermal delivery from eutectic systems: enhanced permeation of a model drug, ibuprofen. J. Control. Release 50(1-3) (1998) 297-308.

[162] Y. Kaplun-Frischoff, E. Touitou, Testosterone skin permeation enhancement by menthol through formation of eutectic with drug and interaction with skin lipids. J. Pharm. Sci. 86(12) (1997) 1394-1399.

[163] P.W. Stott, A.C. Williams, B.W. Barry, Mechanistic study into the enhanced transdermal permeation of a model beta-blocker, propranolol, by fatty acids: a melting point depression effect. Int. J. Pharm. 219(1-2) (2001) 161-176.

[164] P. Mura, F. Maestrelli, M.L. Gonzalez-Rodriguez, I. Michelacci, C. Ghelardini, A.M. Rabasco, Development, characterization and in vivo evaluation of benzocaine-loaded liposomes. Eur. J. Pharm. Biopharm. 67(1) (2007) 86-95.

[165] P.N. Gupta, V. Mishra, A. Rawat, P. Dubey, S. Mahor, S. Jain, D.P. Chatterji, S.P. Vyas, Non-invasive vaccine delivery in transfersomes, niosomes and liposomes: a comparative study. Int. J. Pharm. 293(1-2) (2005) 73-82.

[166] M. Manconi, C. Sinico, D. Valenti, F. Lai, A.M. Fadda, Niosomes as carriers for tretinoin: III. A study into the in vitro cutaneous delivery of vesicle-incorporated tretinoin. Int. J. Pharm. 311(1-2) (2006) 11-19.

[167] N. Dayan, E. Touitou, Carriers for skin delivery of trihexyphenidyl HCl: ethosomes vs. liposomes. Biomaterials 21(18) (2000) 1879-1885.

[168] M.M.A. Elsayed, O.Y. Abdallah, V.F. Naggar, N.M. Khalafallah, Deformable liposomes and ethosomes: mechanism of enhanced skin delivery. Int. J. Pharm. 322(1-2) (2006) 60-66.

[169] I.A. Alsarra, A.A. Bosela, S.M. Ahmed, G.M. Mahrous, Proniosomes as a drug carrier for transdermal delivery of ketorolac. Eur. J. Pharm. Biopharm. 59(3) (2005) 485-490.

[170] J.-Y. Fang, S.-Y. Yu, P.-C. Wu, Y.-B. Huang, Y.-H. Tsai, In vitro skin permeation of estradiol from various proniosome formulations. Int. J. Pharm. 215(1-2) (2001) 91-99.

[171] S. Hatziantoniou, G. Deli, Y. Nikas, C. Demetzos, G.T. Papaioannou, Scanning electron microscopy study on nanoemulsions and solid lipid nanoparticles containing high amounts of ceramides. Micron 38(8) (2007) 819-823.

[172] O. Sonneville-Aubrun, J.T. Simonnet, F. L'Alloret, Nanoemulsions: a new vehicle for skincare products. Ad. Colloidal Interf. Science 108-109 (2004) 145-149.

[173] H. Wu, C. Ramachandran, A.U. Bielinska, K. Kingzett, R. Sun, N.D. Weiner, B.J. Roessler, Topical transfection using plasmid DNA in a water-in-oil nanoemulsion. Int. J. Pharm. 221(1-2) (2001) 23-34.

[174] S.L. Borgia, M. Regehly, R. Sivaramakrishnan, W. Mehnert, H.C. Korting, K. Danker, B. Röder, K.D. Kramer, M. Schäfer-Korting, Lipid nanoparticles for skin penetration enhancement—correlation to drug localization within the particle matrix as determined by fluorescence and parelectric spectroscopy. J. Control. Release 110(1) (2005) 151-163.

[175] S.R. Patel, H. Zhong, A. Sharma, Y.N. Kalia, In vitro and in vivo evaluation of the transdermal iontophoretic delivery of sumatriptan succinate. Eur. J. Pharm. Biopharm. 66(2) (2007) 296-301.

[176] B. Mudry, P.-A. Carrupt, R.H. Guy, M.B. Delgado-Charro, Quantitative structure–permeation relationship for iontophoretic transport across the skin. J. Control. Release 122(2) (2007) 165-172.

[177] S. Tokumoto, N. Higo, K. Sugibayashi, Effect of electroporation and pH on the iontophoretic transdermal delivery of human insulin. Int. J. Pharm. 326(1-2) (2006) 13-19.

[178] H. Ueda, K. Sugibayashi, Y. Morimoto, Skin penetration-enhancing effect of drugs by phonophoresis. J. Control. Release 37(3) (1995) 291-297.

[179] V.M. Meidan, A.D. Walmsley, W.J. Irwina, Phonophoresis is it a reality? Int. J. Pharm. 118(2) (1995) 129-149.

[180] G. Merino, Y.N. Kalia, M.B. Delgado-Charro, R.O. Potts, R.H. Guy, Frequency and thermal effects on the enhancement of transdermal transport by sonophoresis. J. Control. Release 88 (2003) 85-94.

[181] J.W. Hooper, J.W. Golden, A.M. Ferro, A.D. King, Smallpox DNA vaccine delivered by novel skin electroporation device protects mice against intranasal poxvirus challenge. Vaccine 25(10) (2007) 1814-1823.

[182] T.-W. Wong, C.-H. Chen, C.-C. Huang, C.-D. Lin, S.-W. Hui, Painless electroporation with a new needle-free microelectrode array to enhance transdermal drug delivery. J. Control. Release 110(3) (2006) 557-565.

[183] W.-R. Lee, S.-C. Shen, C.-R. Liu, C.-L. Fang, C.-H. Hu, J.-Y. Fang, Erbium:YAG laser-mediated oligonucleotide and DNA delivery via the skin: an animal study. J. Control. Release 115(3) (2006) 344-353.

[184] D. Howes, R. Guy, J. Hadgraft, J. Heylings, U. Hoeck, F. Kemper, H. Maibach, J.-P. Marty, H. Merk, J. Parra, D. Rekkas, I. Rondelli, H. Schaefer, U. Täuber, N. Verbiese, Methods for Assessing Percutaneous Absorption. The Report and Recommendations of ECVAM Workshop 13. ATLA 24 (1996) 81-106.

[185] K. Witt, D. Bucks, Studying in vitro skin penetration and drug release to optimize dermatological formulations. Pharm. Technol. (2003).

[186] N. Leveque, S. Makki, J. Hadgraft, P. Humbert, Comparison of Franz cells and microdialysis for assessing salicylic acid penetration through human skin. Int. J. Pharm. 269 (2004) 323-328.

[187] OECD, OECD guideline for the testing of Chemicals. Draft guideline 428: Skin Absorption in vitro method. (2000) 1-6.

[188] OECD, Draft guidance document for the conduct of skin absorption studies. OECD environmental Health and Safety Publications Series on testing and assessment Nº 28. (2000) 1-23.

[189] N. Sekkat, Y.N. Kalia, R.H. Guy, Biophysical study of porcine ear skin in vitro and its comparison to human skin in vivo. J. Pharm. Sci. 91(11) (2002) 2376-2381.

[190] F.P. Schmook, J.G. Meingassner, A. Billich, Comparison of human skin or epidermis models with human and animal skin in in-vitro percutaneous absorption. Int. J. Pharm. 215(1-2) (2001) 51-56.

[191] M.J. Bartek, J.A. Labudde, H.I. Maibach, Skin permeability in vivo: comparison in rat, rabbit, pig and man. J. Invest. Dermatol. 58(3) (1972) 114-123.

[192] G.A. Simon, H.I. Maibach, The pig as an experimental animal model of percutaneous permeation in man: qualitative and quantitative observations - an overview. Skin Pharmacol. Appl. Skin Physiol. 13 (2000) 229-234.

[193] U. Jacobi, M. Kaiser, R. Toll, S. Mangelsdorf, H. Audring, N. Otberg, W. Sterry, J. Lademann, Porcine ear skin: an in vitro model for human skin. Skin Res. Technol. 13(1) (2007) 19-24.

[194] K. Moser, K. Kriwet, A. Naik, Y.N. Kalia, R.H. Guy, Passive skin penetration enhancement and its quantification in vitro. Eur. J. Pharm. Biopharm. 52 (2001) 102-112.

[195] SCCNFP/075/03, Opinion concerning basic criteria for the in vitro assessment of dermal absorption of cosmetic ingredients (2003).

[196] E. Commission, Guidance Document on dermal absorption, 2000.

[197] W.E. Hennink, C.V.v. Nostrum, Novel crosslinking methods to design hydrogels. Ad. Drug Deliv. Rev. 54 (2002) 13-36.

[198] L. Noble, A.I. Gray, L. Sadiq, I.F. Uchegbu, A non-covalently cross-linked chitosan based hydrogel. Int. J. Pharm. 192(2) (1999) 173-182.

[199] N.A. Peppas, P. Bures, W. Leobandung, H. Ichikawa, Hydrogels in pharmaceutical formulations. Eur. J. Pharm. Biopharm. 50 (2000) 27-46.

[200] P. Gupta, K. Vermani, S. Garg, Hydrogels: from controlled release to pH-responsive drug delivery. Drug Discovery Today 7(10) (2002) 569-579.

[201] J. Berger, M. Reist, J.M. Mayer, O. Felt, R. Gurny, Structure and interactions in chitosan hydrogels formed by complexation or aggregation for biomedical applications. Eur. J. Pharm. Biopharm. 57(1) (2004) 35-52.

[202] J. Berger, M. Reist, J.M. Mayer, O. Felt, N.A. Peppas, R. Gurny, Structure and interactions in covalently and ionically crosslinked chitosan hydrogels for biomedical applications. Eur. J. Pharm. Biopharm. 57 (2004) 19-34.

[203] J.W. Lee, S.Y. Kim, S.S. Kim, Y.M. Lee, K.H. Lee, S.J. Kim, Synthesis and characteristics of interpenetrating polymer network hydrogel composed of chitosan and poly(acrylic acid). J. Appl. Polymer Sci. 73(1) (1999) 113-120.

[204] C.S. Satish, K.P. Satish, H.G. Shivakumar, Hydrogels as controlled drug delivery systems: synthesis, crosslinking, water and drug transport mechanism. Ind. J. Pharm. Sci. 68(2) (2006) 133-140.

[205] S.M. Al-Saidan, B.W. Barry, A.C. Williams, Differential scanning calorimmetry of human and animal stratum corneum membranes. Int. J. Pharm. 168 (1998) 17-22.

[206] B.F.V. Duzee, Thermal analysis of human stratum corneum. J. Invest. Dermatol. 75 (1975) 404–408.

[207] G.M. Golden, D.B. Guzek, R.R. Harris, J.E. Mckie, R.O. Potts, Lipid thermotropic transitions in human stratum corneum. J. Invest. Dermatol. 86 (1986) 255-259.

[208] W.H.M.C. Hinsberg, J.C. Verhoef, H.E. Junginger, H.E. Boddé, Thermoelectrical analysis of the human skin barrier. Thermochim. Acta 248 (1995) 303-318.

[209] R. Neubert, K. Raith, S. Raudenkolb, S. Wartewig, Thermal degradation of ceramides as studied by mass spectrometry and vibrational spectroscopy. Anal. Commun. 35 (1998) 161-164.

[210] T. Ogiso, H. Ogiso, T. Paku, M. Iwaki, Phase transitions of rat stratum corneum lipids by an electron paramagnetic resonance study and relationship of phase states to drug penetration. Biochim. Biophys. Acta 1301 (1996) 97-104.

[211] G.S.K. Pilgram, A.M.E. Pelt, J.A. Bouwstra, H.K. Koerten, Electron diffraction provides new information on human stratum corneum lipid organization studied in relation to depth and temperature. J. Invest. Dermatol. 113 (1999) 403-409.

[212] J.A. Bouwstra, G.S.K. Pilgram, M. Ponec, Does a single gel phase exist in stratum corneum? J. Invest. Dermatol. 118 (2002) 897-901.

[213] S. Engstrom, K. Ekelund, J. Engblom, L. Eriksson, E. Sparr, The skin barrier from a lipid perspective. Acta Derm. Venereol. 208 (2000) 31-35.

[214] J.A. Bouwstra, L.J.C. Peschier, J. Brussee, H.E. Boddé, Effect of n-alkyl-azocycloheptan-2-ones including azone on thermal behaviour of human stratum corneum. Int. J. Pharm. 52 (1989) 47–54.

[215] I. Brinkmann, C.C. Muller-Goymann, Role of Isopropyl Myristate, Isopropyl alcohol and a combination of both in hydrocortisone permeation across the Human stratum corneum. Skin Pharmacol. Appl. Skin Physiol. 16 (2003) 393-404.

[216] P.W. Cornwell, B.W. Barry, J.A. Bouwstra, G.S. Gooris, Modes of action of terpene penetration enhancers in human skin; differential scanning calorimetry, small-angle X-ray diffraction and enhancer uptake studies. Int. J. Pharm 127 (1996) 9-26.

[217] J. Hirvonen, R. Rajala, P. Vihervaara, E. Laine, P. Paronen, A. Urtti, Mechanism and reversibility of penetration enhancer action in the skin - a DSC study. Eur. J. Pharm. Biopharm. 40 (1994) 81-85.

[218] Y.S.R. Krishnaiah, V. Satyanarayana, R.S. Karthikeyan, Effect of the solvent system on the in vitro permeability of nicardipine hydrochloride through excised rat epidermis. J. Pharmacol. Pharm. Sci. 5 (2002) 124-130.

[219] G.S.K. Pilgram, J. Meulen, G.S. Gooris, H.K. Koerten, J.A. Bouwstra, The influence of two azones and sebaceous lipids on the lateral organization of lipids isolated from human stratum corneum. Biochim. Biophys. Acta 1511 (2001) 244-254.

[220] G.S.K. Pilgram, A.M.E. Pelt, H.K. Koerten, J.A. Bouwstra, The effect of two azones on the lateral lipid organization of human stratum corneum and its permeability. Pharm. Res. 17 (2000) 796-802.

[221] H.K. Vaddi, P.C. Ho, Y.W. Chan, S.Y. Chan, Terpenes in ethanol: haloperidol permeation and partition through human skin and stratum corneum changes. J. Control. Release 81 (2002) 121.

[222] R. Neubert, W. Rettig, S. Wartewig, M. Wegener, A. Wienhold, Structure of stratum corneum lipids characterized by FT-Raman spectroscopy and DSC. II. Mixtures of ceramides and saturated fatty acids. Chem. Phys. Lipids 89 (1997) 3-14.

[223] M. Wegener, R. Neubert, W. Rettig, S. Wartewig, Structure of stratum corneum lipids characterized b FT-Raman spectroscopy and DSC. I. Ceramides. Int. J. Pharm. 128 (1996) 203-213.

[224] H. Tanojo, J.A. Bouwstra, H.E. Junginger, H.E. Boddé, Subzero thermal anlysis of human stratum corneum. Pharm. Res. 11 (1994) 1610-1616.

[225] H. Tanojo, J.A. Bouwstra, H.E. Junginger, H.E. Boddé, Thermal analysis studies of human skin and skn barrier modulation by fatty acids and propylene glycol. J. Therm. Anal. Calorim. 57 (1999) 313-322.

[226] G.S. Gooris, J.A. Bouwstra, Infrared spectroscopic study of stratum corneum model membranes prepared from human ceramides, cholesterol, and fatty acids. Biophys. J. 92 (2007) 2785-2795.

[227] J.A. Bouwstra, M.A.d. Vries, G.S. Gooris, W. Bras, J. Brussee, M. Ponec, Thermodynamic and structural aspects of the skin barrier. J. Control. Release 15 (1991) 209-220.

[228] R. Pouliot, L. Germain, F.A. Auger, N. Tremblay, J. Juhasz, Physical characterization of the stratum corneum of an in vitro human skin equivalent produced by tissue engineering and its comparison with normal human skin by ATR-FTIR spectroscopy and thermal analysis (DSC). Biochim. Biophys. Acta 1439 (1999) 341-352.

[229] M. Wegener, R. Neubert, W. Rettig, S. Wartewig, Structure of stratum corneum lipids characterized by FT-Raman spectroscopy and DSC. III. Mixtures of ceramides and cholesterol. Chem. Phys. Lipids 88 (1997) 73-82.

[230] A. Alonso, N.C. Meirelles, M. Tabak, Lipid chains dynamics in stratum corneum studied by spin label electron paramagnetic resonance. Chem. Phys. Lipids 104 (2000) 101-111.

[231] Y. Chen, T.S. Wiedmann, Human stratum corneum lipids have a distorted orthorhombic packing at the surface of cohesive failure. J. Invest. Dermatol. 107 (1996) 15-19.

[232] E. Sparr, L. Eriksson, J.A. Bouwstra, K. Ekelund, AFM study of lipid monolayers: III. Phase behavior of ceramides, cholesterol and fatty acids. Langmuir 17 (2001) 164-172.

[233] J.R. Hill, P.W. Wertz, Molecular models of the intercellular lipid lamellae from epidermal stratum corneum. Biochim. Biophys. Acta 1616 (2003) 121–126.

[234] G.S.K. Pilgram, A.M.E. Pelt, G.T. Oostergetel, H.K. Koerten, J.A. Bouwstra, Study on the lipid organization of stratum corneum lipid models by cryo-electron diffraction. J. Lipid Res. 39 (1998) 1669–1679.

[235] D.C. Swartzendruber, P.W. Wertz, D.J. Kitko, K.C. Madison, D.T. Downing, Molecular models of the intercellular lipid lamellae in mammalian stratum corneum. J. Invest. Dermatol. 92 (1989) 251-257.

[236] B. Glombitza, C.C. Muller-Goymann, Influence of different ceramides on the structure of in vitro model lipid systems of the stratum corneum lipid matrix. Chem. Phys. Lipids 117 (2002) 29-44.

[237] T.J. McIntosh, Organization of skin stratum corneum extracellular lamellae: diffraction evidence for asymmetric distribution of cholesterol. Biophys. J. 85 (2003) 1675–1681.

[238] T.F.J. Pijpers, V.B.F. Mathot, B. Goderis, R.L. Scherrenberg, E.W.V. Vegte, High-speed calorimetry for the study of the kinetics of (de)vitrification, crystallization, and melting of macromolecules. Macromolecules 35 (2002) 3601-3613.

[239] C. McGregor, M.H. Saunders, G. Buckton, R.D. Saklatvala, The use of high-speed differential scanning calorimetry (hyper-dsc) to study the thermal properties of carbamazepine polymorphs. Thermochim. Acta 417 (2004) 231-237.

[240] J.C. Hipeaux, M. Born, J.P. Durand, P. Claudy, J.M. Létoffé, Physico-chemical characterization of base stocks and thermal analysis by differential scanning calorimetry and thermomicroscopy at low temperature. Thermochim. Acta 348 (2000) 147-159.

[241] P.N. Simões, L.M. Pedroso, A.A. Portugal, J.L. Campos, Thermal decomposition of solid mixtures of 2-oxy-4,6-dinitramine-s-triazine (DNAM) and phase stabilized ammonium nitrate (PSAN). Thermochim. Acta 364 (2000) 71-85.

[242] J.D. Dunitz, Phase transitions in molecular crystals from a chemical viewpoint. Pure Appl. Chem. 63 (1991) 117-185.

[243] D. Giron, Investigations of polymorphism and pseudo-polymorphism in pharmaceuticals by combined thermoanalytical techniques. J. Therm. Anal. Calorim. 64 (2001) 37-60.

[244] M.L.P. Leitão, R.A.E. Castro, F.S. Costa, J.S. Redinha, Phase transitions of 1,2-cyclohexanediol isomers studied by polarised light microscopy and differential thermal analysis. Thermochim. Acta 378 (2001) 117-124.

[245] R. Sabbah, A. Xu-Lou, J.S. Chickos, M.L.P. Leitão, M.V. Roux, L.A. Torres, Reference materials for calorimetry and differential thermal analysis. Thermochim. Acta 331 (1999) 93-204.

[246] R. Marks, R. Dawber, Skin surface biopsy: an improved technique for the examination of the horny layer. Br. J. Dermatol. 84 (1971) 117-123.

[247] M.A. Yamane, A.C. Williams, B.W. Barry, Effects of terpenes and oleic acids as skin penetration enhancers towards 5-fluorouracil as assessed with time; permeation, partitioning and differential scanning calorimetry. Int. J. Pharm. 116 (1995) 237-251.

[248] G.L. Wilkes, A. Nguyen, R. Wildnauer, Structure-property relations of human and neonatal rat stratum corneum. I.Thermal stability of the crystalline lipid structure as studied by X-ray diffraction and differential thermal analysis. Biochim. Biophys. Acta 304 (1973) 267-275.

[249] J.W. Han, M. Kamber, Data mining: concepts and techniques, Morgan Kaufmann San Francisco, 2001.

[250] J. Bouwstra, G. Gooris, M. Ponec, The lipid organisation of the skin barrier: liquid and crystalline domains coexist in lamellar phases. J. Biol. Physics 28 (2002) 211-223.

[251] R.N.A.H. Lewis, R.N. McElhaney, Fourier transform infrared spectroscopy in the study of hydrated lipids and lipid bilayer membranes, John Wiley & Sons Ltd, New York, 1996.

[252] M. Mimeault, D. Bonenfant, FTIR spectrocopic analysis of the temperature and pH influences on stratum corneum lipid phase behavior and interactions. Talanta 56 (2002) 295-405.

[253] H.R. Moghimi, A.C. Williams, B.W. Barry, A lamellar matrix model for stratum corneum intercellular lipids. I. Characterization and comparison with stratum corneum intercellular structure. Int. J. Pharm. 131 (1996) 103-115.

[254] W. Potts, D.T. Downing, Deuterium NMR investigation of polymorphism in stratum corneum lipids. Biochim. Biophys. Acta 1068 (1991) 189-194.

[255] W. Potts, D.T. Downing, Lamellar structures formed by stratum corneum lipids in vitro: a deuterium nuclear magnetic resonance (NMR) study. Pharm. Res. 9 (1992) 1415-1421.

[256] B. Ongpipattankul, R.R. Burnette, R. Potts, M.L. Francoeur, Solid phase behaviour of lipids in porcine stratum corneum. Proc. Int. Symp. Control. Rel. Bioact. Mater. 19 (1993) 143-144.

[257] J.J. Bulgin, L.J. Vinson, The use of differential thermal analysis to study the bound water in stratum corneum membranes. Biochim. Biophys. Acta 136 (1967) 551-560.

[258] P. Garidel, Calorimetric and spectroscopic investigations of phytosphingosine ceramide membrane organisation. Phys. Chem. Chem. Phys. 4 (2002) 1934-1942.

[259] P. Garidel, The thermotropic phase behaviour of phytoceramide 1 as investigated by ATR-FTIR and DSC. Phys. Chem. Chem. Phys. 4 (2002) 2714-2720.

[260] J. Pieper, G. Charalambopoulou, T. Steriotis, S. Vasenkov, A. Desmedt, R.E. Lechner, Water diffusion in fully hydrated porcine stratum corneum. Chem. Phys. 292 (2003) 465–476.

[261] A. Alonso, N.C. Meirelles, V.E. Yushmanov, M. Tabak, Water increases fluidity of intercellular membranes of stratum corneum: correlation with water permeability, elastic, and electrical resistance properties. J. Invest. Dermatol. 106 (1996) 1058–1063.

[262] E. Sparr, H. Wennerström, Responding phospholipid membranes- interplay between hydration and permeability. Biophys. J. 81 (2001) 1014-1028.

[263] R.L. Anderson, J.M. Cassidy, J.R. Hansen, W. Yellin, Hydration of stratum corneum. Biopolymers 12 (1973) 2789-2802.

[264] M. Hey, D. Taylor, W. Derbyshire, Water sorption by human callus. Biochim. Biophys. Acta 540 (1978) 518–533.

[265] G. Imokawa, H. Kuno, M. Kawai, Stratum corneum lipids serve as a bound-water modulator. J. Invest. Dermatol. 96 (1991) 845–851.

[266] T. Inoue, K. Tsujii, K. Okamoto, K. Toda, Differential scanning calorimetric studies on the melting behavior of water in stratum corneum. J. Invest. Dermatol. 86 (1986) 689–693.

[267] G.B. Kasting, N.D. Barai, Equilibrium water sorption in human stratum corneum. J. Pharm. Sci. 92 (2003) 1624–1631.

[268] P. Wertz, L. Norlén, "Confidence Intervals" for the "True" Lipid Composition of the Human Skin Barrier?, in Skin, Hair and Nails: Structure and Function, Marcel Dekker, 2004.

[269] D.B. Fenske, J.L. Thewalt, M. Bloom, N. Kitson, Model of stratum corneum intercellular membranes: 2H NMR of macroscopically oriented multilayers. Biophys. J. 67 (1994) 1562–1573.

[270] D.J. Moore, M.E. Rerek, R. Mendelsohn, Lipid domains and orthorhombic phases in model stratum corneum: evidence from Fourier Transform Infrared Spectroscopy studies. Biochem. Biophys. Res. Commun. 231 (1997) 797–801.

[271] B. Ongpipattanakul, M.L. Francoeur, R.O. Potts, Polymorphism in stratum corneum lipids. Biochim. Biophys. Acta 1190 (1994) 115–122.

[272] A. Alonso, J. Silva, M. Tabak, Stratum corneum protein mobility as evaluated by a spin label maleimide derivative. Biochim. Biophys. Acta 1478 (2000) 89-101.

[273] M. Sznitowska, S. Janicki, A. Williams, S. Lau, A. Stolyhwo, pH-Induced modifications to stratum corneum lipids investigated using thermal, spectroscopic, and chromatographic techniques. J. Pharm. Sci. 92 (2003) 173-179.

[274] I. Wadsö, L. Wadsö, A new method for determination of vapour sorption isotherms using a twin double microcalorimeter. Thermochim. Acta 271 (1996) 179–187.

[275] V. Kocherbitov, Salt-saturated salt solution as a standard system for sorption calorimetry. Thermochim. Acta 421 (2004) 105–110.

[276] V. Kocherbitov, A new formula for accurate calculation of water activity in sorption calorimetric experiments. Thermochim. Acta 414 (2004) 43-45.

[277] L. Wadsö, N. Markova, A double twin isothermal microcalorimeter. Thermochim. Acta 360(2) (2000) 101-107.

[278] K. Whittal, A. MacKay, Quantitative interpretation of NMR relaxation data. J. Magn. Reson. 84 (1989) 134-152.

[279] C.J. Johnson Jr, Diffusion ordered nuclear magnetic resonance spectrocopy: principles and applications. Prog. Nucl. Magn. Reson. Spectrosc. 34 (1999) 203–256.

[280] V. Kocherbitov, T. Arnebrant, O. Söderman, Lysozyme-water interactions studied by sorption calorimetry. J. Phys. Chem. B 108 (2004) 19036–19042.

[281] L. Wadsö, N. Markova, A method to simultaneously determine sorption isotherms and sorption enthalpies with a double twin microcalorimeter. Rev. Sci. Instrum. 73 (2002) 2743–2754.

[282] M.H. Levitt, Spin Dynamics: Basics of Nuclear Magnetic Resonance, Chichester, 2001.

[283] D. Topgaard, O. Söderman, Self-diffusion of nonfreezing water in porous carbohydrate polymer systems studied with NMR. Biophys. J. 83 (2002) 3596–3606.

[284] H. Wennerström, Proton nuclear magnetic ressonance lineshapes in lamellar liquid crystals. Chem. Phys. Lett. 18 (1973) 41-44.

[285] K.J. Packer, T.C. Sellwood, Proton magnetic resonance studies of hydrated stratum corneum. Part 1.- Spin-lattice and transverse relaxation. J. Chem. Soc. Faraday Trans. 2 74 (1978) 1579–1591.

[286] Y. Xu, C. Araujo, A. MacKay, K. Whittal, Proton spin-lattice relaxation in wood – T1 related to local specific gravity using a fast-exchange model. J. Magn. Reson. B 110 (1996) 55–64.

[287] A. Alonso, N.C. Meirelles, M. Tabak, Effect of hydration upon the fluidity of intercellular membranes of stratum corneum: an EPR study. Biochim. Biophys. Acta 1237 (1995) 6-15.

[288] M.E. Hatcher, W.Z. Plachy, Dioxygen diffusion in the stratum corneum: an EPR spin label study. Biochim. Biophys. Acta 1149 (1993) 73–78.

[289] D. Parrott, J. Turner, Mesophase formation by ceramides and cholesterol: a model for stratum corneum lipid packing? Biochim. Biophys. Acta 1147 (1993) 273–276.

[290] S. Rehfeld, W. Plachy, S. Hou, P. Elias, Localization of lipid microdomains and thermal phenomena in murine stratum corneum and isolated membrane complexes: an electron spin resonance study. J. Invest. Dermatol. 95 (1990) 217–223.

[291] V. Mak, R. Potts, R. Guy, Does hydration affect intercellular lipid organization in the stratum corneum? Pharm. Res. 8 (1991) 1064–1065.

[292] B. Ninham, V. Parsegian, Electrostatic potential between surfaces bearing ionizable groups in ionic equilibrium with physiologic saline solution. J. Theor. Biol. 31(3) (1971) 405-428.

[293] J. Israelachvili, Intermolecular and surface forces, Academic Press Limited, London, 1992.

[294] G. Charalambopoulou, T.A. Steriotis, T. Hauss, A.K. Stubos, N.K. Kanellopoulos, Structural alterations of fully hydrated human stratum corneum. Physica B 350 (2004) e603–e606.

[295] V. Kocherbitov, O. Söderman, Glassy crystalline state and water sorption of alkyl maltosides. Langmuir 20 (2004) 3056–3061.

[296] V. Kocherbitov, Driving forces of phase transitions in surfactant and lipid systems. J. Phys. Chem. B 109 (2005) 6430–6435.

[297] W. Abraham, D.T. Downing, Deuterium NMR investigation of polymorphism in stratum corneum lipids. Biochim. Biophys. Acta 1068 (1991) 189–194.

[298] S. Raudenkolb, S. Wartewig, G. Brezesinski, S. Funari, R. Neubert, Hydration properties of n-(alpha-hydroxyacyl)-sphingosine: X-ray powder diffraction and FT-Raman spectroscopic studies. Chem. Phys. Lipids 136 (2005) 13–22.

[299] Y.S. Papir, K. Hsu, R.H. Wildnauer, The mechanical properties of water and ambient temperature on the tensile properties of newborn rat stratum corneum. Biochim. Biophys. Acta 399 (1975) 170–180.

[300] H.P. Baden, A.L.A. Goldsmith, L. Bonar, Conformational changes in the α-fibrous protein of epidermis. J. Invest. Dermatol. 60 (1973) 215–218.

[301] J. Garson, J. Doucet, J. Lévêque, G. Tsoucaris, Oriented structure in human stratum corneum revealed by X-ray diffraction. J. Invest. Dermatol. 96 (1991) 43-49.

[302] P. Elsner, E. Berardesca, H. Maibach, Bioengineering of the skin: water and stratum corneum, CRC Press, Switzerland, 1994.

[303] M.A. Kiselev, N.Y. Ryabova, A.M. Balagurov, S. Dante, T. Hauss, J. Zbytovska, S. Wartewig, R.H.H. Neubert, New insights into the structure and hydration of a stratum corneum lipid model membrane by neutron diffraction. Eur. Biophys. J. 34 (2005) 1030-1040.

[304] S.E. Friberg, I. Kayali, L.D. Rhein, F.A. Simion, R.H. Cagan, The importance of lipids for water uptake in stratum corneum. Int. J. Cosmet. Sci. 12 (1990) 5-12.

[305] L. Norlén, A. Emilson, B. Forslind, Stratum corneum swelling. Biophysical and computer assisted quantitative assessments. Arch. Dermatol. Res. 289 (1997) 506-513.

[306] P.K. Dutta, M.N.V. Ravikumar, J. Dutta, Chitin and chitosan for versatile applications. J. Macrom. Sci. Part C: Polymer Reviews C42(3) (2002) 307-354.

[307] A. Denuziere, D. Ferrier, O. Damour, A. Domard, Chitosan-chondroitin sulfate and chitosan-hyaluronate polyelectrolyte complexes: biological properties. Biomaterials 19(14) (1998) 1275-1285.

[308] E. Khor, L.Y. Lim, Implantable applications of chitin and chitosan. Biomaterials 24 (2003) 2339-2349.

[309] S. Rossi, G. Sandri, F. Ferrari, M.C. Bonferoni, C. Caramella, Buccal delivery of acyclovir from films based on chitosan and polyacrylic acid. Pharm. Develop. Technol. 8(2) (2003) 199-208.

[310] P. Torre, Y. Enobakhare, G. Torrado, S. Torrado, Release of amoxicillin from polyionic complexes of chitosan and poly(acrylic acid). Study of polymer/polymer and polymer/drug interactions within the network structure. Biomaterials 24(8) (2003) 1499-1506.

[311] T. Cerchiara, B. Luppi, F. Bigucci, I. Orienti, V. Zecchi, Physically cross-linked chitosan hydrogels as topical vehicles for hydrophilic drugs. J. Pharm. Pharmacol. 54 (2002) 1453-1459.

[312] N.L. Yusof, A. Wee, L.Y. Lim, E. Khor, Flexible chitin films as potential wound dressing materials: wound model studies. J. Biomed. Mater. Res. 66A (2003) 224-232.

[313] A.K. Azad, N. Sermsintham, S. Chandrkrachang, W.F. Stevens, Chitosan membrane as a wound-healing dressing: characterization and clinical application. J. Biomed. Mater. Res. Part B: Appl. Biomater. 69B (2004) 216-222.

[314] J. Nunthanid, S. Puttipipatkhachorn, K. Yamamoto, G.E. Peck, Physical properties and molecular behavior of chitosan films. Drug Dev. Ind. Pharm. 27(2) (2001) 143 - 157.

[315] M.N.V.R. Kumar, N. Kumar, Polymeric controlled drug-delivery systems: perspective issues and opportunities. Drug Dev. Ind. Pharm. 27(1) (2001) 1-30.

[316] P.M. Torre, S. Torrado, S. Torrado, Interpolymer complexes of poly(acrylic acid) and chitosan: influence of the ionic hydrogel-forming medium. Biomaterials 24 (2003) 1459-1468.

[317] A. Gómez-Carracedo, C. Alvarez-Lorenzo, J.L. Gómez-Amoza, A. Concheiro, Glass transitions and viscoelastic properties of carbopol and noveon compacts. Int. J. Pharm. 274 (2004) 233-243.

[318] X.Z. Shu, K.J. Zhu, W. Song, Novel pH-sensitive citrate cross-linked chitosan film for drug controlled release. Int. J. Pharm. 212(1) (2001) 19-28.

[319] K. Kofuji, T. Ito, Y. Murata, S. Kawashima, Effect of chondroitin sulfate on the biodegradation and drug release of chitosan gel beads in subcutaneous air pouches of mice. Biol. Pharm. Bull. 25 (2002) 268-271

[320] O. Munjeri, J.H. Collett, J.T. Fell, Hydrogel beads based on amidated pectins for colon-specific drug delivery: the role of chitosan in modifying drug release. J. Control. Release 46(3) (1997) 273-278.

[321] W. Chen, L. Wang, J. Chen, S. Fan, Characterization of polyelectrolyte complexes between chondroitin sulfate and chitosan in the solid state. J. Biomed. Mater. Res. 75A (2005) 128-137.

[322] J.-S. Ahn, H.-K. Choi, M.-K. Chun, J.-M. Ryu, J.-H. Jung, Y.-U. Kim, C.-S. Cho, Release of triamcinolone acetonide from mucoadhesive polymer composed of chitosan and poly(acrylic acid) in vitro. Biomaterials 23(6) (2002) 1411-1416.

[323] H. Lin, S. Yu, C. Kuo, H. Kao, Y. Lo, Y. Lin, Pilocarpine-loaded chitosan-PAA nanosuspension for ophthalmic delivery. J. Biomater. Sci. Polym. Ed. 18(2) (2007) 205-221.

[324] A.J. Thote, J.T. Chappell, R. Kumar, R.B. Gupta, Reduction in the initial-burst release by surface crosslinking of PLGA microparticles containing hydrophilic or hydrophobic drugs. Drug Dev. Ind. Pharm. 31(1) (2005) 43 - 57.

[325] X. Huang, C.S. Brazel, On the importance and mechanisms of burst release in matrix-controlled drug delivery systems. J. Control. Release 73 (2001) 121-136.

[326] I.S. Arvanitoyannis, A. Nakayama, S. Aiba, Chitosan and gelatin based edible films: state diagrams, mechanical and permeation properties. Carbohydrate Polymers 37 (1998) 371-382.

[327] N.E. Suyatma, L. Tighzert, A. Copinet, Effects of hydrophilic plasticizers on mechanical, thermal, and surface properties of chitosan films. J. Agric. Food Chem. 53 (2005) 3950-3957.

[328] A.M. Wokovich, S. Prodduturi, W.H. Doub, A.S. Hussain, L.F. Buhse, Transdermal drug delivery (TDDS) adhesion as a critical safety, efficacy and quality attribute. Eur. J. Pharm. Biopharm. 64 (2006) 1-8.

[329] S. Venkatraman, R. Gale, Skin adhesives and skin adhesion. 1. Transdermal drug delivery systems. Biomaterials 19 (1998) 1119-1136.

[330] M.M. Feldstein, I.M. Raigorodskii, A.L. Iordanskii, J. Hadgraft, Modeling of percutaneous drug transport in vitro using skin-imitating Carbosil membrane. J. Control. Release 52(1) (1998) 25-40.

[331] A.L. Iordanskii, M.M. Feldstein, V.S. Markin, J. Hadgraft, N.A. Plate, Modeling of the drug delivery from a hydrophilic transdermal therapeutic system across polymer membrane Eur. J. Pharm. Biopharm. 49(3) (2000) 287-293.

[332] M.M. Feldstein, V.N. Tohmakhch, L.B. Malkhazov, A.E. Vasiliev, N.A. Plate, Hydrophilic polymeric matrices for enhanced transdermal drug delivery. Int. J. Pharm. 131(2) (1996) 229-242.

[333] A.A. Chalykh, A.E. Chalykh, M.B. Novikov, M.M. Feldstein, Pressure-sensitive adhesion in the blends of poly(N-vinyl pyrrolidone) and polyethylene glycol of disparate chain lengths. J. Adhes. 78(8) (2002) 667-694.

[334] J.L.G.C. Pereira, A.A.C.C. Pais, J.S. Redinha, Maximum likelihood estimation with nonlinear regression in polarographic and potentiometric studies. Anal. Chim. Acta 433(1) (2001) 135-143.

[335] E. Seyrek, P.L. Dubin, C. Tribet, E.A. Gamble, Ionic strength dependence of protein-polyelectrolyte interactions. Biomacromolecules 4 (2003) 273-282.

[336] T.A. Khan, K.K. Peh, H.S. Ch'ng, Mechanical, bioadhesive strength and biological evaluations of chitosan films for wound dressing. J. Pharm. Pharmaceut. Sci. 3(3) (2000) 303-311.

[337] K.M. Kim, C.L. Weller, M.A. Hanna, Properties of chitosan films according to pH and types of solvents. J. Food Sci. 71(3) (2006) E119-E124.

[338] X. Yan, E. Khor, L. Lim, Chitosan-alginate films prepared with chitosans of different molecular weights. J. Biomed. Mater. Res. (Appl. Biomater.) 58 (2001) 358-365.

[339] A. Roos, C. Creton, M.B. Novikov, M.M.B. Feldstein, Viscoelasticity and tack of Poly(Vinyl Pyrrolidone)-Poly(Ethylene Glycol) blends. J. Polym. Sci. Part B: Polym. Phys. 40(20) (2002) 2395-2409.

[340] L.B. Rockland, Saturated salt solutions for static control of relative humidity between 5ºC and 40ºC. Anal. Chem. 32 (1960) 1375- 1376.

[341] K. Paepe, E. Houben, R. Adam, F. Wiesemann, V. Rogiers, Validation of the VapoMeter, a closed unventilated chamber system to assess transepidermal water loss vs. the open chamber Tewameter®. Skin Res. Technol. 11(1) (2005) 61–69.

[342] H.J.C. Berendsen, D.v.d. Spoel, R.v. Drunen, GROMACS - a message-passing parallel molecular dynamics implementation. Computer Phys. Commun. 91 (1995) 43-56.

[343] E. Lindahl, B. Hess, D.v.d. Spoel, GROMACS 3.0: a package for molecular simulation and trajectory analysis. J. Mol. Model 7 (2001) 306-317.

[344] W.F.v. Gunsteren, H.J.C. Berendsen, Gromos-87 manual, Biomos BV, Nijenborgh 4, 9747 AG Groningen, The Netherlands, 1987.

[345] D.M.F.v. Aalten, R. Bywater, J.B.C. Findlay, M. Hendlich, R.W.W. Hooft, G. Vriend, PRODRG, a program for generating molecular topologies and unique molecular descriptors from coordinates of small molecules. J. Comput. Aided Mol. Des. 10 (1996) 255-262.

[346] H.J.C. Berendsen, J.P.M. Postma, W.F.v. Gunsteren, J. Hermans, Interaction models for water in relation to protein hydration, B. Pullman ed., Reidel, Dordrecht, 1981.

[347] S. Miyamoto, P.A. Kollman, SETTLE : An analytical version of the SHAKE and RATTLE algorithms for rigid water models. J. Comput. Chem. 13 (1992) 952--962.

[348] H.J.C. Berendsen, J.P.M. Postma, W.F.v. Gunsteren, A. DiNola, J.R. Haak, Molecular dynamics with coupling to an external bath. J. Chem. Phys. 81 (1984) 3684-3690.

[349] T. Darden, D. York, L. Pedersen, Particle mesh Ewald. (PME): a N log(N) method for Ewald sums in large systems. J. Chem. Phys. 98 (1993) 10089–10092.

[350] S. Ikeda, H. Kumagai, T. Sakiyama, C. Chu, K. Nakamura, Method for analyzing pH-sensitive swelling of amphoteric hydrogels - Application to a polyelectrolyte complex gel prepared from xanthan and chitosan. Biosci. Biotech. Biochem. 59(8) (1995) 1422-1427.

[351] S. Mao, U. Bakowsky, A. Jintapattanakit, T. Kissel, Self-assembled polyelectrolyte nanocomplexes between chitosan derivatives and insulin. J. Pharm. Sci. 95(5) (2006) 1035-1048.

[352] S.Y. Lin, C.J. Lee, Y.Y. Lin, Drug-polymer interaction affecting the mechanical properties, adhesion strength and release kinetics of piroxicam-loaded Eudragit E films plasticized with different plasticizers. J. Control. Release 33(3) (1995) 375-381.

[353] M.F. Cervera, J. Heinämäki, K. Krogars, A.C. Jörgensen, M. Karjalainen, A. Colarte, J. Yliruusi, Solid-State and mechanical properties of aqueous chitosan-amylose starch films plasticized with polyols. AAPS PharmSciTech. 5(1) (2004) article 15.

[354] S. Mathew, M. Brahmakumar, T.E. Abraham, Microstructural imaging and characterization of the mechanical, chemical, thermal, and swelling properties of starch-chitosan blend films. Biopolymers 82(2) (2006) 176-187.

[355] R.A. Talja, H. Helén, Y.H. Roos, K. Jouppila, Effect of various polyols and polyol contents on physical and mechanical properties of potato starch-based films. Carbohydrate Polymers 67 (2007) 288-295.

[356] M.F. Cervera, M. Karjalainen, S. Airaksinen, J. Rantanen, K. Krogars, J. Heinamaki, A.I. Colarte, J. Yliruusi, Physical stability and moisture sorption of aqueous chitosan-amylose starch films plasticized with polyols. Eur. J. Pharm. Biopharm. 58 (2004) 69-76.

[357] S. Mali, L.S. Sakanaka, F. Yamashita, M.V.E. Grossmann, Water sorption and mechanical properties of cassava starch films and their relation to plasticizing effect. Carbohydrate Polymers 60(3) (2005) 283-289.

[358] S. Despond, E. Espuche, A. Domard, Water sorption and permeation in chitosan films: relation between gas permeability and relative humidity. J. Polym. Sci. Part B: Polym. Phys. 39 (2001) 3114-3127.

[359] A.B. Richards, S. Krakowka, L.B. Dexter, H. Schmid, A.P.M. Wolterbeek, D.H. Waalkens-Berendsen, A. Shigoyuki, M. Kurimoto, Trehalose: a review of properties, history of use and human tolerance, and results of multiple safety studies. Food Chem. Toxicol. 40(7) (2002) 871-898.

[360] Y.N. Kalia, I. Alberti, N. Sekkat, C. Curdy, A. Naik, R.H. Guy, Normalization of stratum corneum barrier function and transepidermal water loss in vivo. Pharm. Res. 17(9) (2000) 1148-1150.

[361] C. Remunan-Lopez, R. Bodmeier, Mechanical, water uptake and permeability properties of crosslinked chitosan glutamate and alginate films. J. Control. Release 44(2) (1997) 215-225.

[362] R. Lamim, R.A. Freitas, E.I. Rudek, H.M. Wilhelm, O.A. Cavalcanti, T.M.B. Bresolin, Films of chitosan and N-carboxymethylchitosan. Part II: effect of plasticizers on their physiochemical properties. Polym. Int. 55(8) (2006) 970-977.

[363] J. Viyoch, T. Sudedmark, W. Srema, W. Suwongkrua, Development of hydrogel patch for controlled release of alpha-hydroxy acid contained in tamarind fruit pulp extract. Int. J. Cosm. Sci. 27 (2005) 89-99.

[364] D.A. Hollingsbee, P. Timmins, Topical adhesive systems, Wissenschaftliche Verlagsgesellschaft, Stuttgart, 1990.

[365] B. Sarmento, A. Ribeiro, F. Veiga, D. Ferreira, Development and characterization of new insulin containing polysaccharide nanoparticles. Colloids and Surfaces B: Biointerfaces 53(2) (2006) 193-202.

[366] M.G. Sankalia, R.C. Mashru, J.M. Sankalia, V.B. Sutariya, Reversed chitosan–alginate polyelectrolyte complex for stability improvement of alpha-amylase: Optimization and physicochemical characterization. Eur. J. Pharm. Biopharm. 65 (2007) 215-232.

[367] X.-D. Fan, Y.-L. Hsieh, J.M. Krochta, M.J. Kurth, Study on molecular interaction behavior, and thermal and mechanical properties of polyacrylic acid and lactose blends. J. Appl. Polymer Sci. 82(8) (2001) 1921-1927.

[368] Y. Huang, J. Lu, C. Xiao, Thermal and mechanical properties of cationic guar gum/poly(acrylic acid) hydrogel membranes. Polym. Deg. Stab. 92(6) (2007) 1072-1081.

[369] J.J. Maurer, D.J. Eustace, C.T. Ratcliffe, Thermal characterization of poly(acrylic acid). Macromolecules 20(1) (1987) 196-202.

[370] C. Rodríguez-Tenreiro, C. Alvarez-Lorenzo, A. Concheiro, J.J. Torres-Labandeira, Characterization of cyclodextrin-carbopol interactions by DSC and FTIR. J. Thermal Anal. Cal. 77 (2004) 403-411.

[371] J. Dong, Y. Ozaki, K. Nakashima, Infrared, Raman, and Near-Infrared Spectroscopic evidence for the coexistence of various hydrogen-bond forms in poly(acrylic acid). Macromolecules 30(4) (1997) 1111 -1117.

[372] K. Brandenburg, U. Seydel, Fourier transform infrared spectroscopy of cell surface polysacharides, Wiley-Liss, New York, 1996.

[373] X. Qu, A. Wirsén, A.-C. Albertsson, Structural change and swelling mechanism of pH-sensitive hydrogels based on chitosan and D,L-lactic acid. J. Appl. Polym. Sci. 74(13) (1999) 3186-3192.

[374] B. Stuart, Infrared Spectroscopy: Fundamentals and Applications, John Wiley & Sons Ltd, West Sussex, England, 2004.

[375] J. Coates, Interpretation of Infrared Spectra, a practical approach, John Wiley & Sons Ltd, Chichester, 2000.

[376] C.D. Brown, L. Kreilgaard, M. Nakakura, N. Caram-Lelham, D.K. Pettit, W.R. Gombotz, A.S. Hoffman, Release of PEGylated granulocyte-macrophage colony-stimulating factor from chitosan/glycerol films. J. Control. Release 72(1-3) (2001) 35-46.

[377] A.C. Moffat, M.D. Osselton, B. Widdop, Clarke's Analysis of Drugs and Poisons, Pharmaceutical Press, 2004.

[378] D.S. Wishart, C. Knox, A.C. Guo, S. Shrivastava, M. Hassanali, P. Stothard, Z. Chang, J. Woolsey, DrugBank: a comprehensive resource for in silico drug discovery and exploration. Nucleic Acids Res. 34 (2006) D668-672.

[379] J.L. Cummings, Alzheimer's disease. N. Engl. J. Med. 351 (2004) 56-67.

[380] P. Tariot, B. Winblad, Galantamine, a novel treatment for Alzheimer's Disease: a review of long-term benefits to patients and caregivers, John Wiley & Sons Ltd Chichester, 2001

[381] M.C. Dale, S.E. Libretto, C. Patterson, J. Anderson, T. Choudhury, F. McCafferty, C. McWilliam, M. Richardson, Clinical experience of galantamine in dementia: a series of case reports. Curr. Med. Res. Opinion 19(6) (2003) 508-518.

[382] R. Katzman, Epidemiology of Alzheimer's Disease and Dementia: advances and challenges, John Wiley & Sons Ltd Chichester, 2001

[383] J. Hadgraft, R.H. Guy, Feasibility assessment in topical and transdermal delivery: mathematical models and in vitro studies, Marcel Dekker, Inc., NY, 2003.

[384] M. Dias, J. Hadgraft, M.E. Lane, Influence of membrane–solvent–solute interactions on solute permeation in skin. Int. J. Pharm. 340(1-2) (2007) 65-70.

[385] N. Leveque, S.L. Raghavan, M.E. Lane, J. Hadgraft, Use of molecular form technique for the penetration of supersaturated solutions of salicylic acid across silicone membranes and human skin in vitro. Int. J. Pharm. 318 (2006) 49-54.

[386] D.A. Godwin, B.B. Michniak, Influence of drug lipophilicity on terpenes as transdermal penetration enhancers. Drug Dev. Ind. Pharm. 25(8) (1999) 905-915.

[387] H.K. Vaddi, P.C. Ho, S.Y. Chan, Terpenes in propylene glycol as skin-penetration enhancers: permeation and partition of Haloperidol, Fourier Transform Infrared Spectroscopy, and Differential Scanning Calorimetry. J. Pharm. Sci. 91 (2002) 1639-1651.

[388] N.A. Megrab, A.C. Williams, B.W. Barry, Oestradiol permeation through human skin and silastic membrane: effects of propylene glycol and supersaturation. J. Control. Release 36 (1995) 277-294.

[389] R.J. Babu, J.K. Pandit, Effect of penetration enhancers on the transdermal delivery of bupranolol through rat skin. Drug Delivery 12 (2005) 165-169.

[390] I.Z. Schroeder, P. Franke, U.F. Schaefer, C.M. Lehr, Delivery of ethinylestradiol from film forming polymeric solutions across human epidermis in vitro and in vivo in pigs. J. Control. Release 118 (2007) 196-203.

[391] V.R. Sinha, M.P. Kaur, Permeation enhancers for transdermal drug delivery. Drug Dev. Ind. Pharm. 26(11) (2000) 1131-1140.

[392] Y. Takeuchi, H. Yasukawa, Y. Yamaoka, Y. Kato, Y. Morimoto, Y. Fukumori, T. Fukuda, Effects of fatty acids, fatty amines and propylene glycol on rat stratum corneum lipids and proteins in vitro measured by fourier transform infrared/attenuated total reflection (FT-IR/ATR) spectroscopy. Chem. Pharm. Bull. 40(7) (1992) 1887-1892.

[393] J.E. Harrison, A.C. Watkinson, D.M. Green, J. Hadgraft, K. Brain, The relative effect of Azone and Transcutol on permeant diffusivity and solubility in human stratum corneum. Pharm. Res. 13(4) (1996) 542-546.

[394] P. Mura, M.T. Faucci, G. Bramanti, P. Corti, Evaluation of transcutol as a clonazepam transdermal permeation enhancer from hydrophilic gel formulations. Eur. J. Pharm. Sci. 9 (2000) 365-372.

[395] J.J. Escobar-Chávez, D. Quintanar-Guerrero, A. Ganem-Quintanar, In vivo skin permeation of sodium naproxen formulated in pluronic F-127 gels: effect of Azone and Transcutol. Drug Dev. Ind. Pharm. 31 (2005) 447-454.

[396] H. Liu, S. Li, Y. Wang, H. Yao, Y. Zhang, Effect of vehicles and enhancers on the topical delivery of cyclosporin A. Int. J. Pharm. 311(1-2) (2006) 182-186.

[397] S. Nicoli, V. Amoretti, P. Colombo, P. Santi, Bioadhesive transdermal film containing caffeine. Skin Pharmacol. Physiol. 17 (2004) 119-123.

[398] A. Femenia-Font, C. Padula, F. Marra, C. Balaguer-Fernandez, V. Merino, A. Lopez-Castellano, S. Nicoli, P. Santi, Bioadhesive monolayer film for the in vitro transdermal delivery of sumatriptan J. Pharm. Sci. 95(7) (2006) 1561-1569.

[399] M. Kim, H. Zhao, C. Lee, D. Kim, Formulation of a reservoir-type testosterone transdermal delivery system. Int. J. Pharm. 219 (2001) 51-59.

[400] R. Rowe, P. Sheskey, S. Owen, Handbook of Pharmaceutical Excipients, Pharmaceutical Press, 2005.

[401] M.A. Bagger, H.W. Nielsen, E. Bechgaard, Nasal bioavailability of peptide T in rabbits: absorption enhancement by sodium glycocholate and glycofurol. Eur. J. Pharm. Sci. 14 (2001) 69-74.

[402] E. Bechgaard, S. Gizurarson, R.K. Hjortkjaer, A.R. Sorensen, Intranasal administration of insulin to rabbits using glycofurol as an absorption promoter. Int. J. Pharm. 128 (1996) 287-289.

[403] U.T. Lashmar, J. Hadgraft, N. Thomas, Topical application of penetration enhancers to the skin of nude mice: a histopathological study. J. Pharm. Pharmacol. 41(2) (1989) 118-122.

[404] A.I. Vogel, A.R. Tatchell, B.S. Furnis, A.J. Hannaford, P.W.G. Smith, Vogel's Textbook of Practical Organic Chemistry, Longman Scientific and Technical, UK, 1989.

[405] ICH, Validation of analytical procedures: text and methodology. Q2 (R1) Current Step 4 (2005).

[406] ISO8466-1, Water quality - Calibration and evaluation of analytical methods and estimation of performance characteristics - Part 1: Statistical evaluation of the linear calibration function, ISO, Geneve, Switzerland, 1990.

[407] ISO8466-2, Water quality - Calibration and evaluation of analytical methods and estimation of performance characteristics - Part 2: Calibration strategy for non-linear second order calibration functions, ISO, Geneve, Switzerland, 1993.

[408] FDA. US Department of Health and Human Services, Center for Drug Evaluation and Research, Guidance for industry: skin irritation and sensitization testing of generic transdermal products. (1999).

[409] S.K. Niazi, Handbook of Pharmaceutical Manufacturing Formulations. Volume 4: Semi-Solid Products, CRC Press, Boca Raton, Florida, 2004.

[410] D. Fitzpatrick, J. Corish, Release characteristics of anionic drug compounds from liquid crystalline gels: I: Passive release across non-rate-limiting membranes. Int. J. Pharm. 301(1-2) (2005) 226-236.

[411] P. Costa, J.M.S. Lobo, Evaluation of mathematical models describing drug release from estradiol transderml systems. Drug Dev. Ind. Pharm. 29(1) (2003) 89-97.

[412] P. Costa, J.M.S. Lobo, Modeling and comparison of dissolution profiles. Eur. J. Pharm. Sci. 13 (2001) 123-133.

[413] A.M. Kligman, E. Christophers, Preparation of isolated sheets of human stratum corneum. Arch. Dermatol. 88 (1963) 702-705.

[414] S.M. Harrison, B.W. Barry, P.H. Dugard, Effects of freezing on human skin permeability. J. Pharm. Pharmacol. 36 (1984) 261-262.

[415] R.L. Bronaugh, R.F. Stewart, M. Simon, Methods for in vitro percutaneous absorption studies VII: use of excised human skin. J. Pharm. Sci. 75 (1986) 1094-1097.

[416] V. Rogiers, E. group, EEMCO guidance for the assessment of transepidermal water loss in cosmetic sciences. Skin Pharmacol. Appl. Skin Physiol. 14 (2001) 117-128.

[417] M. Node, S. Kodama, Y. Hamashima, T. Katoh, N. Nishide, T. Kajimoto, Biomimetic synthesis of (±)-galanthamine and asymmetric synthesis of (-)-galanthamine using remote asymmetric induction. Chem. Pharm. Bull. 54(12) (2006) 1662-1679.

[418] P. Patnaik, J.A. Dean, Dean's analytical chemistry handbook, McGraw-Hill, New York, 2004.

[419] J.H. Kim, H.K. Choi, Effect of additives on the crystallization and the permeation of ketoprofen from adhesive matrix. Int. J. Pharm. 236(1-2) (2002) 81-85.

[420] X.G. Ma, J. Taw, C.M. Chiang, Control of drug crystallization in transdermal matrix system. Int. J.Pharm. 142 (1996) 115-119.

[421] T. Miyazaki, S. Yoshioka, Y. Aso, S. Kojima, Ability of polyvinylpyrrolidone and polyacrylic acid to inhibit the crystallization of amorphous acetaminophen. J. Pharm. Sci. 93(11) (2004) 2710-2717.

[422] S. Wang, S. Lin, Y. Wei, Transformation of metastable forms of acetaminophen studied by thermal fourier transform infrared (FT-IR) microsspectrocopy. Chem. Pharm. Bull. 50(2) (2002) 153-156.

[423] Y.-f. Zhu, J.-l. Shi, Y.-s. Li, H.-r. Chen, W.-h. Shen, X.-p. Dong, Storage and release of ibuprofen drug molecules in hollow mesoporous silica spheres with modified pore surface. Micropor. Mesopor. Mater. 85(1-2) (2005) 75-81.

[424] P.M.d.l. Torre, G. Torrado, S. Torrado, Poly(acrylic acid) chitosan interpolymer complexes for stomach controlled antibiotic delivery. J. Biomed. Mater. Res. Part B: Appl. Biomater. 72B (2005) 191-197.

[425] M. Siewert, J. Dressman, C. Brown, V. Shah, FIP/AAPS guidelines for dissolution/in vitro release testing of novel/special dosage forms. Dissolution Technologies 10(1) (2003) 6-15.

[426] C. Padula, S. Nicoli, P. Colombo, P. Santi, Single-layer transdermal film containing lidocaine: modulation of drug release. Eur. J. Pharm. Biopharm. 66(3) (2007) 422-428.

[427] S. Lieb, R.-M. Szeimies, G. Lee, Self-adhesive thin films for topical delivery of 5-aminolevulinic acid. Eur. J. Pharm. Biopharm. 53 (2002) 99-106.

[428] C. Lin, A.T. Metters, Hydrogels in controlled release formulation: network design and mathematical modeling. Ad. Drug Delivery Rev. 58 (2006) 1379-1408.

[429] F.O. Costa, J.J.S. Sousa, A.A.C.C. Pais, S.J. Formosinho, Comparison of dissolution profiles of ibuprofen pellets. J. Control. Release 89 (2003) 199-212.

[430] C. Padula, G. Colombo, S. Nicoli, P.L. Catellani, G. Massimo, P. Santi, Biodhesive film for the transdermal delivery of lidocaine: in vitro and in vivo behaviour. J. Control. Release 88 (2003) 277-285.

[431] M. Aqil, Y. Sultana, A. Ali, K. Dubey, A.K. Najmi, K.K. Pillai, Transdermal drug delivery systems of a beta blocker: design, in vitro, and in vivo characterization. Drug Delivery 11 (2004) 27-31.

[432] A.F. El-Kattan, C.S. Asbill, B.B. Michniak, The effect of terpene enhancer lipophilicity on the percutaneous permeation of hydrocortisone formulated in HPMC gel systems. Int. J. Pharm. 198 (2000) 179-189.

[433] C. Puglia, F. Bonina, G. Trapani, M. Franco, M. Ricci, Evaluation of in vitro percutaneous absorption of lorazepam and clonazepam from hydro-alcoholic gel formulations. Int. J. Pharm. 228 (2001) 79-87.

[434] P.J. Lee, R. Langer, V.P. Shastri, Role of n-methyl pyrrolidone in the enhancement of aqueous phase transdermal transport. J. Pharm. Sci. 94 (2005) 912-917.

[435] R.J. Babu, J.K. Pandit, Effect of penetration enhancers on the release and skin permeation from bupranolol from reservoir-type transdermal delivery systems. Int. J. Pharm. 288 (2005) 325-334.

[436] J. Hadgraft, J. Peck, D.G. Williams, W.J. Pugh, G. Allan, Mechanisms of action of skin penetration enhancers/retarders: Azone and analogues. Int. J. Pharm. 141 (1996) 17-25.

[437] P.J.S. Gomes, C.M. Nunes, A.A.C.C. Pais, T.P. Melo, L.G. Arnaut, 1,3-Dipolar cycloaddition of azomethine ylides generated from aziridines in supercritical carbon dioxide. Tetrahedron Letters 47(31) (2006) 5475-5479.

[438] A.F. Peixoto, M.M. Pereira, A.A.C.C. Pais, Maximization of regioselectivity in hydroformylation of vinyl-aromatics using simple factorial design. J. Molecular Catalysis A: Chemical 267(1-2) (2007) 234-240.

[439] N.A. Armstrong, Pharmaceutical Experimental Design and Interpretation, CRC press, Boca Raton, FL, 2006.

[440] G.G. Agyralides, P.P. Dallas, D.M. Rekkas, Development and in vitro evaluation of furosemide transdermal formulations using experimental design techniques. Int. J. Pharm. 281 (2004) 35-43.

[441] G.A. Lewis, D. Mathieu, R.P. Tan-Luu, Pharmaceutical Experimental Design, Marcel Dekker, New York, 1999.

[442] J. Siepmann, N.A. Peppas, Modeling of drug release from delivery systems based on hydroxypropyl methylcellulose (HPMC). Adv. Drug Deliv. Rev. 48(1-2) (2001) 139-157.

[443] J.W. Moore, H.H. Flanner, Mathematical comparison of dissolution profiles. Pharm. Tech. 20 (1996) 64-74.

[444] FDA/CDER, Guidance for Industry: dissolution testing of immediate release solid oral dosage forms, Rockville, 1997.

[445] EMEA, Note for guidance on quality of modified release products: A: Oral dosage forms, B: Transdermal dosage forms. Section I (Quality). (1999).

[446] T. O'Hara, A. Dunne, J. Butler, J. Devane, A review of methods used to compare dissolution profile data. PSTT 1(5) (1998) 214-223.

[447] D.L. Massart, B.G.M. Vandeginste, S.N. Deming, Y. Michotte, L. Kaufman, Chemometrics: a textbook, Elsevier, Amsterdam, 1988.

[448] R.G. Brereton, Chemometrics: data analysis for the laboratory and chemical plant, John Wiley & Sons Ltd, Chichester, 2003.

[449] D.C. Montgomery, Design and analysis of experiments, John Wiley & Sons Ltd, Danvers, 2001.

[450] E.-S. Park, S.-J. Chang, Y.-S. Rhee, S.-C. Chi, Effects of adhesives and permeation enhancers on the skin permeation of Captopril. Drug Dev. Ind. Pharm. 27(9) (2001) 975-980.

[451] A. López, F. Llinares, C. Cortell, M. Herráez, Comparative enhancer effects of Span®20 with Tween®20 and Azone® on the in vitro percutaneous penetration of compounds with different lipophilicities. Int. J. Pharm. 202 (2000) 133-140.

[452] O. Diez-Sales, A.C. Watkinson, M. Herraez-Dominguez, C. Javaloyes, J. Hadgraft, A mechanistic investigation of the in vitro human skin permeation enhancing effect of Azone. Int. J. Pharm. 129(1-2) (1996) 33-40.

[453] O. Díez-Sales, T.M. Garrigues, J.V. Herráez, R. Belda, A. Martín-Villodre, M. Herráez, In vitro percutaneous penetration of acyclovir from solvent systems and carbopol 971-P hydrogels: influence of propyleneglycol. J. Pharm. Sci. 94(5) (2005) 1039-1047.

[454] J.H. Ross, M.H. Dong, M.I. Krieger, Conservatism in pesticide exposure assessment. Regulatory Toxicol. Pharmacol. 31 (2000) 53-58.

[455] S. Torrado, P. Prada, P.M.d.l. Torre, S. Torrado, Chitosan-poly(acrylic) acid polyionic complex: in vivo study to demonstrate prolonged gastric retention. Biomaterials 25 (2004) 917-923.

[456] V. Pillay, R. Fassihi, Evaluation and comparison of dissolution data derived from different modified release dosage forms: an alternative method. J. Control. Release 55(1) (1998) 45-55.

[457] M.A. Repka, J.W. McGinity, Bioadhesive properties of hydroxypropylcellulose topical films produced by hot-melt extrusion. J. Control. Release 70(3) (2001) 341-351.

[458] M.A.C. Sánchez, A.I.T. Suárez, M.E.G. Alegre, M.M.O. Sánchez, V.R. Palomar, Validation protocol of analytical methods for finished pharmaceutical products. S. T. P. Pharma Pratiques 3(3) (1993) 197-202.

[459] D. Harvey, Modern analytical chemistry, McGraw-Hill, Boston, 1999.

[460] J.M. Green, A practical guide to analytical method validation. Anal. Chem. 68 (1996) 305A-309A.

[461] C.M. Riley, T.W. Rosanske, Development and validation of analytical methods, Elsevier Science, Oxford, 1996.